CRANFIELD UNIVERSITY

Rudi Kirner

An Investigation into the Benefits of Distributed Propulsion on Advanced Aircraft Configurations

School of Engineering

Department of Power and Propulsion

PhD

Academic Year: 2013 - 2014

Supervisors: Dr. Panagiotis Laskaridis

Prof. Riti Singh

December 2013

CRANFIELD UNIVERSITY

School of Engineering
Power and Propulsion

PhD

Academic Year 2013 - 2014

Rudi Kirner

An Investigation into the Benefits of Distributed Propulsion on Advanced Aircraft Configurations

Supervisors: Dr. Panagiotis Laskaridis
Prof. Riti Singh

December 2013

This thesis is submitted in partial fulfilment of the requirements for the degree of PhD

(NB. This section can be removed if the award of the degree is based solely on examination of the thesis)

ABSTRACT

Radical aircraft and propulsion system architecture changes may be required to continue historic performance improvement rates as current civil aircraft and engine technologies mature. Significant fuel-burn savings are predicted to be achieved through the Distributed Propulsion concept, where an array of propulsors is distributed along the span of an aircraft to ingest boundary layer air and increase propulsive efficiency. Studies such as those by NASA predict large performance benefits when integrating Distributed Propulsion with the Blended Wing Body aircraft configuration, as this planform geometry is particularly suited to the ingestion of boundary layer air and the fans can be redesigned to reduce the detrimental distortion effects on performance. Additionally, a conventional aircraft with Distributed Propulsion has not been assessed in public domain literature and may also provide substantial benefits.

A conceptual aircraft design code has been developed to enable the modelling of conventional and novel aircraft. A distributed fan tool has been developed to model fan performance, and a mathematical derivation was created and integrated with the fan tool to enable the boundary layer ingestion modelling. A tube & wing Distributed Propulsion aircraft with boundary layer ingestion has been compared with a current technology reference aircraft and an advanced turbofan aircraft of 2035 technology. The advanced tube & wing aircraft achieved a 27.5% fuel-burn reduction relative to the baseline aircraft and the Distributed Propulsion variant showed fuel efficiency gains of 4.1% relative to the advanced turbofan variant due to a reduced specific fuel consumption, produced through a reduction in distributed fan power requirement. The Blended Wing Body with Distributed Propulsion was compared with a turbofan variant reference aircraft and a 5.3% fuel-burn reduction was shown to be achievable through reduced core engine size and weight. The Distributed Propulsion system was shown to be particularly sensitive to inlet duct losses. Further investigation into the parametric sensitivity of the system revealed that duct loss could be mitigated by altering the mass flow and the percentage thrust produced by the distributed fans. Fuel-burn could be further reduced by

decreasing component weight and drag, through decreasing the fan and electrical system size to below that necessary for optimum power or specific fuel consumption.

Keywords:

distributed, propulsion, blended, wing, body, boundary, layer, ingestion, aircraft, magneto, plasma, dynamics

ACKNOWLEDGEMENTS

The work in this thesis has involved a large number of people due to the nature of collaborative work and trying to predict the future. My technical supervisor, Panagiotis Laskaridis, has taught me a lot with regards to work strategy, and technical and project direction. I have received much joy from the many thought provoking conversations we shared together. He has endured my sporadic and drastic ideas and has supported me throughout the work in all situations. I am very grateful for all this. I would also like to thank my other supervisor, Riti Singh, for enabling the PhD opportunity with Rolls-Royce, which was very enjoyable and a great contribution to my future career. I can imagine arranging this with Rolls-Royce was not a simple task. The broad view of industry you have shared with me and your insight into the mind-set of those involved in technology, has been invaluable and has ultimately led me to a fantastic job with Rolls-Royce. I am also grateful for the input Vassilios Pachidis has provided in regards to the Rolls-Royce UTC presentations, especially for his unwavering patience with the organising of all UTC events. This appreciation extends to Maria Negus who has always endeavoured to make the UTC operate seamlessly. I would like to thank Rolls-Royce's Andrew Rolt and Lorenzo Raffaelli who have been a pleasure to work with and have spent a considerable portion of their time sharing their gas turbine knowledge with me and assisting with publications. I would like to thank Pericles Pilidis for his support throughout the PhD and the wisdom I was exposed to through the invaluable discussions we had on career direction. I am very grateful to receive the Rolls-Royce/EPSRC Case Studentship award, Voucher Number: 10000780.

TABLE OF CONTENTS

NOMENCLATURE

Acronyms

A	Aspect ratio
a.c	Aerodynamic Centre
AFC	Active Flow Control
AoA	Angle of Attack
AoA	Angle of Attack
BLI	Boundary Layer Ingestion
BWB	Blended Wing Body
c.g	Centre of Gravity
c.p	Centre of Pressure
CADI	Conceptual Aircraft Design Integration tool
CAEP	Committee on Aviation Environmental Protection
CD	Drag Coefficient
CD0	Zero-Lift drag coefficient
CDi	Induced Drag Coefficient
CDw	Wave Drag
CESTROL	Cruise Efficient, Short Take-off and Landing
CF	Fin Coefficient
CFD	Computational Fluid Dynamics
CL	Lift Coefficient
CO2	Carbon Dioxide
COP	Coefficient of Performance
CT	Tail Coefficient
DP	Distributed Propulsion
eBPR	Engine Bypass Ratio
eFPR	Engine Fan Pressure Ratio
EoR	End-Of-Runway
FE	Finite Element
FOD	Foreign Object Damage
FPR	Fan Pressure Ratio
GE	General Electric

HP	High Pressure
HX	Heat Exchanger
IPC	Intermediate Pressure
L/D	Lift-Drag ratio
LAP	Local Air Pollution
LE	Leading Edge
LFC	Laminar Flow Control
MAC	Mean Aerodynamic Chord
MAD	Magnetoaerodynamics
MHD	Magnetohydrodynamics
MLW	Max Landing Weight
MPD	Magnetoplasmadynamics
MTOW	Max Take-Off Weight
MZFW	Max Zero Fuel Weight
NASA	National Aeronautics and Space Administration
NOx	Oxides of Nitrogen
OEW	Overall Empty Weight
OPR	Overall Pressure Ratios
P&W	Pratt and Whitney
RPK	Revenue Passenger Kilometres
SRC	Strategic Research Centre
T&W	Tube and Wing
T/C	Thickness-Chord ratio
T/O	Take-Off
TE	Trailing Edge
TET	Turbine Entry Temperature
TL	Thrust Loading
ToC	Top of Climb
TS	Thrust-Split (DP fan thrust to total thrust ratio)
VELA	Very Efficient Large Aircraft

Symbols

a	Linear Acceleration
A	Volume
Alt	Altitude
b	Span
B	Magnetic Field Strength
C	Constant
C_{la}	Lift Curve Slope
D	Drag Force
d	Diameter
E	Error
E	Electric Field Strength
F	Force
g	Acceleration due to Gravity
h	Height
I	Electric Current
i_{arm}	Moment Arm
j	Current Density
L	Length
$\dot{m}$	Mass Flow
M	Mass
Mn	Mach Number
n	Power Law Index
N	Number of Charged Particles
P	Power
p	Static Pressure
Q	Heat flux
q	Charge on a single Partcicle
R	Gas Constant
r	Radius
S	Area
s	Linear Distance
T	Temperature

u	Velocity
U	Free-stream velocity
V	Voltage
w	Width
X_A	Distance to MAC
y	Integration Length
γ	Heat Capacity Ratio
ρ	Density
δ	Boundary Layer Height
η	Non-dimension coordinate
λ	Taper Ratio
Λ	Sweep
θ	Angle
Φ	Drag Force Component
δ*	Displacement Thickness
δ_m	Momentum Thickness
σ	Electrical Conductivity
ϕ	Load Factor
∂r	Radius Delta
∂t	Thickness delta

Subscripts

A	Aircraft
BL	Boundary Layer
eng	Engine
EoR	End of Runway
eq	Equivalent Airspeed
j	jet
m	Mean
N	Nacelle
n	integer
S	Area

s	Distance From Surface
ss	Speed of Sound
TRUE	True-Airspeed
v	Shear Force
w	Wake
∞	Free-stream

LIST OF FIGURES

LIST OF TABLES

1 Thesis objectives and structure

Due to the well-established environmental, economic and social issues the aviation industry faces, more efficient designs are continually being sought after by airframe and engine manufacturers. Within the civil transport aircraft industry the major advances on current designs are beginning to subside, providing room for the more radical and challenging concepts to be considered. It therefore becomes important to investigate the potential for these unconventional propulsion concepts on conventional and novel aircraft configurations. The Distributed Propulsion (DP) concept has been heavily investigated by NASA and by a number of other key market players. It shows promise in being the propulsion choice for future aircraft, such as on the Blended Wing Body (BWB) and benefits from being able to ingest boundary layer and improve propulsive efficiency, known as Boundary Layer Ingestion (BLI). This PhD project is centred on evaluating the potential of DP by looking at the wide design space it constitutes.

1.1 Objectives

1. Perform a literature review of the key aircraft and propulsion system methodologies that are available in the literature
2. Model and validate the baseline aircraft and engine similar to the A350 and Trent XWB-1000 respectively, using Cranfield University's performance tools Hermes and Turbomatch
3. Build a robust conceptual aircraft design tool capable of modelling a range of different airframe and propulsion system types
4. Validate the conceptual aircraft design tool using public domain literature
5. Model the following chosen concepts using the conceptual aircraft design tool and Rolls-Royce's engine performance tool BD-36:
6. Tube & wing (T&W) aircraft similar to A350-1000
7. Advanced T&W aircraft with an advanced turbofan engine
8. Advanced T&W aircraft with a DP system
9. BWB with an advanced turbofan engine
10. BWB with a DP system

11. Produce alternative aircraft and propulsion system designs to explore system sensitivities and technology dependencies
12. Develop a DP fan tool, turbofan engine model and a BLI methodology in Cranfield
13. Perform a wider design space investigation of DP on a BWB aircraft by assessing the key technology sensitivities and the effects of changing propulsion system configuration
14. Perform a literature review of Magnetoplasmadynamic (MPD) technologies
15. Produce an analytical model for assessing a MPD boundary layer flow control concept that has been devised
16. Evaluate the performance and feasibility of the MPD flow control concept

2 **PhD Scope**

The main target of the PhD research is to investigate the potential of DP relative to competing turbofan engine technology and to understand how aircraft configuration affects the results. This was done by developing tools that are sufficiently accurate to capture all the relevant physics of the system, of which are flexible enough to enable parametric analysis that doesn't require specific geometry and operating conditions. The DP system is highly integrated with the aircraft, since the flow interacts strongly with both the aircraft surface and propulsor. Detailed CFD studies would be needed to understand the flow interactions and enable an accurate prediction of the potential benefits of BLI. However, due to time constraints, a higher level analysis has been conducted. This has required the development of analytical and empirical 1D tools that can be changed and run at ease. Additionally, a number of simplifying assumptions has been made in order to address the problem rapidly, such as treating the boundary layer as a stream of average momentum. These assumptions are clearly stated throughout the thesis.

The aircraft structure and DP fan housing are also tightly integrated since they may be designed to share the same structure for efficiency gains. Typically Finite Element Analysis (FEA) would be used to predict the structural weight and dynamic affects accurately. Also, the aircraft planform shape in terms of taper ratio and sweep would be designed using a code that predicts the air load lift distribution, providing input to the FEA tool. A parametric study would then enable an efficient design to be found. This PhD takes an alternative approach by fixing parameters like taper ratio and sweep and altering other variables that have a larger impact on fuel-burn. This has been primarily done as when comparing propulsion systems the impact of these variables on performance becomes more important and due to time constraints a more rapid and versatile approach was needed.

Cranfield University worked with the Rolls-Royce Strategic Research Centre (SRC) to investigate a number of future civil aircraft concepts based on the Vision 20 initiative. The results are contained within sections 5.1 and 5.2.This initiative set out to evaluate advanced aircraft concepts aimed to exist 20 years from now; focusing

on the 2030 timeframe. The future concepts were to be compared with present day reference aircraft, enabling the quantification of the benefits and risks to current technology. The vehicle specification was a transport aircraft having an 8000nm range with a payload of 350 passengers and a cruise Mach number of 0.85. A variety of concepts were evaluated in a workshop held at Cranfield University and were short-listed to advanced T&W and BWB aircraft, both with and without electrical DP and BLI. The baseline T&W aircraft was set to be similar to an Airbus 350 and the baseline BWB was equipped with the same advanced turbofan engine technology as the advanced T&W carries.

In order to the model both the aircraft and engines, the appropriate tools were first selected. Cranfield University's engine performance tool Turbomatch is capable of modelling gas turbine engines and provides an in-house solution to the engine modelling requirements. It is also written in the Fortran language which facilitates the rapid integration with other Cranfield University tools. However for the Vision 20 project, it was decided that Rolls-Royce would take the engine modelling using their in-house code 'BD36'. Therefore, there would be an iterative process between the Rolls-Royce's engine modelling and Cranfield University's aircraft modelling. Since, Rolls-Royce were unable to provide Cranfield with BD36 for further study, Turbomatch was used for the parametric studies.

Cranfield University's aircraft performance tool Hermes was assessed to check whether its capability was sufficient for aircraft design purposes. It was concluded that the tool doesn't easily enable the aircraft design syntheses, since it is only a performance tool and doesn't enable the resizing and redesign of the wing as the engine performance, flight profile and aircraft weights change. Instead it requires the geometry and weights to be specified in advance. Although it too is written in Fortran and could be manipulated to provide a design tool. However, the level of manipulation and the lack of experience the author held with the code internals rendered the process of editing inefficient. Additionally, the tool cannot model BWB aircraft. Therefore, it was decided to only utilise Hermes as a method for validation by checking the performance of the baseline T&W aircraft.

By creating an aircraft conceptual design tool from scratch using a 'bottom-up' approach, the framework could be customised to allow an effective integration with the engine code. Also, the theory would be primarily based upon analytical formulae, enabling novel designs to be accurately modelled when empirical relations are not reliable. A number of author's aircraft design theories were examined and specific design processes were extracted from each method, ensuring each process was kept consistent with each author's method to avoid the use of incompatible assumptions. The selected aircraft were then modelled and compared using the adopted technology assumptions and predictions.

The next stage of the PhD was to use the knowledge and experience obtained from the Vision 20 studies to assess the wider design space of DP through a parametric investigation. This results of this research is contained with sections 5.3 and 5.4. Rolls-Royce developed a spreadsheet tool for assessing the DP electrical system weight. They produced the electrical system calculations for the Vision 20 study. The tool was subsequently supplied to Cranfield and the author then used it for the parametric studies. The Cranfield in-house performance tool Turbomatch replaced BD-36 and a DP fan methodology was developed by the author. A mathematical derivation was developed by the author to enable accurate BLI modelling. A methodology for scaling the propulsion system weights was developed by the author and a spreadsheet was created. Collectively these tools enabled a parametric assessment of the whole propulsion system to be carried out.

Because of the inherent difficulties in modelling BWB aircraft, T&W and BWB configurations have not been compared explicitly. This is because the BWB mass estimation is based on a very different method which is not fully validated as currently BWB aircraft only exist in concept form. Also, the assumptions made for the T&W and BWB aircraft differ due to the level of information available within the public domain. However, the PhD aims to investigate the potential for DP as a propulsion system choice for future aircraft and therefore the quest is to explicitly compare DP with turbofan engine technology.

The final stage of the PhD work was to devise and evaluate a novel flow control concept that utilises the magnetoplasmadynamic technology. This work is located in Appendix A. This contribution is separate from the main PhD contribution and serves to explore the different technologies that may be synergistic with DP. The feasibility of the concept has been assessed on an initial basis and future recommendations are given.

3 Literature Review

3.1 Current market activity

In 2008 National Aeronautics and Space Administration (NASA) awarded $12.4m to six industrial groups to progress subsonic and supersonic commercial transport aircraft [1]. The agenda was to significantly improve the performance of civil aircraft whilst superseding the environmental targets set by government bodies. The research and development targets are grouped using the notation n+i, where ‘n’ represents current technology and ‘i’ the number of generations ahead of current technology. The n+3 period denotes three generations ahead of current technology and is the basis for most of the funding. Therefore, radical changes are expected in the proposed aircraft and propulsion system concepts in order to produce substantial breakthroughs in the next 25 to 30 years.

The funding is designated to six teams: Northrop Grumman, Boeing, MIT, Lockheed Martin, GE and Boeing. Each team has delegated some of its funding to a number of other organisations, giving some insight into the scale of this research agenda [2].

NASA imposes strict targets including an 80 decibel noise reduction below current levels with the ability to land in smaller airports, both of which would facilitate take-off and landings closer to urban locations. Other targets include an 80%+ Oxides of Nitrogen (NOx) reduction below the Committee on Aviation Environmental Protection 2 (CAEP2) level and a 70% improvement in fuel-burn relative to today’s aircraft; reducing costs for airliners and consumers [1].

General Electric (GE) aviation is working in collaboration with NASA on one of the n+3 projects known as “Small Commercial Efficient & Quiet Air Transportation for 2030-2035” and focuses on the 10-30 passenger size aircraft. A reduced environmental impact is achieved through improvements in airframe and propulsion system overall efficiencies. A key benefit to having smaller more efficient aircraft and implementing multiple smaller airports dispersed throughout communities is the reduction in congestion relative to larger airports. By having localised airports the environmental impact would be spread over a larger area; reducing local

disturbances. Another benefit is found through the increase in local economy where the number of jobs rises [2].

Airbus opposes the development of smaller airports by arguing the cost of developing new airports considerably outweighs the development costs to expand current airports to facilitate larger aircraft [3]. Therefore, it seems that the larger aircraft performance enhancements and airport infrastructure cost savings would need to justify the congestion increase effects.

For a given periodic seating capacity, a larger aircraft has a lower flight frequency which results in less airport noise. A reduction in aircraft movements can also reduce airport and flying delays, including runway congestion, and hence reduces the overall flight time. Consequently Local Air Pollution (LAP) and climate change impacts decrease. Airbus predicts that by 2025 short-haul flights will reach 35% in terms of the world's airliners Revenue Passenger Kilometres (RPK), which translates to 75% of the world's aircraft movement number [4]. It can then be concluded that if small and large aircraft emission reductions evolve at the same rate and worldwide/local concerns with aviation transport increase, smaller airplanes will become more favourable in terms of LAP and larger airplanes with a lower frequency will become favoured for climate change and noise.

It is predicted that wide-body aircraft on short haul journeys would reduce the negative emissions effects, in particular for larger airports, and utilise the limited runway space more effectively [5]. Currently airports use small aircraft for short flights, so this viewpoint does not appear to have been supported by the industry at present. However, as airport congestion becomes more expensive, this solution may become justified. More advanced aircraft such as the BWB aircraft may become available in the future and may be more suitable for short flights, through the ability to take-off and land over shorter distances. Still though, during the next decade the question remains whether current wide-body models, such as the Boeing 787 or the Airbus A350, could be used or adapted for shorter trajectories i.e. less than an 8000nm mission.

GE proposed two propulsion systems for the n+2 aircraft; the open rotor and the conventional ducted fan. The GE36 open rotor was originally designed and tested

within a NASA partnership during the 1980's and demonstrated significant fuel savings, gaining worldwide recognition. Unfortunately, the design was neglected due to the excessive noise created by the fan blades and the sharp fall in oil prices during the late 1980's. Now GE plans to revisit the open rotor and enhance its benefits by utilising the technology and knowledge developed over the years. The key research themes are composite materials and contra-rotating rotor technology, and will be developed using better computational tools and data acquisition systems [6].

In competition, Rolls Royce is currently enhancing open rotor technology through partnerships with various universities and airframe manufacturers, with a matching goal to reduce fuel consumption and noise. They predict a 10-15% reduction in both CO2 emissions and fuel consumption relative to equivalent turbofan technology is possible [7]. These improved values represent a goal for the next decade and provide an improvement to T&W aircraft configurations.

Pratt and Whitney (P&W) have taken another approach to near future technology enhancements and have invested heavily into the geared turbofan engine. This engine incorporates a planetary gear that is situated between the fan and an intermediate pressure compressor (IPC), which replaces the inefficient booster. The IPC rotates at a different speed to the fan without the need of a third shaft. P&W's vice president Bob Saia describes how they feel the open rotor's inherent noise problem may never be properly remedied [8], which describes why P&W decided to pursue the geared turbofan design. Instead P&W are developing the Pure Power PW1000G geared turbofan which boasts fuel savings of 12-15% relative to current turbofans. In addition, it is likely to have significantly reduced noise over turboprop configurations, at 20 less decibels than the most stringent standard. Also P&W estimate the engine produces 50% less NOx emissions than the limits set by the CAEP6 level. The reduction in fuel-burn over successive years would be small, since the configuration is not that dissimilar from today's turbofan engines, although it may be comparable to turboprop engine technology, which would provide a short term solution. The engine class ranges from 15-30,000lbf and are expected to launch from between 2013 to 2016 [8].

MTU Aero Engines Germany has examined a potential novel engine that combines a geared turbofan with inter-cooling/recuperation. This is likely to benefit from significant improvements in specific fuel consumption (SFC) and emissions reductions. An inter-cooler is used to cool the air between the IP and high pressure (HP) compressors, which reduces the power requirement for a fixed compression ratio. This increases the specific power output of the engine because per unit mass flow more heat can be added for the same turbine entry temperature (TET). However, the thermal efficiency diminishes as the extra fuel-flow requirement offsets the additional expansion power output achieved, which therefore increases SFC relative to a non-intercooled engine. Because of this, it is common to incorporate a heat exchanger (HX) to utilise the high temperature turbine exit gases. This is done by preheating the air exiting the HP compressor by absorbing heat from the turbine exit gases in a heat exchanger. This then reduces the fuel flow requirement since the exhaust gases from the heat exchanger with be lower in temperature than the case without a heat exchanger. This leads to an increase in thermal efficiency and a reduction in SFC relative to an intercooled engine [9]. The combined effect of both components provides high core efficiency at lower overall pressure ratios (OPR), which reduces weight and decreases NOx emissions. The intercooler compliments the HX through enabling effective heat exchange at higher TET's. This could be ideal for small aircraft that operate at high TET during take-off when the heat recovery would be high. For longer flights the heat recovery benefits would be offset by the additional energy required to transport the heat exchanger weight. This is because the cruise segment dominates long range missions, where the TET is around 300-400K less than the corresponding take-off condition. However, by changing the inlet guide vane nozzle area for each operating condition, the HP turbine inlet temperature can be kept consistently high [10].

Another advantage of this flat temperature profile is that component thermal fatigue is reduced; enhancing component life, although a creep effect is inevitable given the high operating temperatures. The sum weight of the heat exchanger, flat plate cooler, piping and nozzle system is considerable but leaves room for improvements and the decreased OPR allows the removal of some turbo-machinery stages and thus a reduction in compressor weight. The engine's low OPR and high TET reduces

the core mass flow, resulting in an increased bypass ratio for the same fan diameter. Consequently, the flight speed is limited as the bypass stream jet velocity reduces for a given overall thrust and so the engine becomes used for lower speed applications. MTU Germany predicts SFC savings of 8% over a 2015 geared turbofan engine and 60% lower NOx than the ICAO-96 limit, reaching an 80% NOx reduction through the adoption of novel combustor technologies [10].

One of the most predominant future aircraft concepts that has been heavily invested in by NASA is the novel fixed wing subsonic aircraft for operation during the n+3 era. The baseline designs consist of DP, generally defined as having more than four propulsors, fuelled by liquid natural gas, providing slower aircraft where current technology cannot operate efficiently. NASA has issued the criteria of a 70% fuel-burn reduction and a 75% reduction in NOx emissions. Another target was to enable shorter runway take-off's, which would facilitate access to smaller airports in urban locations. According to MIT's Aero-Astro faculty principle investigator Ed Geitzer, radical changes in airframe and propulsion systems are imminent for the success in meeting future performance targets. The conventional fuselage and protruding wings that has been previously used in many successful designs are now exhausted of any major advancement. Thus unique airframe and engine integration, and geometrical configurations are to be adopted in order to 'break the barrier' [1].

As a response to NASA's requirements, two radical concepts were created for the 180 and 350 passenger size aircraft, replacing the Boeing 737 and 777 classes respectively. The D-Series aircraft (left side of figure 3.1) replaces the Boeing 737 and features a fuselage that comprises two cylindrical sections joined in parallel with a flat top and bottom to provide a smooth transition. The propulsion system incorporates the BLI technology, which increases the aircraft's propulsive efficiency through the ingestion of the aircraft wake's low momentum air. This can be implemented by mounting propulsors centrally in line with the airframe surface to re-energise flow that was slowed by the frictional surface drag (a theoretical explanation of the BLI benefits can be found in Chapter 4 Section 5). However, BLI carries its own disadvantages, such as engine integration difficulties and rotor stressing; both of which could offset the potential benefit. Even so, the wider fuselage in the D-

Series could reduce airport loading times, corresponding to a decrease in airport congestion [1].

Figure 3.1 - NASA's D-Series (left) and H-Series (right) aircraft designs[2]

As the emerging markets around the globe demand slower and cheaper air travel, the D-series could provide an ideal solution. NASA has made many small changes to each aspect of a regular T&W aircraft to result in a large effect that enhances the performance considerably. The director of Federal Aviation Office of Environment and Energy, Carl Burleson, stated that the D-series would require less change to current airport infrastructure due to the relatively similar 'double bubble' fuselage design to conventional designs. He quotes "For some other designs, you could have to fundamentally reshape the gates at airports because the planes are configured so differently" [1].

The H-Series (right side of Figure 3.1) features a BWB design, which has similar aesthetics to swept wing, flying wing and delta wing configurations. However, unlike its military counterparts, the fuselage contains a cabin pressure differential and stores a large payload of passengers or cargo [11]. The next section elaborates further into the BWB design and its synergistic technologies.

3.2 Distributed Propulsion concepts

NASA predicts that the combination of a BWB configuration and DP system produces a 70-72% fuel-burn reduction relative to a B777-200LR reference aircraft

[12]. NASA's quoted fuel savings figures arise from its N3-X concept, where 18-20% of the benefit is attributed to the DP system. A study by C. Lui [13] simulates the N3-X concept using a different methodology and manages to meet similar performance goals, which helps underwrite these significant benefit predictions.

A study has been conducted to investigate the overall performance benefit of DP and BLI technologies at an aircraft level. By analysing previous BWB and DP studies it was possible to select an appropriate aircraft class and develop a novel aircraft and propulsion system.

Both the SAI SAX-29 and its successor, the SAX-40, included three gas generators located above the fuselage mechanically powering nine fans that were semi-buried within the wing to enable BLI [14]. However, the current study focuses on maximising fuel efficiency, therefore there may be potential in locating the gas generators under-wing to provide wing bending relief and enabling reduced wing structural mass.

By decreasing the number of engines from three to two, the maximum thrust per engine requirement would increase due to the required total aircraft thrust during an engine failure. According to [12] this would have implications on the engine design such that noise would increase. However, because the climb-ceiling thrust requirement may already be more severe than that of take-off due to the inherent high BWB cruise altitude and also maintenance costs and core losses would be lower for a twin-engine case. Therefore a two gas generator case is considered in this study.

The SAX-40 favours short distances between the generator and propulsors due to the mechanical transmission system [14]. However, it may be more beneficial to use NASA's approach where superconductive electrical transmission is adopted, due to the large distances between the fans and under-wing engines. The SAX-40 also restricts the fan diameters to increase the length-to-diameter ratio to enable high noise attenuation [4], however, a more fuel efficient method could be to power an array of BLI fans by high engine bypass ratio (eBPR) under-wing turbofans. The TS could then be optimised. In addition, the turbofan diameter would not be restricted or affected by the boundary layer total pressure distortion and aircraft integration issues.

NASA uses turbo-generators to transmit nearly 100% power to the DP fans [12]. But because the electrical system must be sized at the most power demanding condition i.e. at EoR take-off, the study adopts a combination of turbofans and DP fans to help reduce the electrical system weight. A TS of 40% was chosen for the cruise stage but this reduced to 20% at take-off. The climb TS was varied so that the transmitted electrical power remained constant, to best utilise the capability of the electric system.

Ameyugo [15] examines the effectiveness of distributing small gas-turbines along an aircraft span to increase propulsive and airframe structural efficiency. However, the thermal efficiency is reported to be poor for smaller engines due to scaling effects, so the electrical distribution of power to motorised fans may provide a more efficient solution to enable DP. In addition, Lui [13] reports that overall system weight reduces with increasing number of motorised fans, in contrast with Ameyugo's [15] predicted increasing weight for small gas turbines, which get heavier due to their auxiliary systems and non-scalable parts (which will still be present with electric power transmission but to a reduced extent). The success of the concept however, hinges on the superconducting machines power density capabilities, which currently are below the required level [16] and therefore the concept is targeted for a 2035 timeframe. The aircraft may be specifically designed to efficiently carry the extra electrical system associated mass, therefore stressing the highly integrated nature of the DP technology.

Two methods of cooling the superconducting electrical systems exist: cryogenic cooling and cooling with liquid hydrogen. Liquid hydrogen and its required tanks are a lighter option than cryo-coolers, and the hydrogen can be utilised as a fuel after providing cooling. The hydrogen reduces the kerosene required and is lighter by a factor of 2.8, according to a Cranfield University study [17], but the volume is approximately 4 times that of kerosene, increasing fuel tank and airframe weight. The BWB airframe is relatively spacious and more suited to the large volumes required by liquid hydrogen than a conventional aircraft, therefore liquid hydrogen is also considered in this study. Safety issues have not been considered in this study, except that the storage tank must be sized to contain the hydrogen safety through

the relevant gravimetric efficiency which describes the tank weight as a function of hydrogen weight.

At a passenger density similar to conventional aircraft of 1.4 passengers/m^2, the N3-X and SAX-40 aircraft can carry 335 passengers [18]. Other studies assess BWB aircraft of much larger capacities. The Very Efficient Large Aircraft (VELA) developed by Airbus, features four under-wing turbofans and a 750 PAX [19]. However, NASA and McDonnell Douglas have investigated a number of different sized BWB designs and conclude that a payload of 800 is beyond market forecast data and cannot be accurately compared to conventional aircraft [20]. Instead, NASA developed a 450 PAX BWB and the BLI system was replaced by three above-fuselage turbofans in order to mitigate risk.

Larger capacity airframes benefit from the square-cube law, as surface area increases less than volume, thus increasing aerodynamic efficiency [20]. However, all sizes of aircraft may benefit from drag reduction through the inclusion of a BLI system. Therefore long range, medium-sized airliners show potential.

3.3 Wider-design space studies

At present, a parametric study that investigates the wide design space of DP does not exist within the public domain. NASA's N3-X Blended BWB aircraft features 15 electrically distributed BLI fans situated on the aircraft upper surface, as seen in figure 3.2. It is predicted that a fuel-burn reduction of over 70% is possible through this configuration [12]. However, larger benefits may be achievable through comparing different propulsion configurations and evaluating a larger number of parameters.

NASA elected to distribute most of the gas turbine power to the fans, as it enabled the flexibility of positioning the turbo-generator anywhere on the vehicle and provided efficiency gains from the infinitely variable transmission ratio [12]. However, other possibilities exist, such as replacing the turbo-generator with a turbofan with power off-take and optimising the overall bypass ratio (BPR) for installed efficiency. Through this, significant fuel-burn, drag and mass benefits may be achievable. In addition, more degrees of freedom may exist, such as providing thrust during

electrical system failure scenarios. Also, under-wing podded turbofans are a conventional design and therefore adopting them into the system reduces the risk for the DP technology's entrance into the civil aviation market.

Figure 3.2 - NASA N3-X BWB with DP[12]

The N3-X study uses an iterative method of calculating the fan size and number. Because the DP fan pressure ratio (FPR) is fixed, a mass flow is required to generate a specified net thrust. The array width is fixed from aircraft geometry, whilst the fan height is iterated and checked by comparing the required mass flow with the mass flow equated from average boundary layer Mach number and density values obtained from CFD [12]. Therefore by fixing the DP FPR, the specific thrust may only be altered by changing fan number which affects the average inlet properties. In addition, large mass flows require smaller numbers of fans, as this increases intake height. The current study relieves these constraints to explore the benefits achievable through altering DP FPR whilst keeping a large number of fans and large mass flows for added propulsive efficiency. This study also investigates the benefit of ingesting free-stream air in addition to boundary layer air.

NASA recognises that at the cruise condition, decreasing FPR and thus increasing mass flow is beneficial in terms of propulsive efficiency. However, an optimum in SFC is found as when FPR is decreased the boundary layer total pressure loss becomes a larger fraction of the propulsor pressure rise fraction [21]. Another way to view this is that the larger mass flow, employed to sustain constant thrust when FPR

is decreased, multiplies the effect of the boundary layer pressure loss. However, for a fixed boundary layer mass flow, additional mass flow is sourced from the free-stream, which contains no total pressure loss. For the aerofoils investigated in the current study, the boundary layer mass flow was not large enough to exceed the optimum value in terms of fan power requirement. However, inlet DP fan duct total pressure losses must be accounted for when ducting an effective square boundary layer profile to a circular cross-section, as shown in figure 3.3. This restricts the propulsive efficiency gains offered by reducing FPR. NASA also mentions that podded non-BLI fans increase external drag through a diameter increase associated with lower FPR [21]. Therefore, the present study provides an assessment of these maximum efficiencies for varying FPR and compares installed performances. In addition, the turbofan eBPR has been varied to assess the effect of the change in FPR on overall installed efficiency.

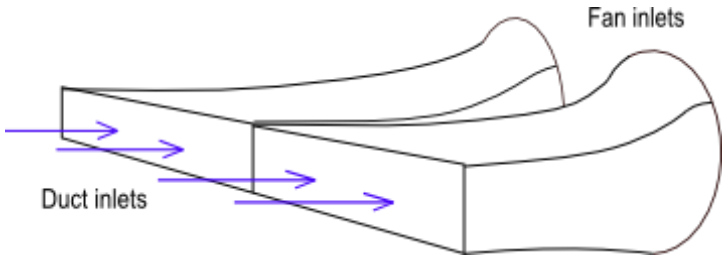

Figure 3.3 - DP fan inlet duct form

The Silent Aircraft Initiative developed the SAX-40 with the principal aim of reducing background noise whilst ensuring an economically competitive and reliable design. The concept consists of three partially embedded gas turbines generators mechanically driving nine BLI fans figure 3.4 displays the discrete units that ingest part of the aircraft upper surface boundary layer. Smaller fans are favoured as the ability to attenuate noise is greater and the close proximity of fans provides an efficient and reliable mechanical arrangement [22]. However, by incorporating electrical transmission, such as in the N3-X [12], and derestricting the fan and engine size, fuel-burn reductions may be traded with noise.

Figure 3.4 - SAI SAX-40 distributed propulsors[22]

A comparison of propulsors that do not ingest boundary layer to BLI propulsors is useful as this helps determine the relative benefits of the two technologies. G.Ameyugo has conducted a study on distributed gas turbines and explains that in theory smaller engines should be lighter due to the square-cube law (area-volume relationship). However, from viewing figure 3.5, this trend is seen to reverse due to non-scalable parts and an inability to use small-scale weight saving technologies [15]. Electrical fans may be scaled down more efficiently as they do not contain core engine components, although the weight of components such as housing and electrical wiring would not decrease significantly.

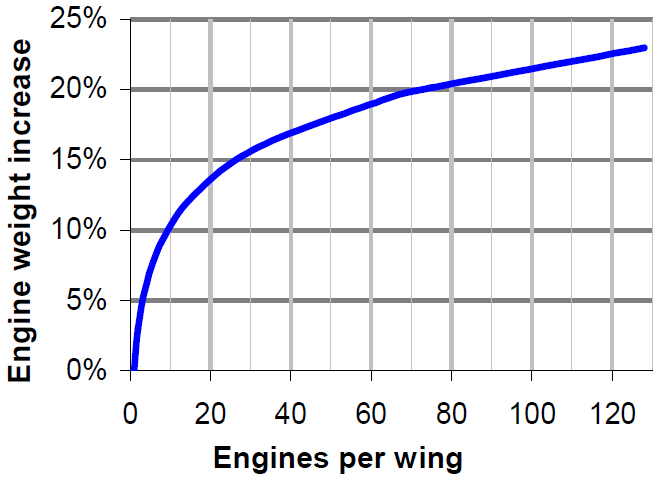

Figure 3.5 - Distributed gas turbine weight analysis[15]

Electric motor torque scales with volume and therefore with mass [4], whilst rotational speed is inversely proportional to torque for fixed power. Therefore large

rotational speeds are desirable for low mass, although small fans suffer from thermal efficiency losses due to Reynolds number effects and relative tip clearance losses. This study evaluates all fan diameters by fixing fan number and optimising mass flow, although diameters above 0.5 metres are considered realistic, in accordance with Rolls-Royce fan loss data.

A.Gohardani [23] discusses the sensitivities of the electrical system, namely the considerable motor/generator weight associated with large numbers of fans, due to the low specific torque associated with small motors. In addition, the location of the core engines affects the cabling weight. For example rear-fuselage mounted engines on a T&W aircraft with DP fans located on the wing would incur a significant cabling weight penalty. Therefore, the optimum fan configurations are expected to be highly dependent on the electrical system capabilities.

Fan nacelle surface area depends on the product of nacelle length and diameter. As nacelle length is generally assumed to be linearly proportional to nacelle diameter, surface area is then proportional to diameter squared. Since thrust is proportional to diameter squared also, engine number should not affect skin-friction drag, if fan specific thrust and mass flow remain constant. However G.Ameyugo correlates engine nacelle length with the 0.9^{th} power of diameter [15], which increases drag with fan number as shown in figure 3.6. Because electric fans are powered by motors alone and may be less affected by non-scalable equipment effects, the change in this power law is unlikely to exist. Therefore, nacelle skin-friction drag is assumed to be only affected by motor sizing and not nacelle number.

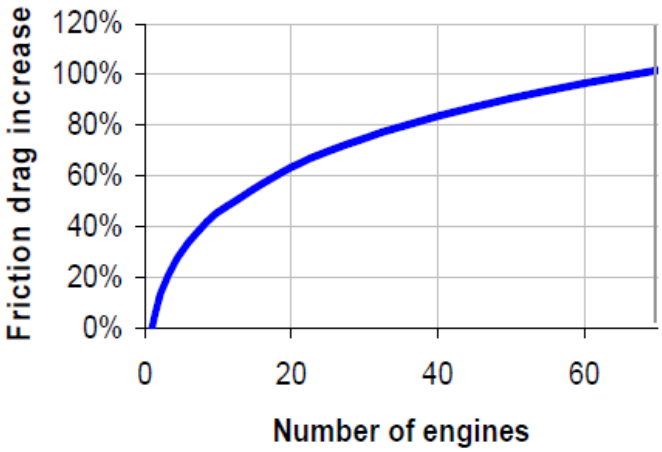

Figure 3.6 - Distributed gas turbine skin-friction drag analysis[15]

3.4 **The BWB aircraft**

The BWB utilises a variety of benefits over conventional T&W configurations, such as the aerofoil shaped fuselage that serves to increase induced lift though the vortex build up around the triangular fuselage edge. This coupled with the low aspect ratio fuselage, pushes the centre of lift further forward in comparison to T&W configurations; reducing the horizontal stabiliser load requirements and removing the need for a tail. The BWB caters for the tail stability and pitch functions using a set of elevons, located along either/both the fuselage and wing's trailing edge (TE). The stability and yaw functions of the fin are provided by rudders which replace the winglets at the wing tips [24].

The BWB also benefits from a reduced wetted area relative to a T&W configuration, decreasing skin friction drag, and a blended wing/fuselage that greatly reduces interference drag associated with the rapid change in profile shape. Collectively, this produces a higher ratio of lift to drag, which reduces fuel-burn.

Another key benefit of the BWB is its large centre-body that facilitates the use of a variety of propulsion systems and fuel types. Because of the many airframe and engine benefits that the BWB provides, NASA states that the H-series has already met its performance targets and they now plan to improve the designs further [1].The NASA N3-X is one of NASA's latest concepts and incorporates DP and BLI [12]. In this context, DP is achieved through using gas turbine engines to electrically power

an array of distributed motors that are connected to fans. The fans are mostly embedded and are therefore able to take advantage of the BLI benefits.

3.5 The BLI technology

BLI concepts favour distributing many propuslors along the span of an aircraft as this configuration ingests the most boundary layer. As the propulsors are positioned on an airframe surface, it becomes difficult to treat the forces associated with the airframe and propulsors separately. To remedy this, a control-volume can be placed around both the propulsor and airframe, and the momentum deltas can be summed to find the net propulsive force [25]. Chapter 4 Section 5.1 expands further on the subject of BLI modelling.

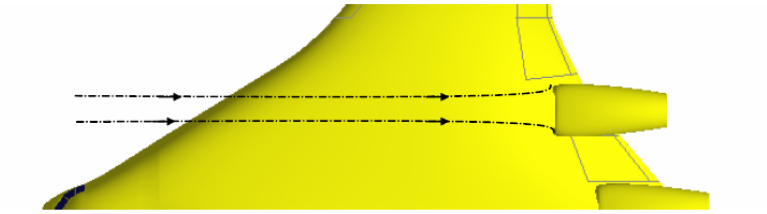

Figure 3.7 - Mass flow ratio upstream to highlight[14]

It is difficult to predict how much of the wing area the ingested flow 'scrubs' prior to entering the propulsor. This is important as it enables the correct boundary layer growth to be equated and an accurate prediction of the drag associated with the rest of the aircraft. Figure 3.7 illustrates the stream tube affect, where the flow area evolves as it nears the propulsor. During cruise flight, the flow is typically diffused at the propulsor inlet. This occurs because for a given inlet area, the high flight velocity provides more mass flow than the fan can ingest, for a given air density. Therefore the flow velocity is reduced and a pre-compression zone develops. The inlet is design like this firstly to reduce the flow Mach number and minimise the total pressure losses due to friction; secondly, the pre-compression reduces the fan or compressor pressure ratio requirement and therefore decreases turbomachinery weight. The ratio of upstream to inlet plane mass flow is termed the mass flow ratio [11]. At take-off the reverse effect happens and the inlet velocity requirement exceeds the flow speed and therefore air is pulled from around the nacelle,

increasing the effective upstream stream-tube area. By assuming the mass flow ratio equals one, the problem can be greatly simplified. This is because the length and size of the pre compression zone doesn't need to be calculated. The propulsor inelt area then defines the aircraft surface area that corresponds to propulsor ingested flow and the rest belongs to the aircraft drag. However, this would only permit the analysis of one stage of flight under ideal conditions.

In the case of having separately cased propulsors above the wing, the flow rapidly decelerates as it reaches the propulsor highlight zone due to the upstream diffusion taking place, resulting in a loss of aircraft lift. However, it is predicted that the lift generated by the flow acceleration around the curved nacelles is more than enough to counteract the diffusion losses and results in a net lift increase [11].

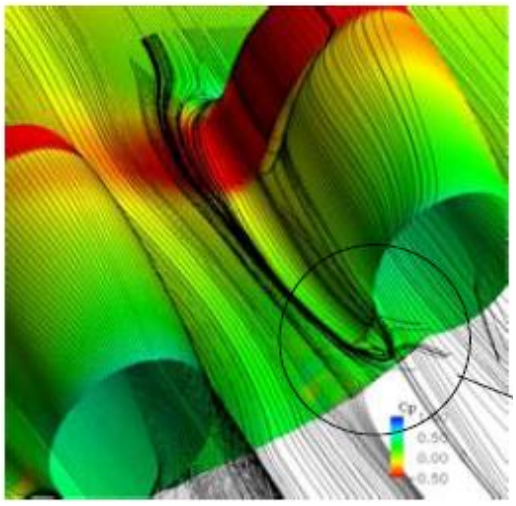

Figure 3.8 - Above wing propulsor CFD model[11]

Figure 3.8 shows an image that displays the coefficient of pressure for flow past individually cased the nacelles [11]. It shows that sufficient gaps must be left between the casings in order to reduce the shock wave occurrences at high subsonic cruise Mach numbers. This can be seen by the darker shading relating to high coefficient of pressure (CP) values that represent the shockwave or flow compression located parallel to the inlet plane. If the nacelles were further apart then the wave drag would be smaller at the location on the aircraft surface between the nacelles and vice-versa. The lines in the flow direction show the streamlines and the

closer together the lines the grater the pressure gradient and therefore a greater boundary layer build up. By packing the fans tightly together to optimise on space and adopting common nacelle housing, the BLI benefits could be augmented further relative to the separate casing configuration. Although, the lift generated by the flow acceleration would decrease, the extra number of units would increase the overall BLI effect and offset the aerodynamic detriment. This would also benefit from a reduced nacelle wetted surface area, decreasing the skin-friction drag.

The boundary layer presents distorted flow to a fan's rotor. Additionally, flow degradation exists when the free stream and boundary layer mix at the nacelle inlet. This non-uniform flow at the fan inlet is detrimental to fan efficiency and can offset any potential benefits. Active Flow Control (AFC) has been investigated as a means of energising the flow to reduce the non-uniformity. This is done by moving the fluid in such a way as to produce a more uniform profile around the circumference of the fan. For example the boundary layer velocity varies away from the surface, however a single point on the fan sweeps all the way through this and sees a varying flow velocity regardless of fan design, causing efficiency loss. If the boundary layer was curved in some way then the point on the fan would see a smaller change in velocity through blade twist design could be optimised for the smaller variation in flow velocity. A study from [26] found that without the inclusion of AFC, the net benefit of BLI would amount to a reduction in fuel-burn of only 0.4% relative to a turbofan engine. By including AFC, the fuel-burn was expected to reduce by 5.5%, although this value did not account for AFC power requirements. From the author's knowledge, a 5.5% benefit sounds realistic. However, from a discussion with Rolls-Royce [27] which relates to the experimental results obtained from BLI fan rig tests at Cambridge University, the distortion penalty of 5.1% seems far too high and it should be possible to redesign a fan so that it incurs a penalty of around 1-2%.

The next section of the literature review is based on noise implications and the technologies associated with reducing it, primarily because the BWB and DP concepts potentially offer considerable benefits in this area.

3.6 **Noise**

From the jet engine's inception of the skies it was generally an object of curiosity rather than a nuisance, due to the limited number that existed relative to piston engines. They were particularly noisy due to the low BPR's that produce high jet velocities and as they became increasingly popular due to their speed of travel, noise has become largely an issue that is being restricted legislatively. Because the jet velocity has been reduced to almost flight speed, further improvements in propulsive efficiency are becoming small and the returns in noise reduction are diminishing [28]. Current engine duct linings decrease take-off and landing noise more effectively as the fan produces predominantly high frequency noise emanating through the intake and exhaust. These are present in most current civil aircraft engines and in order to meet the future targets, other methods must be sought [29].

The interaction between the engine and the non-uniform inlet flow from BLI is an additional engine noise source, where this "distortion noise" tends to be broadband in nature. Similar distortion noise is observed in engines that operate with separated intake flow. There is limited data available on distortion noise, and in the case of a BLI engine the propagation of the noise will be strongly influenced by the installation duct and location on the airframe [30]. Although the magnitude of the distortion noise might be important for a "Silent Aircraft", it may not be for a design in which noise is not the principal objective [5]. This could be the case if fuel-burn was the priority for economic and environmental reasons.

Both engine redesign and modification can reduce noise emissions, although generally a penalty ensues. Redesign includes altering the guide vane number and separation, and blowing bleed air to correct wake velocities. Using a flexible walled intake effectively reduces inlet noise radiation through accelerating the flow to such an amount that the outlet acoustic energy transfer is almost eliminated, although this is a complex design change. Using absorbing linings is a method that requires the least amount of redesign and can be positioned in otherwise difficult areas, such as intakes, outlet splitters and mixing ducts. There are two types of linings: a porous material lining known as an 'absorber' that attenuates a large range of noise, but doesn't respond effectively to large amplitudes; and a 'resonator' that consists of a

honeycomb arrangement of perforated material which attenuates a thin frequency band, but is effective for larger amplitudes. Both the linings have contrasting benefits, and when combined provide an effective solution [30].

Engine positioning is key for both noise and fuel-burn reductions. The BWB promotes the use of noise shielding through possessing a large fuselage area. For above-fuselage located engines, the forward-radiated engine fan noise is shielded by the centre-body and the engine exhaust noise is prevented from reflecting downwards by the lower surface of the wing [24]. It is possible to reduce noise further by increasing aircraft fuselage area. However, doing this for noise purposes alone becomes questionable, as the increased airframe weight and thus engine power requirement would add an additional noise increment that may exceed the noise that was blocked by the airframe. Additionally, aircraft and engine performance would degrade substantially [28]. Rather than increasing wing area, the aspect ratio of the fuselage and wing could be reduced to provide better noise blocking characteristics, accepting a small reduction in lift to drag ratio.

The effect of positioning an engine above-fuselage has been investigated through simple experiments, such as coupling a plate and source amongst a moving fluid to measure noise diffraction. One study concluded that the optimum engine position was central to the plate or fuselage, and that the fuselage TE wake acted as a shield. The wake diffraction effectiveness was dependant on jet velocity, and take-off and landings were found to provide less diffraction relative to cruise, due to the lower wake Mach numbers [31]. Also, it may only be effective to locate the engines at the centre chord of a wing or fuselage when using podded propusors. This is because otherwise the distorted flow associated with BLI propulsors is likely to cause aft-chord wing degradation due to the flow’s unsteadiness; incurring maintenance issues. Additionally, the amount of BLI would be dramatically reduced, as ideally the propulsors should be located at the wing TE to maximise BLI.

A typical BWB design does not tend to possess slotted TE flaps, since its large effective wing lifting surface doesn’t require the extra high-lift devices that a conventional aircraft configuration may require. Therefore a major source of airframe noise is eliminated. Furthermore, the use of TE flaps can be eliminated by obtaining

high lift and longitudinal control through the use of DP and deflection of the TE jet [12]. Since the BWB has lower total installed thrust and lower fuel-burn due to inherent airframe design benefits relative to conventional designs, an equivalent reduction in engine emissions is possible for the same engine technology. So, it seems that the BWB offers a significant reduction in noise without including any specific acoustic treatment.

The next section briefly discusses some of the key merits and drawbacks of placing engines in different locations, although this is also partly relevant to propulsors of any kind. The aim of this review is to highlight the key effects of propulsor placement so that the integrated aircraft and propulsion system design effects are modelled pragmatically.

3.7 **Propulsor placement**

3.7.1 Above-wing mounted engines

NASA has proposed a novel aircraft design known as the Cruise Efficient, Short Take-off and Landing (CESTROL) subsonic aircraft, which incorporates the engine above-wing concept that has previously been used in the 1979 Russian An-72 cargo transport. The configuration utilises the engines position to assist take-off through 'powered-lift', whereby the engine can rotate to blow air over the wing upper surface and use the Coanda effect to augment lift. Georgia Tech Research Institute (GTRI) engineer Robert Englar explains that 'powered-lift' provides the lift that wouldn't usually be available given the low velocities permitted on such runways [32, 33]. As a consequence the engine positioning provides high frequency noise reductions.

NASA's CESTROL is targeted for the n+2 time period (year 2020) and is an example of an advanced aircraft concept that retains the T&W airframe geometry, as can be seen in figure 3.9. The above-wing engine configuration has other advantages; namely Foreign Object Damage (FOD) reduction, as its position reduces the suction effect [34].

Figure 3.9 - NASA's CESTROL aircraft concept[32]

3.7.2 Aft-fuselage mounted engines

Engines mounted on the rear of the fuselage are commonly used in business jet aircraft because of the limited ground clearance that small aircraft possess [35]. However, the long fuselage surface that incurs large drag penalties makes the aft-fuselage an attractive place to position BLI propulsors. Therefore, it is important to identify some of the affects this positioning has on the aircraft. The horizontal tail could enter stall through the incoming flow disturbances created by the engine exhaust, therefore either a larger tail that protrudes out from the wake or a T-tail configuration would need to be employed. Both of these configurations incur weight penalties, such as thickening the vertical fin to sufficiently act as a support structure for the T-tail, which partly offsets the BLI benefits.

Because of the height of the engines, the thrust would create a rotation about the aircraft's centre of gravity. Depending on the position of the aircraft weights and the stabilising control surfaces, the tail size may need to be increased or decreased. Therefore, it becomes important to perform a static stability analysis in order to determine whether the aircraft is stable and to predict the empennage size requirement. Cabin noise would decrease by locating the engines towards the rear. However, this configuration is disadvantaged as access for maintenance becomes more challenging [35].

The wing is essentially a cantilever beam with an airload acting as a distributed force along its span and wing podded engines acting as effective point loads that provide a

bending moment relief [36]. By removing these effective point loads, the wing root must thicken to support the resulting moment; ensuring an overall mass increase.

3.7.3 Wing embedded engines

Early civil aircraft such as the Dehavillad Comet embedded engines within the wings to benefit from reduced parasite drag (pressure drag + skin friction drag) [35]. This location for embedding the engines has not found its way on to toady's aircraft since it was disadvantaged by aircraft damage during blade or disc failures, maintenance issues due to difficulty in accessing the engine and the wing would need to be redesigned if the engine was re-sized. However, the embedded feature has been partly replicated in future aircraft concepts that feature BLI propulsors located on the wing, where the casing must be partly embedded in order to immerse the fans within the boundary layer to maximize the benefit. Consequently, the casing would act as a support rib in the wing structure, which simplifies the integration with the airframe and removes rib weight. However, if the propulsors were fully embedded, then a significant s-shaped duct would be required and the total pressure losses associated with its curvature may offset the added BLI benefit.

Unfortunately, if the propulsor dimensions or major attachments were to be redesigned after the aircraft design was complete or the aircraft was in service, the aircraft wing would need to be altered. This would hinder the aircraft's model evolution due to the expense. Fortunately, it's likely that the propulsors would only occupy the volume where the TE high-lift device mechanisms retract to. In this case, the wing fuel tanks and structure would remain unaffected [35].

4 Vision 20 study methodology

4.1 Review of available methods

This section is based on the first objective in Chapter 1 and discusses various methods of assessing the key aircraft design areas found from the literature. These were chosen as they were predicted to impact the aircraft results substantially and were directly related to the novel propulsion systems being investigated. The conceptual aircraft design tool was then developed by adopting the preferred methods and adapting them to suit the specific aircraft requirements. Additionally, BLI methodologies have been reviewed in a quest for a method sufficient for the conceptual study.

4.1.1 Wave drag

Because the BWB is similar to swept wing, flying wing and delta wing aircraft, some of its components can be modelled in a similar fashion. However, it's larger centre-body becomes more difficult to model, due to its complex drag and structural characteristics. The inner wing and centre-section are thicker and produce complex systems of local shock waves at high subsonic Mach numbers. Conventional design methodology for T&W aircraft calculates wave drag, due to shockwaves, through the use of empirical correlations. In the case of the BWB configuration, a more analytical or experimental based method is preferred when sufficient data on BWB's is not available.

Raymer mentions that currently the industry relies on linearised computer codes such as 'PANAIR' to model aircraft wave drag. However, if the flow around the aircraft is unsteady (not the cruise condition) then either empirical corrections or Computational Fluid Dynamics (CFD) modelling should be sought [37]. In either case, these methods can be cumbersome at the conceptual design stage.

Jenkinson estimates the overall aircraft wave drag contribution by adding 5-20 drag counts or a drag coefficient of 5-20e-4 for cruise Mach numbers above 0.7. This approximation enables a rapid drag assessment, although, it doesn't capture any specific aircraft geometrical characteristics [28]. Collingbourne has developed an

analytical-empirical method that calculates the wave drag as a function of a wing's thickness to chord ratio, aspect ratio, lift coefficient and sweep [3]. The formula differentiates aircraft age technologies through including a year-of-manufacture coefficient, which can be calibrated with previous aircraft. The formula's accuracy was assessed through running the developed aircraft design tool and producing results that show its variation with wing geometry, shown in Chapter 5 Section 6.2. The method yields a more accurate correlation of wave drag over the purely empirical relations. Wilson advises to use a wave drag of 8 counts for the baseline aircraft [30]. This aligns with the range predicted in [27] and enables the calibration of the technology coefficient used in the method developed in [29]. Wilson also describes how future aerofoil improvements manifest in the aircraft wing as structural benefits rather than reduced drag, permitting a higher wing thickness to chord ratio for the same wave drag count [30]. This convention has been adopted for the current tool. This method was incorporated within the aircraft design code 'CADI' in the subroutines entitled 'Drag' and 'DragBWB' in Appendix B.

4.1.2 Wing mass

A similar problem exists when designing the structure of the aircraft, as the BWB's unusual shaped fuselage acts as a pressure vessel. Unlike conventional tube fuselages that rely on the intrinsic strength properties of a circular cross-section, the BWB uses an almost elliptical cross-section that requires strengthening spars/ribs to withstand the cabin pressure differential [24].

Most aircraft design methodologies, such as those from [28,32-34], use empirical equations based on previous aircraft to calculate the component weights. Raymer suggests using a slightly alternative method in which empirical fudge factors are used to calibrate the wing and fuselage weights. The fudge factors are equated as the ratio of a similar aircraft's actual component weight to its calculated weight, which in turn is found using empirical relationships from [27]. This factor then multiplies the calculated weight of the aircraft under investigation. Clearly this relies on the 'similar aircraft' being close to that of the investigated aircraft. Unfortunately, BWB aircraft possess some integral dissimilarity with the flying wing and broad delta aircraft, such as a cabin differential. Because, in addition, the empirical equations become difficult

to modify when design changes are required, this method has not been implemented into the current tool.

Ideally a Finite Element (FE) structural analysis would be undertaken to calculate the thickness and shape of the supporting components. However, at the conceptual design phase the exact inputs are not known and many simplifying assumptions must be made in order to evaluate a number of designs rapidly. This warrants the use of a simpler method that has a predominantly analytical framework.

One such method is known as the Raleigh-Ritz method, which makes use of the theory of virtual work and is essentially a step down from FE analyses in terms of complexity. The method has been adapted to first equate the wing stresses and then to reverse the process and calculate the thickness required to resist deformation [35]. It simplifies the wing by assuming it to be a solid flat plate split into two segments; inner wing and trapezoidal outer wing. The equivalent flat plate represents the individual components (spars, longerons, ribs etc...) and the bending, shear and torsion stresses are evaluated for a given loading situation. It requires only basic inputs, such as shape and material, and therefore can be effectively used at the conceptual design level. The method represents the wing as a set of mathematical infinite series terms which enable the computation of the method. Because of this though, it takes considerable time to set up the complex programming requirements. Also, unpredictable results can be obtained due to the over simplifications produced by assuming a flat plate. In reality, the high lift device support structure and other additions to the main wing box would affect the failure modes. Therefore, it seems that the unpredictable results do not warrant the time consuming set-up process of the Raleigh-Ritz method.

[32] comprises a fairly detailed method to calculate the wing weight by Torenbeek. It is mostly an analytical method that allows for additions such as leading edge (LE) and TE support structures through the use of empirical relations. It assumes all loads are supported by the main wing box and simplifies the calculation process by replacing its sub-parts with a mode of stress. The problem is a statically determinate

one and simple beam theory is used to determine the bending absorbed by the stiffened skin panels and spar flanges. The ribs and spar webs support the shear stresses and are treated as point loads on the skin panels. The torsion loads are not dealt with explicitly, although the wing box is checked for sufficient stiffness and otherwise compensated for. The method is designed for conventional aircraft synthesis and the BWB requires a method that is more suitable to its unconventional shaped structure that contains both a cabin pressure differential and the bending/shear forces due to the air load. This method was employed and is contained within the 'Wing' subroutine in the aircraft design code 'CADI' in Appendix B.

4.1.3 Fuselage mass

Crawford suggests a simple analytical approach to calculating the fuselage structure of a BWB [47]. It assumes the fuselage consists of two horizontal and two semi-circular sections that provide an almost elliptical cross-section, illustrated in figure 4.1. The top and bottom horizontal sections are split into a lattice of supporting I-beams and flat plates. The flat plate and beam thicknesses are sized to contain the cabin pressure differential. The distance between the beams (plate size) is optimised for the lowest overall weight for a given strength. The semi-circular sections connect the top and bottom sections and are identical to a conventional tubed fuselage; reducing the complexity of the task. This method assumes that the fuselage is rigid and maintains its shape to enable the calculation of the beams/plates under ideal conditions. It also does not account for the bending stresses created by the axial moments about the aircraft's centre of gravity. However, the method is highly adaptable and offers an alternative to using empirical expressions designed for conventional aircraft.

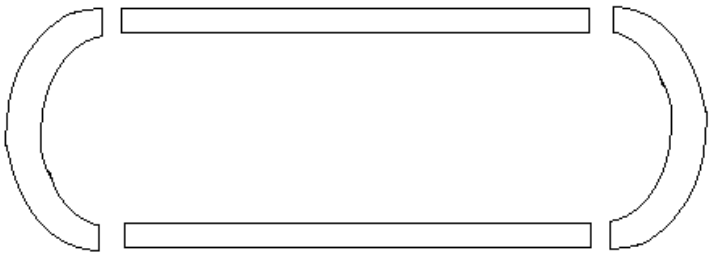

Figure 4.1 - BWB fuselage structure sections

A Cranfield University BWB mass estimation method was chosen for implementation into the tool as it more accurately accounts for secondary items, such as control surfaces, and generally provides a complete method that has been validated with various BWB designs. It is based upon splitting the airframe into three sections: inner wing, outer wing and fuselage. The inner and outer wings are subject to the bending and shear air-loads and the fuselage contains the cabin pressure differential; greatly simplifying the stress analysis. The component mass is found by integrating the thickness required to resist the 0.2% proof stress (an allowable stress relating to the percentage of strain for typical aircraft structures that is used when the materials elastic limit is difficult to define). The rib mass is calculated from the stiffness required to preclude covers from compressive failure and is a semi-empirical approach. The secondary weights are empirical functions derived from traditional aircraft data [37]. Further details on this method can be found in Chapter 6 Section 3.1. This method was employed and is contained within the 'BWB' subroutine in the aircraft design code 'CADI' in Appendix B.

4.1.4 High-lift devices and control surfaces

High-lift device issues arise when positioning the propulsors on the wing, as around 70% of the TE wing span is utilised by flaps. If the TE devices on the portion of wing 'wetted' by the propulsor wake were to be removed, then the remaining TE devices would require an increased lift coefficient to compensate for the loss in lift. Current large civil aircraft such as the Boeing 747 employ triple-slotted TE flaps to create large lift coefficients [38]. However, as the effective wing chord increases due to flap extension, the increase in lift coefficient reduces exponentially and the added weight becomes detrimental [37]. Therefore, another method to generate the extra lift would be preferred. Figure 4.2 shows a simplified schematic of a blown-flap arrangement and the propulsion system fans. This concept has been devised to illustrate a potential configuration with DP fans. The propulsors are located from the aircraft fuselage to the kink point, as the wing chord is largest there and produces a worthwhile amount of BLI. A bleed off-take is taken from the compressor stages of the engine and ejected from the blown-flap arrangement.

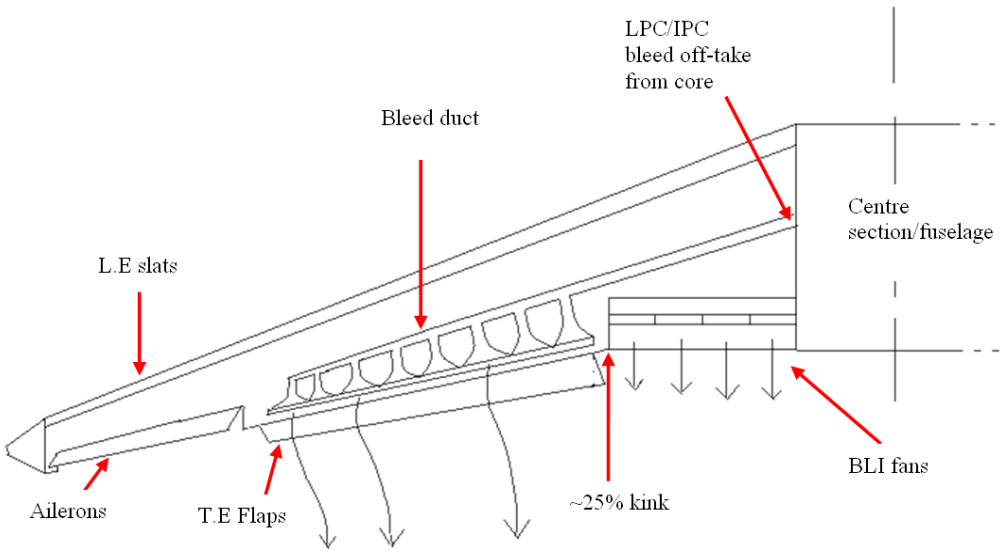

Figure 4.2 – Blown-flap and DP configuration concept

The jet flap is conventionally used for short take-off and landings, but could be utilised in the case of reduced control surface area for conventional distances. It is a simple TE flap with a jet flowing over its upper surface and avoids separation through exercising the Coanda effect (the curved fluid flow profile that is caused by the imbalance of pressure forces around a shape). Lift is generated not only by the redirection of the jet to create a vertical reaction force component, but also by the pressure differential over the flap. This pressure force increases efficiency of lift as it is distributed over a large flap area and effectively raises propulsive efficiency by reducing the kinetic energy of the expelled air. The upper image in figure 4.3 shows the streamlined flow that generates this vertical component of lift, whilst the lower image in figure 4.3 shows various configurations of blown-flap technology. Williams developed a semi-analytical theory that is based upon experimental results obtained from wind tunnel tests [39]. Very high lift coefficients in excess of eight can be achieved, although, they come with a number of issues. These include a fuel-burn penalty due to the high velocity air required from compressor bleed off-takes, weight effects, blockage in the piping due to debris, insulation to prevent icing and reduced wing volume for fuel.

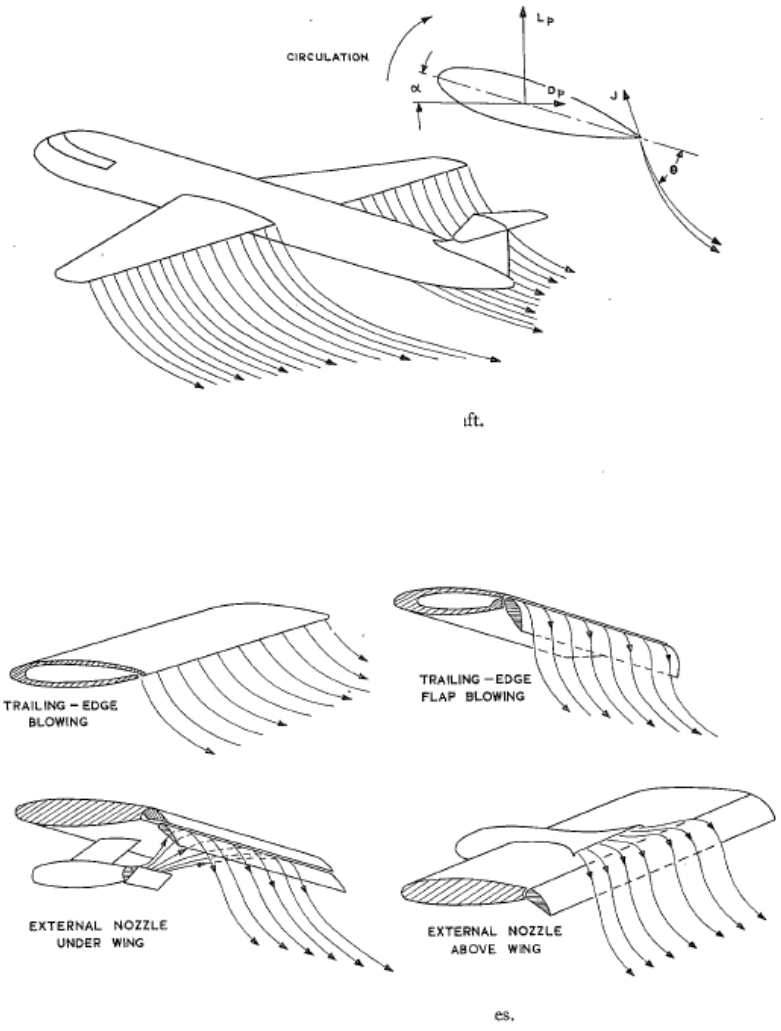

Figure 4.3 – Blown-flap configurations[39]

The lower right concept in figure 4.3 shows an external blown-flap arrangement which provides the most controlled blowing method as the bleed air is ejected as a thin stream over the flap surface. A slot between the wing and flap sucks air through and onto the upper surface, which augments the system capability by reducing the onset of separation. However, the required ducts incur significant total pressure losses and weight penalties, partly offsetting the lift benefits [40]. Optimisation of the ducting diameters and the angle of the blown-flaps have shown to reduce the bleed off-take considerably and at the same time increase the lift coefficient, without incurring detrimental profile drag over the blown-flaps [41].

The lower left concept in figure 4.3 uses an external blown-flap arrangement that

creates a similar effect by deflecting the exhaust from a podded engine using the upper and lower surface of a flap. The Airbus 380 is one of the key commercial aircraft to utilise the external blown-flap arrangement due to its significant wing loading [40]. However, the engine exhaust gas temperatures are high enough to cause considerable maintenance issues and future aircraft concepts tend to position the engines above the wing or use DP.

Historically, aircraft that used a blown-flap arrangement that require ducting were neglected due to their tendency to clog up; incurring considerable maintenance issues and rendering them useless as a landing aid [40]. However, blown-flaps were predominantly used to generate huge lift coefficients which required a large air mass flow. In the context of the current study, above wing DP propulsors are likely to reduce the flap area by only a small amount and the take-off and landing distance would remain at the same conventional distance of approximately 10500ft [28]. The mass flow required would be relatively small and cause fewer maintenance issues. Therefore, the internally blown-flap may still be feasible for these purposes.

Figure 4.4 shows the correlation between a parameter known as the 'jet coefficient', defined as the jet momentum to dynamic flow force ratio, and the flap lift-curve slope (units are 1/rad) of a simple flap, for different flap lengths (plotted as non-dimensional fractions of the wing chord). The jet coefficient is essentially the mass flow rate and consequently increases with lift coefficient. It can be seen that small values of jet coefficient provide sufficient lift for a regular take-off and landing situation. Therefore, the blown-flap arrangement could successfully remedy the reduced flap area problem.

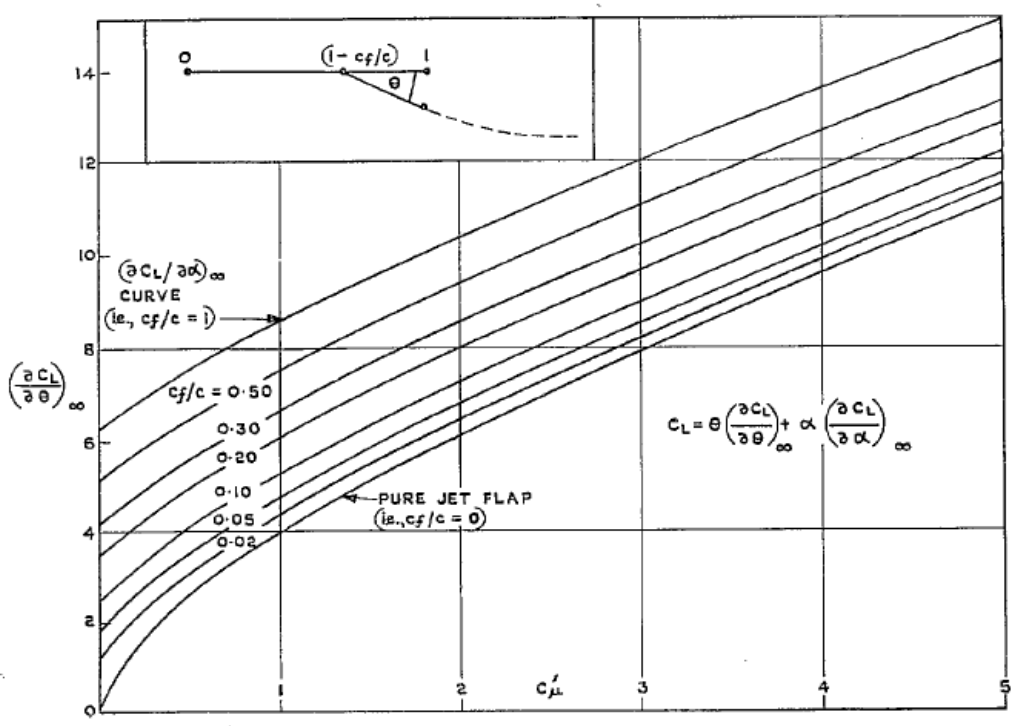

Figure 4.4 - Flap lift-curve slope vs Jet coefficient[39]

Another method of generating the extra lift required could be through vectoring the thrust of the above wing propulsors to create an externally blown-flap arrangement. In this case, the propulsors would be hinged and could mechanically rotate about the wing TE, enabling the thrust to be partly ejected downwards. Lift would be generated through the vertical change in momentum with the free stream air and flaps would not be required. However, the Coanda effect produced be locating flaps in the propulsor exhaust could augment the lift through a pressure effect. In the event of an engine blow-out, a number of distributed fans could act as electrical generators for the remaining fans by wind-milling freely using the free-stream air velocity. This would provide a convenient redundancy option [42] and would enable some fans to power other fans in order to focus the thrust for lift or to provide thrust vectoring. Blown-flaps have not been modelled in the current study due to time constraints and the lack of knowledge available on their reliability. Instead, the propulsors as assumed not to interact with the high-lift devices.

4.1.5 BLI methodology

This section provides a review of the current methods of assessing BLI. The theory of the benefit that BLI provides is best explained through mathematical expressions [25]. Figure 4.5 compares a podded engine case that ingests only free-stream air at a velocity of u_∞ and an idealised BLI case, in which an engine ingests 100% aircraft boundary layer air wake that has an area-averaged velocity u_w. Here it is assumed that all the aircraft drag is from skin-friction, which is just an example to show the principal physics. The mass flow interacting with the aircraft is assumed to be the same as that ingested by the propulsor. The flow is accelerated to a jet velocity u_j, which enables the engine net thrust F_{eng} to equal the airframe drag D_A, as shown in equation 4.1.

$$F_{eng} = \dot{m}(u_j - u_\infty) = \dot{m}(u_\infty - u_w) = D_{A.} \quad \textbf{(4.1)}$$

The rate of mechanical energy provided to the flow, $P_{added,\ no\ BLI}$, is given by,

$$P_{added,noBLI} = \frac{\dot{m}}{2}({u_j}^2 - {u_\infty}^2) = \frac{F}{2}(u_j + u_\infty). \quad \textbf{(4.2)}$$

Supposing the whole boundary layer is ingested, the engine must accelerate the wake back to the free-stream velocity in order to maintain flight speed. In other words the propulsive force, $\dot{m}(u_j - u_w)$, must equal the drag force, $\dot{m}(u_\infty - u_w)$. Therefore the propulsive force $F_{eng,BLI}$ then becomes,

$$F_{eng,BLI} = \dot{m}(u_j - u_w) = \dot{m}(u_\infty - u_w) = D_A, \quad \textbf{(4.3)}$$

and the power provided to the flow $P_{added,BLI}$ becomes,

$$P_{added,BLI} = \frac{\dot{m}}{2}({u_j}^2 - {u_w}^2) = \frac{\dot{m}}{2}({u_\infty}^2 - {u_w}^2) = \frac{F}{2}(u_w + u_\infty). \quad \textbf{(4.4)}$$

The power required for flight P_{useful} is the same for both cases as the force and flight speed are the same, shown by,

$$P_{useful} = D_A u_\infty = \dot{m}(u_j - u_\infty)u_\infty = \dot{m}(u_j - u_w)u_\infty. \quad \textbf{(4.5)}$$

Since, $u_w < u_j$, the BLI case requires less power to generate the same thrust.

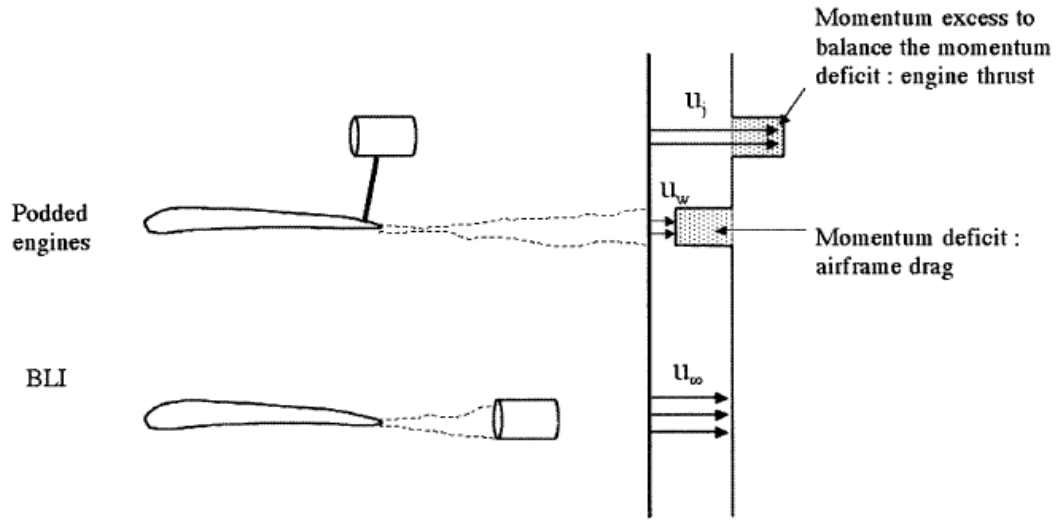

Figure 4.5 - BLI vs free-stream ingestion[25]

Control-volumes

[43] defines the "Trefftz-Plane" as a plane downstream of the aircraft where the flow has returned to free-stream static pressure. The control-volume is illustrated in figure 4.6, where the boundaries are assumed to be far enough away from the propulsor that the flow is undisturbed. The engine thrust is then equated using equation 4.1. The thrust balances the airframe drag (assuming nacelle drag is neglected), which is found by integrating wake velocity across the control-volume and multiplying by the mass flow, as shown in equation 4.6.

$$D_A = \int \rho(u_\infty - u_w)u_w dA \qquad \textbf{(4.6)}$$

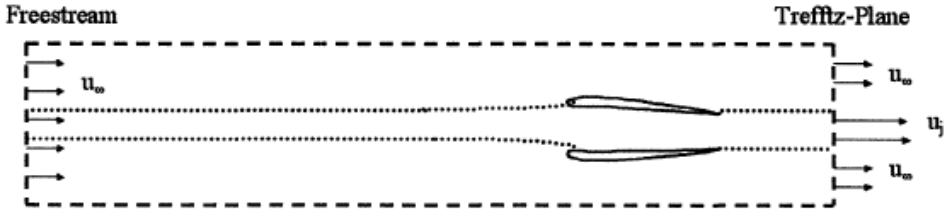

Figure 4.6 - Trefftz-Plane[43]

Embedded engines require an integrated approach to calculating thrust as they cannot be separated from the airframe. There are two main techniques that account for the forces; inner and outer control-volumes. The forces on an inner control-volume from the start of the pre-compression zone to the Trefftz-Plane, as illustrated in figure 4.7, originate from not only the propulsive forces provided by the engine, but also the “potential field effect” due to the aerofoil curvature, described by Smith [44]. Additionally, the flow that enters the inner control-volume boundaries is not at free-stream conditions and therefore its momentum needs to be accounted for.

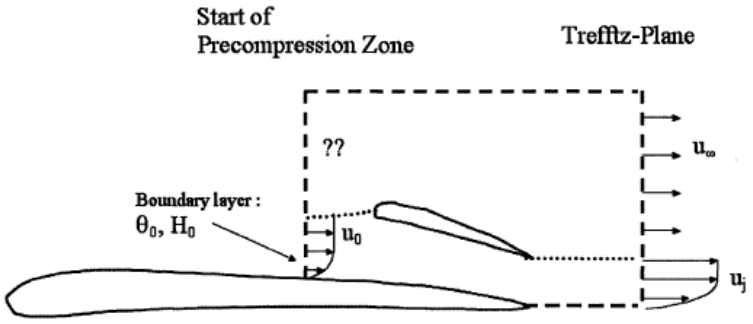

Figure 4.7 - Inner control-volume[43]

The outer control-volume approach addresses this problem by calculating the fan performance using free-stream inlet conditions, illustrated by the schematic in figure 4.8. The thrust is then equated as the integral of the jet velocity multiplied by the mass flow.

$$T_N = \int \rho(u_j - u_\infty)u_j dA \qquad \textbf{(4.7)}$$

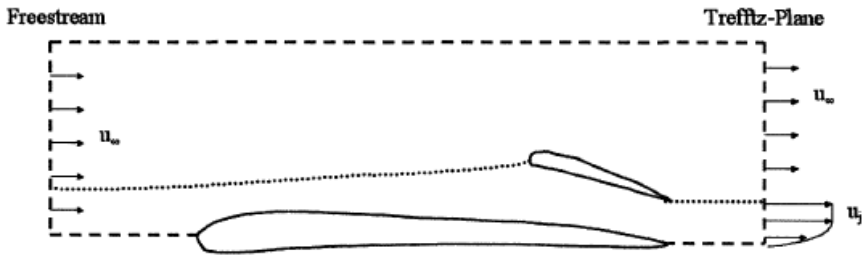

Figure 4.8 - Outer control-volume[43]

The net drag force $D_{N,}$ which the thrust balances, is then equal to the overall airframe drag D_A plus the nacelle drag $D_{nacelle}$ minus the skin-friction drag associated with the flow ingested by the propulsor D_w, as shown in equation 4.8.

$$D_N = D_A + D_{nacelle} - D_w \quad \textbf{(4.8)}$$

The BLI benefit in the outer control-volume approach manifests itself as a reduction in thrust requirement, associated with D_w. The advantage in doing this is that the velocity profile of the boundary layer does not have to be known and instead the drag force D_w can be equated directly, from either flat-plate turbulent boundary layer relations or a CFD tool. Additionally, the fan performance calculation can be done with the known free-stream conditions.

However, as the engine changes in geometry or location, or the airframe size changes, the engine must be provided with an updated thrust requirement. This complicates the design process. Another issue is that because the engine is not 100% efficient, the engine power requirement that is calculated to generate the required thrust is different between the two control-volume approaches. This is because the inlet velocity differs from reality, which affects the thermal efficiency of the components. Because the engine is actually exposed to the lower inlet velocities, the inner control-volume method has been adopted for the current studies to provide the most accurate BLI benefit prediction. Chapters 5, 6 and 7 provide more detail into the methods used for each study.

A ‘Distributed Propulsion fan tool’ was created in a spreadsheet and is based on the theory and methodology described here, details of which can be found in Appendix B.

4.2 Aircraft design methodology

A conceptual aircraft design tool was developed to model the selected aircraft and is known as ‘CADI’ – Conceptual Aircraft Design Integration tool. It is based on the theory and methodology described in this section, details of this and the coding can be found in Appendix B. Figure 4.9 illustrates the general process adopted for designing the aircraft within the conceptual design tool. Before the iterative sequence begins, a set of requirements is fixed for design purposes, such as payload, range and cruise Mach number. The approach and cruise Lift Coefficients (CL) are specified from empirical values and have been set to 1.6 for current civil aircraft with triple-slotted fowler flaps and 0.5 for current civil aircraft with supercritical aerofoils respectively.

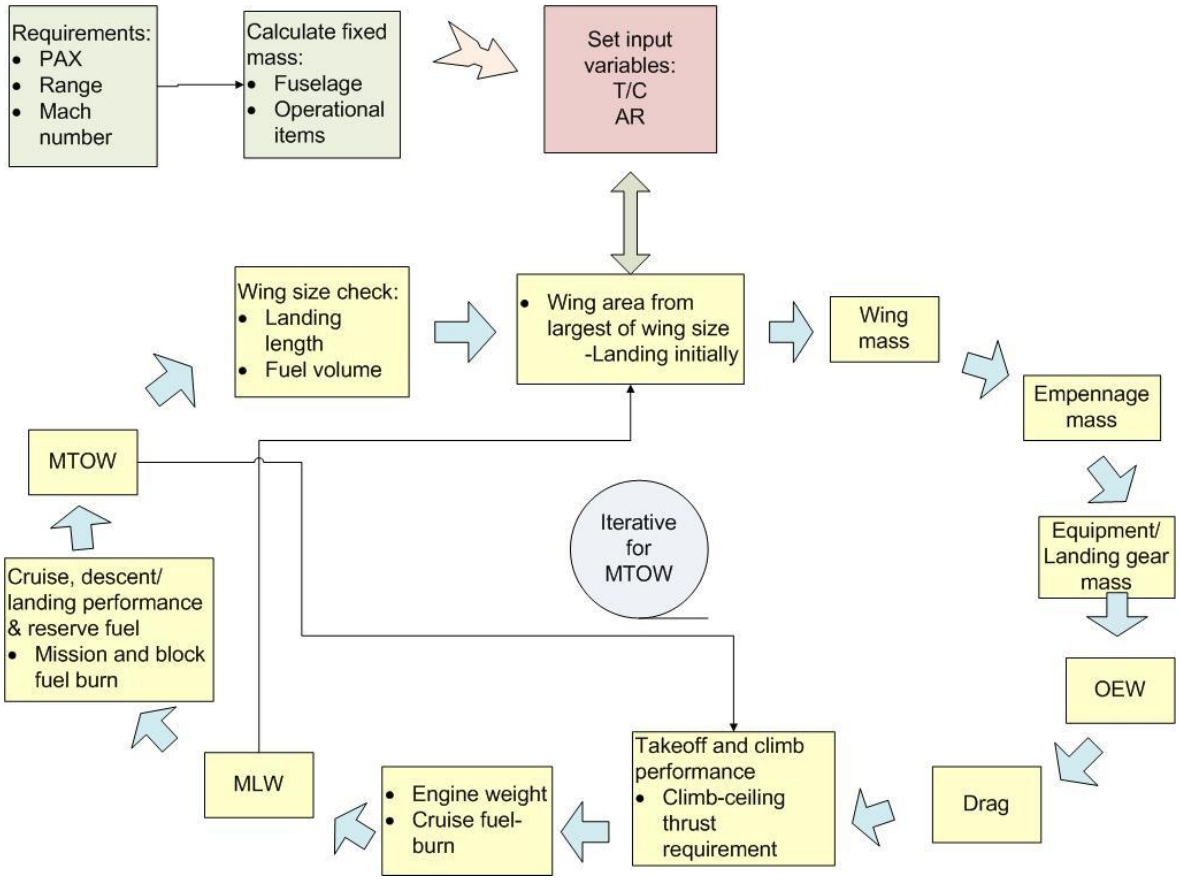

Figure 4.9 - Conceptual aircraft design tool iterative layout

The fixed weights are then calculated as a function of the payload using the relations in [10]. The T&W fuselage is calculated as a function of cabin pressure, material density, exterior dimensions and an empirical aircraft-type constant.

The aircraft is optimised in terms of trapezoidal wing Aspect Ratio (AR) and mean wing thickness to chord ratio (T/C). A combination of these two variables produces a specific design. The loop is initiated to sum the variable weights until the Max Take-Off Weight (MTOW) has converged. The loop is iterative as the variable weights are a function of the MTOW and Max Landing Weight (MLW).

The sequence begins by calculating the MLW as a sum of the fixed weights and reserve fuel. The payload weight is doubled as an assumption to account for any additional mass, such as freight. Although this assumption is rather crude, each aircraft manufacturer has a different method of calculating MLW and the methods a fairly longwinded. It was found that this assumption provided reasonably accurate results. The reserve fuel is assumed to be 9% of the mission fuel and is an empirical value taken from a Boeing 787 Piano simulation [45]. The A350 is very similar in technology, design and mission to the Boeing 787. The key difference is the larger passenger payload. This chiefly affects planform area and MTOW, which is directly proportional to fuel-burn. For a similar design, payload alone doesn't affect the aerodynamic efficiency, where fuel-burn is related exponentially with the inverse of the Lift to Drag ratio (L/D). Therefore, this assumption is considered sufficiently accurate.

The wing planform area is calculated from the largest of three requirements; landing length, take-off length and fuel volume. Generally the most critical phase is landing and this is calculated first as a function of approach speed, MLW and approach CL. An approach speed of 145kts is assumed.

The wing mass is then calculated using the analytical/empirical process developed by Torenbeek [42] for transport aircraft. The method computes the mass through integrating the span-wise material required to resist bending and shear loads from the air-load distribution. Mass penalties are added to allow for non-optimum effects, such as extra stiffness required for aero-elastic effects. Statistical relations are then used to equate the secondary weights, such as high lift devices.

Both quarter-chord sweep and taper ratio, defined as the ratio of wing tip chord to structural wing root chord, are extracted from existing aircraft of a similar design and have been fixed at 32.5 degrees and 0.12 respectively. These parameters vary significantly less between different civil aircraft in comparison with other design parameters, such as AR and T/C. The LE and half-chord sweep angles are calculated from the quarter-chord sweep using the expressions in [37]. The wing root chord is calculated assuming a straight tapered wing and multiplying the result by an assumed empirical constant with the value of 1.3, which has been estimated from existing aircraft to account for the kink and sweep geometry.

The empennage mass is estimated by multiplying the wing mass by the ratio of empennage to wing mass for a similar aircraft. The fin and tail areas are calculated from equation 4.9 and 4.10, where CT and CF correspond to tail and fin coefficients respectively that denote aircraft type and are taken from [37], S_{wing} is the reference wing area and i_{arm} is the moment arm.

$$S_{tail} = CT \cdot MAC_{wing} \cdot S_{wing}/i_{arm} \quad \textbf{(4.9)}$$

$$S_{fin} = CF \cdot Span \cdot S_{wing}/i_{arm} \quad \textbf{(4.10)}$$

The empennage AR's are taken from existing aircraft and the spans are then calculated. By assuming the LE tip point aligns in the stream-wise direction with the TE root point, two triangles are formed and the empennage areas can be equated. The wing Mean Aerodynamic Chord (MAC) and sweep parameters can then be obtained using the method for the wing and taking values for taper ratio from existing aircraft.

The fuselage, wing and empennage zero-lift drag coefficients are calculated using the equations in [27]. The wing drag coefficient is equated using the MAC definition, which assumes a trapezoidal wing section. The nacelle zero-lift drag coefficient can be accounted for once the propulsion system is sized at a later stage. The nacelle diameter and length were assumed to be 1.3 and 1.5 times the fan diameter respectively.

The induced drag calculation is based on the Oswald Span Efficiency method and is a function of AR. An effective-AR is produced by multiplying AR by a factor of 1.2, which account for the reduction in induced drag with winglets [37]. The wave drag estimation is based upon an iterative empirical method by Collingbourne [39], which is calculated as a function of T/C, cruise CL, quarter-chord sweep, AR and taper ratio. There is also a technology factor which is chosen according to the level of aerofoil technology used and was found for the baseline T&W by varying it until five wave drag counts was achieved for the selected A350 wing dimensionless parameters.

Initially, the take-off and climb phase performance is calculated, which enables the propulsion system to be sized. The take-off segment fuel is estimated by assuming take-off thrust for two minutes and using the take-off specific fuel consumption (SFC). This thrust is defined at the take-off End-Of-Runway (EoR) condition as F_{EoR} and is calculated by first obtaining the required acceleration 'a' through using the kinematic expression in equation 4.11, where the initial velocity u_1 is zero, the final velocity u_2 is the sea-level velocity at Mach 0.25 (taken from A350 take-off requirement) and s is the runway length.

$$u_2{}^2 = u_1{}^2 + 2 \cdot a \cdot s \qquad \textbf{(4.11)}$$

Newton's second law of motion, equation 4.12, is then used to attain the thrust required and the value is multiplied by two, to reflect a one-engine-inoperative state. This approach to predicting F_{EoR} is fairly simplistic, however, the engine was found to be sized at the climb-ceiling, due to the high cruise altitude, and the fuel-burn during take-off is small relative to other flight phases. Therefore, for conceptual design purposes this is acceptable.

$$F_{EoR} = 2 \cdot a \cdot MTOW \qquad \textbf{(4.12)}$$

The climb performance of the aircraft is calculated using the method in [13] and the altitude and Mach numbers used are listed in table 4.1, where TET is the turbine entry temperature, TET_{max} refers to the maximum TET the engine is capable of and was set by Rolls-Royce, OPR is the overall pressure ratio of the engine, OPR_{max} denotes the largest value at the climb-ceiling condition and Mn is Mach number. The

method discretises the climb into numerous segments, in which average aircraft and flight parameters are used to provide fuel-burn estimation for each segment. The first two altitude segments at Mach 0.85 were duplicated except for slightly different altitudes, to provide a more accurate fuel-burn prediction due to the change in calibrated-airspeed. This method was employed in the 'Performance' subroutine of CADI code, detailed in Appendix B.

OPR/OPR_{max}	TET/TET_{max}	Mach number	Altitude (kft)
0.7	0.905	0.39	1.5
0.74	0.905	0.41	5
0.79	0.905	0.45	10
0.75	0.905	0.58	10
0.8	0.905	0.63	15
0.85	0.905	0.69	20
0.9	0.905	0.76	25
0.95	0.905	0.83	30
0.95	0.905	0.85	30.6
0.95	0.905	0.85	30.7
1	0.891	0.85	37.1

Table 4.1 – Aircraft climb profile

If absolute thrust values were used during low MTOW values, the aircraft would operate outside of the code's convergent conditions since the aircraft mass would be low and the climb rate would be very high and convergence issues would arise because the altitudes would be out of the range of the empirical equation limits. Instead, a climb thrust-factor, defined as the ratio of datum climb segment thrust to datum ceiling thrust, multiplies the new climb-ceiling thrust in equation 4.13 to give the new thrust for each segment during the climb phase. The value is then corrected by the ratio of new to datum climb-ceiling densities. The datum point is taken from a previous simulation where the SFC was calculated. This procedure accounts for the

variation in thrust requirement during the iterations, which allows convergence during low MTOW values.

The climb time is then calculated. For civil transport aircraft this is approximately 25 minutes. However, if the rate of climb exceeds 10-15m/s, then the thrust-factors are reduced and the climb time is extended.

$$\text{Segment thrust} = \text{Thrustfactor} \cdot \text{New ceiling thrust} \cdot \frac{\text{New ceiling density}}{\text{Datum ceiling density}} \quad \textbf{(4.13)}$$

The climb-ceiling altitude is calculated by adding 3-4kft to the optimum-start-cruise altitude which is a general requirement for civil aircraft to allow a buffer for the engine to operate safely under adverse flow conditions or in case the aircraft is perturbed in some way. The climb-ceiling thrust is equated through imposing a rate of climb of 300ft/min at the cruise Mach number. The climb-ceiling conditions are usually the most demanding and the engine is sized using an engine performance tool.

The total installed power-plant mass, M_{pp}, is calculated from an engine weight tool. However, for small thrust variations, M_{pp} is calculated using equation 4.14, where thrust loading (TL), defined as the ratio of sea level static thrust to engine weight, sea-level-static aircraft thrust F_{sls} and aircraft type coefficient C_3 are found from [10].

$$M_{pp} = C_3 F_{sls}/TL \quad \textbf{(4.14)}$$

The EoR thrust attained from equation 4.12 is increased by an assumed value of 33% to approximate F_{sls}; a fraction that was taken from the B787 simulation [55]. The aircraft produces thrust requirements at climb-ceiling, cruise and EoR and the propulsion system then returns the design point and off-design point thrust and SFC values. The calculation of the optimum-start-cruise altitude is iterative and, using the Newton Raphson method, requires two initial altitude guesses, Alt_{n-1} and Alt_{n-2}. Figure 4.10 shows the sequence, where the atmospheric conditions are found using the relations in [19]. This method has been incorporated into the 'Alitud' subroutine in the code, detailed in Appendix B. E_n denotes the error between altitudes during the

iterations and the subscripts denote the iteration number relative to the current iteration n. u_{true} corresponds to the true-airspeed, γ is the heat capacity ratio and R is the gas constant.

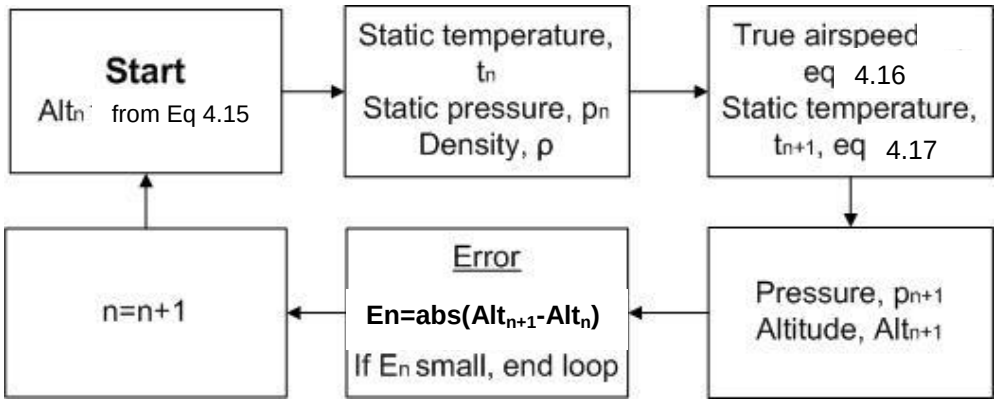

Figure 4.10 - Altitude iterative sequence

$$\mathrm{Alt_n} = \mathrm{Alt_{n-1}} - \frac{\mathrm{f(Alt_{n-1})}}{\mathrm{f'(Alt_{n-1})}}$$

$$= \mathrm{Alt_{n-1}} - \frac{\mathrm{E_{n-2}}}{(\mathrm{E_{n-1}} - \mathrm{E_{n-2}})/(\mathrm{Alt_{n-2}} - \mathrm{Alt_{n-1}})} \quad \textbf{(4.15)}$$

$$\mathrm{CL} = \frac{(\mathrm{MTOW} - \text{takeoff fuel} - \text{climb fuel}) * 9.81}{\frac{1}{2}\rho \mathrm{u}_{true}{}^{2}\mathrm{S_{wing}}} \quad \textbf{(4.16)}$$

$$\mathrm{Mn} = \frac{\mathrm{u_{true}}}{\sqrt{\gamma \mathrm{R T_{n+1}}}} \quad \textbf{(4.17)}$$

The end-cruise altitude is calculated using the same method, and when knowledge of the cruise fuel-burn is unavailable, an initial guess is made. Depending on the start-cruise and end-cruise altitude, the last few climb and first few descent altitudes can be altered to form evenly distributed flight segments; increasing the fuel-burn result accuracy. In reality, the cruise would have several stepped climb segments rather than a gradual climb, however this analysis assumes a constant L/D for a

given aircraft geometry and therefore a smooth climb for simplicity. Also, the difference is expected to be relatively small and is constant between the different aircraft being compared thus reducing any relative performance prediction inaccuracies.

The cruise segment fuel-burn is estimated using the Breguet range equation, equation 4.18; where u_{eq} is the equivalent-air-speed, Range is in km and g is assumed to be 9.81. L/D is fixed once the aircraft geometry is set for a given simulation, since CL, lift coefficient, is an input and CD, drag coefficient, is calculated from the geometry.

$$\text{Fuel burn} = \text{MTOW}_{\text{start-cruise}} \cdot \left(1 - \frac{1}{\exp\left(\frac{\text{Range} \cdot \text{SFC} \cdot \text{g}}{u_{\text{eq}} \cdot \text{L/D}}\right)}\right) \quad \textbf{(4.18)}$$

The cruise altitude is estimated as an empirical function of the start and end cruise altitudes, taken from the A350 mission (similar to the B787 mission requirement). Setting the cruise-fraction to 3/8 in equation 4.19, estimates the cruise altitude for a long range medium-sized civil airliner.

$$\text{Cruise altitude} = \text{Cruise fraction} \times (\text{Alt}_{\text{end}} - \text{Alt}_{\text{Start}}) + \text{Alt}_{\text{Start}} \quad \textbf{(4.19)}$$

The descent phase is then calculated using the same method as the climb phase [38] but with the altitudes reversed. The landing fuel mass is assumed to be 50% of the fuel mass required for take-off, which is taken from the Boeing 787 simulation in [55]. Taxi-out fuel is neglected as it doesn't affect aircraft weight during flight and the fuel tanks are sufficiently large. Taxi-in fuel is assumed to be taken from the reserve fuel; in line with [55].

The MTOW is then updated with the newly found weights. The aircraft systems, equipment and landing gear are then calculated as a single mass by multiplying the MTOW by an empirical aircraft type factor from [43]. This mass is then added to the MTOW to enable the calculation of the final MTOW, MLW and OEW for the current iteration. The iterations continue until the error between the new and old MTOW is smaller than 1kg.

4.3 Overall DP methodology

Figure 4.11 displays the specific functions in the global methodology that was employed to assess DP. The origin of the tools used is detailed in Appendix B. The CADI and XFoil codes are used for the 'Aircraft Design' function to simulate the aircraft design and mission to obtain the thrust requirement, and to retrieve the aircraft boundary layer results, respectively. The 'Propulsion System' function constitutes the 'DP Fan Performance' tool used to obtain the fan power requirements, and the 'Turbomatch' engine performance code which was used to model the turbofan engine and obtain the overall propulsion system SFC. The 'Electrical System Mass' tool was used to find the weight of the super-conducting electrical system and hydrogen coolant required by the DP fans. Fan power along with values for technology level parameters served as input. The 'Weighting Tools' function, used to predict the engine and DP fans/housing mass, initially consisted of Rolls-Royce's engine weighting tool 'Genesis' for the Vision 20 studies. This was changed to a set of scaling laws for the parametric investigation. After this point, the aircraft design would iterate until MTOW convergence was met and the propulsion system sizing iterations were complete. Fuel-burn would then be the final output metric. Finally, the parametric variables were altered and the sequence restarted.

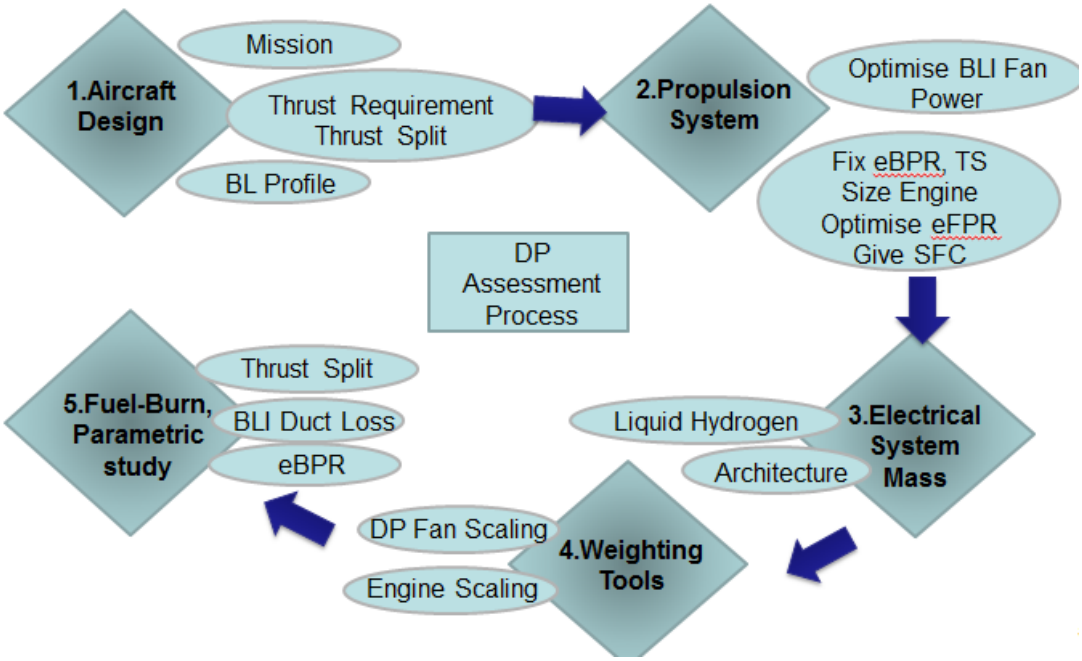

The following sections describe the number of modifications and additions that are required when modelling advanced technologies, together with the assumptions made for the advanced T&W-turbofan and DP aircraft variants.

4.4 Advanced T&W assumptions

4.4.1 Engine assumptions

Table 4.2 contains the relative change in engine parameters from the reference engine. A geared turbofan with a 0.6% mechanical efficiency loss was adopted and a 2:1 gear ratio to enable the reduction in LP turbine stage number. The turbofan engine fan pressure ratio (eFPR) was optimised to a value of 1.5 for the selected eBPR. The TET and OPR were not optimised, but were set from the predicted technology advance.

Parameter	Delta %
Max TET (EoR)	+12.2
Max OPR (climb-ceiling)	+40.3
Isentropic efficiencies	+2.0
eBPR (cruise)	+64.1

Table 4.2 - Advanced turbofan parameters relative to Trent XWB reference engine

The engine and installation weight was calculated using a weight prediction code.

4.4.2 Aircraft assumptions

By reviewing historical trends of aircraft technology it was possible to formulate key assumptions as to the technological advances achievable by 2035.

Brown [56] states that a 30% reduction in structural mass due to composites is achievable relative to a 1990's aircraft. The A350 has approximately 20% less structural mass due to its composite wing/empennage, therefore accordingly a 10% reduction remains possible within the fuselage. Raymer [37] predicts a 10% fuselage mass reduction due to composites, which is in line with the aforementioned

prediction. Assuming that these reductions are made for the same size structure (ignoring aircraft resizing effects), the fuselage mass is reduced by 10%.

A 10% reduction in landing gear/equipment mass due to composites and aluminum power cables was made in line with Raymer's predictions [27]. Also a 5% reduction in operational items is assumed, due to general design advances.

The wave drag calculation method by Collingbourne [29] was adopted. The method contains a technology parameter that represents aerofoil technology advances, which is one per cent higher for current aircraft relative to 1990's aircraft through designing for lower peak lift using supercritical aerofoil technology. A further one per cent increase is predicted due to the enhanced supercritical aerofoil. Typically for conventional aircraft the T/C has been increased for a fixed value of wave drag. Therefore five to ten wave drag counts, which are typical of a conventional aircraft, were expected for a thicker wing.

Figure 4.12 displays the baseline and advanced T&W aircraft. The results section 6.1 explains the reasons for the differences.

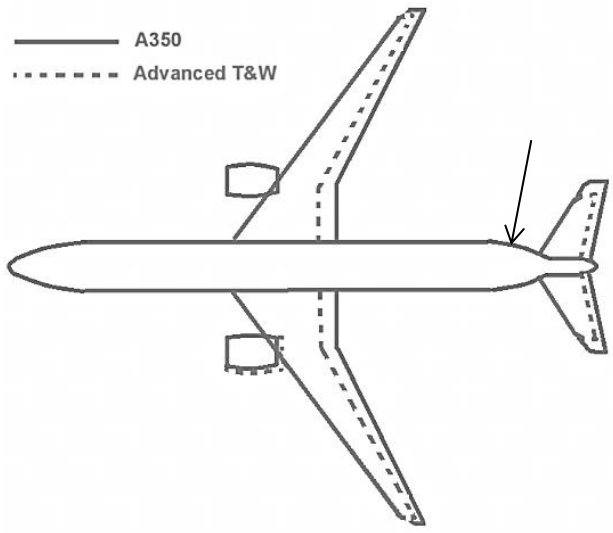

12

4.5 T&W with DP assumptions

4.5.1 Propulsion system assumptions

The same advanced turbofan technology was used to provide thrust and power to

the distributed fans, but the engine mass flow and BPR was altered to meet the Thrust-Split (TS) requirements, defined as the DP fan thrust to total thrust ratio. The turbofan cruise eFPR was fixed at 1.5 to provide the same specific thrust as the advance turbofan; providing a fair comparison with BLI effects.

During initial studies it was found that high mass flows were susceptible to large duct total pressure losses and therefore it was preferable to ingest only boundary layer air that contained a high momentum deficit to mass flow ratio. As this ratio was relatively low on the T&W wing section due to the relatively short chord, it was decided to implement DP and BLI on the fuselage surface alone. Therefore the turbulent flat-plate equation 4.20 that utilises the 1/7 power law was used for the T&W assessment, where u is the velocity, U is the boundary layer edge velocity and is taken as 99% of the free-stream velocity, y_s is the distance from the wall and δ is the boundary layer height.

$$\frac{u}{U} = \left(\frac{y_s}{\delta}\right)^{1/7} \quad \textbf{(4.20)}$$

The inner control-volume approach [25] was adopted, where the skin friction drag relating to the aircraft surface that the flow scrubs prior to ingestion is equal to the propulsion system thrust. The inlet momentum to the DP fans was calculated from the boundary layer properties and a total pressure loss was included in the thermodynamic calculations.

To minimise electrical system weight and maximise DP fan performance, the DP fan power requirement was kept constant during the climb phase. This meant the TS was lower during take-off than during cruise. The cruise DP FPR was parametrically varied between 1.4 and 1.7, where 1.4 provided the minimum value achievable without incurring significant fan efficiency losses. An inlet total pressure loss of 2% was invoked to represent the DP fan inlet ducts. In addition, a 2% loss in isentropic efficiency of the DP fans relative to the advanced turbofan was introduced to account for their smaller size and flow distortion at the fan face produced by the boundary layer.

It was decided to locate the DP fans at the rear of the fuselage and size the fans by the boundary layer thickness, giving a diameter of 0.78m, which was equal to the boundary layer height. Sixteen fans were employed to surround the fuselage; providing enough room for installation. The mass-flow-ratio, which here is defined as the ratio of area-averaged intake throat velocity to area-averaged boundary layer velocity, is assumed to be equal to unity at the cruise condition; simplifying the BLI area calculation. Fixing the mass flow gave the TS for each DP FPR case. The main engines are still mounted ahead and beneath the wings.

The electrical system consisted of motors, generators, cabling, protective earth system and cooling system. The motors and generator mass calculations required knowledge of rotational speed and power, whilst assuming a capability of 70Nm/kg. The cabling mass was calculated assuming 2kV and 1000Amps/kg/m capability, where current is equated from knowledge of power and voltage, and the lengths were obtained from the aircraft geometry.

Liquid hydrogen cooling was adopted and was carried in a tank capable of containing the required pressure. The hydrogen coolant mass was calculated from the internal heat generation during flight, which was equated to the product of the mission time, distributed fan power and a 0.2% transmission loss. The mass was then found using the latent heat of evaporation of hydrogen. Equation 4.21 was used to calculate the storage tank mass, where a tank efficiency of 60% was assumed and accounts for the structure required to contain the pressure differential and carry the insulation.

$$0.6 = \frac{\text{Hydrogen mass}}{\text{Hydrogen mass} + \text{tank mass}} \quad \textbf{(4.21)}$$

As the liquid hydrogen coolant can be utilised as a secondary fuel after the cooling stage, the kerosene fuel mass was reduced accordingly. The amount of hydrogen required was predicted to be small enough to be carried within the wing without resizing, since the fuel burn reduced more for the DP concept than the wing size reduced.

4.5.2 Aircraft assumptions

Figure 4.13 shows an image of the DP fans, where the boundary layer is ingested from the fuselage section and the propulsors are located at the rear of the fuselage to maximise BLI. The wing chord is relatively small on this T&W configuration and therefore the wing BLI benefits are predicted to be small relative to that of the fuselage, therefore propulsor have not been place there. The DP fans are assumed to have common nacelle housing. The surface area of the housing was approximately equal to the fuselage area occupied by the fans, therefore the increase in skin-friction drag is assumed to be minimal. Also, form and wave drag changes have not been accounted for as these require a detailed investigation into specific geometries. Therefore drag additions were not implemented.

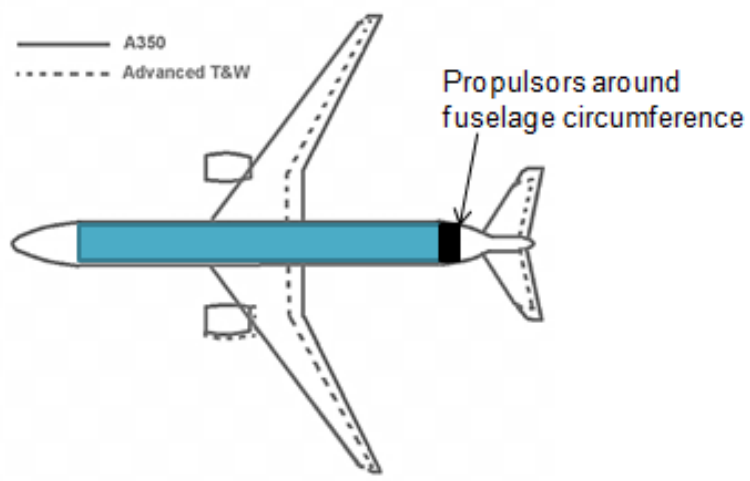

13

Wing structural weight can be reduced by positioning propulsors along the wing span to oppose the upward acting air-load moment. The main engines and wing-mounted DP propulsors (if there had been any) act as point loads and can be accounted for by summating each propulsor's contribution to the wing bending relief function. Torenbeek's [12] $delta_{pp}$ function in equation 5.22 was used to account for this effect, where $\eta_{propulsor}$ is defined as the ratio of the distance between the centre-line and propulsor to semi-span, MTOM is the same as MTOW and $M_{propulsor}$ is an individual propulsor mass. η_{cp} is the ratio of the lateral coordinate of c.p. (centre of pressure) to structural semi-span and is defined by equation 5.23, where λ is wing taper ratio.

$$\mathrm{Delta_{pp}} = \sum -1.5 \frac{{\eta_{\mathrm{fan}}}^2}{\eta_{\mathrm{cp}}} \frac{\mathrm{M_{fan}}}{\mathrm{MTOM}/2} \quad \textbf{(4.22)}$$

$$\eta_{\mathrm{cp}} = \frac{1 + 2\lambda}{3(1 + \lambda)} \quad \textbf{(4.23)}$$

The DP T&W has the DP propulsors located close to the centre-line at the rear of the fuselage and do not provide much wing-bending relief, so they were neglected from the calculation. Instead this method was used for the BWB aircraft in Chapter 6 of this paper.

The electrical transmission wiring and hydrogen coolant weights are also treated as point loads at their mean distances, and together with the main engine $delta_{pp}$, summate to give the total power-plant bending relief function.

The fin and tail size were altered as the distributed propulsor positions affect the pitch and yaw aircraft moments during an engine failure due to asymmetric thrust. Raymer [27] estimates a 5% reduction in fin and tail areas by moving engines from under-wing to aft-fuselage, resulting in a reduced stabiliser area and mass. This estimation was used for the change in distributed propulsor position, where the stabliser's size has been calculated using equations 4.9 and 4.10. Equations 4.24 and 4.25 were used to modify the coefficients to 'new' coefficients that account for the reduction in size, using the EoR TS. The 0.95 represents a 5% reduction for moving propulsors from the wing to fuselage. To account for the propulsors spread along a wing, an interpolation between 0-5% is done with respect to propulsor position. The T&W study retains both 0.95 values, whilst the BWB study uses a value of 0.975 for CF_{new} to account for inner wing spread and 0.95 for CT_{new}.

$$\mathrm{CF_{new}} = \mathrm{CF}\left(0.95 \cdot \mathrm{TS_{EoR}} + (1 - \mathrm{TS_{EoR}})\right) \quad \textbf{(4.24)}$$

$$\mathrm{CT_{new}} = \mathrm{CT}\left(0.95 \cdot \mathrm{TS_{EoR}} + (1 - \mathrm{TS_{EoR}})\right) \quad \textbf{(4.25)}$$

The empennage mass has been equated as a fixed proportion of wing weight. Assuming the reduction in empennage area directly reduces its weight, equation 4.26 is used to produce a mean factor C, which is used to scale the empennage mass to account for the distributed propulsors.

$$C = \frac{CF_{new} + CT_{new}}{CF + CT} \quad \textbf{(4.26)}$$

4.6 BWB design methodology

The same vehicle specification as the T&W aircraft in Chapter 5 was used for the BWB aircraft, namely 350 PAX, 8000nm mission and 0.85 cruise Mach number. The overall design methodology used for the BWB was the same as the T&W aircraft, although modifications were made to account for the novel design, such as the structural mass tool. However, the BWB was not explicitly compared to the T&W aircraft due to incompatible methods and assumptions, such as the different wing bending theory methodology used in calculating the structural mass and the different empirical data used in the secondary items such as high lift devices.

4.6.1 BWB mass method

A Cranfield University BWB mass estimation method was implemented and is based upon splitting the airframe into three sections (shown in figure 4.14); inner wing, outer wing and fuselage. The inner and outer wings are subject to the bending and shear air-loads and the fuselage contains the cabin pressure differential; which greatly simplifies the stress analysis. The component mass is found by integrating the thickness required to resist the 0.2% proof stress. The rib mass is calculated from the stiffness required to preclude covers from compressive failure and is a semi-empirical approach. The secondary weights, such as control surfaces, are empirical functions derived from traditional aircraft data.

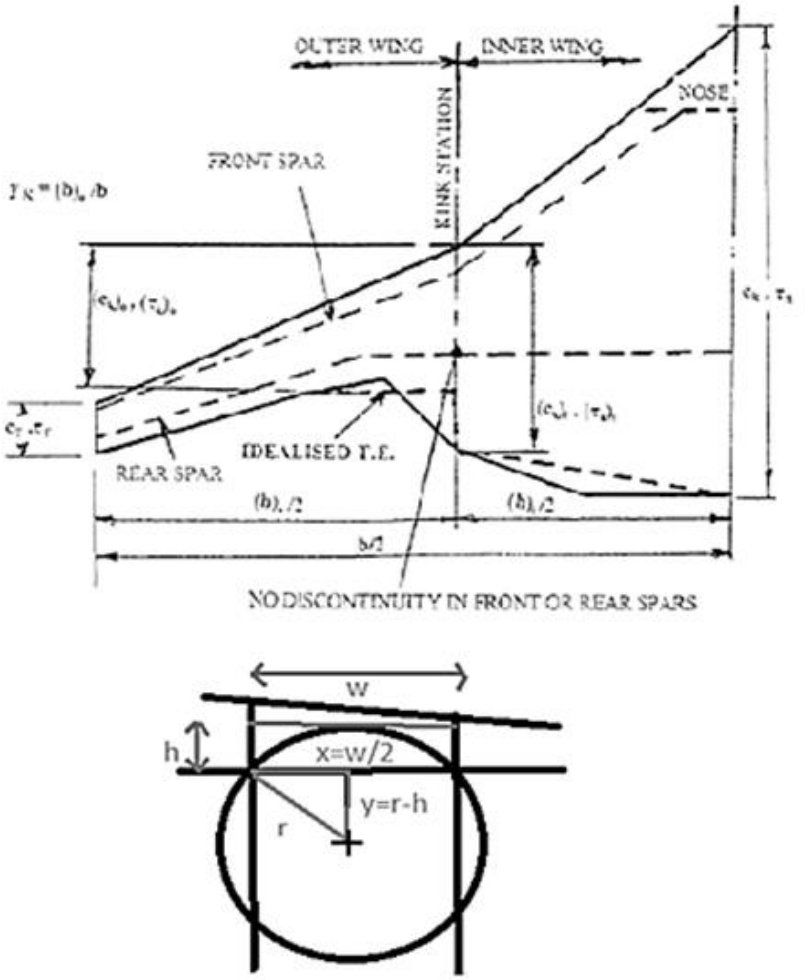

Figure 4.14 - Cranfield University BWB inner/outer wng (top) and fuselage (bottom)

The effective radius of curvature for each cabin segment was calculated from equation 4.27 using the geometry in figure 4.14.

$$r = \frac{w^2}{8h} + \frac{h}{2} \qquad \textbf{(4.27)}$$

The inner wing planform area and thickness-chord ratio were sized by the payload requirement (outlined by the boxes in the figure 4.14). A single decked cabin was assumed in the payload area and structural calculations. The outer wing was then free to be optimised in terms of structural weight, drag and stability. Taper ratio and sweep remained fixed at values taken from existing aircraft, as the structural method requires these to produce an elliptical air-load distribution. The inner wing taper ratio

was fixed at 50 degrees and the inner wing taper ratio was fixed at 0.476 as this approximately provided the required distribution as seen in the study by Kane [47]. The outer wing sweep was fixed at 32.50 degrees which was the same as the T&W aircraft in Chapter 5 and the outer wing taper ratio was set to 0.316 to give the same ratio of sweep to taper ratio as the inner wing to approximate the required distribution.

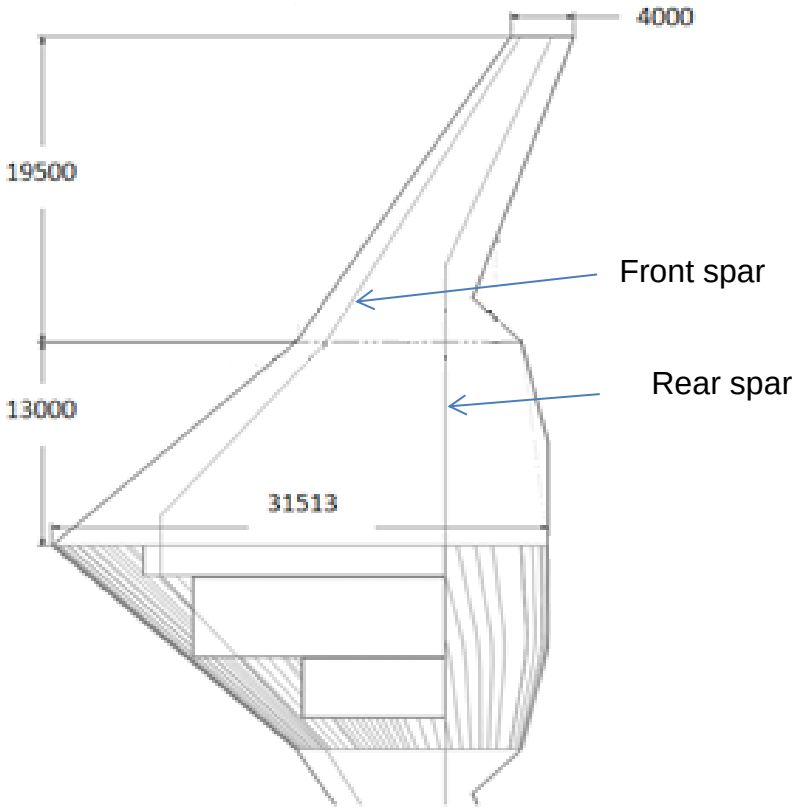

14

A number of restrictions applied to the aircraft's geometrical design. The passenger payload is located between the front and rear spars of inner wing with a two metre minimum cabin height. The fuel tanks are located between the front and rear spars, and up to 85% span. The rear spar remains continuous and the control surfaces/actuators are located behind the rear spar.

4.6.2 BWB stability

A static stability analysis was performed to certify the basic stability of the aircraft and check its component weights were in permissible locations. CMo denotes the

centre moment in which the aircraft rotates about. It can be seen from the second schematic in figure 4.16 that if the aircraft Angle of Attack (AoA) increases, the moment about the centre of gravity (c.g) from the aerodynamic centre (a.c) force will produce a clockwise rotation and the aircraft wing will stall. Conventional T&W aircraft are designed to be statically stable, shown in the first schematic in figure 4.16. A statically stable aircraft operates by producing a counter-clockwise rotation to correct a clockwise rotation that may have been cause by a flow perturbation.

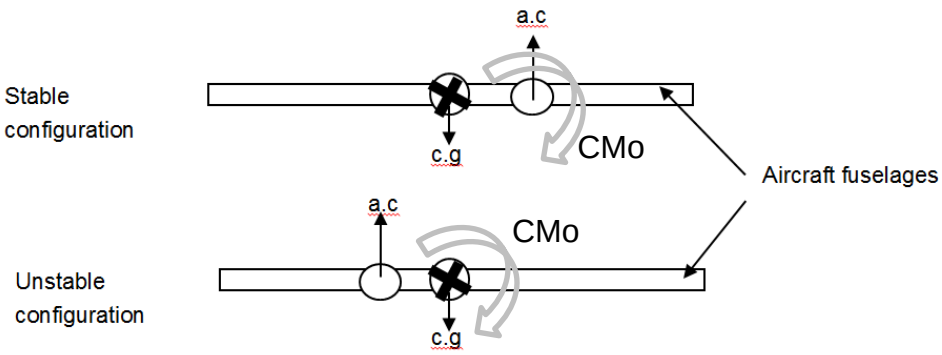

15

In order to trim an aircraft such as the A350, a horizontal stabilizer (elevator) is required to generate either upwards or downwards lift depending on whether a stable or unstable configuration is adopted. A stable configuration induces negative lift in order to balance the lifting moment, which therefore requires a further increment in AoA to sustain the required lift force to maintain altitude. Figure 4.17 shows two statically stable aircraft: BWB1 and BWB2; and two statically unstable aircraft: BWB3 and BWB4. The unstable configurations require a small change in AoA relative to the stable configurations when the aircraft is trimmed [48]. This effect diminishes at higher speeds, although landing would occur at around 145kts. T&W aircraft have a long moment arm (distance between stabiliser and c.g) due to their long fuselage and suit a statically stable configuration. However, [48] discusses the benefit of considering an unstable configuration as the reduced moment arm of the BWB aircraft would require particularly large elevators that would be detrimental to performance and therefore it becomes attractive to have a low AoA due to the low drag incurred when trimmed. Therefore, it has been assumed that an electrical system provides stability control and both positive and negative stability margins are

permitted in the range of ±5%, although currently there are no examples of civil airliners with an unstable configuration.

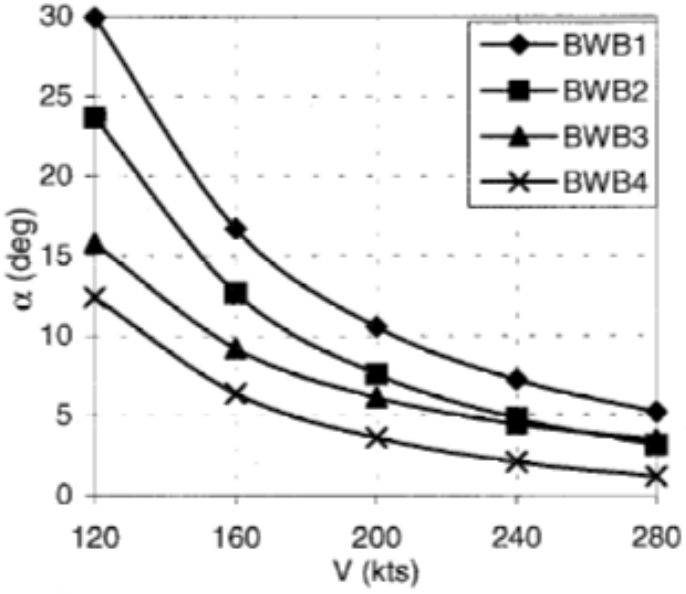

16

Detailed information on aircraft stability can found in [49]. The aerodynamic centre is defined as the point on a specific chord line that has a zero rate of change of moment with respect to AoA i.e. δM/δα=0. This is commonly assumed to be the quarter-chord point (quarter of the chord from the wing leading edge). The mean quarter chord point or wing aerodynamic centre (a.c), is found by integrating these points across the semi-span. The distance from a datum point 'A' to the a.c is defined as X_A, which is found using equation 5.28, which divides the integral over the span 'b' of the mean lift moment and the integral of the mean lift force, where Clα is the derivative of the cruise lift coefficient CL with respect to AoA 'α', and can be assumed constant over the wing section. The schematic in figure 4.18 illustrates that this must be done for both wing sections, where c is the chord (function of y), y is the semi-span and Λ is the quarter-chord sweep.

$$X_A = \frac{\int_0^{b/2} cC_{l\alpha} y \cdot \tan(\Lambda) dy}{\int_0^{b/2} cC_{l\alpha} dy} \quad \textbf{(4.28)}$$

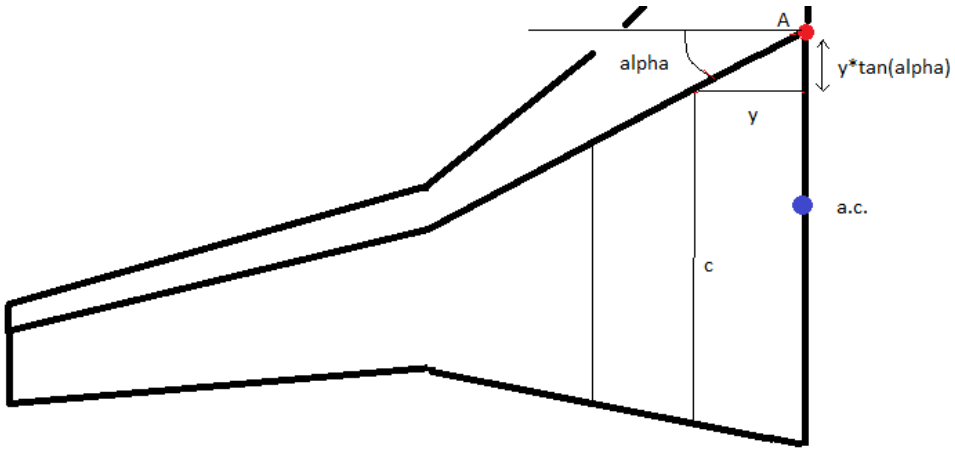

17

The aircraft c.g can be found by summing each of the aircraft components product of mass and distance to the datum point ‘A’ and dividing it by the sum of all the masses. The static stability margin is defined as the percentage distance between the a.c and c.g of the MAC.

The locations of the aircraft component weights were altered until an acceptable static stability margin was achieved. Table 6.12 in the results section shows that the margins do slightly exceeded the ±5% range when the fuel tanks were full, at take-off, in the aft-fuselage turbofan cases. Decreasing the cruise Mach number reduces the margin slightly due to the fuel-burn reduction, although, the values are generally acceptable for a conceptual design study.

4.6.3 Propulsion system assumptions

The same engine and DP fan technology used in Chapter 5, was used for all the BWB aircraft variants. The cruise eFPR for the turbofan and DP fan was fixed at 1.5 and 1.4 respectively. The lower DP fan FPR of 1.4 was chosen as it provided an optimal combination of fan efficiency and specific thrust for the DP T&W aircraft in Chapter 5. Once the boundary layer properties were known, the DP mass flow and DP thrust was fixed, which enabled the turbofan sizing.

4.6.4 Engine spacing

Two cases have been investigated to help understand the performance/stability benefits and drawbacks of changing the engine location; turbofan engines located

under-wing and at the aft-fuselage. The above-fuselage case required the engines to be in close proximity to each other and therefore a calculation was required to determine the minimum spacing needed in the event of a blade disc failure. Figure 4.19 shows the geometry considered in the spacing analysis that is used in equations 4.29 and 4.30. In the event of an engine 'one third blade disc radius' failure scenario, the angle limit percentage used is ±5% (a nominal value provided by Rolls-Royce).

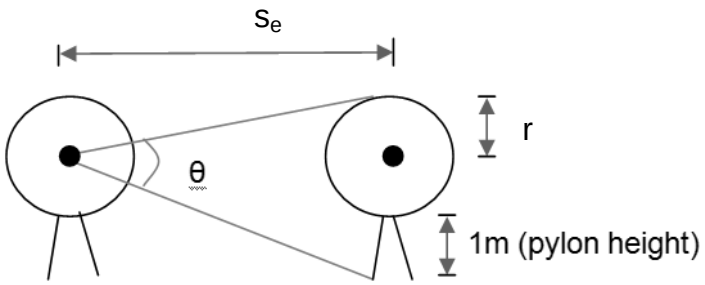

18

$$\text{Angle limit percentage} = 100 \times \frac{\theta}{360} \quad \textbf{(4.29)}$$

$$\theta = 2 \times \sin^{-1}\left(\frac{r}{s_e}\right) \quad \textbf{(4.30)}$$

4.6.5 DP system design

Figure 4.20 shows the embedded location of the distributed propulsors. Common nacelle housing was incorporated to reduce profile drag. An inlet duct was also used to maximize BLI, where the associated duct total pressure losses were varied to highlight the sensitivity.

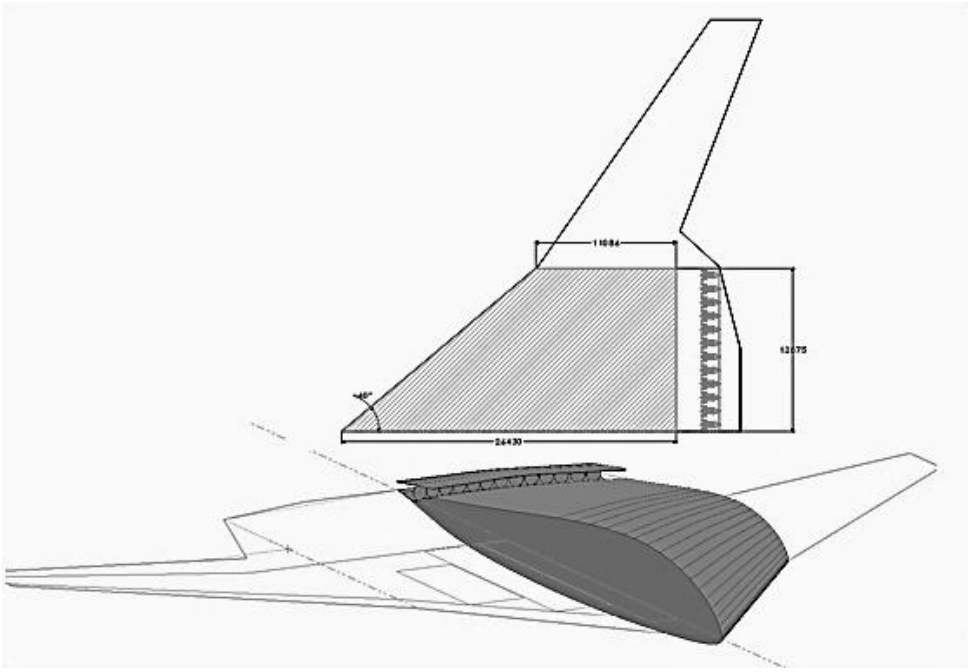

19

Figure 4.20 displays the inner wing area that the boundary layer ‘wets’ before it’s ingested by the fans. It was decided to not ingest the outer wing boundary layer due to the limited benefit available and adverse interactions with the aircraft control devices. It was also assumed that shock waves only existed on the outer wing; an assumption that is realistic through altering the local lift CL’s over the aircraft span (highlighting the importance of an integrated design approach between the propulsion system and the whole aircraft).

Flat plate and aerofoil boundary layer properties are compared in figure 4.21. The flat plate model was based on the 1/7 power law index used in Chapter 5 and the aerofoil section at the BWB’s inner-wing MAC was modelled using the 2D CFD tool XFoil. The benefit of using the XFoil CFD code over the simplified flat-plate equations can be seen by the exponential growth of the momentum thickness (theta) and displacement thickness (delta), where the upper surface adverse pressure gradient of the aerofoil is accounted for in 2D analysis. It should be noted that Figure 4.21 shows the displacements thickness and not the boundary layer height. This study implements the XFoil results into the BLI methodology described in Chapter 5, although both methods are compared in the results section. The momentum and displacement thicknesses were used to find an effective power law to equation 5.20

in Chapter 5 Section 5, which was then integrated numerically to give the boundary layer mass flow, boundary height and mean inlet velocity. The resulting power law ‘n’ equated to 0.25 at a Reynolds number of 8.668x10^7. This calculation was done by Rolls-Royce for the Vision 20 study. Section 5.1 describes the method developed by the author to enable the boundary layer to be evaluated for the parametric investigation.

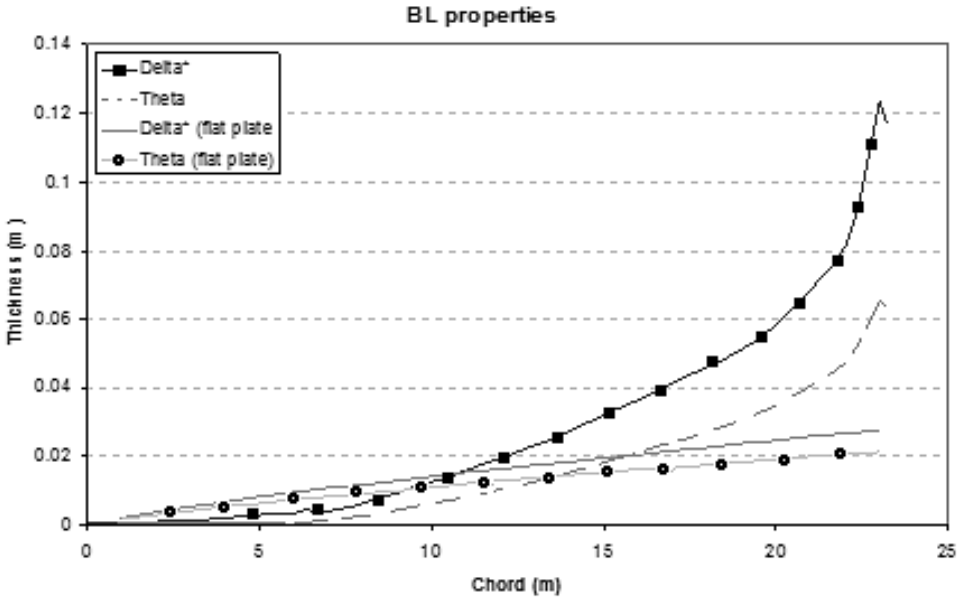

20

The study implemented twenty fans, of 0.89m diameter to match the boundary layer height in the centreline. The DP fan number and size together with the cruise DP FPR fixed the DP fan cruise thrust and produced a cruise TS of 56%. The DP fan mass flow was set by the fixed intake height and therefore the TS has not been optimised. However, ingesting the whole boundary layer is assumed to be not far from the optimal mass flow. The fans, nozzle and inlet duct stretched five times the fan diameter from the trailing edge. The wing structural bending relief and nacelle drag were accounted for using the same methods as in the T&W studies.

5 Parametric investigation methodology

5.1 Uninstalled DP study

5.1.1 Objectives and rational

It was shown that the overall propulsion system performance was particularly sensitive to duct loss and BLI benefit in the Vision 20 studies in chapters 5 and 6. Therefore, this study aims to build on the knowledge of DP obtained from the previous studies by assessing the impact of various propulsion parameters on the system configuration and performance.

The first objective was to define a methodology of assessing BLI parametrically. This required the development of a mathematical derivation that converts the boundary layer properties from CFD to averaged values that can be used to rapidly assess different DP fan intake heights. A DP fan tool was then developed to enable the evaluation of the fan performance, with the objective of showing how flow parameters such as mass flow and FPR affect fan performance. The DP fan tool was then combined with the Cranfield engine performance tool Turbomatch to enable the assessment of the whole propulsion system in terms of SFC. The aim was then to understand how technology assumptions affect the optimum configurations of the DP fans and engines.

It was shown in Chapter 6 that the boundary layer properties on an aerofoil vary considerably over the chord length than on a flat-plate. Therefore, the final objective was to assess the performance impact of varying propulsor location on the rear part of the upper surface of the aerofoil. In addition, the aerofoil type was altered to assess the change in BLI benefit available.

The BWB aircraft and propulsions systems used in this study are based on a 2030-2035 service entry. The study's novelty lies in the modelling of an A350-1000 sized BWB airliner that incorporates both under-wing and above-fuselage turbofan configuration with a TS. In addition, a parametric optimisation of the DP system has been carried out to assess its performance potential.

5.1.2 Engine and aircraft

Table 5.1 displays the key data, taken from the BWB aircraft in Chapter 6, which was used to fix the aircraft thrust requirement, boundary layer properties, and the engine technology level.

Parameter	Value
Cruise thrust (kN)	82.9
Cruise altitude (m)	13,654
Cruise Mach no.	0.85
Mission range (km)	14,820
Engine cruise OPR	56
Engine cruise TET (K)	1680
Engine cruise eBPR	15.0
DP fan isentropic efficiency	0.90
Electrical efficiency	99.9%

Table 5.1 - Key BWB data

The low pressure turbine of the turbofan engine included a power off-take (identified under auxiliary power in Turbomatch) to match the DP fans power requirement. As one engine was modelled, half the DP fan power was required in Turbomatch.

Figure 5.1 shows the process of designing the engine for the cruise design-point so that it provides the correct amount of thrust and DP fan power. The TS, defined as the ratio of DP fan thrust to total thrust, is one of the key parameters to be investigated in the parametric study. The process initiates by selecting a TS and proceeding to optimise fan power. The engine is then sized by selecting the required mass flow. The SFC is minimised by altering eFPR to invoke the optimum ratio of bypass velocity to core velocity that is required for constant eBPR. The SFC represents the efficiency of the DP fans and engine, and is calculated by taking the fuel flow of a single engine and dividing it by half the total aircraft thrust requirement

or aircraft drag force. This process is repeated to assess the performance of different TS cases.

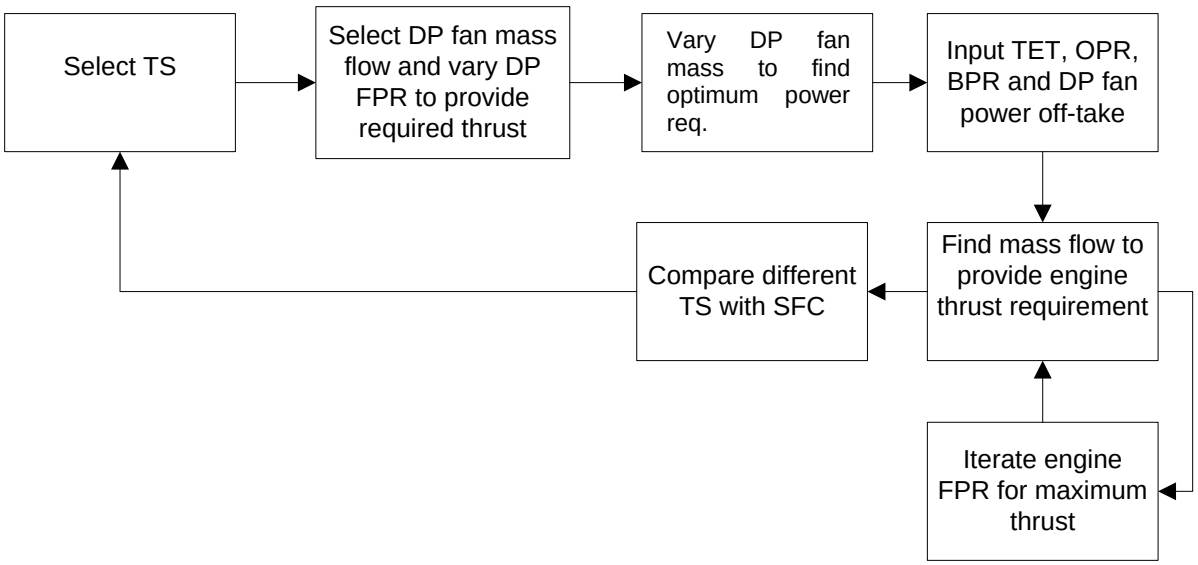

Figure 5.1 - Propulsion system design-point process

5.1.3 BLI method and assumptions

Figure 5.2 illustrates the parallel stream method adopted to model the flow properties through the fan and nozzle, where the free-stream and boundary layer stream through the fan are modelled separately and are subsequently mixed before the nozzle. This method provides a more accurate prediction of the fan power than through assuming a single stream with average flow conditions. This is because the fan is not 100% efficient and the mass flow average inlet total pressure of the two streams would invoke a different thermal efficiency to if two different inlet total pressure streams were modelled. The conditions at station 2 are found from the boundary layer properties, which are obtained from the derivation within this section. In order to calculate the pressure ratio of one stream by knowing that of the other, either use of a fan map must be made or a constant static pressure assumption must be adopted. If a fan map were available, then by choosing a FPR and calculating the non-dimensional mass flow for one stream, a constant speed line could be chosen for both streams and by calculating the non-dimensional mass flow of the other stream, a FPR for that stream would be obtained. However, developing an iterative

based procedure to do this would require more time than by assuming a constant static pressure at the fan outlet and obtaining the missing FPR through knowledge of the inlet conditions. Therefore, the latter method has been adopted for the parametric analysis. The mixing zone enables the total temperatures and pressures to be equated from mass flow averaged values at stations 3 and 4. Averaging these quantities is useful as it simplifies the thrust calculation process and the error in doing so is assumed to be small.

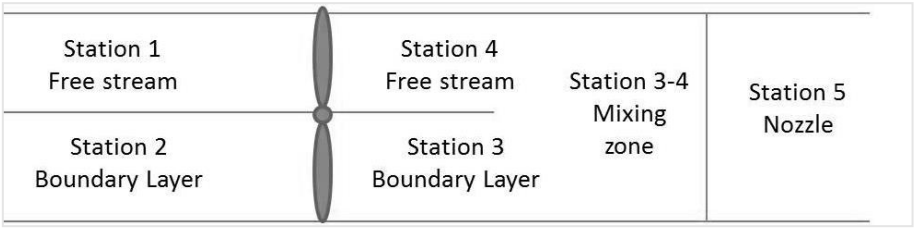

Figure 5.2 - Parallel stream method

Two methods exist that account for the benefit available through ingestion of the boundary layer stream and are described in detail in Chapter 4. The first method is known as the outer control-volume method. It assumes the mean boundary layer velocity is equal to the free-stream velocity and the DP fan net thrust requirement is equal to the aircraft drag multiplied by the TS minus the profile drag (skin-friction + form drag) that relates to the flow that scrubs the aircraft surface before ingestion into the DP fans. The second method is known as the inner control-volume method and is illustrated in figure 5.3. Equation 5.1 is used to calculate the DP fan net thrust requirement and is equal to the total aircraft drag multiplied by the TS. The ϕ terms represent the forces acting from the aircraft to the flow and F denotes forces acting from the propulsor to the flow, where subscripts $_{G1}$ and $_{G9}$ denote gross thrust and momentum drag respectively. The method assumes the DP fan intake velocity is equal to an area-averaged value. The advantage of this method is that the aircraft drag accounting remains unchanged, simplifying the aircraft drag calculation, and the boundary layer effects are only accounted for by the propulsion system. The difference in inlet velocity requires that the DP FPR changes between the outer and

inner control-volumes to provide a fixed thrust. As a result the power output varies for the same overall thrust requirement. This is due to the difference in thermal efficiency caused by varying the DP FPR, as in the case of the single versus parallel stream method. The inner control-volume is the best representation of reality as the reduced momentum is what the fan would actually be exposed to.

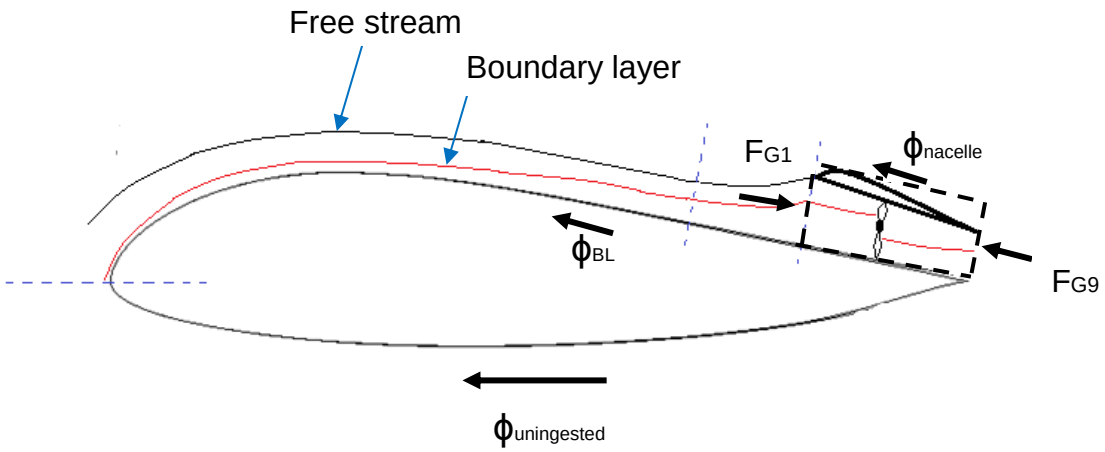

Figure 5.3 - Inner control-volume method

$$F_{net,DP\ fan} = F_{G1} - F_{G9} = \left(\phi_{uningested} + \phi_{BL} + \phi_{nacelle}\right) \cdot TS \qquad \textbf{(5.1)}$$

In order to calculate the boundary layer flow properties at the fan inlet, the 2D CFD code XFoil was used to obtain the momentum and displacement thicknesses of the Eppler 336 aerofoil used in Chapter 6. A mathematical derivation was developed by the author to convert these parameters to boundary layer mass flow and average velocity. It should be noted that this is all original work by the author.

The displacement thickness δ* is a theoretical quantity that is equivalent to having a thickness of zero flow that has been removed from a free-stream velocity flow that is equivalent to the flow reduction caused by a boundary layer of height δ. The momentum thickness δ_m is based upon the same premise but describes the momentum lost in the boundary layer. The displacement and momentum thicknesses are defined in equations 5.2 and 5.3 respectively. U denotes the

boundary layer edge velocity and is approximated as 99% of the free-stream velocity. u denotes the velocity as a function of y, which is the distance from the wall. ρ is density and subscripts $_{BL}$ and ∞ denote boundary layer and free-stream conditions respectively, where ρ_{BL} is a function of y.

$$\delta^* = \int_0^\infty \left(1 - \frac{u}{U}\right) \frac{\rho_{BL}}{\rho_\infty} dy \qquad \textbf{(5.2)}$$

$$\delta_m = \int_0^\infty \frac{u}{U} \left(1 - \frac{u}{U}\right) \frac{\rho_{BL}}{\rho_\infty} dy \qquad \textbf{(5.3)}$$

An empirical constant has been assumed that converts the displacement thickness to the boundary layer height using equation 5.4. For a flat plate the constant C is roughly 8.0, however the value of 4.0 was assumed to account for the adverse pressure gradient effect an aerofoil has on boundary layer growth, which was taken from a previous study by Rolls-Royce and the origins of it are confidential. It should be noted that if δ* is fixed, the smaller C gives a smaller boundary layer height, δ. This shows that flows with lower values of C have a lower momentum per unit mass flow. Aerofoils actually possess much larger values of δ* for at a given length of plate than flat-plates do (illustrated in figure 4.21), therefore if δ happened to be equal in both cases then the mass flow reduction due to the boundary layer or equivalently δ* would be much lower for aerofoils.

$$\delta = \delta^* \cdot C \qquad \textbf{(5.4)}$$

The average velocity u_m is obtained by first defining the boundary layer flow rate per unit depth for constant density, using equation 5.5. Equation 5.6 is the well-established Law of the Wall expression that assumes the velocity magnitude away form a wall is logarithmic, where n is the index to be prescribed for a given boundary layer. Inserting equation 5.6 into 5.5 and integrating with respect to y within the limits of zero and δ yields equation 5.7. This shows that the area averaged boundary layer velocity does not explicitly depend on δ, although n does depend on δ.

$$u_m \cdot \delta = \int_0^{\delta} u \, dy \tag{5.5}$$

$$\frac{u}{U} = \left(\frac{y}{\delta}\right)^n \tag{5.6}$$

$$\frac{U}{n+1} = u_m \tag{5.7}$$

The next stage is to obtain an expression for n. Inserting equation 5.6 into equation 5.3 and assuming $\delta\rho_{BL} / \delta y = 0$ or in other words $\rho_{BL}=\rho_\infty$, gives equation 5.8.

$$\delta_m = \int_0^{\delta} \left(\frac{y}{\delta}\right)^n \left(1 - \left(\frac{y}{\delta}\right)^n\right) dy \tag{5.8}$$

Integrating with respect to y and rearranging into a quadratic of n produces,

$$\delta_m = \delta\left[\frac{1}{n+1} - \frac{1}{2n+1}\right] = \delta\frac{n}{2n^2+3n+1}$$

$$2n^2 + n\left(3 - \frac{\delta}{\delta_m}\right) + 1 = 0 \tag{5.9}$$

Using the quadratic equation formula to solve equation 5.8 for n gives,

$$n = \frac{\left(\frac{\delta}{\delta_m} - 3\right) - \sqrt{\left(3 - \frac{\delta}{\delta_m}\right)^2 - 8}}{4} \tag{5.10}$$

u_m is now obtained by inserting equation 5.10 into 5.7. The boundary layer mass flow is then simply equal to the product of u_m, δ, ingested span and ρ_∞.

A numerical analysis was performed by assuming $\delta\rho_{BL} / \delta y \neq 0$ and the results showed that $\delta\rho_{BL} / \delta y$ was small and therefore had a small effect on δ_m. Therefore, density variation effects were omitted from the method.

However, density variations can be accounted for by assuming a constant static pressure p throughout the boundary layer and a gas constant R. ρ_{BL} is then a function of boundary layer temperature t_{BL}, as show in the ideal gas law in equation

5.12. t_{BL} is a function of u in equation 5.11, where 'a' is the speed of sound and γ is the heat capacity ratio, and is inserted into equation 5.12 to give ρ_{BL} as a function u. Inserting the result into equation 5.3 yields an equation that replaces equation 5.8 and requires integration with respect to y to give a value of n. However, the author found that after integration the equation could not be written in terms of n, as δ_m became a function of n^3 .This required numerical techniques for solving and was not attempted due to time constraints.

$$T_{BL} = T_{\infty}\left[\frac{1+\frac{\gamma-1}{2}\left(\frac{u}{u_{ss}}\right)^2}{1+\frac{\gamma-1}{2}\left(\frac{u_{\infty}}{u_{ss}}\right)^2}\right] \quad \textbf{(5.11)}$$

$$\rho_{BL} = \frac{p}{RT_{BL}} \quad \textbf{(5.12)}$$

In order to obtain values of u_m for intake heights less than δ, equation 5.6 was used to find the value of u that corresponded to a value of y equal to the intake height, and then the value of u was set to equal U in equation 5.7.

5.1.4 Cooling power requirement

The first option considered for cooling was through the use of cryogenics. The cryogenic power required to cool the superconducting wiring and motors is added to the fan power requirement and is obtained using equation 5.13. The Coefficient of Performance (COP) greatly limits the achievable overall efficiency and is defined by equation 5.14, where T_{hot} and T_{cold} are the ambient and electrical temperatures respectively. Equation 7.13 includes a 33% cooler efficiency and a 99.7% overall system efficiency. The 33% encapsulates the effect that the actual efficiency will be less than the Carnot efficiency.

$$Cryo\ power = \mathrm{COP} \times 0.33 \times (\text{fan power} \times 0.997) \quad \textbf{(5.13)}$$

$$COP_{cooling} = \frac{Q_{cold}}{Q_{hot} - Q_{cold}} = \frac{T_{cold}}{T_{hot} - T_{cold}} \quad \textbf{(5.14)}$$

The second option for cooling was through the use of liquid hydrogen. Some other studies were done in parallel to the current study and showed that liquid hydrogen was a lighter and less energy demanding source of coolant. It was therefore adopted for the installed analysis in Chapter 8. However, this study had already adopted the cryo-power and so it is based upon it and it does give some insight into its effects on the propulsion system configuration.

5.2 DP installed effects study

5.2.1 Objectives and rational

This study aims to build on the results obtained in Chapter 7 by investigating the effect of varying propulsion system parameters at an installed aircraft level, using fuel-burn as the primary metric. Firstly, fuel-burn results show the potential of DP from looking at a wide design space and can be compared with previous DP studies. Secondly, knowledge of the sensitivity of the propulsion system configuration can be useful in order to understand how technology level and system design influence the overall DP performance.

Chapter 7 evaluated the propulsion system by optimising the DP fans through varying DP FPR and mass flow to minimise the power requirement. The engine performance was then accounted for through assessing SFC. However, fuel-burn may be reduced further if the DP fan mass flow is reduced to below that corresponding to the optimal DP fan power requirement, due to the reduced mass and drag.

Since DP system installed effects have been shown to affect the optimal DP system configuration significantly, an off-design assessment has been carried out to understand the implications of sizing the propulsion system at climb-ceiling and take-off EoR.

5.2.2 Component installation effects

The drag of the DP fans and engine were accounted for in the same way as in Chapter 6. The DP nacelle drag was assumed to be zero due to the mostly embedded nacelle positioning in the aircraft surface and the common nacelle housing. The engine nacelle drag was accounted for using the nacelle dimensions, where the nacelle width was estimated to be 1.3 times the fan diameter and the nacelle length estimated to be 1.5 times the nacelle width. These values were provided by Rolls-Royce as an approximation to their empirical data.

5.2.3 DP fan system mass

The DP fan system mass, M_{fan}, consists of the fan, inlet and outlet ducts and nacelle housing and was estimated in Chapter 6 using the in-house engine tool. However, the full calculation process is time consuming and a more rapid method is required to parametrically assess a number of fan sizes. Therefore, the mass was approximated using a developed simple scaling law, equation 5.15. This assumes the DP fan system mass is proportional to its area and therefore the square of its diameter. $M_{fan,1}$ denotes the fan system mass corresponding to the fan diameter d_{fan1}, and $M_{fan,2}$ denotes the fan system mass corresponding to the fan diameter $d_{fan,2}$. $M_{fan,1}$ of 2150kg and $d_{fan,1}$ of 0.56m were taken from a simulation in Chapter 6 and used as the datum values for this study.

$$M_{fan,2} = \frac{{d_{fan,2}}^2}{{d_{fan,1}}^2} M_{fan,1} \quad \textbf{(5.15)}$$

5.2.4 Engine mass

The turbofan engine mass was estimated in Chapter 6 using an in-house tool that accounts for each component of a gas turbine. Again, in order to rapidly parametrically assess a number of engines, a scaling method has been developed for the current study and it uses the engine mass results from a previous simulation of the in-house weighting tool used in Chapter 6. In order to account for both changes in engine size and eBPR, equation 8.2 and equation 8.3 were used to obtain the final engine weight, $M_{eng,3.}$ The datum engine weight $M_{eng,1}$ was taken from the study in Chapter 6 as 6900kg per engine with a diameter $D_{eng,1}$ of 2.565m for a

EBPR=15. If the new eBPR changed, then the new fan weight was calculated by multiplying a proportion of the datum engine mass by a scaling factor. The datum fan weight was found to be approximately 10% of the datum engine weight for the BWB aircraft turbofan engine in figure 5.4 (rotors plus stators mass) taken from a simulation in the Chapter 6. Figure 5.4 was taken from a simulation done on T&W and BWB turbofan engines with Rolls-Royce's engine weighting tool Genesis [50]. The scaling factor, $\frac{{d_{eng,2}}^2}{{d_{eng,1}}^2}$, was obtained by assuming the core size remained fixed and using equation 5.16 to equate the new fan mass flow M_{total}, giving the fan diameter $d_{eng,2}$. A mass flow ratio, defined as the ratio of fan face flow velocity to free-stream velocity, was assumed equal to unity, along with the equivalent density ratio, as this simplified the diameter calculation. If the eBPR remained constant, then $d_{eng,1} = d_{eng,2}$ and the term in the brackets equals unity and the scaling is done on the whole engine alone with $\frac{{d_{eng,3}}^{2.7}}{{d_{eng,2}}^{2.7}}$. Once the eBPR has been accounted for, the change in engine mass flow is accounted for by scaling with the 2.7 power law. This index was taken from [61] and has been reduced from the third power to account for non-scalable items such as bolts and sheet thickness. $d_{eng,3}$ denotes the fan diameter that corresponds to $W_{eng,3}$ and is found from the mass flow of that engine.

$$BPR = \frac{M_{total}}{M_{core}} - 1 \qquad \textbf{(5.16)}$$

$$M_{eng,3} = M_{eng,1}\left(0.9 + 0.1\frac{{d_{eng,2}}^2}{{d_{eng,1}}^2}\right)\frac{{d_{eng,3}}^{2.7}}{{d_{eng,2}}^{2.7}} \qquad \textbf{(5.17)}$$

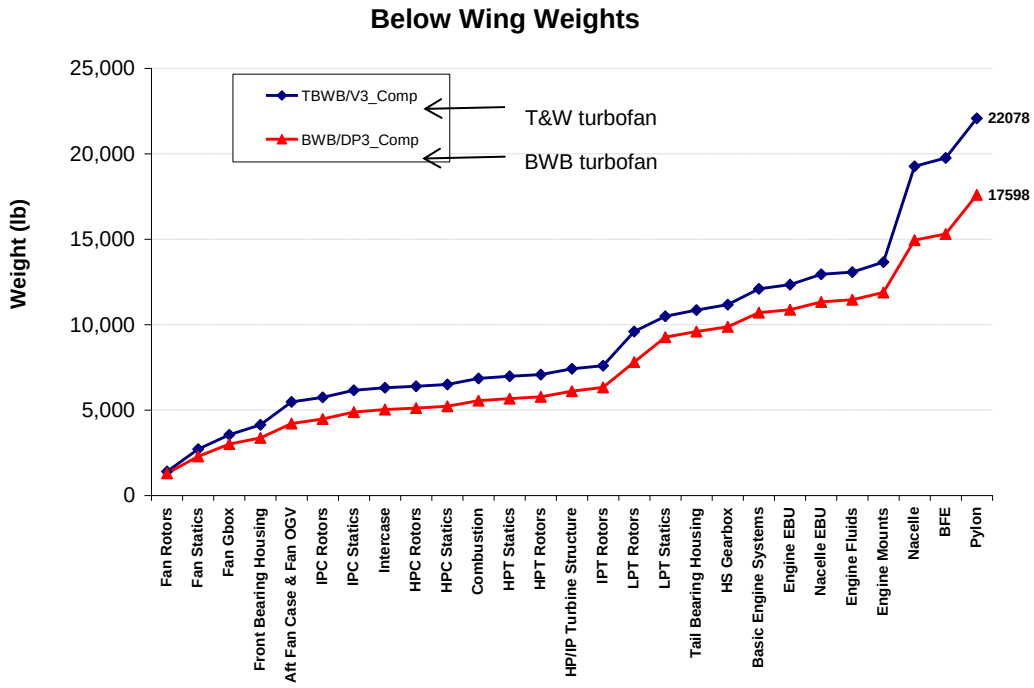

Figure 5.4 - Weight component build up for BWB turbofan[2]

5.2.5 Electric system mass

The electrical system consisted of motors, generators, cabling, protective earth system, superconducting fault current limiter and cooling system. The method used is the same as that in Chapter 5 Section 6. The motors and generator mass calculations required knowledge of rotational speed and power, whilst assuming a capability of 70Nm/kg. The cabling mass was calculated assuming 2kV and 1000Amps/kg/m capability, where current is equated from knowledge of power and voltage, and the lengths were obtained from the aircraft geometry.

Liquid hydrogen cooling was adopted. The hydrogen coolant mass was calculated from the internal heat generation during flight, which was equated to the product of the mission time, distributed fan power and a 0.2% transmission loss. The mass was then found using the latent heat of evaporation of hydrogen. Equation 5.18 was used to calculate the storage tank mass, where a tank efficiency of 60% was assumed.

$$0.6 = \frac{Hydrogen\ mass}{Hydrogen\ mass + tank\ mass} \qquad \textbf{(5.18)}$$

As the liquid hydrogen coolant can be utilised as a secondary fuel after the cooling stage, the kerosene fuel mass was reduced accordingly.

5.2.6 Off-design modelling

The engine performance tool Turbomatch is capable of modelling the engine in off-design, although a fan alone cannot be modelled in off-design. Therefore, the DP system and engine were accounted for by treating them as one engine with some modifications to approximate the overall performance in Turbomatch. This was done by assuming a bigger turbofan fan that represented the DP fans and turbofan fan and making the following changes.

It was found that the optimum DP fan mass flow increased with TS, defined as the ratio of DP fan thrust to total thrust, and therefore different TS's have been accounted for by changing the eBPR. As the isentropic efficiency and the inlet/bypass duct loss of the DP fans and engine are different, a mass flow mean average value for each parameter was taken to account for both systems. Table 5.2 shows the parameter values used.

	DP fans	**Engine**
Isentropic efficiency	0.92	0.945
Duct pressure loss	2%	1%

Table 5.2 - DP fan and engine parameters

The BLI method chosen for the design point studies uses the inner control-volume method, where the DP fan intake velocity equals the average boundary layer velocity. It is difficult to change this intake velocity to an average value that accounts for the different effects on the engine bypass and core streams. Therefore, the outer control-volume was adopted as this requires an intake velocity equal to the free-stream velocity and the total thrust requirement is reduced to account for the BLI benefit; both of which can be modelled using Turbomatch. The climb-ceiling condition was found to require the largest thrust relative to the cruise and EoR conditions. Therefore, it is expected that the boundary layer drag force would be

higher. Rather than obtaining the BLI benefit for the climb-ceiling condition through CFD calculation, which takes significant time, the same proportion of the total thrust requirement for the cruise case was used for the climb-ceiling case.

The cruise condition was kept as the design-point as the overall engine efficiency should be highest during this phase. A maximum TET of 2100K was selected from the Vision 20 studies in chapters 5 and 6 to simulate the same engine technology level and the value was adopted for the climb-ceiling. The mass flow was then varied to provide the climb-ceiling thrust and the cruise TET was altered to provide the cruise thrust. The cruise eFPR was optimised whilst keeping the OPR fixed at 56.0 and ensuring the intermediate and high pressure compressor ratios were equal. An EoR condition was simulated, where the max TET was input and a check was done to establish whether the EoR thrust was sufficient. The EoR SFC was not required as the aircraft tool calculates take-off fuel-burn by using an empirical expression, given in chapter 5.

6 Results and analysis

6.1 Vision 20 T&W aircraft

6.1.1 Tool validation and baseline T&W design

Once the conceptual design tool was built, it was used to model the Boeing 787 and compared with data from a Piano simulation from public domain data [55]. The non-dimensional geometry parameters such as AR and T/C were input, which provided an assessment of the mass, drag and performance prediction modules. During the conceptual design tool simulation the engine tool was omitted from the process and replaced by a linear thrust variation with a density delta function for simplicity. This method disregards specific thrust effects and captures the overall thrust effects. The errors between the tools in table 6.1 are relatively low for a first attempt synthesis, where the highest errors occur from the use of empirical formulae and the simplistic thrust assumption. MZFW denotes Max Zero Fuel Weight. Here n/a means that the information was not available in the public domain.

Parameter	Boeing	Piano	Current tool	Tool delta %
MTOW (kg)	227,933	215,912	210,987	-2.3
OEW (kg)	n/a	108,500	107,752	-0.7
MZFW (kg)	n/a	154,223	150,426	-2.5
MLW (kg)	n/a	165,563	158,228	-4.4
Wing mass (kg)	n/a	27,233	27,327	0.3
Power-plant mass (kg)	n/a	16,090	15,120	-6.0
Fuel total mass (kg)	n/a	87,044	82,002	-5.8
Span (m)	60	59	62	4.75
Wing area (sqm)	n/a	359	359	-0.2
Net cruise thrust (kN)	n/a	113.5	106.7	-6.0

Table 6.1 - B787 data comparison; delta column compares Piano [55] and current tool studies

Next, the conceptual design tool, coupled with an engine performance tool was used to model the baseline A350 aircraft, providing a second comparison and further calibration of the tool. The empirical engine mass relation was replaced with the engine weight tool and the climb-ceiling thrust requirement was calculated using the more accurate aircraft mass, as well as the increased accuracy of the SFC and thrust values from the engine performance tool. AR and T/C were varied to assess their drag and mass effects and the optimum values, in terms of fuel-burn, were similar to the public domain values in table 6.2. The largest difference occurred in the wing area, resulting from the low MLW. This is due to the approximate freight mass assumption, described in Section 3 of this chapter, which directly affects the MLW. The calculated L/D was 20.8, and although public domain data for the L/D could not be found, it is expected to be similar to the B787 value from [45].

Parameter	Public domain (A350)	Current tool (A350)	Tool delta %
MTOW (kg)	298,013	298,618	0.2
OEW (kg)	150,005	149,630	-0.2
MLW (kg)	228,522	225,889	-1.2
Wing area (sqm)	440	434	-1.4

Table 6.2 – A350 simulation tool comparison

The A350 simulation gave a close match to the public domain data confirming the tool's accuracy for conceptual design modelling purposes.

6.1.2 Advanced vs baseline (A350) T&W aircraft

The key variables for the T&W aircraft were AR and T/C. Figure 6.1 shows a plot of various advanced T&W designs, which are determined by the specific AR and T/C combinations. Mission fuel-burn was used as the performance metric. The optimum AR is 11.0 and whilst a T/C of 0.11 provides an optimum, the value of 0.115 is chosen as the efficiency penalty is small and in reality the extra fuel-burn would be offset by the structural benefits obtained through having a thicker wing.

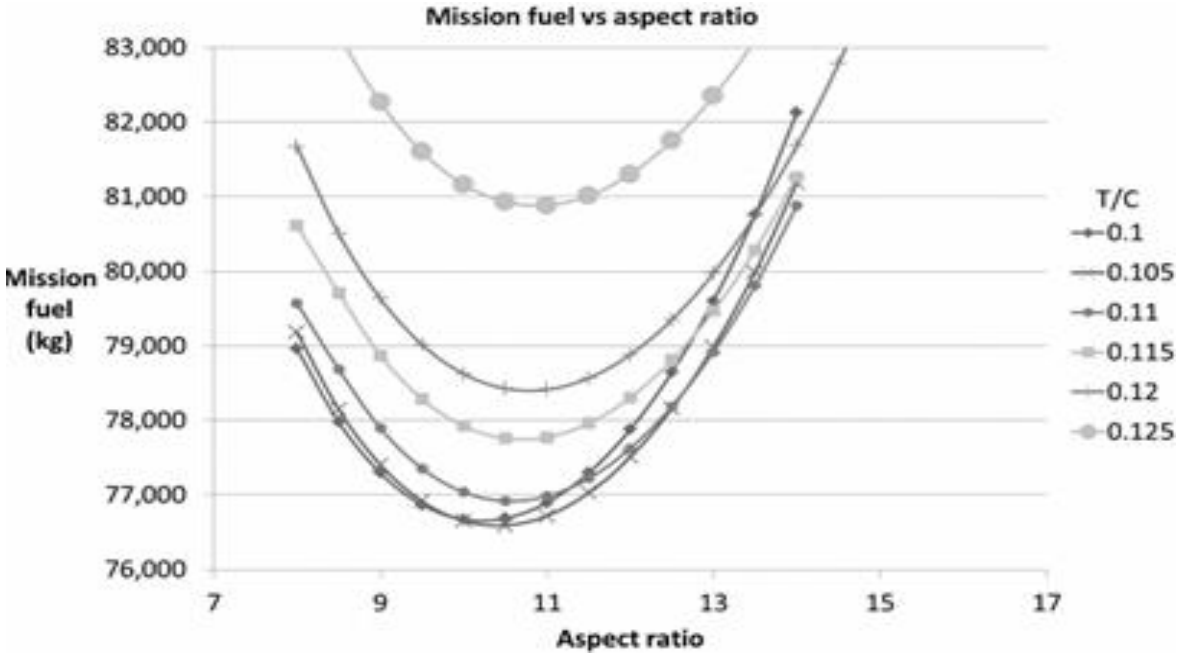

Figure 6.1 - Advanced T&W fuel vs. aspect ratio plot

The advanced T&W's trend of L/D with T/C in figure 6.2 elaborates on the result found in figure 6.1. As the wing thickens, the wave drag increases exponentially; producing an expected result.

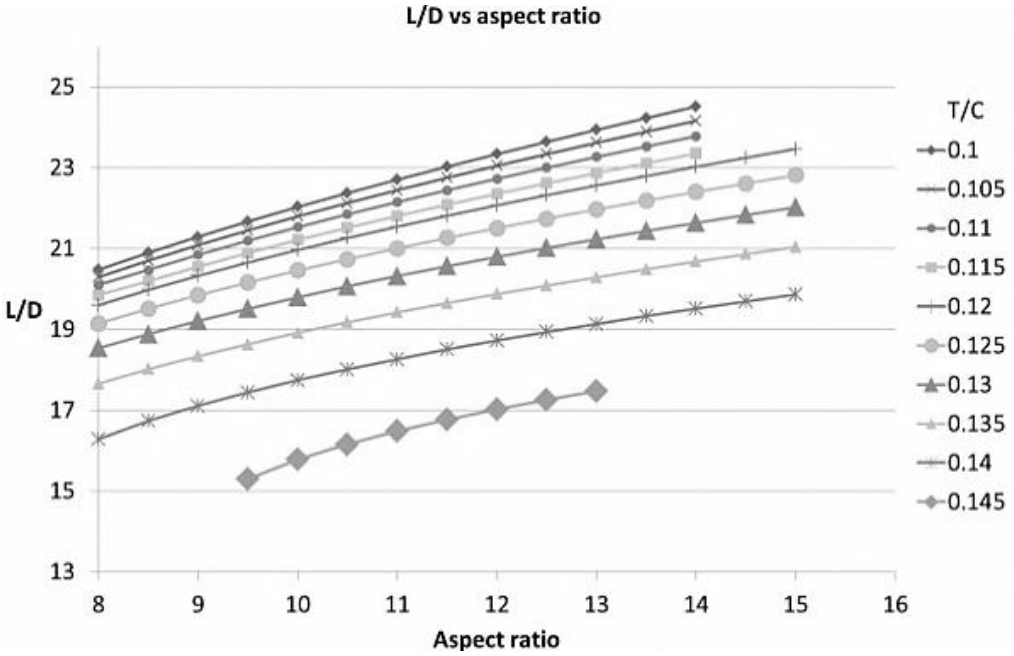

Figure 6.2 - Advanced T&W L/D vs. aspect ratio plot

The optimum design was compared with the baseline aircraft and the results are presented in table 6.3. The delta column is defined as the advanced T&W minus the baseline T&W and reflects the benefits from the future technology assumptions. The climb-ceiling altitude has risen as a result of the lower MTOW and higher L/D. This coupled with the increased propulsion system efficiency has reduced the fuel-burn by 27.5%. This increased efficiency is around half of what is required to meet NASA's N+3 target. The N+2 aircraft for 2020 service entry, targets a 50% fuel-burn reduction relative to a B777-200LR powered by GE90-115B engines, whilst the N+1 aircraft for 2015 service entry targets a 33% relative reduction [2]. Because the A350 is due in 2013, the N+2 aircraft is likely to be fairly optimistic and the advanced T&W performs somewhere between the N+2 and N+3 aircraft.

Parameter	**Baseline**	**Adv. T&W Delta %**
Aspect ratio	9.60	16.7
Thickness/chord	0.105	6.7
Wing area (sqm)	434	-19.7
Span (m)	65	-4.7
MTOW (kg)	298,618	-23.4
Wing mass (kg)	35,261	-22.8
Fuselage mass (kg)	33,008	-12.5
Empennage mass (kg)	4,430	-22.8
Equipment/Gear mass (kg)	47,779	-31.5
Operational mass (kg)	5,250	0.0
Payload design mass (kg)	33,310	0.0
Mission fuel mass (kg)	**106,038**	**-27.5**
Mid-cruise altitude (ft)	34,883	3.7

Table 6.3 - Baseline and advanced T&W aircraft data compared

The schematic in figure 4.12 displays the reduction in wing and empennage size, and increased nacelle size for the advanced T&W, due to the added efficiency induced by the future technology assumptions.

Both aircraft were designed to reach climb-ceiling, defined as the start cruise altitude, in approximately 25 minutes, as shown in figure 6.3. The kink in the graph is due to the acceleration from 250kts to 320kts at 10kft, shown in table 4.1. This is normal for civil airliners in order to decrease climb fuel and time and was taken from Jenkinson's mission profile [38]. The advanced T&W climbs faster due to its increased aerodynamic efficiency and higher climb TET. However, it may be advantageous to maintain the same climb rate for both aircraft, to increase component life and enhance propulsion system reliability. This provides an area for further study.

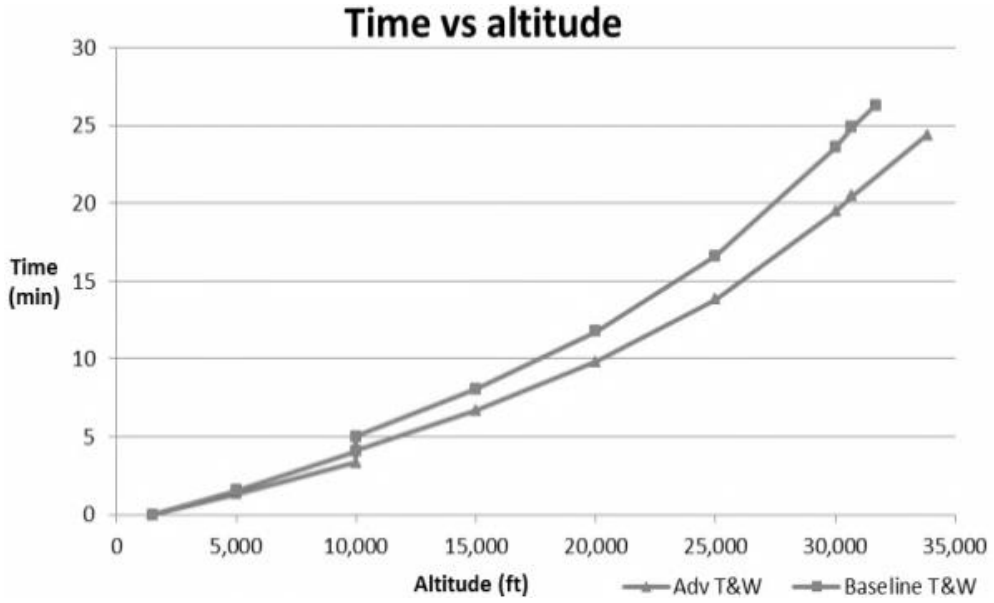

Figure 6.3 - Climb time vs. altitude comparison

6.1.3 DP T&W vs. advanced T&W performance

Figure 6.4 provides a visual comparison of the DP and advanced turbofan engines. By having a TS, the DP system mass flow enables the main turbofan eBPR to decrease; decreasing engine mass flow and hence engine fan diameter. This,

coupled with the lower SFC and thrust requirement, reduced the turbofan fan diameter by 19.2%.

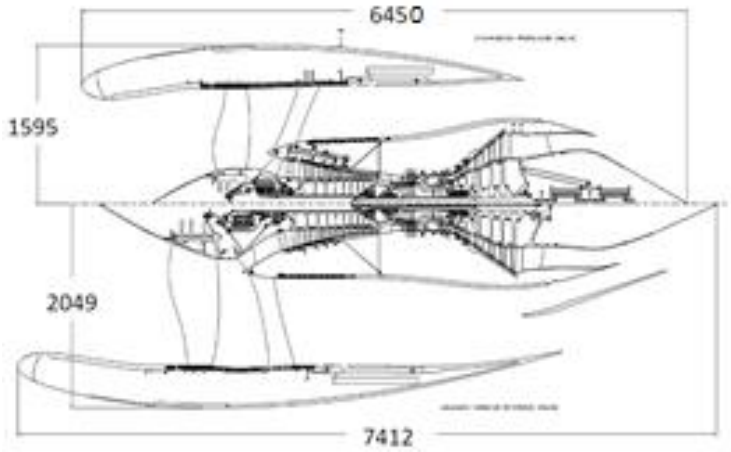

Figure 6.4 - DP T&W (top) and advanced T&W (bottom) turbofan engine comparison (dimensions in mm)

Table 6.4 shows the effect of reducing DP FPR, where for a fixed turbofan specific thrust, turbofan eBPR increases. Collectively the engine and DP system increase propulsive efficiency and reduce SFC. For this study the 1.4 DP FPR case has been chosen.

Parameter	**DP T&W**			
DP FPR	1.7	1.6	1.5	**1.4**
SFC delta (%)	1.5	-1.3	-2.1	**-2.5**
Thrust-Split	0.64	0.57	0.51	**0.45**
Turbofan BPR	4.3	6.08	8.03	**10.26**

Table 6.4 - DP system optimization; SFC data relative to Advanced Turbofan

Table 6.5 shows the comparison between the advanced T&W and the DP T&W. The reduction in mission fuel mass achievable shows potential in the DP and BLI technologies. Even though the overall propulsion system weight increased, the lower SFC and turbofan nacelle profile drag is sufficient to provide a modest benefit.

Parameter	DP T&W
Turbofan engine mass delta	-6.7%
DP fans/housing/ducts mass (kg)	2,118
Electrical system mass (kg)	1,331
Total propulsion system mass delta	17.9%
Aspect ratio	1.8%
Thickness/chord	0.0%
MTOW	-0.6%
Mission fuel mass delta	**-4.1%**

Table 6.5 - DP T&W results; delta values (DP FPR=1.4) relative to advanced T&W

Table 6.6 shows the results from a sensitivity analysis that was conducted by varying the propulsion system mass to a high and a low technology value, by assuming realistic technology assumptions. The corresponding fuel-burn delta values show that the original case was fairly optimistic and assumes fairly advanced technology advances, although turbofan improvements inevitably become harder to achieve and therefore the potential for future weight reduction is limited.

Parameter	DP T&W (low) %	DP T&W (high) %
Power-plants mass	-4.7	24.5
Mission fuel mass	-0.87	5.8

Table 6.6 - Power-plant sensitivity analysis; fuel mass relative to original DP T&W case

6.1.4 Conclusions

Matching the baseline aircraft to B787 and A350 public domain data provided a convenient method to compare and calibrate the conceptual aircraft design tool. Simulating the baseline A350 aircraft gave a design to within a few per cent of the actual design and the variables optimised closely to the actual values.

The advanced T&W aircraft was modelled using advanced technology assumptions, of which the key changes were the reduced weight through composites, increase in aerofoil efficiency, increase in engine thermal and propulsive efficiency. The design produced a 27.5% fuel-burn decrease.

The DP T&W design provided a further 4.1% fuel-burn reduction, where the increased propulsion system weight and inlet duct pressure losses restricted any extra potential benefit. The duct loss is assumed to be based on historic S-shaped duct design and the design has not been optimised.

6.2 Vision 20 BWB aircraft

6.2.1 Validation exercise

A validation exercise was carried out on the BWB structural mass calculation method to check its accuracy. Cranfield University has previously modelled a variety of civil/military BWB's and has created a statistical average of the structural component weights as a fraction of the MTOW [37]. The current study BWB design was compared with the statistical values and the results are shown in table 6.7. It was found that the individual component weights were different due to the unique aircraft geometry, however, the total airframe mass difference was small; an important result as this directly affects performance.

% MTOW			
	Current study BWB	**Cranfield BWB's**	**% Difference**
Covers/spars	5.73	6.53	-12.3
Ribs	2.74	3.83	-28.4
Secondary items	4.24	3.39	25.1
Nose	1.44	0.79	82.1
Payload provision	3.46	2.37	46.0
Apertures	0.53	1.30	-59.3
Total	18.14	18.10	0.2

Table 6.7 - Cranfield airframe component mass fraction comparison47

Another validation study was performed on the BWB mass estimation method. A comparison was made by modelling a BWB designed by Bristol University using extensive public domain data from [47]. Initially the overall drag and mass values were artificially set to that of Bristol's results and the calculation of the airframe components were compared as shown in table 6.7. It can be seen that the conceptual design tool (current tool) under-estimates the airframe mass. However

the Bristol method uses finite element analysis and the analysis in [47] describes the mass as particularly conservative. Through speaking with an expert from Rolls-Royce's aircraft performance department, the Cranfield design project was deemed higher fidelity than the Bristol University design project, which helps underwrite the Vision 20 BWB's accuracy.

Component (kg)	Bristol tool	Current tool	% Difference
Outer wing	22548	18619	-17.4
Control surfaces/winglets	5097	13687	168.5
Inner wing	83898	52487	-37.4
Nose	2933	7307	149.1
Overall airframe	114476	92100	-19.5

Table 6.8 – Bristol BWB simulations compared using current tool and Bristol tool [52]

Table 6.9 shows a comparison between the drag coefficients of a BWB design by Bristol University [62], the same design modelled using the current study design tool and the Boeing Sugar Ray BWB [63]. CDi denotes the induced drag coefficient, CDw is the wave drag coefficient and V_{App} is the approach velocity. The zero-lift drag (CD0) differed the most from the Bristol and Boeing studies, although this difference was virtually eliminated by changing the reference area from the planform area to a trapezoidal wing section, and therefore the total CD was similar to the other aircraft.

Parameter	Current study	Bristol University[52]	Boeing Sugar Ray[53]	Cambridge/ MIT/ Cranfield[18]
CD0	0.0025	0.0064	0.0060	n/a
CDi	0.0045	0.0042	0.0047	n/a
CDw	0.0006	0.0004	0.0006	n/a
Total CD	0.0076	0.011	0.0127	n/a
W/S	**184**	**346**	**203**	**207**
VApp (kts)	**145**	**185**	**103**	**N/A**
Cruise Mach	**0.85**	**0.85**	**0.7**	**0.8**
Cruise altitude (ft)	**44,605**	**37,000**	**40,800**	**~42,000**

Table 6.9 - Aircraft data comparison [52,53,18]

The aircraft tool doesn't account for wave drag on the inner wing due to the assumption that shock waves do not form on the adopted reflex aerofoil. This assumption is imposed since it was not possible to calculate the complex effect of boundary layer and shockwave interactions with fan blades. Also, the shock waves were predicted to be detrimental to fan performance from past Rolls-Royce experience and were therefore not desired in the flow. Instead, the inner wing was assumed to have a low enough CL from the aerofoil shape and geometric twist, whilst the outer wing was supercritical and the wave drag equations were able to account for the shock waves.

The BWB turbofan aircraft was then modelled using the current tool and table 6.9 shows a comparison of the performance results with the Bristol, Boeing and Cambridge / MIT / Cranfield BWB aircraft, where W/S is the ratio of MTOW to reference wing area. The Bristol BWB adopts a high landing speed and a high wing-loaded design; jointly producing a lower cruise altitude. The Boeing BWB cruises at a lower altitude through the lower Mach no. The Cambridge / Cranfield / MIT BWB is the closest design to the Vision 20 BWB, whilst all three designs demonstrate that high cruise altitudes are intrinsic to BWB configurations.

6.2.2 BWB turbofan results

Figure 6.5 illustrates the basic geometry of the BWB turbofan and table 6.10 provides the results. The geometry is a direct output of the aircraft codes structural and aerodynamic calculations and therefore doesn't include some of the characteristics seen on other BWB concepts, such as emergency exit fuselage roof geometry and gradual contours.

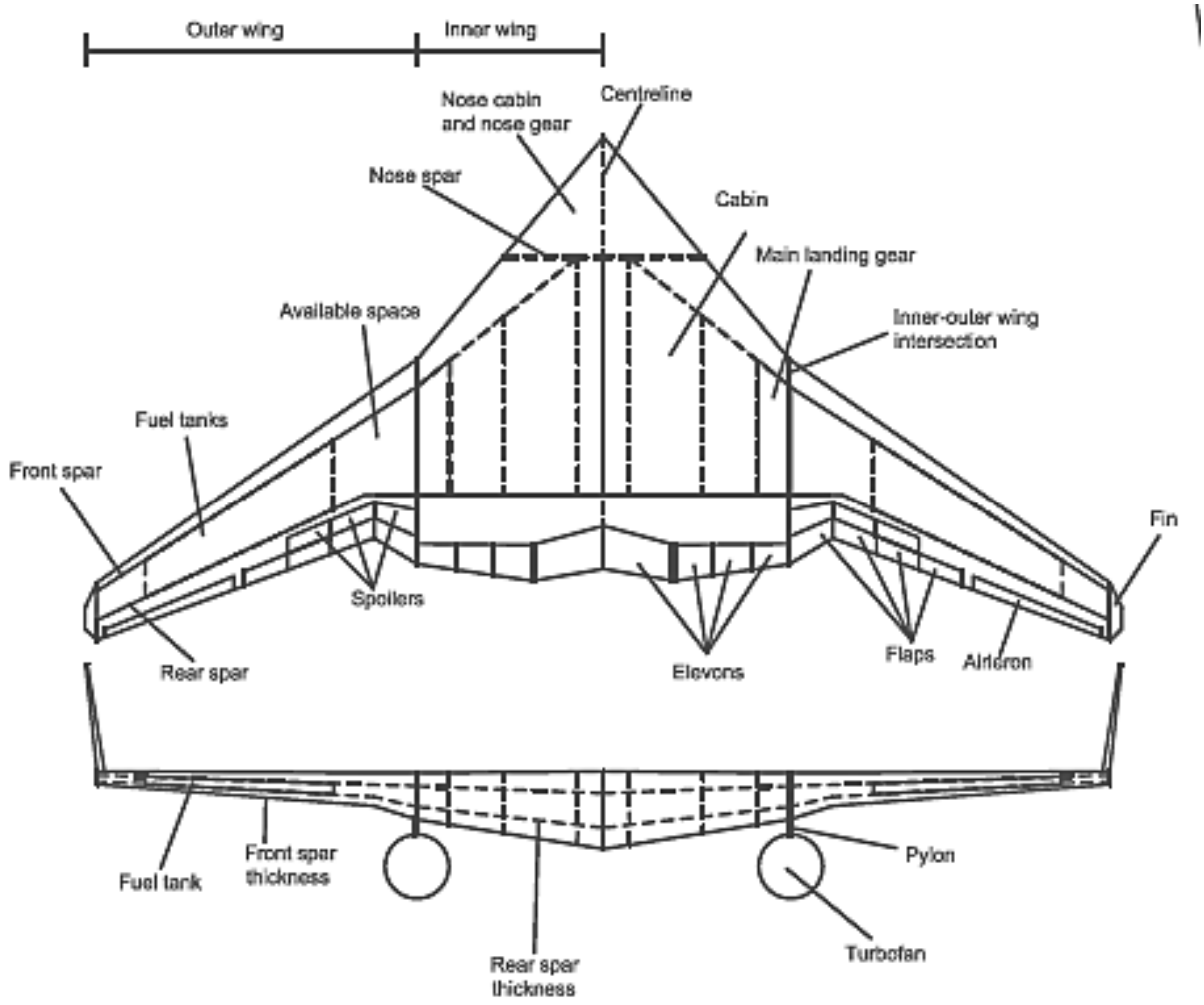

Figure 6.5 - BWB planform and side view

The BWB benefits from a large amount of free space at the inner-outer wing interconnection area. This is due to the relatively small fuel tanks required for such an efficient aircraft and the cabin geometry. Currently part of this space is allocated to the hydrogen coolant in the DP BWB variant, however, other novel propulsion related systems could also be included, such as heat exchangers and DP

mechanical transmission. Also extra freight can be positioned in these areas to help reduce the static stability margins depending on the cabin and fuel tank payloads.

Parameter	Baseline BWB
Aspect ratio (outer-wing)	5.43
Thickness/chord (MAC)	0.195
Gross wing area (sqm)	937
Span (m)	71
MTOW (kg)	203,675
Airframe mass (kg)	46,005
Power-plant mass (kg)	19,259
Equipment/Gear mass (kg)	29,145
Operational mass (kg)	5,250
Payload design mass (kg)	33,309
Mission fuel mass (kg)	**64,814**
Cruise altitude (ft)	44,605

Table 6.10 - BWB turbofan results

Due to the high aerodynamic efficiency of the BWB concept, the cruise altitude was relatively high and a 3.38m fan diameter was required to provide enough thrust at the top-of-climb altitude where the air density is particular low. As a result the engine weight, as well as nacelle profile drag increased significantly. In addition, flying at a high altitude can cause issues for the crew such as excess solar radiation exposure. This, together with the aforementioned issues, provided the rational to investigate three alternative BWB-turbofan designs.

6.2.3 High approach speed – 147kts

The wing area is sized by the landing condition and becomes smaller as the landing speed is increased for a given CL and MLW. Because a smaller wing will optimise at a lower cruise altitude for a given MTOW, the landing speed was increased from

145kts (which is standard for A350 type aircraft) to 147kts to assess the sensitivity. The result in table 6.11 shows that a much larger velocity increase would be required to affect the cruise altitude sufficiently, and the fan diameter only reduced from 3.38m to 3.25m. Also because the inner wing (payload area) is fixed, the reduction in overall area forces the outer-wing AR to decrease, increasing vortex drag and reducing L/D.

Parameter	High V_{App}	Low CL	0.8 Mach
Mission fuel mass delta	-0.1%	+10.3%	-3.8%
Cruise altitude delta	-1.2%	-15.2%	-5.2%

Table 6.11 - Alternative BWB designs

6.2.4 Lower CL - 38000ft cruise altitude

The BWB was then restricted to flying at a cruise altitude of 38kft through reducing the cruise CL by 27%. The fuel-burn increased drastically due to the significant reduction in L/D, despite the fan diameter reducing from 3.38m to 2.98m. This case was neglected for further study due the severe lack in efficiency.

6.2.5 0.80 cruise Mach number

The cruise Mach number was then reduced from 0.85 to 0.80 to allow the aircraft to fly lower with the same aircraft CL's and wing sizing requirements. This design offers the best solution due to the significant reduction in cruise altitude and fuel-burn. The fan diameter reduces to 3.18m and the engine weight was considerably less. Most other BWB designs in public domain literature fly slower to obtain the benefits from flying lower, however the 0.85 Mach design provides a more competitive solution and therefore both designs are retained for further study. It is also worth noting that the 0.85 Mach design benefits from a larger wing area and more BLI.

6.2.6 Turbofan engine positioning

The aft-turbofan positioning resulted in a separation of 20.7% of aircraft span between the engine centre-lines. This meant that the benefit from the reduced fin

area associated with moving the engines laterally inwards was partially offset by the wing structural bending relief reduction from the engines and the reduced fin size. This effect is evident in both the 0.85 and 0.80 Mach number aircraft designs, as can be seen in table 6.12, where the cruise altitude and fuel-burn difference are negligible.

6.2.7 BWB stability results

The locations of the aircraft component weights were altered until an acceptable static stability margin was achieved. Table 6.6 shows that the margins only exceeded the ±5% range when the fuel tanks were full at take-off, in the aft-turbofan cases. Reducing the cruise Mach number reduces the margin slightly due to the fuel-burn reduction. It is worth noting that currently there are issues with unstable aircraft both technologically and legislatively. However, BWB aircraft hinge on unstable aircraft being acceptable and electrical systems being reliable enough, therefore the values here are considered generally acceptable for this conceptual design study.

Comparison type	Parameter	0.85 Mach	0.80 Mach
Aft-turbofan vs under-wing turbofan delta %	Mission fuel mass	-0.2	-0.2
	Cruise altitude	0.0	0.0
BWB under-wing turbofan stability margin %	MTOW	-5.5	-5.0
	MLW	5.1	5.9
BWB aft-turbofan stability margin %	MTOW	-8.1	-7.9
	MLW	2.2	2.7

Table 6.12 - 0.85 and 0.8 Mach no. aft-turbofan vs under-wing turbofan configurations

6.2.8 DP BWB results

The DP turbofan diameter reduced to 1.93m and the DP FPR was kept at 1.4 in accordance with the T&W DP system. Table 6.13 shows the small reduction in SFC achievable with the DP system relative to the BWB turbofan variant. This is in part because the BWB contains a large mass flow to boundary layer momentum deficit ratio, which amplifies the effect of the assumed duct losses relative to the DP T&W aircraft. Additionally, the large TS of 56% lowers the turbofan eBPR and thus results in a small SFC difference. However, the DP benefit is transferred into a reduction in propulsion system weight, of which was due to the reduction in engine weight. Because the BWB has a high cruise altitude and large engine diameter, and thrust and weight vary with the fan diameter, the reduction in the turbofan BPR and increase in DP fan size produces a net saving in weight and drag. The overall fuel-burn reduction is then largely due to the installed effects with the current assumptions for intake pressure losses.

It can be seen that the DP fans weight has increased relative to the DP T&W due to the larger fan diameter and number adopted. However, the BWB's reduced cruise thrust and thus power requirement decreases the electrical system weight relative to the T&W DP variant.

Parameter	DP BWB
DP FPR	1.4
SFC delta	-0.3%
Cruise TS	0.56
Turbofan eBPR	7.48
Turbofan engine mass delta	-29.8%
DP fans/housing/ducts (kg)	2,648
Electrical system (kg)	1,192
Total mass delta	-9.8%

Table 6.13 - DP BWB power-plant results (DP FPR=1.4); delta values relative to BWB turbofan

Figures 6.6 and 6.6 show the fuel-burn saving of the DP BWB relative to the BWB turbofan baseline aircraft, for two per cent and one per cent BLI duct total pressure loss cases. These losses are associated with both the inlet and nozzle outlet ducts of the BLI fans. The fuel savings are shown in incremental form to signify the relative effects of each aircraft and propulsion attribute. The line correlation shows the summation of the increments in sequence. The total fuel-burn reduction for the design case with two per cent DP fan duct total pressure loss gives a 5.3% fuel-burn saving, but if duct loses were to decrease to one per cent the fuel-burn saving would increase to 7 per cent. Therefore very low loss inlet and outlet ducting is an essential design requirement for the DP fan installation.

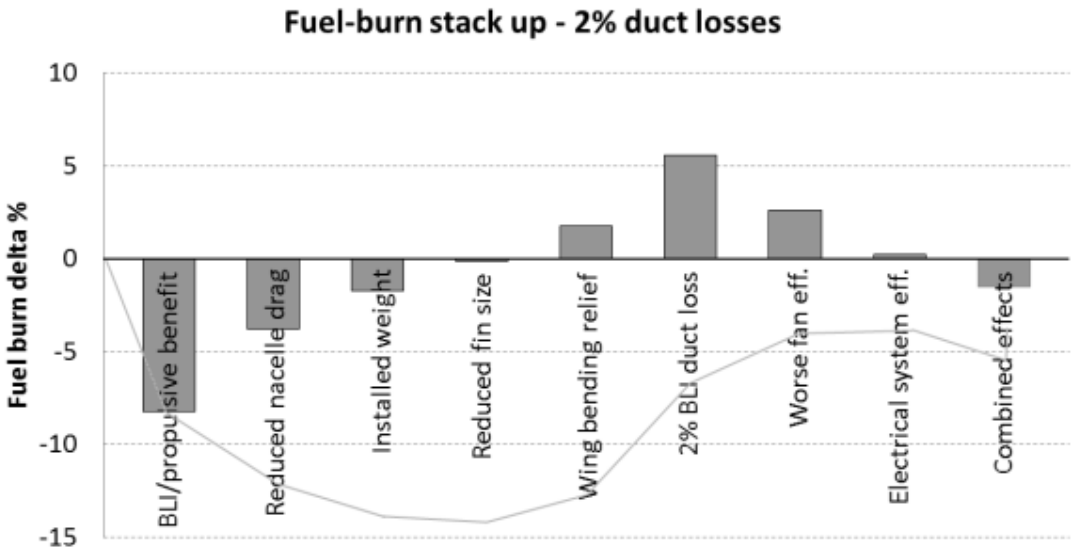

Figure 6.6 - DP BWB fuel-burn relative to baseline BWB turbofan – 2% duct loss

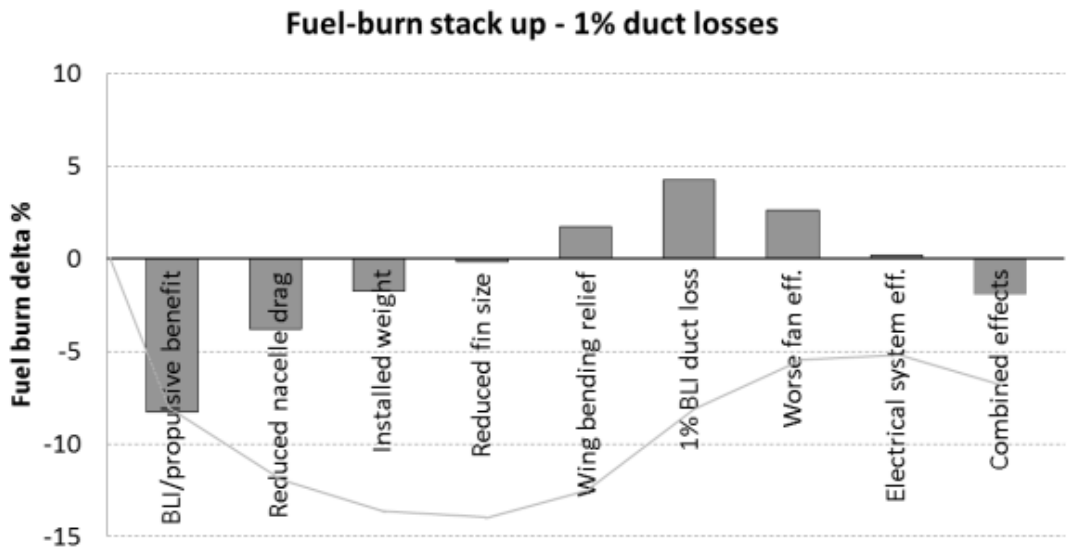

Figure 6.7 - DP BWB fuel-burn relative to baseline BWB turbofan – 1% duct loss

In general, a comparison between the BWB and T&W aircraft performance is not made due to incompatible assumptions and the inherent difficulty in validating the BWB. Instead, the turbofan and DP system have been compared as competing technologies on the same aircraft configuration. However, the DP concept appears to provide a larger proportional benefit to the BWB aircraft, although this is not the same as actual fuel-burn difference. A full parametric analysis remains to be conducted to identify the maximum potential of both aircraft. It can be predicted that the industry is unlikely to adopt both electrical superconductivity and DP technologies simultaneously.

6.2.9 Conclusions

The conceptual aircraft design tool used in Chapter 5 has been modified to enable the BWB modelling. A validation exercise has been conducted to assess the mass and drag accounting results and close agreement was found with previous BWB studies.

A BWB turbofan was successfully modelled to provide a baseline for DP assessment. Alternative BWB designs were produced to reduce the cruise altitude in aid of reducing the engine size and weight.

The DP BWB was modelled and the results showed a 5.3% reduction in fuel-burn relative to the BWB turbofan baseline when two per cent duct losses were included. The fuel savings rose to seven per cent when duct losses were reduced to one per cent; highlighting the sensitivity of DP to duct losses.

It is unlikely that the DP system will buy itself onto the market with a 5% reduction in fuel-burn relative to the turbofan, since the expensive redesign of other dependant systems would render it unfavourable. However, the analysis so far has been fairly restrictive due to the assumptions made. Instead by exploring the wider design space more deeply, further reductions in fuel-burn may be possible.

6.3 Parametric study results and discussion

6.3.1 BLI fan performance

An initial study assessed the performance of the BLI fans with a 4% duct total pressure loss for a TS of 40%. In general, the parametric investigation considers 2% and 4% duct losses, rather than 1% and 2% losses, as the 4% case was assumed to be a worst case scenario that would enable a clear comparison with the 2% case, and the 2% case was assumed to be a realistic case. The 40% TS case values were taken from the Vision 20 BWB study in Chapter 6 as they provided a good starting point. Figure 6.8 shows that increasing DP FPR up to a critical point produces choked fans. Further increases in FPR require a relatively higher pressure rise to generate the same increase in specific thrust, for constant total thrust. This is because the added pressure cannot be converted to momentum thrust and is expelled from the nozzle as pressure thrust, which is less efficient since the force vectors point in all directions. The boundary layer stream experiences a higher pressure rise as more energy is added to the flow relative to the free-stream, due to fan's ability to impart more energy to the lower momentum flow. This effect becomes more pronounced as the pressure differential becomes larger.

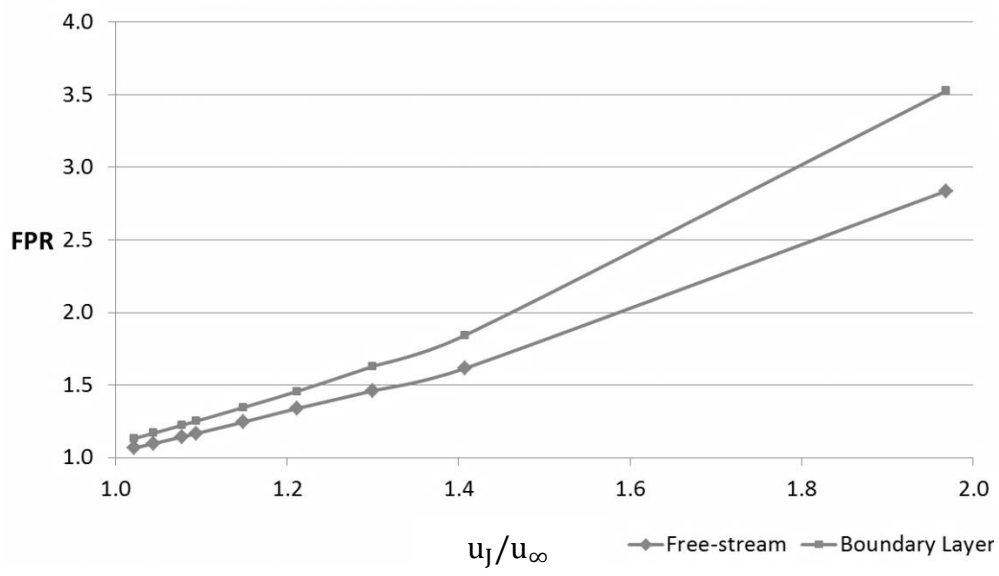

Figure 6.8 - FPR vs uJ/u∞ - 40% TS, 4% duct loss

Figure 6.9 shows that mass flow decreases with increasing pressure ratio for constant thrust, thus providing an increase in specific thrust. As DP fan mass flow

decreases it has been assumed that the boundary layer mass flow remains constant and the free-stream mass flow reduces until the only the boundary layer mass flow is available. This provides an optimal solution due to the boundary layer benefits. A letter box intake has been assumed, such as in figure 6.9, and the total mass flow is reduced by decreasing the vertical height.

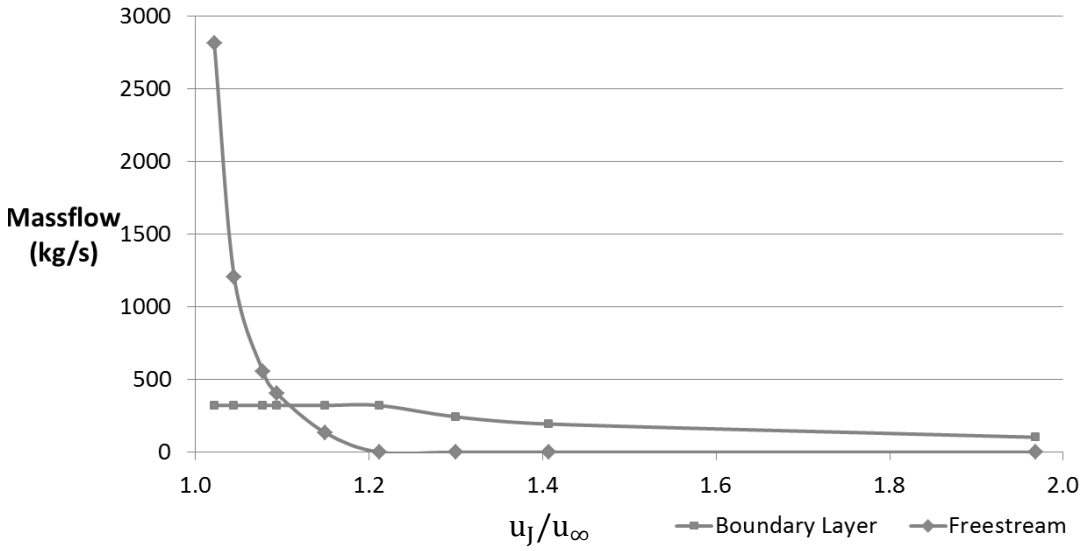

Figure 6.9 - Mass flow vs uj/u∞ - 40% TS, 4% duct loss

Figure 6.10 shows the mean inlet velocity reduces asymptotically with increasing u_j/u_∞ which is normal for fixed free-stream conditions. Under BLI conditions, decreasing the intake height within the boundary layer to reduce mass flow reduces the intake velocity more rapidly (due to the boundary layer profile). Therefore, the specific thrust increases faster, and both the mass flow and mean Mach no. decrease progressively more to account for this, thus increasing the gradient.

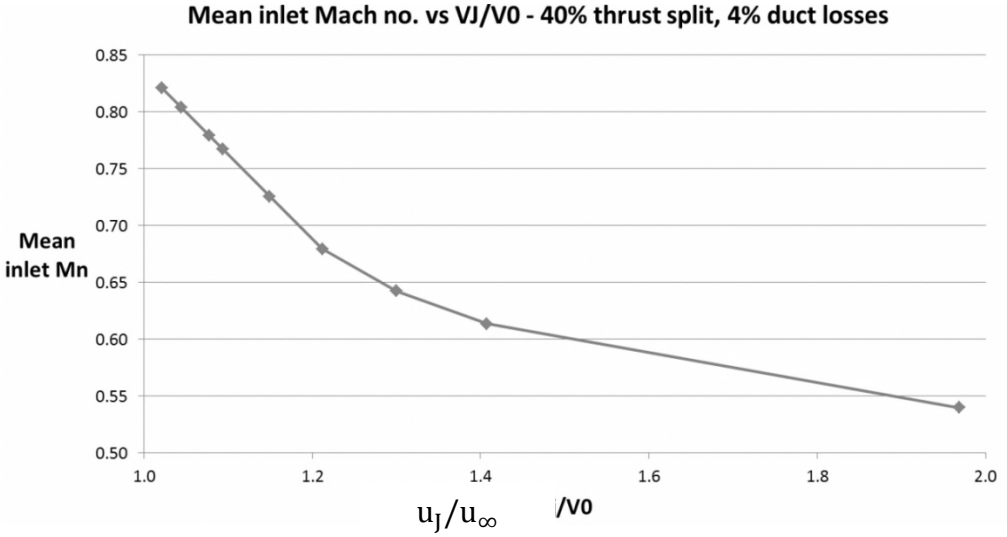

Figure 6.10 - Mean inlet Mach no. vs uj/u∞

Figure 6.11 shows a minimum DP fan power requirement at an intake height of 80% of the boundary layer height. Free-stream air and BLI cases, both without duct loss, are included for reference. A minimum power requirement in figure 6.11 exists for the BLI with 4% duct loss case. This is because the pressure rise required to overcome the duct pressure loss becomes a larger fraction of the overall pressure rise as DP FPR decreases, and FPR decreases as mass flow or intake to boundary layer height ratio increases for fixed total thrust. At low mass flows the gradient is large as the BLI benefit adds further to the propulsive efficiency effects as mass flow is increased. At higher mass flows the detrimental duct loss dominates and increases the power requirement, although the gradient is more gradual because the added propulsive efficiency associated with lower specific thrust partly offsets the duct loss effects.

Two alternative cases were simulated to provide insight into each effect; free-stream air ingestion and BLI, both without duct loss. The BLI case has an incremental power reduction over the free-stream case, which gradually diminishes as the boundary layer mass flow becomes a smaller proportion of the total mass flow. If DP were utilised without BLI, an optimum would still exist in reality due to the duct loss associated with the podded nacelle housing. However, BLI ducts are likely to incur larger duct losses due to the curved duct geometry that is required to capture the

boundary layer and enable the nacelle to be embedded into the wing.

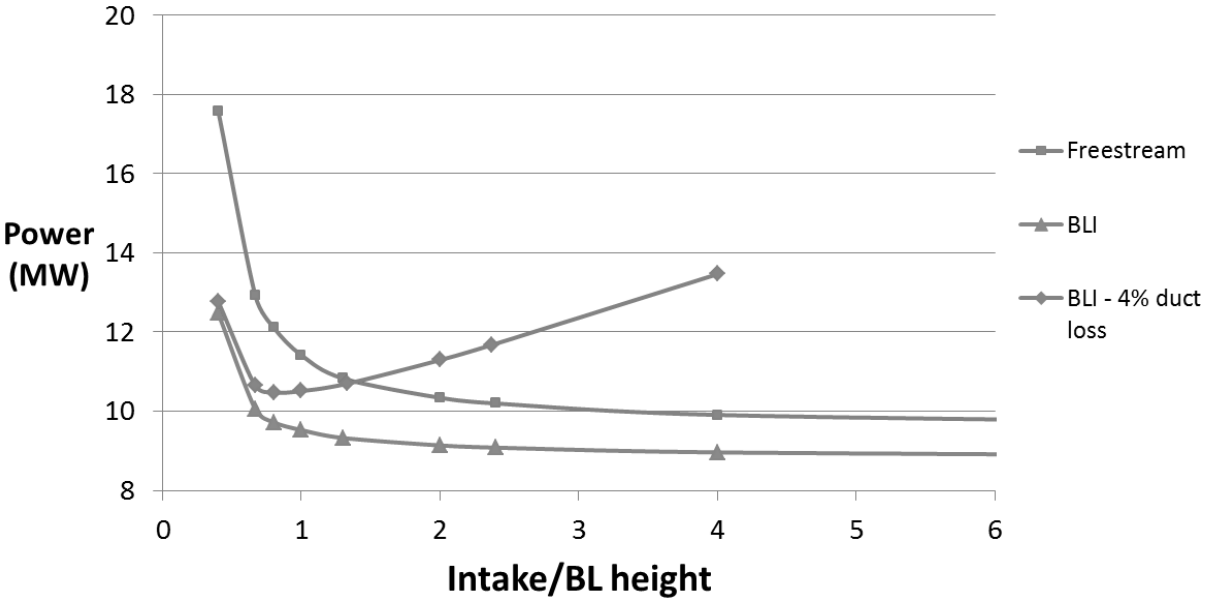

Figure 6.11 - Fan power vs intake/BL height – TS=40%

6.3.2 Whole propulsion system performance

By assessing DP at a propulsion systems level through the inclusion of a turbofan engine, a more optimal solution can be obtained. Figure 6.12 shows the results from simulating an engine that provides thrust and power to the DP fans. eFPR has been varied for each TS (defined as DP fan thrust % in the graphs) and a curve has been drawn that connects the minimum SFC for each TS case. Initially a turbofan with a eBPR of 15 was used to compare a variety of TS cases. Figure 6.12 shows a minimum SFC at around 24% TS, which is approximately 2% lower in SFC than the 40% TS case. The SFC increases dramatically at TS below 20%. This is because the optimum DP mass flow is reduced to a point where the BLI becomes small. At high TS the mass flow to achieve minimum SFC becomes larger and the duct loss dominates, providing a gradual slope similar to that identified in figure 6.11. It is worth noting that this similarity is because increasing TS effectively increases the overall propulsion system BPR for a fixed eBPR.

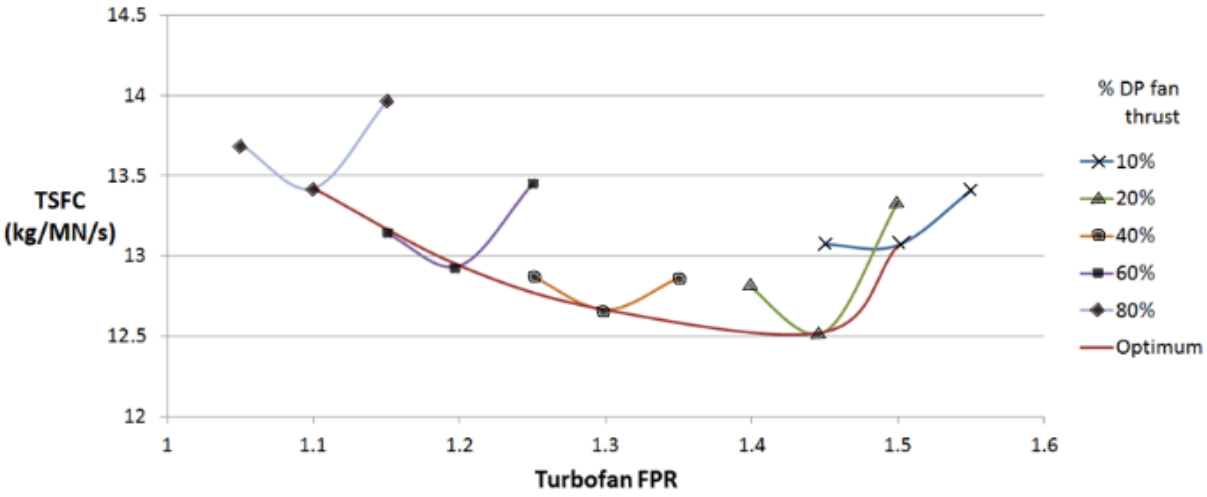

Figure 6.12 - Overall SFC vs eFPR – eBPR=15, 4% duct loss

Figure 6.12 shows eFPR increasing with decreasing TS. This can be explained by considering the average of the DP fan velocity and engine bypass stream velocity to be equivalent to an overall bypass stream velocity. If DP FPR decreases with TS, then to maintain the optimum ratio of overall bypass stream to engine core velocity (relating to internal engine and duct pressure losses), the engine bypass velocity and hence eFPR must increase.

The next step was to parametrically investigate the effect of duct loss and eBPR on SFC and to determine the change in DP system configuration. Figure 6.13 shows for fixed duct loss, increasing the eBPR raises the overall efficiency. This is due to the combined effect of the benefit in reduced turbofan specific thrust and the optimal DP fan intake height, which ingests only the lowest momentum part of the boundary layer air, therefore reducing the detrimental duct loss effects.

Figure 6.13 shows the low eBPR case to maximise performance at higher TS, since the turbofan thrust is now less efficient. Figure 6.14 shows for optimum performance a significant increase in DP fan mass flow is required at large TS to increase propulsive efficiency. It is to be expected that the added mass and drag associated with the increased DP fan duct size would reduce the effectiveness of this design, although the reduced engine weight associated with lower eBPR may offset some of this weight penalty.

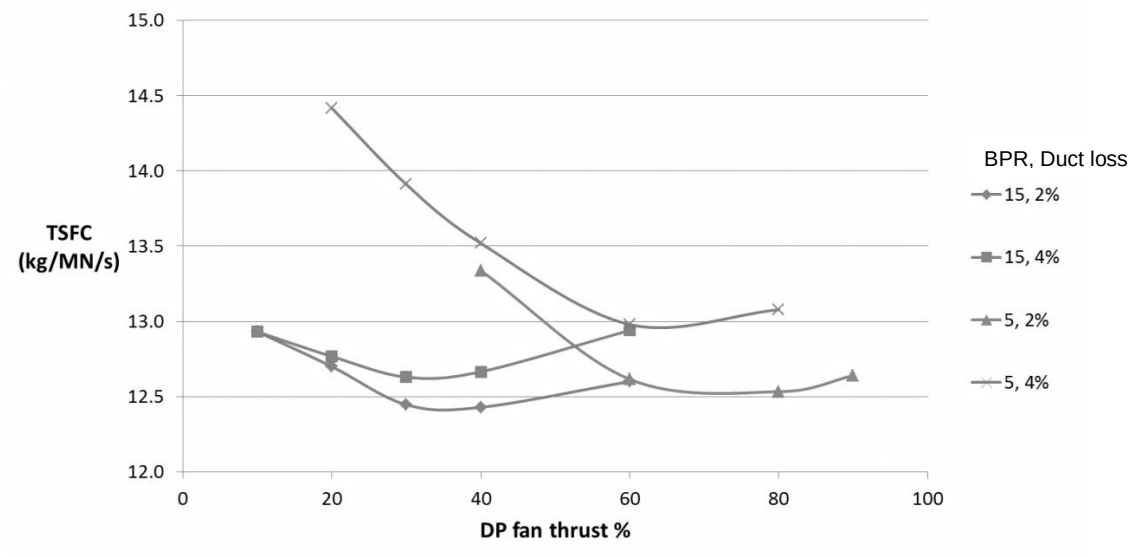

Figure 6.13 - Overall SFC vs DP fan thrust %

Changing eBPR doesn't affect the DP fan mass flow values as the DP fans are optimised for power independently. Therefore, the curves in figure 6.14 represent both eBPR cases. However, changing duct loss does have a considerable effect on mass flow. The sensitivity of the performance to duct losses is illustrated in figure 6.13, where the overall efficiency is increased substantially for the lower duct loss. Figure 6.14 shows for maximum performance the intake height increases, which allows the system to benefit from a reduced specific thrust, thus augmenting the SFC reduction. Therefore, the optimum TS also increases as a result. This benefit obtained through reducing duct loss is greater for the higher eBPR case as the larger mass flow is more sensitive to duct loss changes. As a result, the difference between the SFC values of both eBPR cases becomes small with low duct loss, illustrating both are competitive designs.

Figure 6.13 also shows how duct loss effects can be mitigated by changing mass flow. The Vision 20 study in Chapter 6 fixed the DP fan mass flow and proceeded to vary duct loss to ascertain its effect on fuel-burn. It was found that a 1% increase in duct loss resulted in around a 2% increase in fuel-burn. However, it is shown in figure 6.13 that by optimising mass flow, the TS can be lowered to decrease the SFC

penalty, where the benefit is greater for the lower eBPR case. Therefore, the 1% duct loss results obtained in the Vision 20 may be improved further.

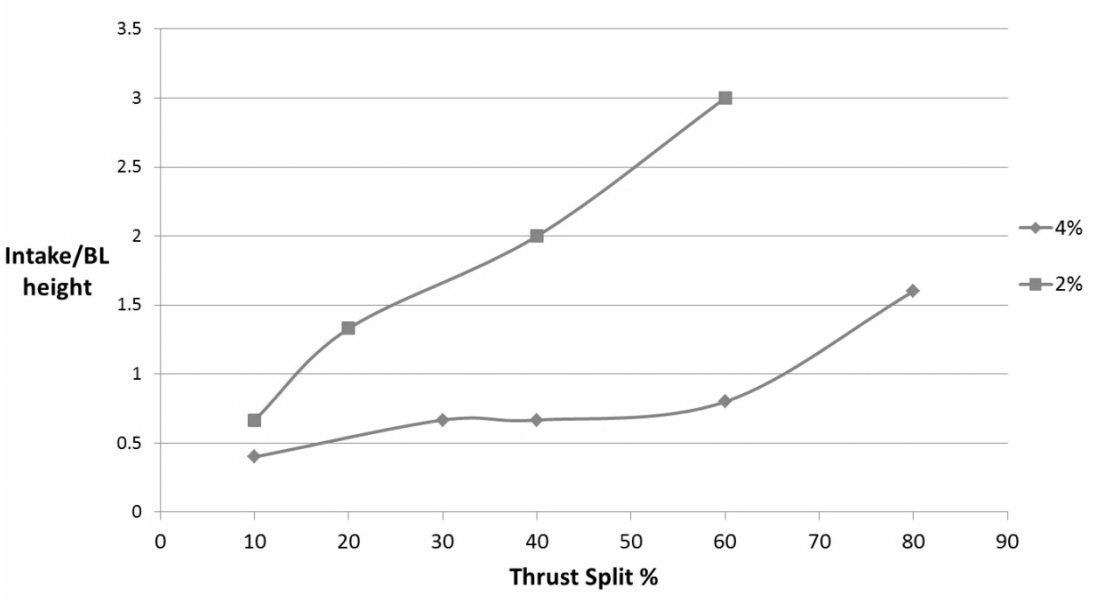

Figure 6.14 - Intake/BL height vs TS %

6.3.3 Installed propulsion system performance

Figure 6.15 provides a comparison between the theta or momentum thickness available at the nacelle highlight zone for varying number of fans and a datum point of 95% chord from the aerofoil leading edge. The nacelle size is calculated from the wing span and assumes half fan diameter spacing. Therefore, reducing fan number increases fan diameter for a fixed ingested aircraft span. As DP nacelle length is proportional to fan diameter, the fan inlet is located further upstream on the aircraft surface as fan diameter is increased. Therefore, the available theta reduces since the boundary layer is smaller further upstream. The reduction in theta becomes considerable at low fan numbers, firstly because nacelle diameter is inversely proportional to fan number and secondly because the rear aerofoil upper surface includes an adverse pressure gradient, as was seen in figure 4.21. This gradient greatly enhances the boundary layer growth (assuming the fan doesn't interact with the aircraft skin-friction drag) and therefore the performance is very sensitive to fan inlet position.

Figure 6.16 shows that for the 20% TS case, power increases with decreasing fan number, since large mass flows are not favoured due to duct loss. In addition, the installed effects become more significant as the fan number delta (relative to the reference value of 25 fans) becomes larger. The benefits are small when increasing fan number beyond the reference value, as this is region of optimum mass flow. DP now becomes a tradeoff between the fan efficiency and duct loss effects caused by scaling the propulsors, and the BLI benefits related to chord-wise nacelle positioning.

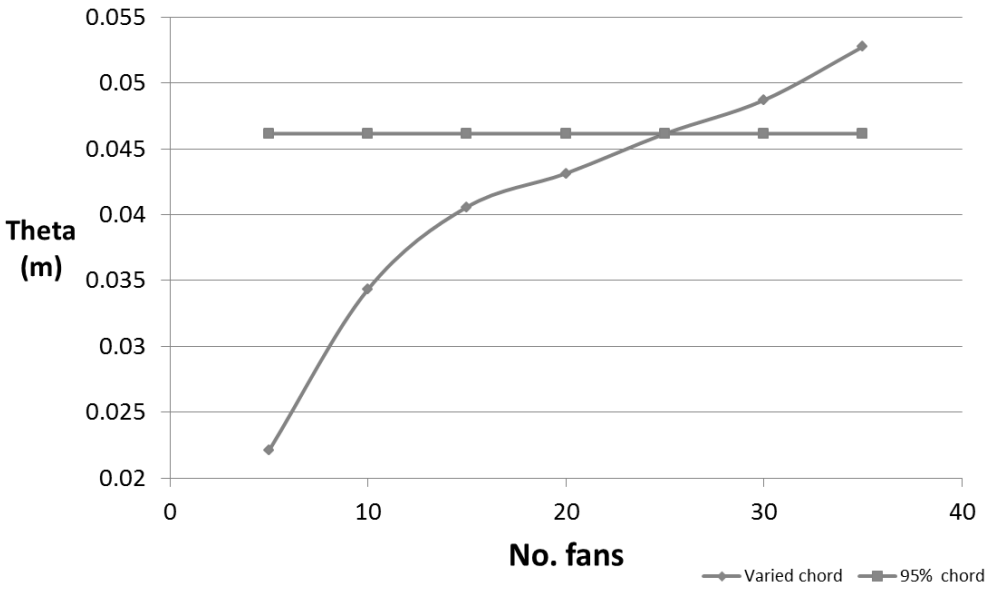

Figure 6.15 - Theta vs no. fans compared to reference study – 20% DP fan thrust

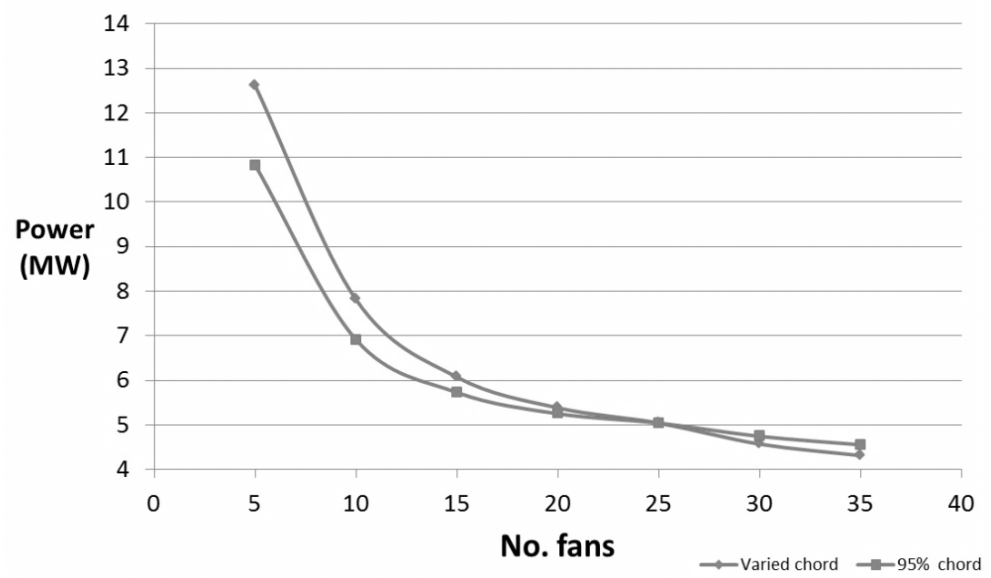

Figure 6.16 - Power vs no. fans compared to reference study – 20% DP fan thrust

6.3.4 Conclusions

A 1D performance methodology has been developed to rapidly assess DP. A mathematical derivation has been produced that converts 2D CFD results to 1D flow property relations. The Vision 20 BWB aircraft requirements were used to parametrically explore the wide design space of the DP system.

DP fan duct pressure loss was shown to produce a minimum DP fan power requirement, as large mass flows become unfavourable. SFC was evaluated by simulating the engine and the DP system. Changes in TS were found to alter the overall BPR. This meant an optimum TS existed for each case explored.

eBPR and duct loss were varied with TS to gauge the sensitivity on performance. The lower eBPR case was shown to be less efficient than the higher eBPR case, although it benefited more when duct loss was reduced due to its increased sensitivity; thus reducing the difference in performance at lower duct loss. Therefore, the possibility remains that the reduced weight of the eBPR engine may offset its propulsive performance penalty relative to a higher eBPR case.

An installed analysis was conducted to establish what effect DP fan number had on performance. Increasing fan number was shown to reduce fan size and increase the BLI benefit, as the fans were located further towards the wing trailing edge and benefited more from BLI. Detailed thermal efficiency effects associated with reduced fan and electric motor size losses were not accounted for, and would be required to accurately determine the optimum fan number and size.

6.4 Installed effects of Distributed Propulsion

The BWB design sequence used in the Vision 20 study in Chapter 4 was adopted, although, the thrust requirement of the aircraft was not iterated with the propulsion system. This reduced the assessment time considerably and was not predicted to have a large effect on the relative assessment of varying propulsion system parameters.

6.4.1 Installed aircraft performance

Figure 6.13 shows that for the eBPR of 15, increasing the duct loss from 2% to 4% provides an increase in SFC and a small decrease in TS for minimum SFC. Both duct loss cases have a minimum SFC at around 35% TS for the eBPR of 15.

By accounting for propulsion system installation effects such as drag and mass, and simulating the BWB aircraft design and mission, the fuel-burn results in figures 6.17 and 6.18 were obtained; for the 4% and 2% duct loss cases respectively. Both eBPR cases have a second curve included which is exactly the same as the standard case except the installation effects are fixed at the values obtained for the minimum fuel burn TS (defined as DP fan thrust % in the graphs) for both eBPR cases. This is at 30% for the eBPR of 15 case and 60% for the eBPR of 5 case. By doing this, it is possible to separate the effects of SFC and mass/drag on fuel-burn. For example by beginning at a TS of 30% for the eBPR of 15 case in figure 6.17 and then reducing the TS slightly, it is found that the fuel burn decreases. For the case where installed effects are fixed at 30%, reducing TS slightly actually increases fuel-burn. Therefore, the reduction in fuel-burn is due to the decreased installation effects alone which offset the detrimental SFC increase.

For the eBPR of 15 and when installation effects are included for the 4% duct loss case, figure 6.17 shows the TS for minimum SFC occurs at around 25%, which is slightly less than the uninstalled case. Figure 6.18 shows that for the 2% duct loss case the minimum TS has reduced to around 30%. Therefore, there appears to be potential in having a higher than optimal SFC in order to obtain low mass and drag, and consequently lower fuel-burn than for an optimal SFC case.

The 4% duct loss case was found to benefit more from a reduction in mass flow than the 2% loss case, since large mass flows increase the effect of the duct loss. However, the higher duct loss case does still produce a larger fuel-burn requirement and this then simply shows that duct loss effects can be mitigated by altering the design of the system but not recovered.

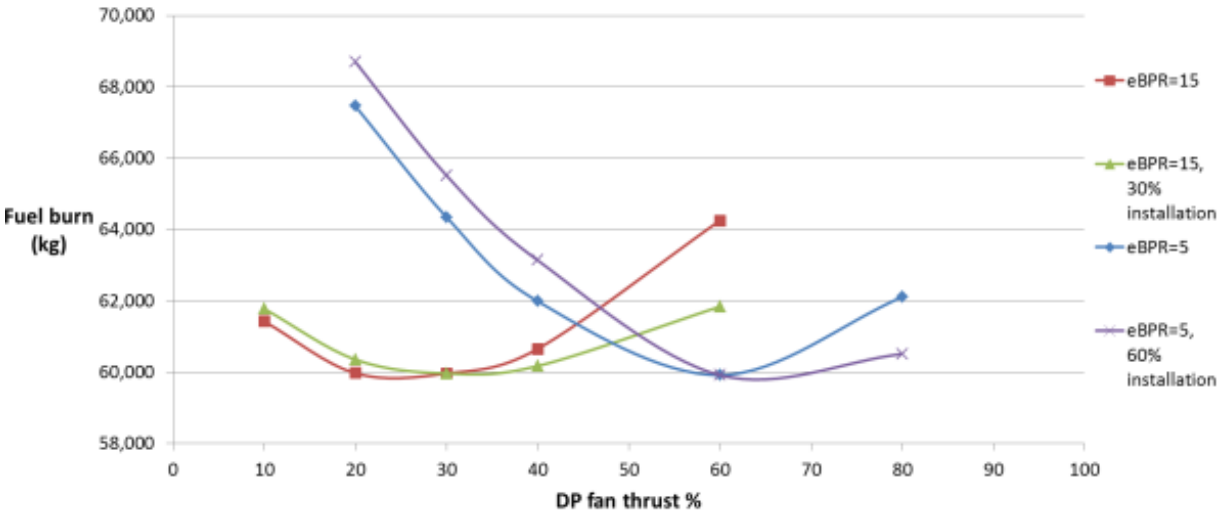

Figure 6.17 - Fuel-burn vs SFC; 4% duct loss

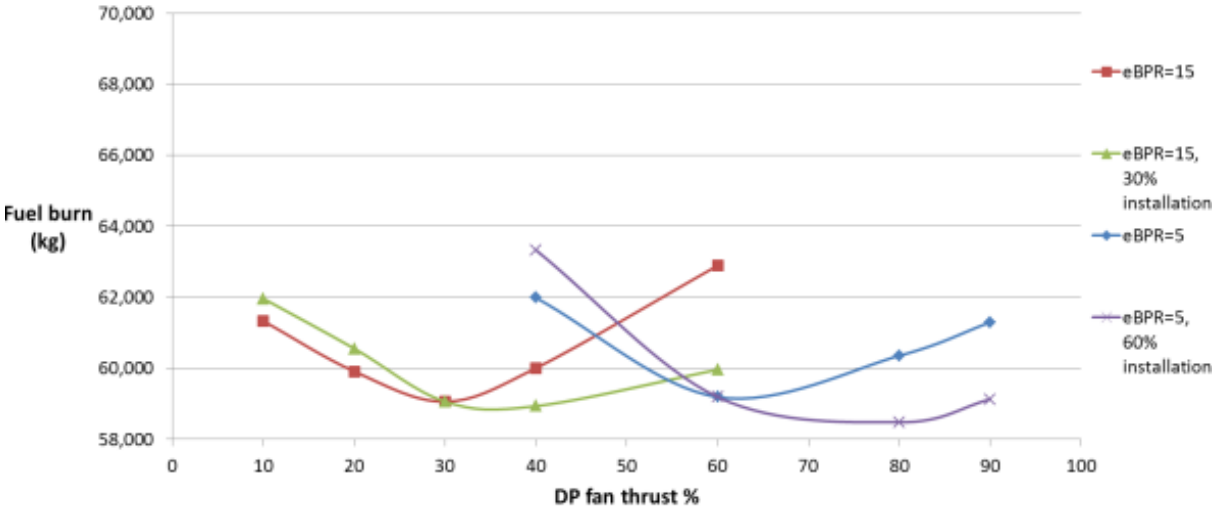

Figure 6.18 - Fuel-burn vs SFC; 2% duct loss

At a lower eBPR of 5, figure 6.13 showed that increasing the duct loss has a larger effect on SFC relative to the higher eBPR case. This is because the DP fan mass flow is larger at higher TS and therefore is more sensitive to pressure losses. As a result, the lower duct loss case has a minimum SFC at a significantly larger TS than the higher duct loss case. Figure 6.17 shows that for the 4% duct loss case the minimum fuel-burn TS reduces by around five per cent relative to the uninstalled case to around 60%. However, by decreasing the duct loss to 2% the minimum fuel-burn TS shifts from the uninstalled value of around 75% to the installed value of around 60%. This considerable change in TS can be attributed to the penalty for having heavy electrical and fan systems at larger TS and is not offset by the enhanced efficiency of having large DP fan mass flows. Therefore, it seems that for installed aircraft, TS's in the region of 80-100% are unlikely to provide an efficient option for DP.

Figure 6.19 shows the mass component breakdown for the 2% duct loss case, where for each curve the different symbols represents the different eBPR cases. Both the DP fan and electrical system mass increase with TS, due to the increases in DP fan mass flow and power requirement respectively. The electrical system mass is relatively small compare with the other masses as this study replaces the cryo-coolers with liquid hydrogen. The hydrogen has a higher calorific content than kerosene and actually reduces the kerosene fuel requirement as it serves as a secondary fuel, which is accounted for in the electrical system mass.

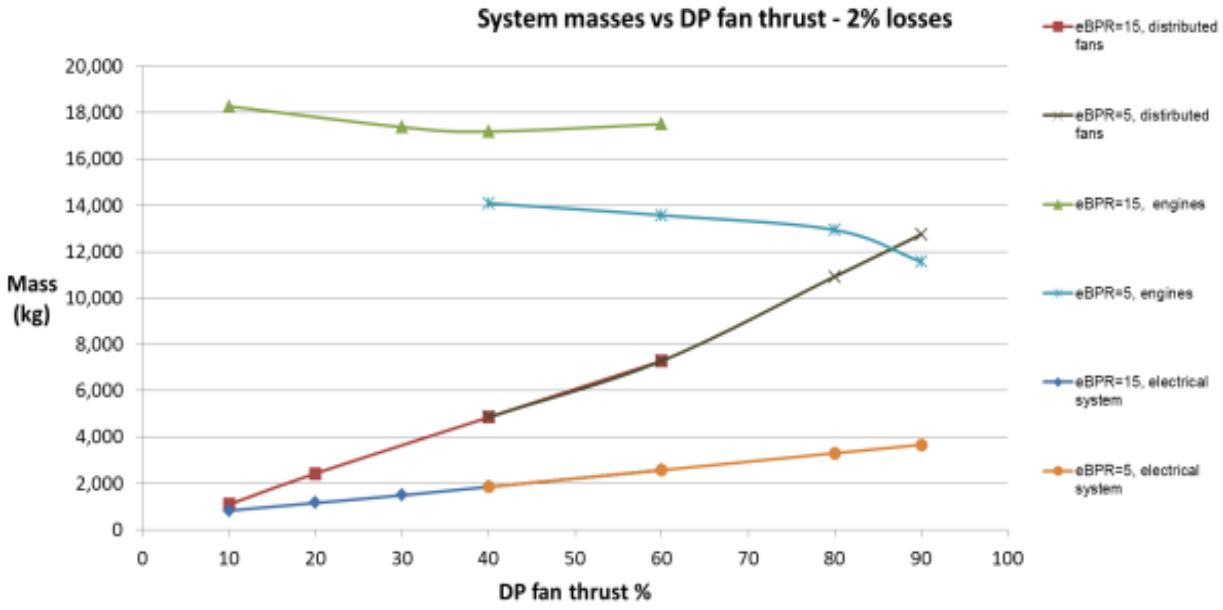

Figure 6.19 - System masses vs DP fan thrust

Both engines are shown in figure 6.19, where the step change in mass is due to the change in eBPR. This illustrates the benefit of the lower eBPR engine, as the increased specific thrust is partially off-set by this reduced mass. The engine mass varies little with TS as the overall thrust requirement remains fixed and the engine fan's mechanical power is transferred to the electrical DP fans. The small differences are then due to the changes in the overall system SFC, since the aircraft's thrust requirement is not iterated with the propulsion system in this study.

6.4.2 Optimising installed performance

Chapter 7 explored DP fan performance by first optimising fan power and then minimising SFC by varying TS. This section investigates the benefit of adopting a non-optimum DP fan performance in order to reduce installation effects to produce a net reduction in fuel-burn. This was done by using DP fan mass flow as a handle.

Figure 6.20 shows the mass flow reductions made to the DP fans for the 2% duct loss case. Both eBPR cases are included. Two TS cases were used due to time constraints; the value for the previous minimum fuel-burn and the TS below that value. The points that lie on the x-axis represent the cases for the optimum DP fan power and the SFC delta refers to the percentage change in SFC relative to those points. It can be seen that all the cases have a higher SFC due to the higher specific

thrust and lower BLI benefits incurred through lowering the mass flow. In general, higher TS cases are less sensitive to changes in mass flow, which is partly due to the BLI mass flow of 321kg/s being unaffected when the mass flow is reduced and also partly because the change is a smaller percentage of the total mass flow. Since the lower eBPR case minimises SFC at higher mass flows, it shows more potential in reducing fuel-burn relative to its optimum SFC case.

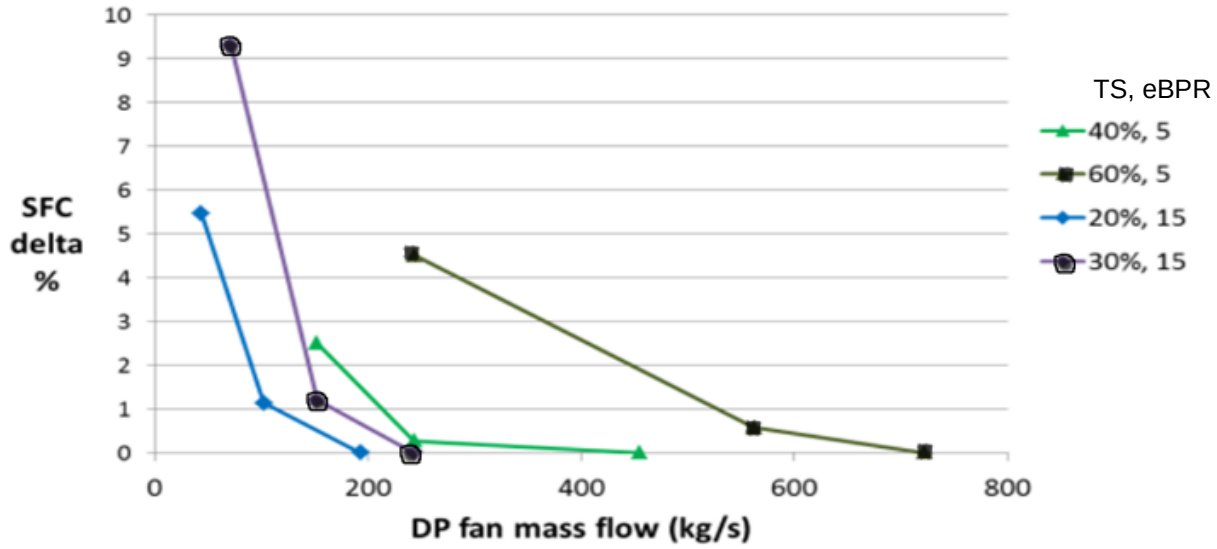

Figure 6.20 - SFC delta vs DP fan mass flow – 2% duct loss

Figure 6.21 shows the variation of fuel-burn with mass flow delta, where the fuel-burn delta is the percentage difference in fuel burn relative to the case where SFC was minimised. In general, it was found that having a non-optimum DP fan performance provided an increase in fuel-burn. However, the lower eBPR cases both provide benefit when reducing the DP fan mass flow slightly, where a 2.2% and 0.5% fuel-burn reduction is achievable for the 40% and 60% TS cases, respectively. It now becomes a question of whether these reductions in fuel-burn manage alter the optimum TS for each eBPR from those in Figure 6.18. Figure 6.18 shows that for an eBPR of 5, the 40% TS case burns 4.7% more fuel than the 60% TS case. Therefore, the results from figure 6.21 show the benefit in reducing mass flow for the 40% TS case is not enough to provide an overall reduction in fuel-burn, since it only reducs fuel-bunr by 2.2% relative to the 60% TS case.

Similarly, for the higher eBPR case, figure 6.18 shows the 20% TS case burns 1.5% more fuel than the 30% TS case. Figure 6.21 shows that a 0.5% fuel-burn reduction is achievable for the 20% TS case relative to the 30% TS case. This does not offset the 1.5% fuel-burn increase.

Overall, it has been shown that eBPR doesn't produce a large effect on fuel-burn, since the DP system can be optimised. The results in figures 6.20 and 6.21 are however only for two extra points, and there may be added benefit in reducing mass flow by a smaller amount.

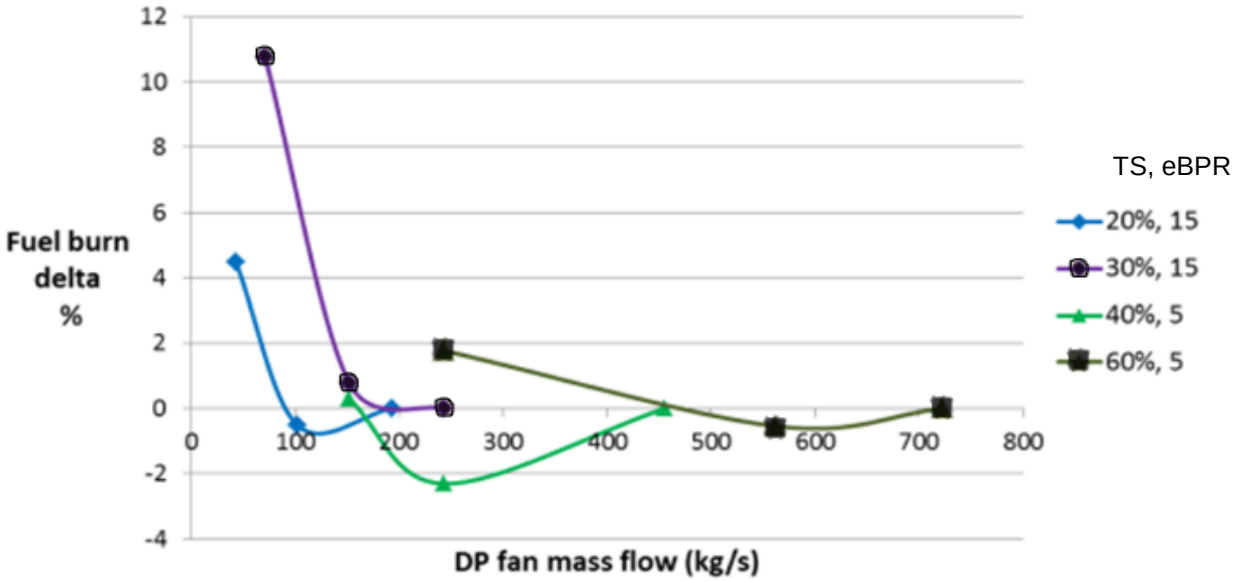

Figure 6.21 - Fuel-burn delta vs DP fan mass flow – 2% duct loss

6.4.3 Off-design performance effects

So far the DP system has been assessed at the cruise condition, where the minimal fuel-burn configuration has found to occur at a TS of around 30-60%. However, the engine is usually sized at an off-design condition, either climb-ceiling or EoR, and therefore a study has been conducted to understand what effects this has on performance and design.

It was found from the Vision 20 study in Chapter 6 that a cruise TET of approximately 1850K was required. Therefore, this value was implemented into a reference case, of which was compared with the off-design sized case. The cruise

average FPR was optimised for both cases, which gave the mass flow average of the DP FPR and eFPR. An eBPR of 15 was chosen for this study, due to its superior performance. Table 6.14 contains the key information for the off-design cases considered, where the climb-ceiling was at an altitude of 3000ft above the cruise altitude with a climb-rate of 300ft/min.

Parameter	Cruise	Climb-ceiling	EoR
Altitude (ft)	44,788	47,788	0.0
Mach no.	0.85	0.85	0.25
ISA Temp Dev. (K)	0.0	0.0	15
TET (K)	Variable	2100	Variable
Power off-take (kW)	472.5	472.5	375.0

Table 6.14 - Off-design engine data

Figure 6.22 shows how the overall mass flow at cruise, which is the sum of the DP fan mass flow and engine mass flow, increases with TS. This was shown before for the DP fan mass flow in figure 6.14 and the engine mass flow varies little as reflected in the small weight variation with TS in figure 6.19. Two sets of results are shown, a case with BLI included and a case without BLI. For both cases the climb-ceiling sized engine requires a significantly larger mass flow at a given TS. This is because the larger climb-ceiling TET of 2100K does not generate enough power to provide the extra thrust needed relative to the cruise condition, and therefore the engine size and mass flow must also be increased.

Figure 6.23 illustrates how mass flow delta, defined as the difference between the cruise mass flow for the cruise and climb-ceiling sized engines, varies with TS. The case where BLI has not been included has a linear increase in mass flow delta as TS increases. This increased mass flow requirement is due to the greater effect the reduced density at climb-ceiling has on larger engines. Because of this, the climb-ceiling sized engine will have an additional weight and fuel-burn penalty relative to the cruise sized engine, and this penalty will grow with TS.

Figure 6.22 shows the cruise mass flow requirement ceases to decrease with TS at around 20% TS when BLI is included. This is due to the rapid reduction in BLI benefit that occurs when decreasing TS lower than around 20%. Figure 6.14 showed the DP fan mass flow rapidly drops off at 20% TS for minimum power. Because the lower momentum portion of the boundary layer is being reduced below this TS, the increase in SFC is causing the engine size to increase. Combining these effects with the installed analysis may alter the optimum TS from the value of the previous installed analysis that sizes the engine for cruise.

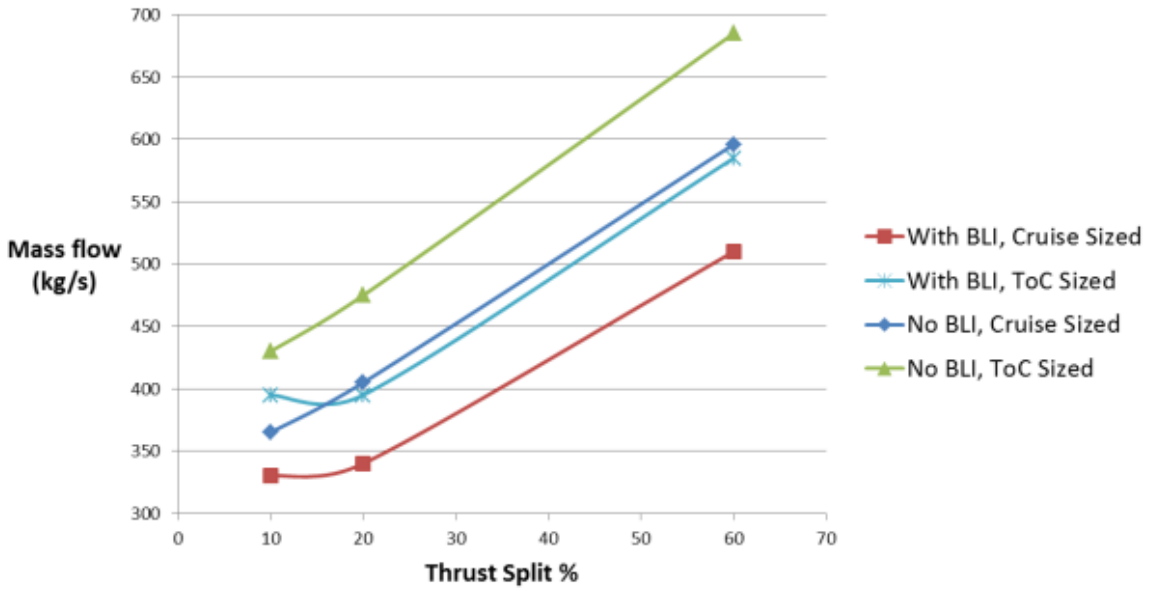

Figure 6.22 - Overall cruise mass flow vs TS

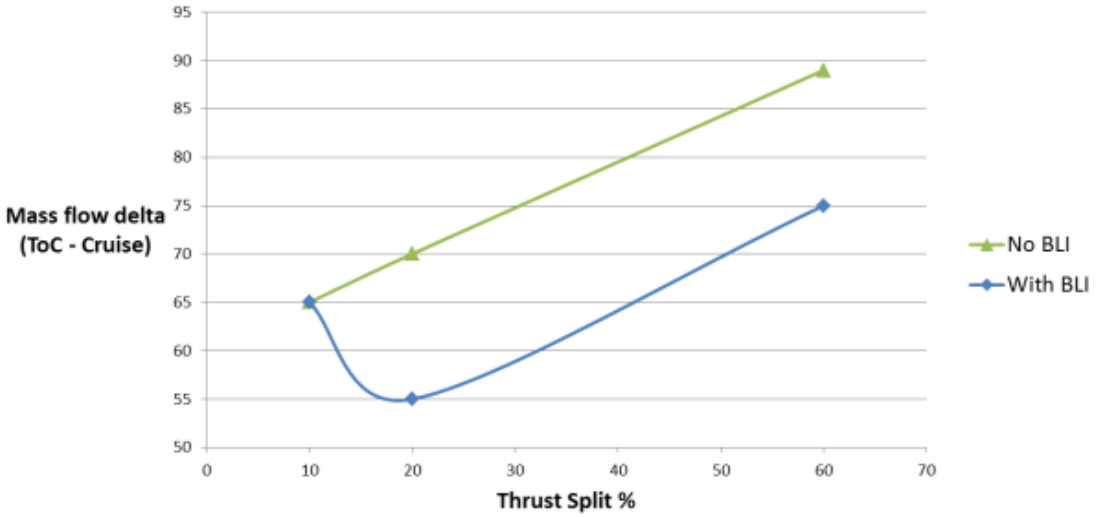

Figure 6.23 - Overall cruise mass flow delta vs TS

Figure 6.24 shows the cruise SFC for both sizing cases. The trend shows that in general a minimum SFC is invoked through the trade-off between low specific thrust and duct loss; as seen before in figure 6.13. The minimum SFC for the climb-ceiling sized case occurs at around 5-10% higher TS than the cruise sized case.

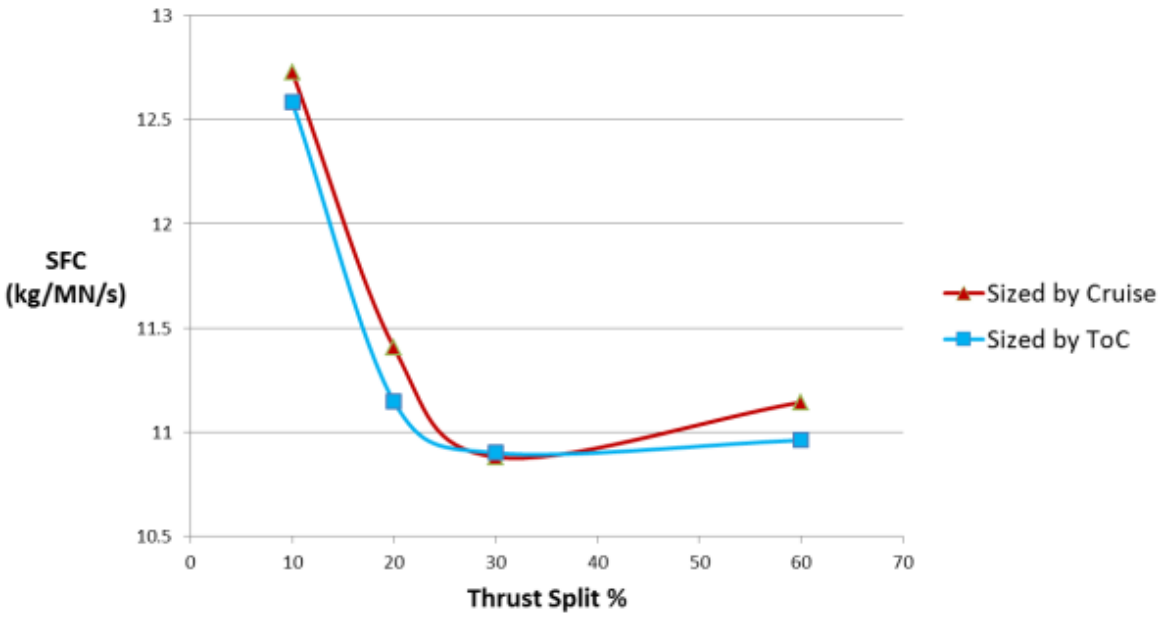

Figure 6.24 - Cruise SFC vs Thrust-Split

Figure 6.25 shows how the cruise TET is constant with TS for the cruise sized case and varies by only a small amount for the climb-ceiling sized case. The climb-ceiling sized case has approximately a 150K reduction in TET, which partly reduces the thermal efficiency of the engine relative to the cruise sized case. However, because the eBPR and DP fan power is fixed for both cases, the engine specific thrust reduces with TET and therefore the higher propulsive efficiency of the climb-ceiling case offsets the lower thermal efficiency effects. Therefore, the SFC is similar for both cases as shown in figure 6.24. In reality the cruise sized engine would be designed with a larger eBPR to utilise the higher TET by reducing the specific thrust and increase propulsive efficiency. More underwing space would be needed since for a given thermal efficiency and core size, the engine diameter would need to increase for eBPR to increase. In this case, the fuel-burn difference, shown in figure 6.26, would become smaller. However, the installed effects of the engine sized at climb-ceiling would still produce a significant fuel-burn penalty due to the added weight and drag of the engines. It was found that the climb-ceiling case burned 11% more fuel than the cruise sized case. It can also been seen that the two cases have different minimum fuel-burn TS values, where the engine sized at climb-ceiling invokes a value of around 20%, as large mass flows are detrimental to performance.

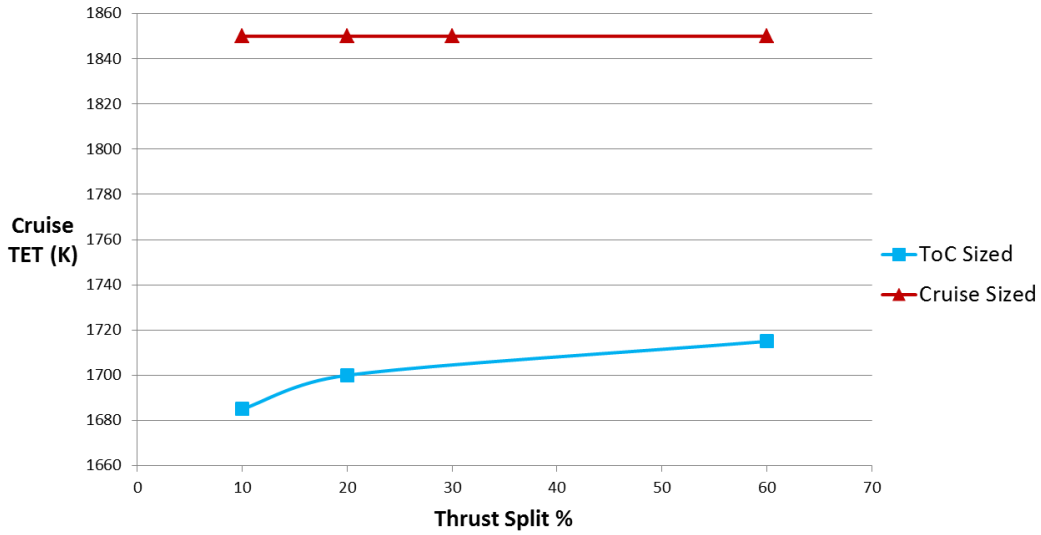

Figure 6.25 - Cruise TET vs TS

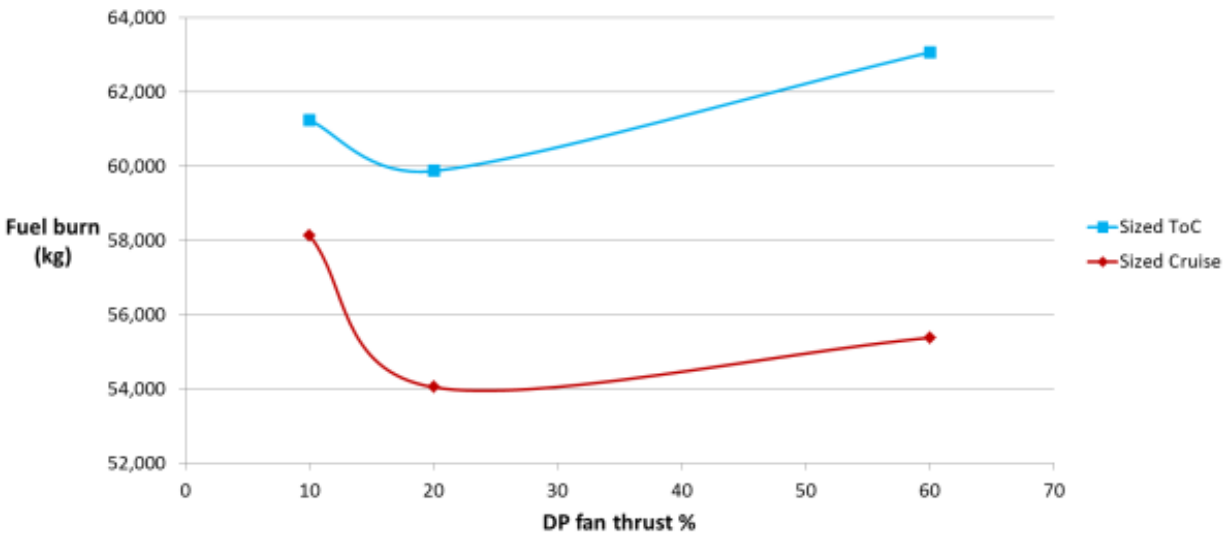

Figure 6.26 - Fuel-burn vs TS

6.4.4 Conclusions

It has been shown through an installed aircraft analysis of the propulsion system that the overall performance is particularly sensitive to the mass and drag of the DP fans, electrical system and engines. In general, the differences in SFC between the different duct loss and EBPR cases become small when installed effects are accounted for. It was shown that in order to minimise fuel-burn a lower TS was required relative to the value that minimised SFC. This has been found for all cases and the lower eBPR case invokes the largest reduction.

The propulsion system mass breakdown shows that the DP fans, including housing and ducting, vary the most with TS. This explains why the DP system performance is particularly sensitive to mass flow changes. The engine fan was assumed to be 10% of the engine weight, however, after discussion with Rolls-Royce this value was deemed low and a value between 15 and 20% is more probable. In this case, the higher eBPR cases would burn more fuel and may become less favourable. Therefore, the lower eBPR design performance is predicted to be conservative.

The installed analysis had optimised DP fan mass flow to require a minimum fan power before assessing fuel-burn. However, for some cases, a reduction in fuel-burn was achievable relative to the value obtained through optimising fan power. This was

despite the SFC increasing. An assessment that includes all the TS cases would provide a full comparison of the installed effects versus the fan performance.

Off-design effects were accounted for by sizing the engine at the climb-ceiling condition, where the thrust requirement is highest. It was found that larger engine and DP fan cruise mass flows require a greater increase in mass flow than those of smaller mass flows. This was because for a given thrust increase, larger mass flows are more sensitive to air density changes. This was due to the reduction in thrust associated with low air densities at high altitudes. Therefore, the minimum fuel-burn TS for the climb-ceiling case was reduced relative to a cruise sized case. Further TS reductions were not beneficial, as reducing cruise mass flow further resulted in a significant BLI benefit reduction. Overall, it was found that the optimum climb-ceiling case burned 11% more fuel than the optimum cruise sized case. Additionally, it was found that the optimum TS case was approximately 20%.

7 Discussion and Conclusions

7.1 Vision 20 Distributed Propulsion studies

An investigation into the feasibility of DP as a future propulsion system choice for advanced aircraft has been conducted. Current literature contains few studies on DP and therefore studies of this nature provide a contribution to knowledge. NASA state that public domain studies of DP on T&W aircraft have not been explored and would be useful in gauging the concepts applicability, especially in comparison with DP on novel airframes. This statement was underwritten by a literature review that was conducted from which the same conclusion was drawn. BWB aircraft DP studies are relatively sparse and a study that integrates the aircraft and propulsion system design for the quest of minimal fuel-burn provides a unique contribution. Therefore, T&W and BWB airframes were chosen as a base to assess current turbofan, advanced turbofan and DP with BLI propulsion systems.

It was decided to build a conceptual aircraft design tool from scratch to enable the design of conventional and novel aircraft. The initial objective was to assess the current methodologies that enable the aircraft modelling. A semi-analytical approach based on Torenbeek's method was adopted to model the T&W wing mass and a Cranfield University BWB airframe mass prediction method was adopted. These were chosen due to the high level of detail in the design methods and the rapid synthesis that is effective at the conceptual design stage. A semi-analytical approach was used to model the aircraft wave drag associated with shock waves as this enhanced the aircraft design sensitivity to wing geometry. Other component prediction models were incorporated from many authors; ensuring only one method was used for a given component to avoid incompatible assumptions. The integration of the all the methods, in particular the BWB method, into a complete conceptual modelling tool provided the initial PhD contribution, as currently access to a BWB modelling tool is not possible within the public domain since they remain proprietary.

The T&W and BWB mass estimation methods assume an elliptical air-load distribution, as it simplifies the calculation process and is generally the most efficient airframe loading. The distribution is affected by wing taper ratio and sweep affect

and can be equated through computation techniques. Due to time constraints, values for wing sweep and taper ratio for the T&W and BWB aircraft were taken from similar type aircraft, since these do not vary significantly between aircraft, unlike aspect ratio and thickness to chord ratio. However, it may be beneficial not to have an elliptic distribution and exchange the airframe benefits for DP benefits, since reshaping the airframe may enhance the boundary layer properties, and alter the optimum number of DP fans and their performance. Therefore, it is recommended that the aircraft design tool be made capable of evaluating these parameters.

The aircraft tool was validated by modelling the Boeing 787 aircraft and Airbus 350 baseline T&W aircraft. The key parameters were then compared with public domain data. The maximum errors for the Boeing 787 were around six per cent and the power-plant mass contributed the largest error, due to the simplified thrust prediction method adopted. The Airbus 350 model contained errors of less than two per cent; the largest being the Maximum Landing Weight, which was because it was based on a simple estimate of payload as manufacturers use a lengthy prediction method.

The next stage consisted of modelling the advanced Vision 20 concepts. Assumptions were made as to the technology improvements achievable for T&W aircraft for the future timeframe, including weight and drag reductions due to composite materials and aerofoil advances respectively. Assumptions relating to advances in turbofan engine technology were provided by Rolls-Royce and amounted to a significant reduction in SFC and weight. The advanced T&W geometry was optimised in terms of aspect ratio and thickness to chord ratio and the results showed almost a 28% fuel-burn reduction relative to the baseline T&W aircraft.

A number of aircraft and propulsion system assumptions were made for the DP variant T&W aircraft. The aircraft wing bending moment relief and empennage size calculations reflected the positioning of the DP fans. The inner control-volume method was adopted for the DP fan BLI modelling due to its enhanced accuracy over the outer control-volume method. The DP electrical system load was varied to optimise its weight for cruise. By sizing the DP fans by the boundary layer mass flow over the fuselage, the DP FPR was then optimised to give the lowest SFC.

Consequently, the DP T&W aircraft provided a 4.1% reduction in fuel-burn relative to the advanced T&W aircraft. This was despite the overall propulsion system mass increasing by 18%, through which the aircraft reshaping reduced the impact of the additional mass.

The BWB turbofan variant aircraft features the same propulsion system technology as the advanced T&W aircraft. The BWB aircraft was not explicitly compared with the T&W aircraft since the assumptions made in the predictive methods are incompatible with each other and the BWB aircraft is difficult to validate as only theoretical modelling data is currently available in the public domain. However, some general comparisons can be made regarding the DP system. The BWB structural mass as a percentage of MTOW was validated with Cranfield BWB studies and showed that the percentage differed by a small amount. This result gave some indication of the BWB designs validity. However, because the Cranfield mass estimation method was used in the validation cases, the difference only signifies that the design is not radically different from other proposed BWB designs. Further validation of the mass estimation method was performed by modelling a Bristol Univeristy BWB and showed substantially different results, although the accuracy of the validation case is questionable. Therefore further validation is advisable with data from different methods.

It was found that the Vision 20 BWB cruised at an exceptionally high altitude, which required a particularly large engine that incurred a considerable weight and drag penalty. The aircraft performance was compared with a number of BWB designs to ascertain whether there was an issue with the design or specification. The other designs were found to achieve lower cruise altitudes by imposing either lower cruise Mach numbers or increased landing speeds. Therefore the Vision 20 design was deemed reasonable. A number of alternative designs were produced to investigate the effect of reducing cruise altitude and a lower cruise Mach number design was chosen for further study due to its high efficiency.

The DP BWB aircraft features DP BLI fans along the inner-wing section and CFD was used to predict the boundary layer growth along the aerofoil section; greatly enhancing the accuracy relative to flat-plate equation results. The DP BWB achieved

a 5.2% fuel-burn reduction relative to the BWB baseline aircraft when assuming 2% BLI duct loss and a 7% fuel-burn reduction when BLI duct loss decreased to 1%. This illustrates the significance of duct loss on performance and further analysis on duct design must be done to ascertain the potential DP benefits. The DP system benefit was found to manifest itself in a reduction in propulsion system mass rather than a large decrease in SFC, due to the greater impact of the turbofan size reduction compared to the DP fan size increase.

7.2 Parametric investigation into the wider design space

The Vision 20 studies served as a preliminary evaluation of DP that provided insight into the potential level of benefits achievable and formed a basis from which more in-depth studies were conducted. The tools and knowledge obtained from the work provided a contribution to knowledge and were used to investigate the wider design space. A parametric investigation was conducted to ascertain the DP concepts design sensitivities and dependencies, relating in particular to intake layer height, BLI duct total pressure loss and engine bypass ratio.

The Vision 20 study sized the DP fans by the boundary layer height which provided a rapid method of assessing BLI. The parametric study aimed to investigate how ingesting different portions of the boundary layer affected overall propulsion system performance and therefore a more detailed method of calculating the boundary layer flow properties was required. A novel mathematical derivation was developed that transforms the 2D CFD results to 1D flow equations and enables the boundary layer to be assessed at any height. This technique is original and provided a further contribution to knowledge; since present studies in the public domain either use costly detailed CFD simulations for specific intake heights or empirical flat-plate equations that don’t accurately account for boundary layer pressure gradient effects. Additionally, the method does not require numerical integration and enables a rapid BLI assessment.

The first stage of the parametric assessment focused on the propulsion system and used power and SFC as the metrics of performance. TS was initially varied to determine its effect. It was found that for a fixed eBPR, changes in TS effectively alters the overall BPR, since optimum DP fan mass flow changes to suit its thrust

requirement. Therefore, curves of power vs mass flow and SFC vs TS showed similar trends, where a minimum power or SFC was found due to the opposing effects of low specific thrust benefits associated with high mass flows and BLI, and detrimental duct losses.

If the maximum eBPR were limited by an aircraft's ground clearance and the losses associated with a reduced core size, then the DP system acts as a means to increase the overall BPR. It was found that a minimum SFC existed between a TS of 30% and 80% for two duct loss and two eBPR cases considered. Like the Vision 20 study, increasing duct loss was found to induce a significant SFC increase. The lower eBPR case minimised its SFC at higher mass flows and therefore was more sensitive to duct loss. Because of this, it was possible to mitigate the increased duct loss effects by lowering the TS. The benefit of doing this decreased as eBPR was increased. However, the Vision 20 study in Chapter 6 adopted a relatively low eBPR, signifying that the difference in fuel-burn between the two duct loss case results in figures 6.10 and 6.11 are not fully optimised and may not be of such magnitude. Though, in general the higher eBPR design was more efficient. This study assumed a constant duct loss for both the engine nacelle and DP fan ducts. By implementing a duct loss as a function of inlet size, the assessment of eBPR with TS could be improved further.

An installed analysis was conducted to understand how mass and drag affected the performance of the DP system. The Vision 20 BWB aircraft was adopted and fuel-burn was used as the primary performance metric. In general, fuel-burn was found to be minimised at a lower TS than for SFC. This was because the large DP fan mass flows associated with high TS required large ducting and heavy motors and fans. Additionally, high TS's introduce added electrical system weight. Therefore, in order to minimise fuel-burn, a balance must be met between propulsive performance and the effects associated with weight and drag. As was the case for larger duct loss, this effect was found to be more pronounced for the lower eBPR case due the greater mass flows. By optimising the TS it was found that an extra 2.5% fuel-burn reduction could be achieved relative to case where the same TS was used as for the minimum SFC case.

It was shown that further reductions in fuel-burn could be achieved through considering the installed effects from the start of the design process. Usually the DP fans mass flow is optimised for power and the TS was varied to obtain the lowest SFC or fuel-burn. However, it was found that by adopting non optimum fan performance through increasing their specific thrust, additional fuel-burn savings of up to two per cent could be achieved. Collectively, optimising TS and DP fan size can produce fuel-burn savings of around 4.5%. This step by step approach to gauging the sensitivity of the DP system is novel within the public domain. It can be concluded that the DP system is highly dependent on many aspects that affect fuel-burn and should be designed using a multi-disciplinary approach for accurate performance predictions.

The optimum TS was found to decrease even further when off-design conditions were accounted for. The climb-ceiling condition required the engine diameter to increase significantly in order to provide sufficient thrust, resulting in an overall engine mass and drag penalty. This caused approximately a ten per cent increase in fuel-burn relative to an engine that was sized for cruise. Since the sensitivity to the off-design conditions increases with mass flow, a lower TS became preferable. In general, it has been shown that only the lowest portion of the boundary layer should be ingested, as this reduces installed losses and utilises BLI in the most resourceful manner. The difficulty comes when justifying the move to a novel propulsion system such as DP, for only a small TS.

8 References

[1] Bettex, M., MIT-led team designs 'green' airplane, MITnews, [Online] (May 2010). Available at: <http://web.mit.edu/press/2010/green-airplanes.html>

[2] NASA, NASA Aeronautics and Space Administration. [Online] (2008). Available at: <http://www.aeronautics.nasa.gov/nra_awardees_10_06_08.htm> [Accessed December 2010].

[3] Aviation Week, N+3 Small Commercial Efficient & Quiet Air Transportation for Year 2030-2035. [Online] (2010). Available at: <http://aviationweek.typepad.com/files/nasa_ge_final_report_out_4.22.10.pdf> [Accessed August 2011].

[4] Airbus, Flying by Nature: Global Market Forecast 2007–2026, Airbus S.A.S, Blagnac Cedex [Report, Online] (2007).

[5] Givoni, M.. Comparing the Environmental Impact from Using Large and Small Passenger Aircraft on Short Haul Routes, Oxford University Centre for the Environmentk, 1033 [Working Paper No.1033] (2008).

[6] Green Energy News, Efficient Open Rotor Jet Engine – Revisited. [Online] (2008). Available at: <http://www.green-energy-news.com/arch/nrgs2008/20080093.html> [Accessed August 2011]

[7] Karp, A., Rolls-Royce touts industry investment in trimming emissions, ATWonline, [Online] (2009). May 2009. Available at: <http://atwonline.com/aircraftenginescomponents/news/rolls-royce-open-rotor-real-pratt-pushes-geared-turbofan-03-09> [Accessed January 2011]

[8] Moxon, J., Open rotors brushed off by Pratt & Whitney, AINonline, [Online] (May 2009). Available at: http://www.ainonline.com/news/single-news-page/article/open-rotors-brushed-off-by-pratt-whitney-25521/. [Accessed January 2011]

[9] Pilidis.P, Gas Turbine Theory and Performance, Cranfield, Cranfield University [Lecture notes] (2010).

[10] Boggia, S. and Rud, K., Intercooled Recuperated Aero Engine, MTU Aero Engines [Online] (2004). Available at: <http://www.mtu.aero/en/technologies/engineering_news/development/Rued_Intercooled_recuperated_en.pdf >

[11] Kawai, R.T., Blended Wing Body (BWB) Boundary Layer Ingestion (BLI) Inlet Configuration and System Studies, National Aeronautics and Space Administration, [Conference Paper - NASA/CR-2006-214534] (2006).

[12] J.L. Felder et al., Turboelectric Distributed Propulsion in a Hybrid Wing Body Aircraft, [Conference Paper - ISABE-2011-1340] (2011).

[13] C.Lui et al., Turboelectric Distributed Propulsion System Modelling for Hybrid-Wing-Body Aircraft, [Conference Paper - AIAA 2012-3700] (2012).

[14] J.I. Hileman, Z.S. Spakovszky, M. Drela, Airframe Design for “Silent Aircraft”, [Conference Paper - AIAA 2007-453] (2007).

[15] G.Ameyugo, et al., Distributed Propulsion Feasibility Studies, [Conference Paper - ICAS-2006] (2006).

[16] C.A. Luongo, Next Generation More-Electric Aircraft: A Potential Application for HTS Superconductors, [Conference Paper - IEEE Transactions on Applied Superconductivity, Vol. 19, No. 3] (2009).

[17] F. Haglind, R. Singh, Potential of reducing the environmental impact of aviation by using hydrogen Part I: Background, prospects and challenges, The Aeronautical Journal, 533 (2006).

[18] J.I. Hileman, et al., Airframe Design for “Silent Aircraft”, [Conference Paper - AIAA 2007-453] (2007).

[19]

http://www.mp.haw-hamburg.de/pers/Scholz/ewade/2007/EWADE2007_Scholz.pdf

[Online] - accessed Nov 2012.

[20] R.H. Liebeck, Design of the Blended Wing Body Subsonic Transport, Journal of Aircraft, Vol.41, No.1 (2004).

[21] J.L. Felder, et al., Turboelectric Distributed Propulsion Engine Cycle Analysis for Hybrid-Wing-Body Aircraft, [Conference Paper - AIAA-2009-1132] (2009). Available at: https://mdao.grc.nasa.gov/publications/AIAA-2009-1132-622.pdf

[22] E.R. Blanco, et al. Challenges in the Silent Aircraft Engine Design, [Conference Paper - AIAA 2007-454] (2007).

[23] A. Gohardani, et al., Challenges of future aircraft propulsion: A review of distributed propulsion technology and its potential application for the all electric commercial aircraft, [Journal Paper - Progress in Aero. Sci., 47, 369-391] (2011).

[24] Liebeck, R.H., Innovative Configurations and Advanced Concepts for Future Civil Aircraft: Design of the Blended-Wig-Body Subsonic Transport, Rhode Saint Genese. von Karman Institute for Fluid Dynamics [Book from Cranfield Library] (2005).

[25] Plas, A.P. et al., Performance of a Boundary Layer Ingesting (BLI) Propulsion System, American Institute of Aeronautics and Astronautics, [MSc Thesis MIT, pp. 22-23, available online] (2006).

[26] Daggett, D.L. et al., Blended Wing Body Systems Studies: Boundary Layer Ingestion Inlets With Active Flow Control, National Aeronautics and Space Administration , [Conference Paper - NASA/CR-2003-212670], (2003).

[27] Rolt, A., Rolls-Royce Experimental Fan Efficiency Discussion (2012).

[28] Broadbent E.G., Noise Shielding For Aircraft, [Journal Paper – Progress in Aerospace Sciences, 17] (1977).

[29] Casalino, D. et al., Aircraft noise reduction technologies: A bibliographic review, Journal of Aerospace Science and Technology, 12(1) (2008).

[30] Mangiarotty R.A., The reduction of aircraft engine-fan compressor noise using acoustic linings, Journal of Sound and Vibration, 18(4) (1971).

[31] Rawlins A.D., The Engine-Over-The-Wing Noise Problem, Journal of Sound and Vibration, 50(4) (1977).

[32] Ailiners.net, The Antonov An-72/74, [Online] (2011). Available at: <http://www.airliners.net/aircraft-data/stats.main?id=39>

[33] Ailiners.net, The Antonov An-72/74, [Online] (2011). Available at: http://5magazine.wordpress.com/2010/11/24/cestol-aircraft-concept

[34] The Aviation Zone, The Antonov An-72 & An-74 (Coaler), [Online] (2011). Available at: <http://www.theaviationzone.com/factsheets/an72.asp>

[35] Stanford University Department of Aeronautics and Astronautics, Engine Placement, [Online] (2006). Available at: <http://adg.stanford.edu/aa241/propulsion/engineplacement.html>

[36] Torenbeek, E., Development and Application of a Comprehensive, Design Sensitive Weight Prediction Method for Wing Structures of Transport Category Aircraft, Delft, Report LR-693, Department of Aerospace Engineering (1992).

[37] Raymer, D.P., Aircraft Design: A conceptual Approach. 4th ed. Virginia. American Institute of Aeronautics and Astronautics, Inc. [Book] (2006).

[38] Jenkinson, L.R. et al., Civil Jet Aircraft Design, London, American Institute of Aeronautics and Astronautics, Inc. [Book] (1999).

[39] Collingbourne, J., Multivariate Optimisation Applied to the Initial Design of Transport Aircraft, Royal Aircraft Establishment, [Report – 84044, pp.73-77] (1984).

[40] Wilson, R., Discussion on wave drag, Rolls-Royce Plc. [Email] (Personal communication, March 2011)

[41] Liebeck, R.H., Innovative Configurations and Advanced Concepts for Future Civil Aircraft: Design of the Blended-Wig-Body Subsonic Transport, Rhode Saint Genese. von Karman Institute for Fluid Dynamics [Book] (2005).

[42] Torenbeek, E., Development and Application of a Comprehensive, Design Sensitive Weight Prediction Method for Wing Structures of Transport Category Aircraft, Delft, Report LR-693, Department of Aerospace Engineering (1992).

[43] Howe, D., Aircraft Conceptual Design Synthesis, London, Professional Engineering Publishing Ltd. [Book] (2000).

[44] Roskam, J., Airplane Design Part V: Component Weight Estimation, DARcorporation [Book] (1999).

[45] Banerjee, D., Conceptual mass estimation of civil subsonic aircraft wings. [MSc. Thesis Cranfield University] (2007).

[46] Crawford, T., Design of a Blended Wing Body Business Aircraft. [Msc. Thesis Cranfield University] (2002).

[47] D. Howe, Blended Wing Body Airframe Mass Prediction, Journal of Aerospace Engineering 215: 319 (2001).

[48] Jackson, P.A., Janes world of aircraft, Jane's Information Group; 99th edition edition [Book] (2008).

[49] Williams, J. et al., The Aerodynamics of Jet Flaps, Ministry of Aviation [Report no.3304] (1963).

[50] Filippone, A., "Powered Lift Systems, Propulsion Systems." Advanced Topics in Aerodynamics [Online] (2008).

[51] Twisk, J.V., Design Study of STOL Transport Using Internally Blown Flaps, [MSc. ThesisCranfield University] (1971).

[52] Rolt, A., Discussion on distributed BLI fan redundancy option, Rolls-Royce Plc. [Email] (Personal communication, June 2011).

[53] P.G.Hill and C.R.Peterson, Mechanics and thermodynamics of propulsion, Reading, Massachusetts: Addison Wesley, [Book] (1992).

[54] A.M.O. Smith and H.E. Roberts, “The Jet Airplane Utilizing Boundary Layer Air for Propulsion”, Journal of the Aeronautical Sciences, Vol. 14, no. 2, pp.97-109, (1947).

[55] B787 simulation. Website: http://www.lissys.demon.co.uk/. Accessed Nov 2012.

[56] Brown, R., Airline Fuel Conservation Equals Reduced Emission, [Report - NASA ECR Workshop], (1998).

[57] J. Kane, Planform Optimisation of a Blended Wing Body, [Cranfield University PhD Thesis] (2004).

[58] H.V. de Castro, The longitudinal static stability of tailless aircraft, [Cranfield University PhD Thesis] (2001).

[59] J. Roskam, Airplane Flight Dynamics and Automatic Flight Controls, Part 2, 6th ed., DARcorporation [Book] (2001).

[60] L. Raffaelli, Rolls-Royce Genesis engine weights communication (2011).

[61] T. Jackson, Optimisation of aero and industrial gas turbine design for the environment, [Cranfield University PhD Thesis] (2009).

[62] M. Peric et al., G1F-BWB: Final Engineering Definition Report, [Bristol University Report] (2003).

[63] http://aviationweek.typepad.com/files/boeing_sugar_phase_i_final_review_v5.pdf - The Boeing Company, Accessed Nov 2012.

Appendix A - Magnetoplasmadynamic Flow Control

A1 Magnetoplasmadynamic Flow Control Concept

Figures 6.10 and 6.11 show that a two per cent reduction in fan efficiency (shown by the fuel-burn increase associated with the 'worse fan efficiency' increment in both figures), due to the ingestion of boundary layer air into the fan, produces around a 2.5% increase in fuel-burn. This fuel-burn increase doesn't account for the detrimental aircraft and propulsion system resizing effects. In addition, the fan efficiency penalty may be worse than two per cent. This efficiency penalty arises because boundary layers possess both a radial and circumferential total pressure distortion, and when presented to the fan face they produce varying velocity triangles that effectively invoke inlet flow angles similar to off-design. Additionally, transient flow may become more prominent and separation may occur. Figure A.1 illustrates the boundary layer lines of constant total pressure running horizontally and increasing upwards from a surface to free-stream conditions. The lines of constant angular velocity of the fan are represented by the concentric circles and they clearly show how the oncoming flow conditions change through rotation at a single radial point on the fan.

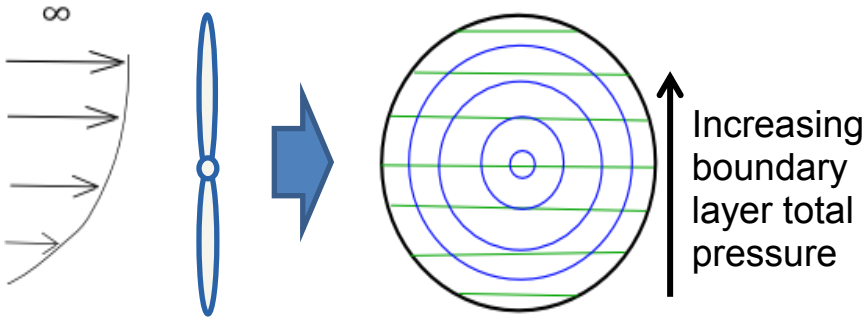

Figure A.1 - Boundary layer fan distortion

A novel flow control method has been devised in which the circumferential distortion of the boundary layer is reduced. The purpose of this chapter is to provide insight into the concept and to generate inspiration that may enable future ideas. It is by no means a rigorous description of the concept.

Radial distortion can be dealt with through fan geometric twist at a design point condition. This novel concept aims to reduce the circumferential distortion, but could also act as a means of correcting radial distortion at off-design conditions. Figure A.2 shows a schematic that illustrates a 2D view of the flow sequence as it travels down the 3D view of the duct. The boundary layer has been simplified to a portion of constant velocity flow that fills part of the duct cross-section, which simplifies the representation. The flow is turned to produce the required flow evolution. The other portion of flow in the duct section is assumed to be at free-stream conditions. The fan face is located at the duct exit, where the transition from free-stream to boundary layer is only encountered by travelling radially outwards from the fan centre, rather than circumferential around.

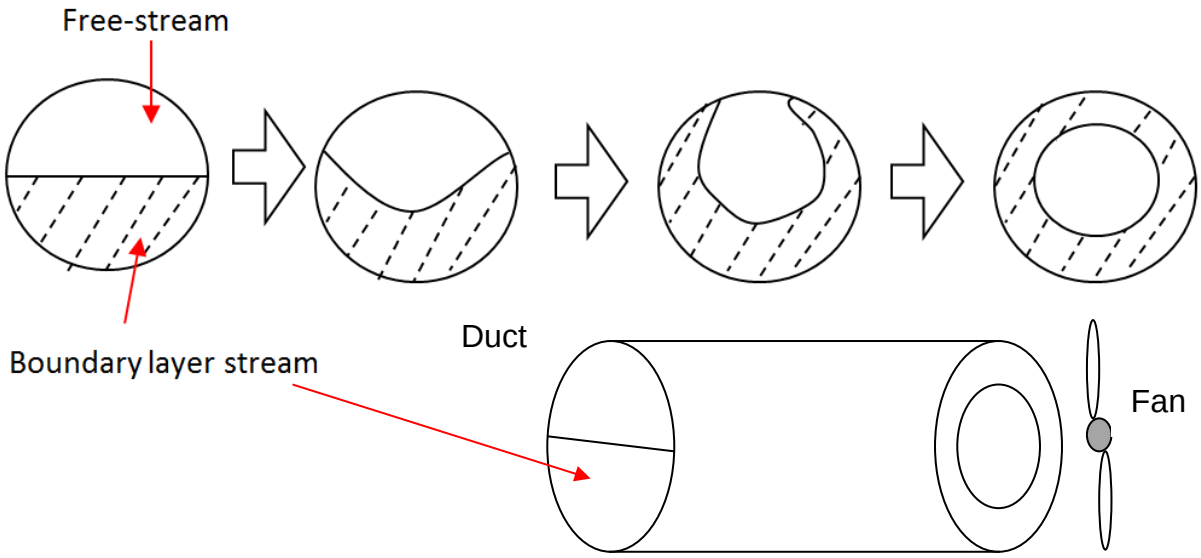

Figure A.2 - 2D face view and 3D isometric view of duct

One possible concept that may produce the required 'turning' of the flow to generate this flow sequence is a complex duct geometry that uses the wall to provide pressure force to deflect the fluid. The duct would turn the fluid through a geometry transformation that begins as a circular cross-section and ends as a concentric cylinder, resulting in the boundary layer being curved around the fan. However, it is predicted that the contours would induce large flow separations on a reasonable length duct and therefore a method of energising the fluid is likely to be needed for acceptable efficiency. Also, this would only suit one design pint condition. Instead,

the devised concept uses body forces to generate fluid momentum in order to turn the flow, reducing the aforementioned issues.

Marine ships have already incorporated BLI in their designs, and since saltwater is partially conductive, boundary layer flow control using magnetohydrodynamics (MHD) may provide a synergy. Additionally, the boundary layer invokes significant radial loading on rotor blades, which can produce mechanical issues and impede the fan's flow separation control. Therefore, the efficiency of a flow control system must be weighed up against the overall advantage associated with introducing BLI. The next section provides a brief review of the magnetoplasmadynamic principles and some of its applications.

A2 MPD theory and background

Magnetoplasmadynamics (MPD), in this context, is the effect of producing a Lorentz force on a conducting fluid using an externally applied magnetic field. Figure A.3 illustrates a basic thruster design that produces thrust in the x-direction and helps describe the fundamentals of MPD. An electric discharge E_y is required to both charge the fluid to enable conductivity (as air is usually an insulator) and provide electric current from the cathode to the anode terminals (electrons travel from anode to cathode). The electric field is positioned orthogonal to the externally applied magnetic field B_x. Using Fleming's left hand rule (usually associated with motors), the resulting Lorentz force is directed perpendicular to E_y and B_x.

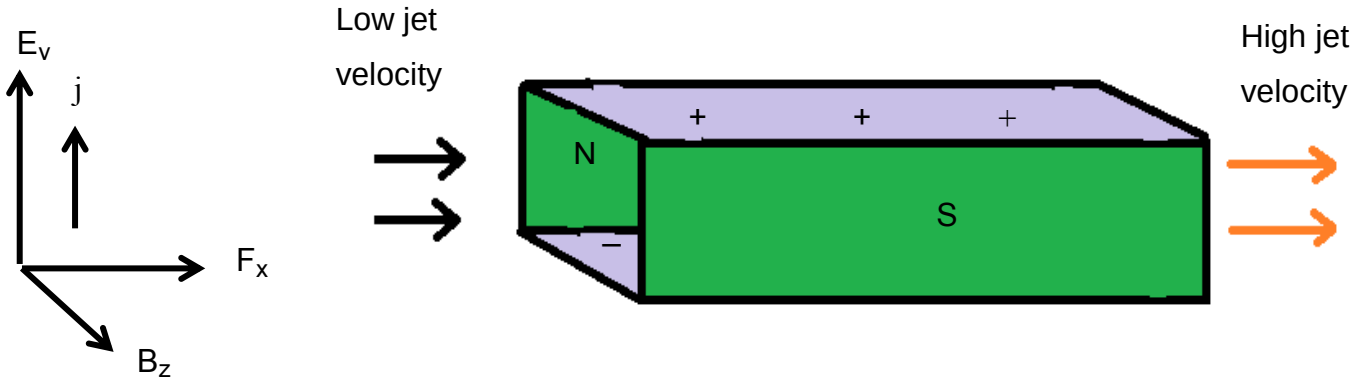

Figure A.3 – Simplified MPD thruster

Within aerospace, thrusters are usually only designed for craft outside the earth's atmosphere, due to the large ionisation power required at high air pressures. However, during the 1950's a number of MHD flow control concepts had been envisioned on the basis that at high enough speeds air becomes ionised by frictional heating and shock wave actions, producing a conductive medium [A1]. Research on magnetoaerodynamics (MAD) has been conducted on boundary layer and shock wave flow control for hypersonic vehicles. [A3] is a Cranfield University PhD thesis that describes the development of a numerical code for assessing hypersonic flow control. It also provides results on the technology's feasibility to reduce skin-friction drag and heat transfer.

NASA has developed a theoretical concept that integrates MPD with a turbojet engine. A component diagram is shown in figure A.4, where in this case the MHD term is equivalent to MPD (more usually MHD refers to saltwater applications and MPD refers to ionised air applications). The MHD generator acts as a dynamo to extract power from the flow prior to compressor ingestion. By using the MPD 'motor' effect, this power is then used to accelerate the flow after exiting the turbine stages, although for a fixed compression ratio, a greater fuel-flow would be needed to achieve the same TET since energy would be extracted from the flow. This Since the MHD generator serves to reduce the turbojet inlet Mach number, the compressor operates efficiently at high flight Mach numbers and NASA predict the turbojet's operating conditions may be extended to a Mach number of around seven. Current turbojet's are limited to a Mach number of around three. NASA's MHD generator concept extracts 30-40% of the energy in the flow, corresponding to between a half and three-quarter flow speed reduction. This reduces the turbojet inlet Mach number to around 2.8 [A1]. Additionally, since a large diffuser precedes a turbojet's compressor in order to reduce the flow Mach number, the MHD generator may partly replace the diffuser requirements and therefore reduce its associated detrimental weight and drag effects. Since the MHD generator loading is controlled electrically through voltage, the off-design conditions may be catered for more effectively than having moving mechanical parts.

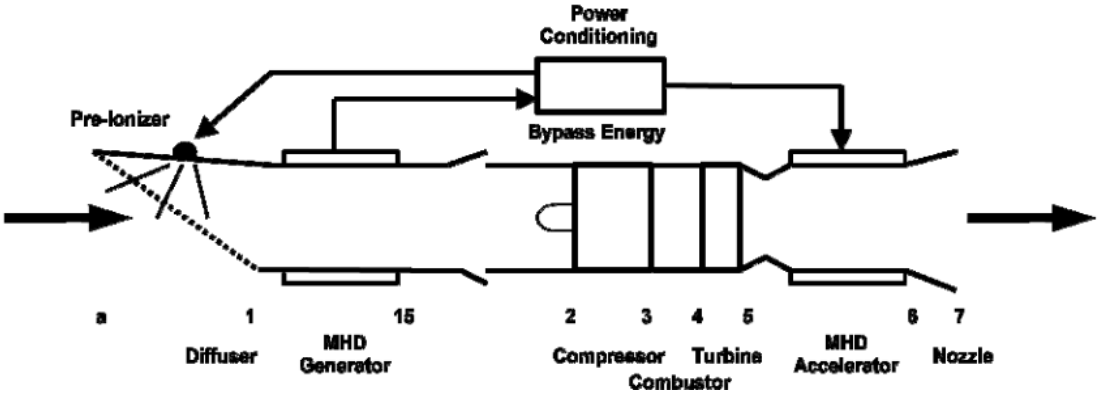

Figure A.4 - Air-breathing MHD controlled turbojet engine [1]

Sea water MHD propulsion was proposed in the 1960's due to the seemingly elegant operation that required no moving parts and was used on the YAMATO-1 vehicle, shown in figure A.5. The concept also benefits from silent operation, high speed flow without cavitation and offers increased payload volume due to the removal of the sizable shaft required for a propeller or the electrical system used to connect the engine to the motors. However, the concepts success was limited by some fundamental problems with MHD propulsion efficiency and the period of active research declined. The reason for the efficiency deficit can be explained by the following equation that were obtained from [A1]. Regardless of the electromagnetic propulsion method, the Lorentz force density **f** produces thrust when the current density **j** crosses a magnetic induction field **B**, shown by,

$$\mathbf{F} = \mathbf{j} \times \mathbf{B}, \tag{A.1}$$

where bold font represents vector quantities. Since the conductivity of sea water is low, the magnetic Reynolds number, defined as the magnetic advection to diffusion, is small and the induced magnetic fields are negligible, so **B** becomes the applied field only. Ohm's law provides the current density,

$$\mathbf{j} = \sigma(\mathbf{E} + \mathbf{u} \times \mathbf{B}). \tag{A.2}$$

E denotes electric field strength, σ the electric conductivity and **u** the flow field, and figure A.3 shows the direction of each vector for a propulsor or 'motor'.

The ideal electrical to mechanical efficiency η is the ratio of propulsive power juB to power supplied per unit volume jE, given by,

$$\text{Efficiency} = \frac{\text{uB}}{\text{E}} = \frac{1}{\emptyset} \qquad \textbf{(A.3)}$$

where U denotes flow velocity. The ideal efficiency is the reciprocal of the load factor $\emptyset$. Rearranging equation A.1 for current density and inserting it into equation A.2 and accounting for the induced electric field acting against the applied field, the electromagnetic thrust F is given by,

$$\text{F} = \sigma \text{UB}^2(\emptyset - 1)\text{A}, \qquad \textbf{(A.4)}$$

where A denotes the duct volume. Therefore the thrust is zero for maximum ideal efficiency. If total drag D is equal to thrust force F, and an approximation for turbulent flows is invoked to give $D=ku^2$ where k is a constant of proportionality, then the ideal efficiency can be written as,

$$\text{Efficiency} = \frac{1}{1+\frac{ku}{\sigma AB^2}}. \qquad \textbf{(A.5)}$$

At a given velocity U, the product AB^2 should be the highest possible. This had been understood from the 1960's and concepts devised throughout the following decades aimed at maximising the magnetic field strength B. The most noticed device that was built was the YAMATO-1, as illustrated in figure A.5. This ship was 30m long with a 185 tonne displacement and produced 8kN thrust in each of its two engines using a mean induction of 4 Tesla. However, this system only produced a top speed of 6.6knots and maximum electrical efficiency of 1.4%.

Figure A.5 - YAMATO-1, Mitsubishi Heavy Ind. 1992[2]

Much higher efficiencies have been achieved under laboratory conditions. In 1999, a Chinese-Japanese group [A4] tested a 14T thruster in a closed seawater loop and exceeded an ideal efficiency of 60%, although the magnet weight was very large and the maximum efficiency including all losses was 13%; offsetting the benefit relative to competing technologies. The superconducting dipole magnets used in the previous concepts could be replaced by superconducting solenoids, shown in figure A.6, in order to increase magnetic field strength and reduce weight for the same bore diameter [A1]. This concept may be synergistic with the boundary layer flow control requirements, through the turning of the flow, although the large total pressure losses associated with the helical duct may be significantly detrimental to performance.

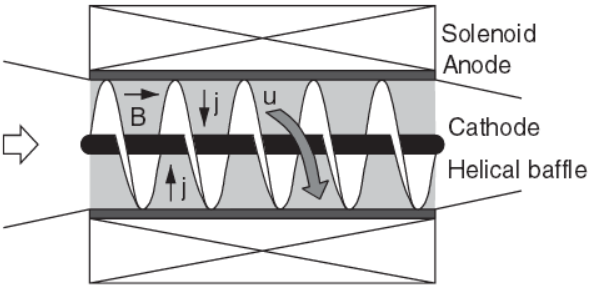

Figure A.6 - Superconducting solenoid magnet configuration[1]

In general, superconductive magnets are being researched through a variety of industries. To date, most superconducting magnets are built from superconducting niobium titanium (NbTi), including the magnets used in the Large Hadron Collider (LHC). However, research into new materials beyond the niobium family is under weigh, such as Bi-2212 (bismuth strontium calcium copper oxide) [A5]. Fermilab scientist Tengming Shen is studying a group of high-field superconductors; in particular Bi2Sr2CaCu2Ox which is expected to achieve a magnetic field strength of up to 50T [A6]. Additionally, in 2000, the U.S. Navy announced that future Naval destroyer ships would all be electrically propelled, due to improved fuel efficiency, flexible design and improved signatures, among other things. Through this, superconducting motors and other related technologies will be researched further [A7]. A combination of the aforementioned programs and other research is likely to enhance the feasibility of MHD propulsion, although it is difficult to say whether magnets will ever be light enough for aeronautical applications.

A3 MPD boundary layer flow control concept

Figure A.7 shows a schematic of the MPD duct that precedes the fan. An electric discharge device is located at fore and aft locations of the duct, stretching a portion of the circumference, as shown in figure A.7. A portion of the boundary layer is then ionised through the creation of an electric field travelling in the axial direction, requiring a voltage of the order of a kV. Electromagnets are positioned around the outer circumference of the duct. A Lorentz force vector F, orthogonal to the electric field and magnetic field is produced, as shown in figure A.8, and acts upon a small strip of fluid to provide a circumferential and radial momentum increase. Additionally,

the movement of the fluid segment entrains the neighbouring fluid; producing a swirl effect. This has the advantage over just swirling the duct that the body forces act on the whole fluid rather than just the outer layer of fluid, therefore enhancing the control of the boundary layer. The electromagnets circumferential position is varied over the axial duct length, such that a flow pattern is produced similar to that in figure A.8. In addition to flow distortion reduction, the concept also produces a total pressure increase that can be translated to thrust using outlet stator vanes and a nozzle, as well as the ability to redirect oncoming flow axially that may originate from crosswinds.

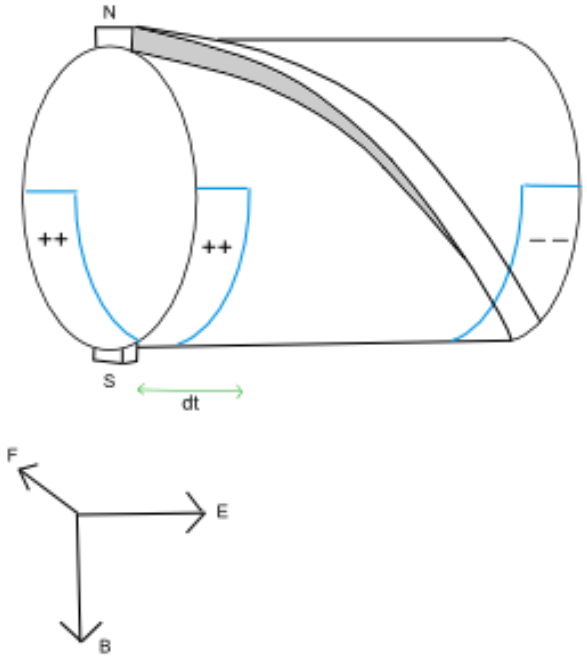

Figure A.7 - MPD duct schematic

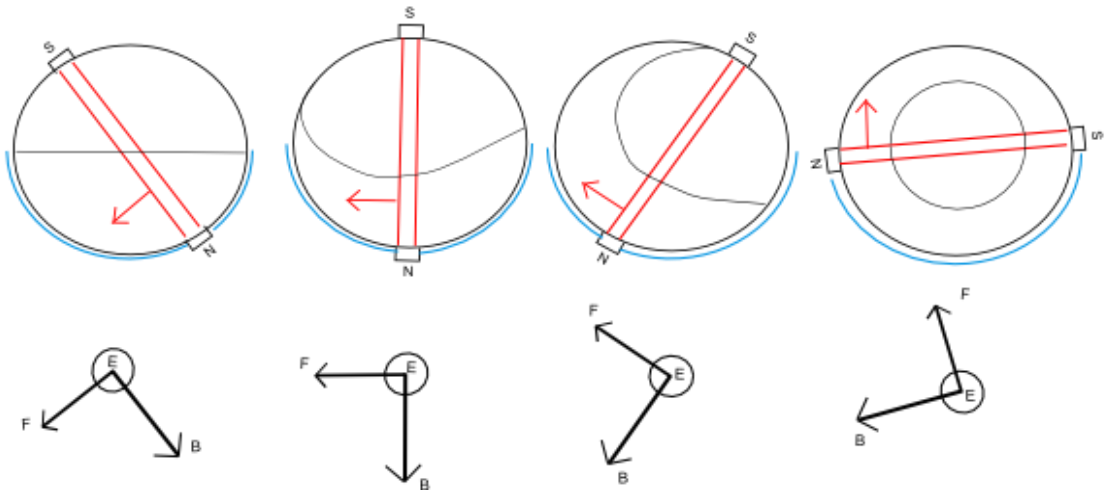

Figure A.8 - MPD force and flow sequence

Figure A.9 shows in detail that an electric field is applied over the boundary layer alone, which provides enough ionization to enable the flow turning whilst restricting the amount of energy lost in the flow due to ionization. By having a small magnetic pole width a small segment of the flow is then forced. The direction of the force provides both a radial and a circumferential pressure gradient, which displaces the inner volume of fluid radially outwards in a swirling motion. Consequently, the circumferential distortion reduces as the fluid moves radially outwards. This is because the neighbouring lower velocity flow closer to the bottom of the duct is being stretched around the circumference and thinned in the outwards radial direction, providing room for the flow at slightly higher velocity to move radially outwards in its place. This effect continues until the highest velocity flow is contained within the inner radius section and the velocity varies in the radial direction alone.

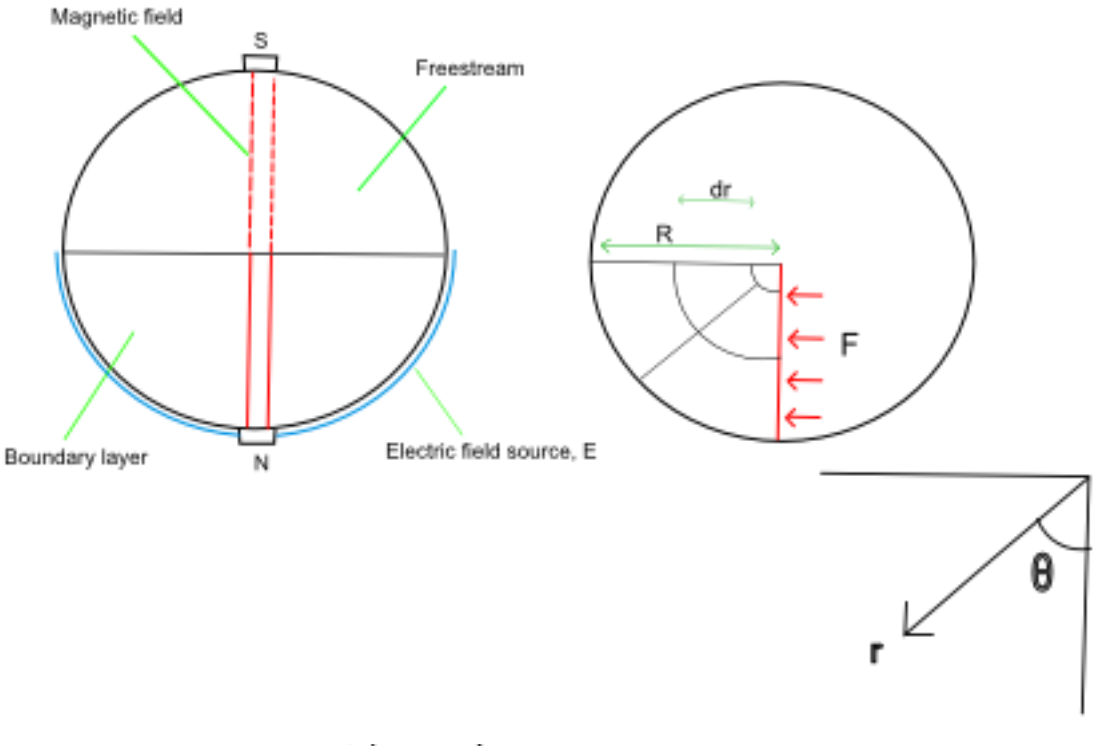

Figure A.9 - MPD force diagram

Figure A.10 presents a slight alternative to the design in figure A.9. Here the radial pressure would be increased by the angle of the applied force relative to the radial segments of flow, producing larger radial flow acceleration. This is the case because the direction of the force vector points more radially outwards. The vector could be changed by changing the position of the magnets around the duct. The exact angle would need to be optimised to obtain the best balance between the stretching of the flow at a specific velocity and the radial motion, otherwise excessive flow mixing would occur and the boundary layer profile would become distorted. The force would remain roughly constant since the magnetic field is applied and the current density is a function of the applied voltage.

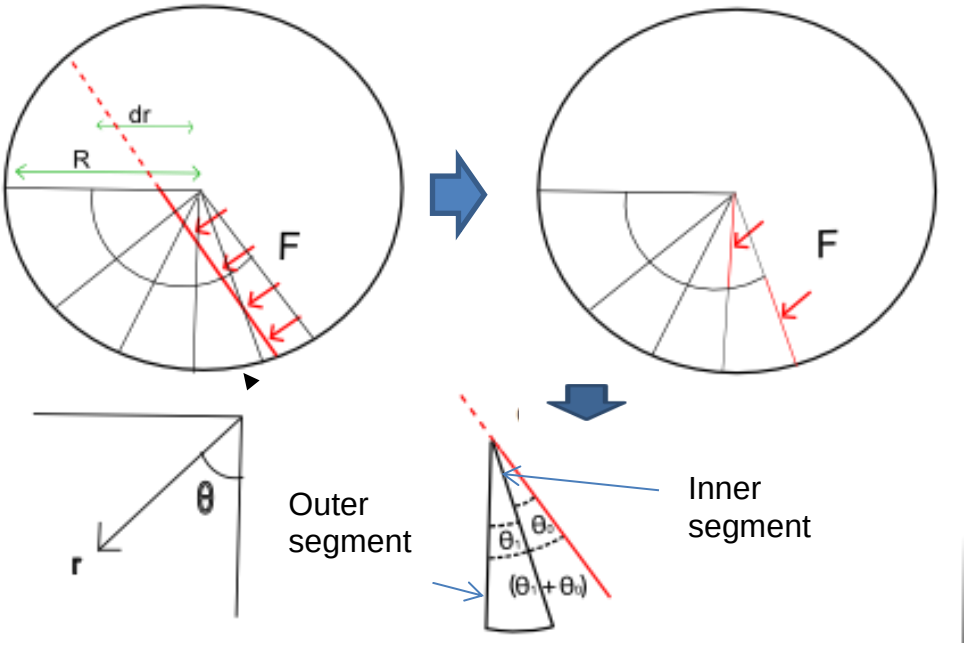

Figure A.10 - Alternative MPD force diagram

The free-body-diagram in figure A.11 gives insight into why a larger radial pressure would exist and is based on the schematic in figure A.10. It contains a number of segments, taken from radial and circumferential directions relative to the applied force position in figure A.10 and shows how the fixed force vector relates to the different segments. The inner and out segment is in contact with the Lorentz force and the other segments to the left circumferentially are affected by resulting pressure forces. p denotes static pressure, F the body force, subscript v the viscous force, δr/R converts the total body force to the force on an individual segment, δt is the unit depth (axially or into the page) and the δrδt transforms the segment force to a pressure or shear stress, depending on if the force vector is oriented normal or tangential to the segment edge, respectively. The cut-away section at the bottom of figure A.10 shows the two angles between the applied body force and two arbitrary segments; inner and outer. The force intersects the radially outer segment at an angle of θ_0, whereas, a force intersects the radially inner segment at a larger angle of $(\theta_0+\theta_1)$. This results in a lower shear stress at a larger radius for a given force angle. This can be shown by the following: the inner radius segment has a shear stress that is equated using the multiplying factor $\sin(\theta_0+\theta_1)$, shown in figure A.11.

The shear stress for the next segment radially outwards is produced using the factor $\cos(\theta_0)\sin(\theta_1)$. This is made up of; the $\cos(\theta_0)$ factor that translates the Lorentz force that is applied to the neighbouring segment at the same radius on the anti-clockwise side to a circumferential force; and the $\sin(\theta_1)$ that translates the angle of the circumferential force to a shear force on the segment in question. Shear stress then decreases with radius, since $\sin(\theta_0+\theta_1) > \cos(\theta_0)\sin(\theta_1)$. Rotational flow effects, compressibility and other fluid flow phenomena may augment or suppress the desired radial displacement of fluid depending on the boundary conditions. Additionally, the normal/circumferential pressure is found to increase radially, since $\cos(\theta_0+\theta_1) < \cos(\theta_0)\cos(\theta_1)$, although an increased Lorentz force may be required to overcome the forces associated with larger energy dissipation due to viscous heating, relating to a large outer surface area.

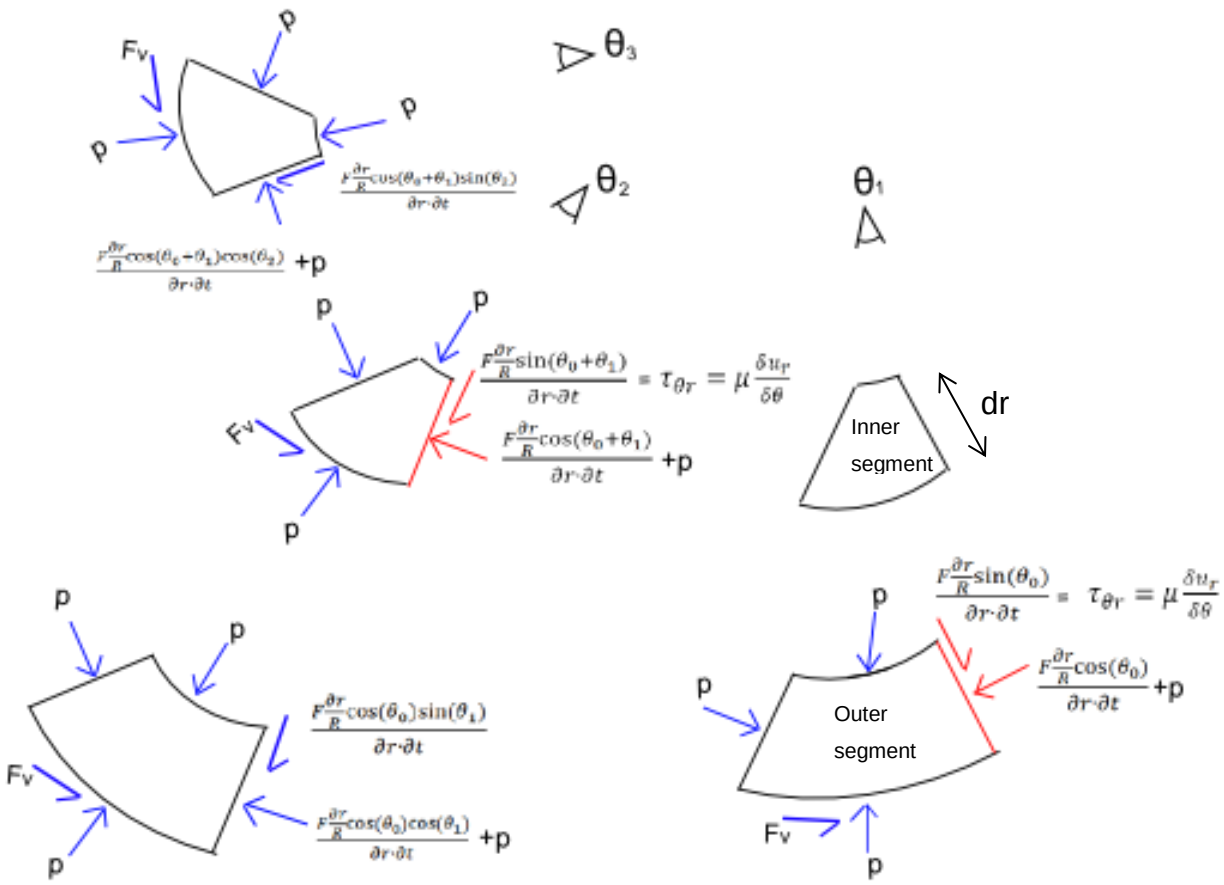

Figure A.11 - MPD free-body force diagram

A4 Non-thermal plasma

One of the main characteristics of plasma is the high bulk fluid temperatures associated with ionisation. High fan entry temperatures would render the concept ineffective because of fan material limits and low thermal/propulsive efficiency. Fortunately, so called ‘non-thermal-equilibrium’ plasmas exist, where the bulk fluid temperature remains at room temperature and only the electron temperature is increased. Using non-homogeneous magnetic fields, the ionisation instability that occurs under non-thermal equilibrium conditions, could be greatly reduced. Therefore the fans would be unaffected. The conditions under which the non-thermal plasma would exist need to be properly understood in order to accurately predict the concept’s performance potential. But roughly speaking, these conditions are achieved through pulsing the electric fields to prevent the bulk fluid temperature from equilibrating with the electron temperature. However, due to time constraints, it has been assumed that the temperature of the bulk fluid remains at ambient temperature.

A5 Modelling methodology

In order to assess the benefit of using MPD to reduce boundary layer distortion, a simplified 1D analytical model was developed to rapidly give a general idea of the system performance. The loss associated with the worse DP fan efficiency due to BLI can be translated into an extra power increment. If the MPD power requirement is similar to this power increment, then the concept should be investigated further.

The method assumes incompressible and inviscid flow and calculates the power required to turn the boundary layer through 180 degrees; from the initial to final positions, as illustrated in figure A.12. The circumferential distortion has been assumed to reduce to a satisfactory level at the final position. The path is simplified to a 1D problem and kinematic expressions are used to enable the force calculation process, which is as follows:

1. Given a boundary layer mass flow and number of fans, the fan radius r is obtained, shown in figure A.12.
2. Using the area-averaged boundary layer axial velocity U (vector points into page in figure A.12) and by choosing a duct length, the time t required for the flow to travel from the entrance to the exit is equated.

3. Assuming the mass flow mean circumferential flow path distance s is located at the equivalent radius of 66% of the outer radius, as illustrated in A.12, the required circumferential acceleration a can be obtained. s is then equal to π multiplied by the equivalent radius.
4. Combining equations A.6 and A.7 and assuming the initial circumferential velocity $u_1$is zero, gives equation A.8; enabling a to be calculated.
5. The final circumferential velocity u_2 is then obtained from equation A.6.

$$u_2 = u_1 + at \quad \textbf{(A.6)}$$

$$u_2{}^2 = u_1{}^2 + 2as \quad \textbf{(A.7)}$$

$$a = \frac{2s}{t^2} \quad \textbf{(A.8)}$$

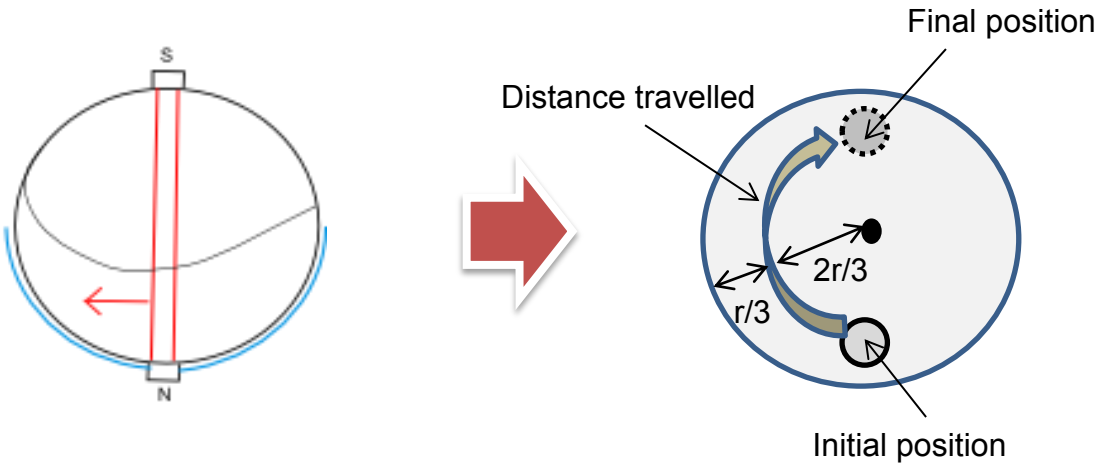

Figure A.12 - Simplified flow path model (view of duct cross-section)

6. The force or momentum increase required is obtain from: mass flow multiplied by u_2, where $u_2$is equivalent to δu_2 since $u_1$is zero.

The MPD power relates to the electromagnetics and the calculation is as follows:

7. The required force from step 6 is equal to the Lorentz force. Equation A.9 provides another different way of expressing the Lorentz force on a single particle to equation A.1, where q is the electric charge for a single particle, n is the number of particles, u is the velocity of the charged particles and is assumed to

equal the axial velocity of the bulk fluid U and therefore the component of velocity of the particles that are associated with the electric field is assumed to be negligible. Another way of viewing this is that the electric field serves to only ionise the air and the charged particles then move with the bulk fluid to provide a current. Additionally, the electrostatic force qE is assumed to be small, the energy density of air is poor which is limited by the electrical breakdown at a value of 3MV/m yielding low pressures that enable work to be done. Instead, magnetic fields can augment the system to produce much large forces. The Lorentz force then simplifies to the electromagnetic force qvB, noting that the cross symbol and bold type can be dropped for a 1D problem.

$$\mathrm{F} = \mathrm{Nq}(\mathrm{E} + \mathrm{u} \times \mathrm{B}) \qquad \textbf{(A.9)}$$

Equation A.10 gives the definition of current I, where L_{duct} is the duct length (since this gives the number of charge particles to pass a cross-sectional plane in the duct per unit time, which is in the direction of the bulk flow).

$$\mathrm{I} = \frac{\mathrm{Nqu}}{\mathrm{L}_{duct}} \qquad \textbf{(A.10)}$$

Current can then be expressed by known parameters by combining equations A.9 and A.10 to yield equation A.11.

$$\mathrm{I} = \frac{\mathrm{F}}{\mathrm{L}_{duct}\mathrm{B}} \qquad \textbf{(A.11)}$$

8. Warrington's empirical formula, equation A.12 [A8], approximates the voltage V required to ionise air, where L_{arc} is the length of the arc or the distance between the anode and cathode, which in this case is equivalent to the duct length. The formula is only valid for still air, however, it provides a good starting point.

$$\mathrm{V} = \frac{28740 * \mathrm{L}_{arc}}{\mathrm{I}^{0.4}} \qquad \textbf{(A.12)}$$

9. Finally, MPD power can be obtained from equation A.13.

$$\mathrm{P} = \mathrm{IV} \qquad \textbf{(A.13)}$$

A6 Results and discussion

A parametric assessment of the MPD system was conducted to ascertain the performance of the system under different conditions and to highlight the key sensitivities. Figures A.13 and A.14 are based on 50kg/s mass flow split over six ducts, 160m/s duct inlet axial velocity. From viewing equation A.11 and A.12, it can be seen that large voltages and low currents are required in order to minimise power, since a reduction in current produces a smaller increase in voltage. As was shown in equation A.5, raising the magnetic field strength increases the ideal efficiency. Since a too larger magnetic field strength requires heavy electromagnets, a magnetic field of five Teslas has been assumed for this study.

Figure A.13 shows tangential velocity or circumferential velocity V_{tan}, and the resultant velocity V_{res} of tangential and axial velocities; both at the duct exit. Both velocities reduce as duct length increases since the flow turning can be achieved in a longer period of time. V_{res} is larger as it also represents the fixed axial velocity component, and is used as the fan inlet velocity and in the fan inlet total pressure calculation. Therefore, the force required also reduces with increasing duct length, which opposes the benefits of BLI.

Figure A.14 shows that power decreases with increasing duct length. This is partly due to the reduced force requirement and partly because power relates to $L_{duct}^{-0.6}$, as can be seen by combining equations A.11 and A.12 to yield an equation for power. Unfortunately, duct weight and drag increase with length, and therefore a trade-off is produced. Because the rate of change in power decreases with duct length, it is likely that a medium sized duct would be chosen and therefore a two metre duct was assumed for further studies. To give an indication of the effect a 2MW power requirement may have, the distributed fans for the 40% TS case, defined by the ratio of distributed fan thrust to total thrust, required around 20MW; therefore 10% power.

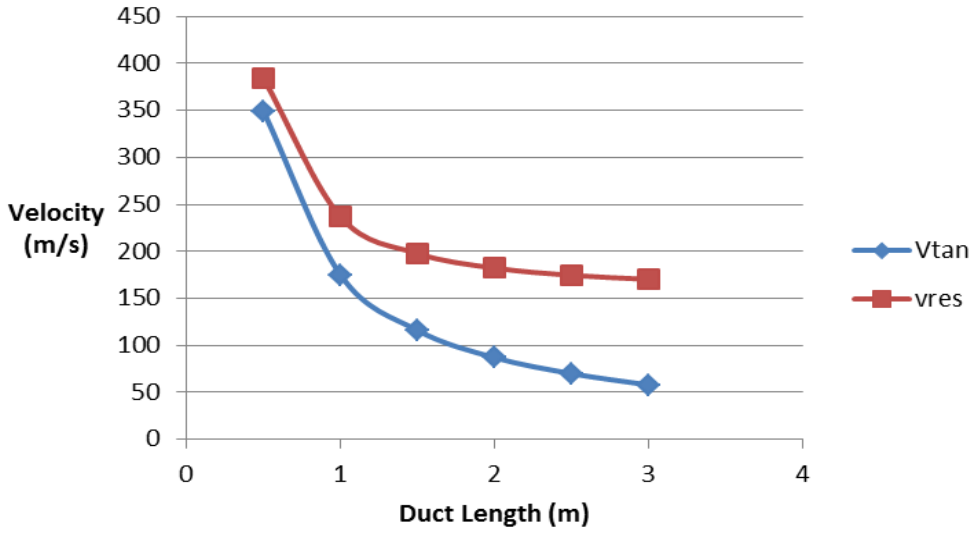

Figure A.13 - Duct outlet velocity vs duct length

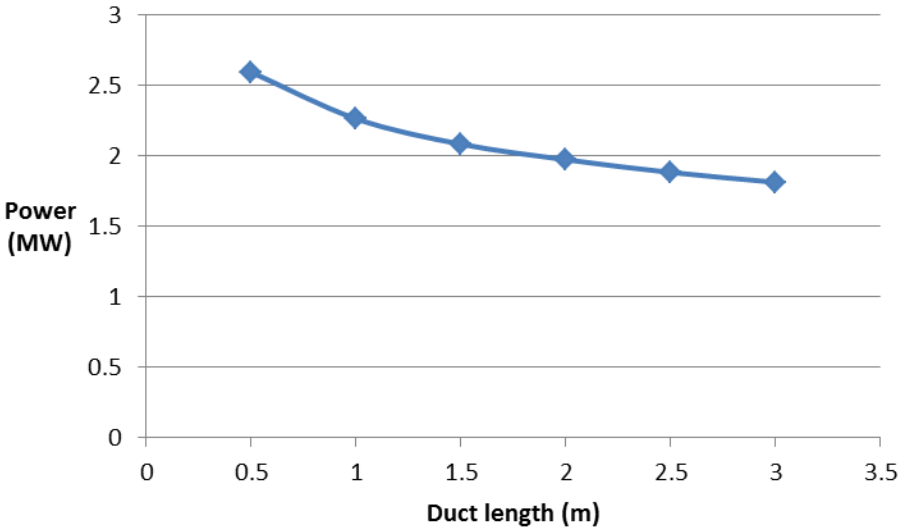

Figure A.14 - Duct outlet velocity vs duct length

Figure A.15 displays the results for a number of cases where the mass flow has been varied to assess the impact on a less efficient fan that has a lower isentropic efficiency due to flow distortion effects. The 'power delta $_{loss}$', defined by equation A.14, is the percentage difference in power of a case with a fan isentropic efficiency of 86% to a normal fan efficiency reference case of 90% efficiency. It can be seen that higher mass flows suffer more from the reduced fan efficiency and therefore show more potential for a flow control concept. This is partly because lowering FPR

doesn't offset the increased mass flow effects on power in relation to a change in fan isentropic efficiency. It is also because power reduces with increasing mass flow due to propulsive efficiency and BLI benefits, and therefore the change in power is relative to a smaller reference power. Additionally, the lower TS cases have a higher power delta, due to the power relative to the higher TS.

$$\text{Power delta}_{\text{loss}} = \frac{P_{86\%} - P_{90\%}}{P_{90\%}} \cdot 100 \qquad \textbf{(A.14)}$$

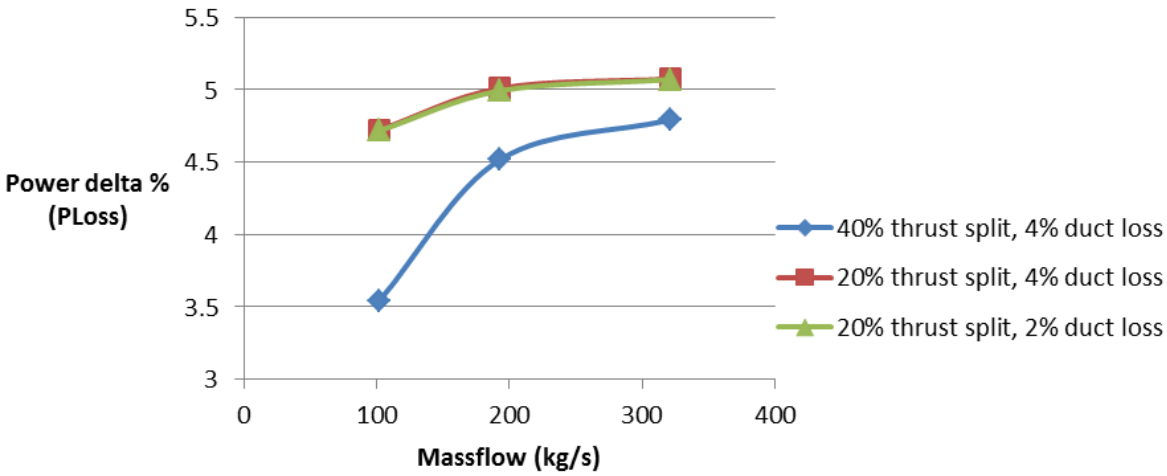

Figure A.15 - Power delta $_{loss}$ vs mass flow

The next task was to compare the MPD power requirement with the power lost through fan distortion effects. Equation A.15 defines the 'power delta $_{MPD}$' parameter that was used to compare the flow control concept with the normal reference case with an isentropic efficiency of 86%. The MPD case assumes that the flow control removes the 4% efficiency penalty.

$$\text{Power delta}_{\text{MPD}} = \frac{(P_{90\%} + P_{\text{MPD}}) - P_{86\%}}{P_{86\%}} \cdot 100 \qquad \textbf{(A.15)}$$

Figure A.16 shows the percentage increase in power required by the case with MPD and the effect of changing mass flow. The vertical lines intersect the corresponding curves to show the mass flow required for optimum fan performance. All cases have a particularly large increase in power requirement, due to the inefficiency of the MPD

system. Unfortunately, the smallest $\text{Power delta}_{\text{MPD}}$ occurs at a low mass flow, whilst the largest losses due to fan distortion occur at high mass flows, as was shown in figure A.15. This lack of synergy is due to the following: Increasing mass flow requires larger duct diameters and therefore the MPD turning force increases due to the increased mass flow and the higher duct exit circumferential velocity. Current is directly proportional to the force requirement, and increases linearly with force for fixed magnetic field strength and duct length. Since high currents are undesirable, the MPD power increases by a greater amount than the losses increase power.

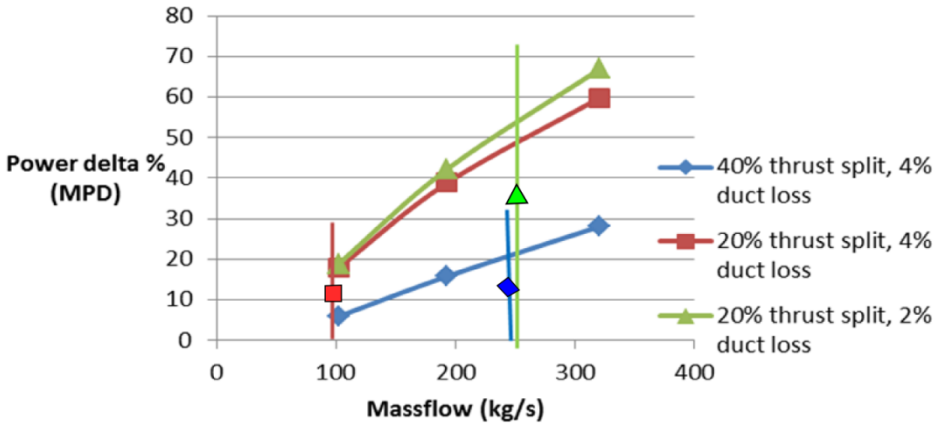

Figure A.16 - Power delta $_{\text{MPD}}$ vs mass flow

Figure A.16 shows that the lower TS case with 4% duct loss has more benefit from the MPD system as the optimum mass flow occurs at a lower $\text{Power delta}_{\text{MPD}}$. Additionally, any further reduction in mass flow will generate a greater reduction in $\text{Power delta}_{\text{MPD}}$ than the 40% TS case. However, since it is more likely that the DP system will be designed for a 40% TS, this case has been chosen for further study.

Figure A.17 shows how the actual power of the different systems varies with mass flow. The case without fan efficiency losses is shown to require around 600kW more power than the case with losses, at the optimum mass flow of which is discussed in Chapter 7 Section 5. Both curves show the power reduces with mass flow due to the reduced specific thrust and BLI benefits, described in Chapter 7 Section 5. The power does increase at higher mass flows, although this graph doesn't contain the needed mass flow range to show this. The 'Without V_{in}' case shows that by ignoring the thrust produced by the MPD system, the power rapidly increases with mass flow,

since the MPD input energy is essentially wasted. However, the 'MPD fan' case shows the MPD thrust production reduces the overall power as mass flow increases, although there is still a significant performance penalty relative to the 'with fan losses' case.

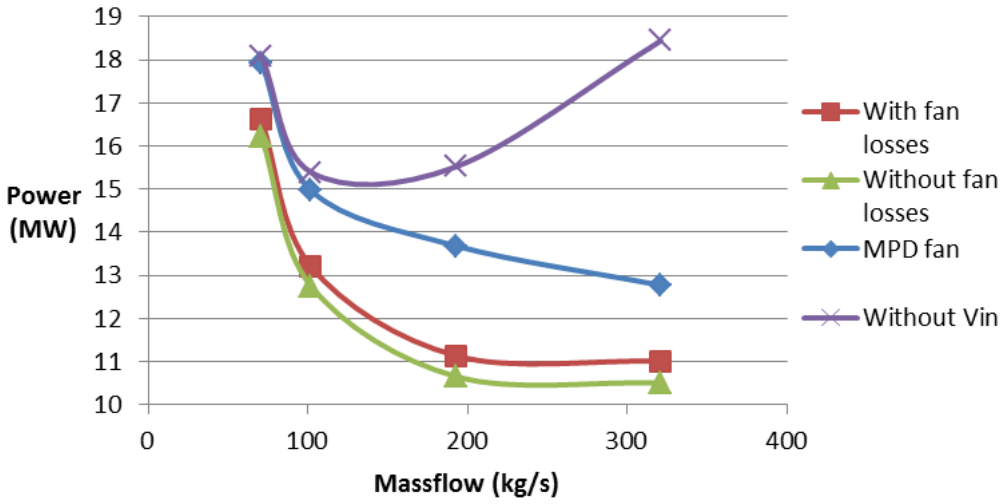

Figure A.17 - Power vs mass flow – TS=40%, 4% duct loss

It was found that by increasing the magnetic field strength, the MPD power requirement could be reduced. However, by using the simple analytical model it was possible to achieve power requirements below the theoretical minimum, or in other words the ideal efficiency could exceed 100%. This is predominantly due to the use of Warrington's formula for voltage and the assumption of still air plasma. In reality, the larger magnetic field strength would interact more strongly with the moving charges and the voltage required for ionization would increase more. In order to fully assess the feasibility of the concept, a 3D simulation using CFD software should be used to model the electromagnetics dynamically, as well as to assess the non-linarites of the flow and magnetic phenomena.

A7 Conclusions

It was found that a fan with a 4% decrease in fan isentropic efficiency due to boundary layer distortion requires around 600kW more power. This gave rise to the development of a flow control concept has been devised in order to reduce the fan distortion associated with BLI. The concept provides an additional contribution to the

PhD, since there is currently no concept of the sort and is effectively a side study that may enhance the feasibility of the DP concept. A literature review was conducted to understand the current state of MPD research and it was found that some aerodynamic flow control studies exist that are based on reducing hypersonic aircraft wing drag. Additionally, there is some MHD research on marine propulsion systems. This pointed towards the concept's applicability in marine craft that utilise BLI.

A 1D model has been developed to rapidly predict the performance of the MPD system. The model is a simplified approach and aims to only approximate the concept's potential, in order to justify further study. The MPD system was assessed through a comparison of an MPD case with high fan efficiency and a case without MPD with a lower fan efficiency. It was shown that higher mass flows induced the greatest performance penalty from the reduced fan efficiency. Unfortunately, electric current increases with mass flow, and since large currents degrade electrical efficiency, the MPD system favours smaller mass flows. In general, the power required for the MPD system was very large and significantly offset the benefit of the flow distortion reduction, under a magnetic field strength of five Teslas. The MPD power requirement drops rapidly as magnetic field strength increases, although the simple 1D model doesn't accurately predict the results.

It was predicted that a higher magnetic field strength would increase the efficiency of the system, However, the current model was found to over predict the benefits of raising magnetic field strength and it was recommended that CFD be used to accurately predict the non-linear flow properties and 3D electromagnetic flow dynamics, of which were the main cause of the inaccuracies.

Other issues associated with the system include: The complication of introducing the technology with other systems in such a compact space; additional propulsion system mass which would reduce the benefit of the whole DP system; and the effect of the large electromagnetic fields on metal aircraft structures.

A8 References

[A1] T. Weier et al., Flow Control and Propulsion in Poor Conductors, Magnetohydrodynamics – Historical Evolution and Trends – Springer, 295–312 (2007).

[A2] YAMATO-1, Mitsubishi Heavy Ind. (1992)

[A3] T.L. Benyo, The Effect of Magnetohydrodynamic (MHD) Energy Bypass on Specific Thrust for a Supersonic Turbojet Engine, AIAA-216734–232 (2010).

[A4] Yan L, Sha C, Peng Y, Zhou K, Yang A, Qing Q, Nishigaki K, Takeda M,Suyama D, Kiyoshi T, Wada H (2002) Results from a 14 T superconducting MHD propulsion experiment. AIAA-paper 2002-2172, (2002).

[A5] G. Sabbi, Website: http://newscenter.lbl.gov/feature-stories/2010/09/10/superconductors-future/ (last accessed Aug 2013).

[A6] B. Wang, Website: http://nextbigfuture.com/2012/05/superconducting-50-tesla-magnet.html (last accessed Aug 2013).

[A7] RAND Corporation, http://www.rand.org/natsec_area/products/electricships.html (last accessed Aug 2013).

[A8] C. Bright, Rolls-Royce SRC Email Correspondence (29/08/2012).

Appendix B – Tools description and origin

The following is a list of the tools used and developed for the PhD work. The data and tools are held on CD with the Rolls-Royce UTC at Cranfield University in the Department of Power and Propulsion. Panagiotis Laskaridis or Maria Negus may be contacted to gain access to the CD.

- Turbomatch – Cranfield University in-house engine performance code used to simulate the turbofan engine for both design point and off design analysis. Access to the code can be sought through Dr. Vassilios Pachidis of the Power and Propulsion Department at Cranfield University.
- Hermes – Cranfield University in-house aircraft performance code used to simulate T&W aircraft for validation of the developed aircraft code CADI. The tool can be accessed through Dr. Panagiotis Laskaridis of the Power and Propulsion Department at Cranfield University.
- XFoil – Panel method tool used to model the boundary layer over the selected aerofoils and provided the input to the DP fan tool. Developed by Prof. Mark Drela and can be obtained easily from the internet as it is freeware in the public domain.
- DP fan performance tool – spreadsheet tool developed by the author to enable the calculation of the distributed fan performance at design point conditions. The XFoil results are input, along with fan technology assumptions. The tool outputs the power requirement of the fans, which is subsequently fed into Turbomatch for overall propulsion system performance. The tool can be accessed through Dr. Panagiotis Laskaridis of the Power and Propulsion Department at Cranfield University.
- CADI – Conceptual Aircraft Design Integration tool – Fortran tool developed by the author to enable the modelling of both conventional and novel aircraft. The tool designs the aircraft by resizing the wing and empennage and requires as input fixed values for a number of parameters, such as overall propulsion system SFC, payload and mission. Key outputs include fuel-burn, static stability and cruise altitude. The code is split into a number of subroutines, which are described below. The code can be accessed through Dr. Panagiotis Laskaridis of the Power and Propulsion Department at Cranfield University.

CADI Code

1. Text input file

```
2       ! BWBTOGG - 2=BWB, 1=T&W
14820000. ! RANGE (m)                    ---------- SI UNITS UNLESS STATED OTHERWISE ---------
```

0.85 ! MCR - MACH NO. CRUISE

74.59 ! VA - APPROACH SPEED (m/s) 93.86 (OLD VALUE)

0.3 ! CL - LIFT COEFFICIENT (CLEAN/CRUISE) 3.265 OLD RATIO CLA/CL ** BWB **

2 !CLATOGG ! 1 FOR AUTOMATED CALCULATION, 2 FOR USER DEFINED INPUT

0.529 ! CLA - APPROACH LIFT COEFF 0.81 - PLAIN FLAPS - 0.55

0.49 ! CL - LIFT COEFFICIENT (CLEAN/CRUISE) 3.265 OLD RATIO CLA/CL ** t&w **

1.6 ! CLA - APPROACH LIFT COEFF

1. !PLANFORMAREAFACTOR - COEFFICIENT THAT MULTIPLIES THE WING AREA

350. ! PAY - PAYLOAD

0.69 ! CABPRESS - CABIN PRESSURE DIFFERENTIAL

5.96 ! W - WIDTH !********** TUBE & WING **********!

7.33 ! H - HEIGHT

73.88 ! L - LENGTH

0.7 ! CM - MATERIAL COEFF

15. ! CO - OPERATIONAL MASS COEFFICIENT

0.79 ! C2 - AIRCRAFT TYPE

5. !LNOSE - FUSELAGE NOSE LENGTH

13.57 !LTAIL - FUSELAGE TAIL LENGTH

45116. !ALTITUDECRUISE - CRUISE ALTITUDE (FT) -- changed in code --

40000 !END CRUISE ALTITUDE (FT) !--A350 ALT--!

1.4216E-05 !MUCR - (CRUISE AIR PROPERTIES)1.4216 !!!-- Requires iterating --!!!

1.52 !VC - CLIMB RATE AT CEILING ALTITUDE 1.52=300FT/MIN

1500. 5000. 10000. 10000. 15000. 20000. 25000. 30689. 30690. 35000. 45071. 48071. ! CLIMB ALTITUDE (FT)

250. 250. 250. 320. 320. 320. 320. 320. 320. 290.9 246.5 229.9 !CAS (KTS)

249.761 249.144 248.096 316.154 313.601 310.506 306.753 301.519 301.519 272.7 229.6 213.6 !EAS(KTS)

259.8 273.2 294.0 374.7 402.9 433.9 467.7 510.1 510.1 501.0 498.7 498.7 !TAS(KTS)

12191.41 10667.48 9143.55 8533.98 7619.63 6095.7 4571.78 3047.85 1523.95 457.18 0. ! DESCENT ALTITUDE

252.4 240.0 227.6 215.3 202.9 190.5 178.1 165.7 153.4 141.0 128.6 ! TAS (M/S)

10.2 !MIN --ASPECT RATIOS-- !********** TUBE & WING PROPERTIES **********!

10.2 !MAX

0.2 !STEP

0.114 !MIN --THICKNESS/CHORDS--

0.114 !MAX

0.002 !STEP

0.12 !TAPER - WING TAPER RATIO

0.8 !BFPERC - PERCENTAGE SPAN FUEL TANK

32.5 !SWEEP - (DEGS)

11. !STEPERC - PERCENTAGE TRAILING EDGE AREA OF WING (REFERENCE AREA)

7.8 !SSLATPERC - PERCENTAGE SLAT AREA OF WING (REFERENCE AREA)

2. !SKRUGPERC - PERCENTAGE KRUGER AREA OF WING (REFERENCE AREA)

1700. !RHOT - WING LOWER SKIN (TENSION) DENSITY

300000000. !SIGMAT - WING UTS LOWER SKIN (TENSION)

1700. !RHOC - WING UPPER SKIN (COMPRESSION) DENSITY

250000000. !SIGMAC - WING UCS UPPER SKIN (COMPRESSION)

1700. !RHOR - RIB DENSITY

1700. !RHOS - SLAT DENSITY

3.81 !NULT - ULTIMATE LOAD FACTOR

5000000000 !G - SHEAR MODULUS

1.4 !LETOG - LEADING EDGE FLAPS PRESENT; 1.4 YES, 1.0 NO

105. !FF - FLAP FACTOR; 0. SINGLE/ 45. DOUBLE/ 105. TRIPLE SLOTTED FLAPS

0.1 !TCEMP - THICKNESS/CHORD OF TAIL AND FIN (USUALLY 0.1)

38. !SWEEPTAILMASTER - SWEEP OF TAIL

38. !SWEEPFINMASTER - SWEEP OF FIN

5.5 !CRTAIL - ROOT CHORD TAIL

7.2 !CRFIN - ROOT CHORD FIN

4.52 !ATAIL - ASPECT RATIO TAIL --SET TO A350--

1.77 !AFIN - ASPECT RATIO TAIL --SET TO A350--

0.33 !TAPERTAIL - TAPER RATIO TAIL -- MEASURED --

0.38 !TAPERFIN - TAPER RATIO FIN -- MEASURED --.28

1. !CT - TAIL VOLUME COEFFICIENT 1.3

0.09 !CF - FIN VOLUME COEFFICIENT 0.106

0.1 !TCTAIL - THICKNESS/CHORD TAIL

0.1 !TCFIN - THICKNESS/CHORD FIN

10.2 !MIN --INNER WING ASPECT RATIOS-- ! ********** BWB PROPERTIES **********!

10.2 !MAX

0.2 !STEP

8. !MIN --OUTER WING ASPECT RATIOS--

8. !MAX

1. !STEP

0.11 !MIN --INNER WING THICKNESS/CHORDS--

0.11 !MAX

0.002 !STEP

0.105 !MIN --OUTER WING THICKNESS/CHORDS-- AT TIP; OUTER KINK IS FIXED

0.105 !MAX

0.002 !STEP

0.2 !MIN --SRATIO; SOUTER/STOTAL--

0.2 !MAX

0.1 !STEP

0.12 !TAPERINNER

0.316 !TAPEROUTER

50. !SWEEPLEINNER

7.36 !SWEEPTEINNER

35. !SWEEPLEOUTER

25. !SWEEPTEOUTER

1900 !RHOBWB

2. !GEARINNERNUM - NUMBER OF MAIN LANDING GEAR UNITS

4.9 !NOSEDIAMETER - DIAMETER OR WIDTH OF NOSE CABIN !******** END OF BWB ********!

1 ! TOGPROPULSION - PROPULSION TOGGLE (1= ONE PODDED PER WING, 2=ONE PODDED PER WING PLUS DISTRIBUTED PROPULSORS - DETAILED BELOW)

16 ! PROPULSORNUMWING - NUMBER OF PROPULSORS FOR HALF WING

12.875 ! PROPULSORWINGDISTANCE - DISTANCE FROM OUTER PROPULSOR TO CENTRE SECTION (M) (FUSELAGE) - ASSUMES EQUAL SPACING

3.42 ! *PROPULSORWINGLENGTH - LENGTH OF PROPULSORS ON WING (CHORDWISE) AND FUSELAGE

0 ! PROPULSORNUMFUSELAGE - NUMBER OF PROPULSORS AROUND FUSELAGE

0.0 ! *PROPULSORFUSELAGEDISTANCE - CIRCUMFERENTIAL DISTANCE COVERED BY FUSELAGE MOUNTED PROPULSORS

0.56 ! PROPULSORTHRUSTFACTOR - RATIO OF DISTRIBUTED PROPULSORS (WING+FUSELAGE) THRUST TO TOTAL THRUST

2. ! PPNUM - TOTAL NUMBER OF UNDERWING PODDED POWERPLANTS

0.29 ! ETAPP - RELATIVE SPANWISE DISTANCE TO ENGINES (ENGINE FROM CENTRE LINE/SEMISPAN); ONLY ALLOWED AT CENTRE LINE IF TOGPROPULSION=1 (AS FANS FIN SIZE REDUCTION IS FUNCTION OF ENGINE DISTANCE)

0.87 ! THETAAREA - MOMENTUM THICKNESS AREA REMOVAL FOR OUTER CONTROL VOLUME (TOTAL I.E. WING+FUSELAGE)

0.05 ! DPFINFRAC - BWB ONLY; NON-AXISYMETIC FIN SIZE REDUCTION DUE TO ENGINE FROM WING TO CENTRE (NORMALLY 5% = 0.05)

6.59 !LNAC - NACELLE LENGTH

4.39 !HNAC - NACELLE HEIGHT

4.39 !WNAC - NACELLE WIDTH

1.915 !C3 - ENGINE COEF !!!!-- INCREASED TO MEET RR VALUE GIVEN --!!!! 1.815

19259. !MPPFIXED - TOTAL POWERPLANT MASS (0.0 IF USER WANTS CODE TO COMPUTE VALUE)

6.5 !THUSTLOAD - THRUST/Mg

0.0 !LAMPERCWING - LAMINAR FLOW PERCENTAGE OVER WING

0.0 !LAMPERCFUS - LAMINAR FLOW PERCENTAGE OVER FUSELAGE

0.0 !LAMPERCNAC - LAMINAR FLOW PERCENTAGE OF NACELLE

0.0 !LAMPERCEMP - LAMIAR FLOW PERCENTAGE OVER EMPENNAGE

0.0 !LFCFUS - FUSELAGE MASS/AREA FOR LAMINAR FLOW CONTROL (WETTED)

0.0 !LFCEMP - EMPENNAGE MASS/AREA FOR LAMINAR FLOW CONTROL

0.0 !LFCWING - WING MASS/AREA FOR LAMINAR FLOW CONTROL (REF)

0.000005 !TRIM DRAG COEFF

0.0010 !WAVE DRAG COEFF

1.105 !TCK - CONSTANT FOR YEAR OF AIRCRAFT

0.0115 !SFCCLIMB - CLIMB SFC !!!!!!!!! sfc includes future reduction and 1% lfc hit

0.0078 !SFCTO - TAKEOFF SFC

0.01351 !SFCCR - CRUISE SFC

0.01745 !SFCD - SFC DESCENT

0.1431 !C4 - EQUIP/SYSTEMS/GEAR COEF (INCLUDES FUEL SYSTEMS MASS FOR AIRCRAFT/ENGINE)

0.5 !DELTASFACT - FACTOR FOR SHEET TAPER REDUCTION (RATIO, 1=NONE REDUCED)

0.009660057 0.009830028 0.010113314 0.011643059 0.012067989 0.012521246 0.012974504 0.013569405 0.013654391 0.013654391 0.013824363 0.0 !sfc

4.782833251 4.468683391 4.054763076 3.719626168 4.378914576 4.073782587 4.802016724 3.523610428 3.785948516 3.785948516 2.152975898 1. !THRUST FACTOR

45013. !ALTCEILING – MAY NEED ITERATING, UNLESS DONE AUTOMATCIALLY IN CODE

2. ‘Main’ subroutine – this routine is the base of the code for the T&W aircraft and reads in data from the input file entitled ‘Input’.

```
SUBROUTINE MAIN(BWBTOGG)


IMPLICIT NONE


!************************************************ CLIMB ARRAYS

DOUBLE PRECISION,DIMENSION(12)::ALT
DOUBLE PRECISION, DIMENSION(12)::TEMP
DOUBLE PRECISION,DIMENSION(12)::RHO
DOUBLE PRECISION,DIMENSION(12)::TAS
DOUBLE PRECISION,DIMENSION(12)::EAS

DOUBLE PRECISION,DIMENSION(12)::ALTMASTER
DOUBLE PRECISION, DIMENSION(12)::TEMPMASTER
DOUBLE PRECISION,DIMENSION(12)::RHOMASTER
DOUBLE PRECISION,DIMENSION(12)::PRESSUREMASTER
DOUBLE PRECISION,DIMENSION(12)::TASMASTER
DOUBLE PRECISION,DIMENSION(12)::CASMASTER

DOUBLE PRECISION,DIMENSION(12)::MACH
DOUBLE PRECISION,DIMENSION(12)::CAS
DOUBLE PRECISION,DIMENSION(12)::MASS
DOUBLE PRECISION,DIMENSION(12)::CLC
DOUBLE PRECISION,DIMENSION(12)::CD
DOUBLE PRECISION,DIMENSION(12)::DRAGS
DOUBLE PRECISION,DIMENSION(12)::THRUST
DOUBLE PRECISION,DIMENSION(12)::SFC
DOUBLE PRECISION,DIMENSION(12)::ROC
DOUBLE PRECISION,DIMENSION(12)::CORR
DOUBLE PRECISION,DIMENSION(12)::ROCCORR
DOUBLE PRECISION,DIMENSION(12)::ROCMEAN
DOUBLE PRECISION,DIMENSION(12)::T
DOUBLE PRECISION,DIMENSION(12)::TCUM
DOUBLE PRECISION,DIMENSION(12)::FFLOW
DOUBLE PRECISION,DIMENSION(12)::F
DOUBLE PRECISION,DIMENSION(12)::FCUM
DOUBLE PRECISION,DIMENSION(12)::RANG
DOUBLE PRECISION,DIMENSION(12)::RCUM

DOUBLE PRECISION,DIMENSION(12)::THRUSTFACTOR
DOUBLE PRECISION,DIMENSION(12)::PRESSURE


!********************************************************** DESCENT ARRAYS
```

```
DOUBLE PRECISION,DIMENSION(11)::ALTD
REAL,DIMENSION(11)::TEMPD
DOUBLE PRECISION,DIMENSION(11)::RHOD

DOUBLE PRECISION,DIMENSION(11)::TASD
DOUBLE PRECISION,DIMENSION(11)::MACHD
DOUBLE PRECISION,DIMENSION(11)::CASD
DOUBLE PRECISION,DIMENSION(11)::MASSD
DOUBLE PRECISION,DIMENSION(11)::CLD
DOUBLE PRECISION,DIMENSION(11)::CDD
DOUBLE PRECISION,DIMENSION(11)::DRAGSD
DOUBLE PRECISION,DIMENSION(11)::THRUSTD
DOUBLE PRECISION,DIMENSION(11)::ROCD
DOUBLE PRECISION,DIMENSION(11)::CORRD
DOUBLE PRECISION,DIMENSION(11)::ROCCORRD
DOUBLE PRECISION,DIMENSION(11)::ROCMEAND
DOUBLE PRECISION,DIMENSION(11)::TD
DOUBLE PRECISION,DIMENSION(11)::TCUMD
DOUBLE PRECISION,DIMENSION(11)::FFLOWD
DOUBLE PRECISION,DIMENSION(11)::FD
DOUBLE PRECISION,DIMENSION(11)::FCUMD
DOUBLE PRECISION,DIMENSION(11)::RANGD
DOUBLE PRECISION,DIMENSION(11)::RCUMD


!*****************************************************************  -- OUTPUT ARRAYS --

DOUBLE PRECISION,ALLOCATABLE :: ARESULT(:)
DOUBLE PRECISION,ALLOCATABLE :: TCRESULT(:)
DOUBLE PRECISION,ALLOCATABLE :: SWINGRESULT(:)
DOUBLE PRECISION,ALLOCATABLE :: LDRESULT(:)

DOUBLE PRECISION,ALLOCATABLE :: CD0WINGRESULT(:)
DOUBLE PRECISION,ALLOCATABLE :: CD0FUSRESULT(:)
DOUBLE PRECISION,ALLOCATABLE :: CD0NACRESULT(:)
DOUBLE PRECISION,ALLOCATABLE :: CD0TAILRESULT(:)
DOUBLE PRECISION,ALLOCATABLE :: CD0FINRESULT(:)

DOUBLE PRECISION,ALLOCATABLE :: CD0TOTRESULT(:)
DOUBLE PRECISION,ALLOCATABLE :: CDIRESULT(:)
DOUBLE PRECISION,ALLOCATABLE :: CDTRESULT(:)
DOUBLE PRECISION,ALLOCATABLE :: CDWRESULT(:)
DOUBLE PRECISION,ALLOCATABLE :: CDTOTRESULT(:)

DOUBLE PRECISION,ALLOCATABLE :: MTOWRESULT(:)
DOUBLE PRECISION,ALLOCATABLE :: OEWRESULT(:)
DOUBLE PRECISION,ALLOCATABLE :: MLWRESULT(:)
DOUBLE PRECISION,ALLOCATABLE :: MFUSRESULT(:)
DOUBLE PRECISION,ALLOCATABLE :: MEMPRESULT(:)
DOUBLE PRECISION,ALLOCATABLE :: MWINGRESULT(:)
DOUBLE PRECISION,ALLOCATABLE :: MEQRESULT(:)
DOUBLE PRECISION,ALLOCATABLE :: MOPSRESULT(:)
DOUBLE PRECISION,ALLOCATABLE :: MPAYRESULT(:)
DOUBLE PRECISION,ALLOCATABLE :: MPPRESULT(:)
DOUBLE PRECISION,ALLOCATABLE :: MFUELTOTRESULT(:)
DOUBLE PRECISION,ALLOCATABLE :: MFUELRESRESULT(:)
DOUBLE PRECISION,ALLOCATABLE :: MFUELTORESULT(:)
DOUBLE PRECISION,ALLOCATABLE :: ALTRESULT(:)
DOUBLE PRECISION,ALLOCATABLE :: THRUSTCEILINGRESULT(:)
DOUBLE PRECISION,ALLOCATABLE :: THRUSTCRRESULT(:)
DOUBLE PRECISION,ALLOCATABLE :: MLFCTOTRESULT(:)


REAL MCR, L, CABPRESS, CM, NULT, LAMPERCWING, RHOSLS, &
& VA, PAY, W, H, CO, C2, AMIN, AMAX, CLA, TAPER, BFPERC, SWEEPMASTER, STEPERC, SSLATPERC, &
& SKRUGPERC, ETAPP, PPNUM, LETOG, FF, TCEMP, CRTAIL, CRFIN, ATAIL, AFIN, CT, &
& CF, R, ACR, VD, VS, SWEEPHALF, TCROOT, LAMPERCFUS, LNOSE, LTAIL, LNAC, LAMPERCNAC, HNAC, &
& WNAC, MACTAIL, MACFIN, LAMPERCEMP, TCTAIL, TCFIN, STAIL, SFIN, CL, THRUSTLOAD, &
& C3, SFCD, SWEEPLE, LD, C4, SWETFUS, DELTASFACT, CROOT, CTIP, SPAN, TCS, TCK, &
& SWEEP, PROPULSORWINGDISTANCE, PROPULSORNUMFUSELAGE, PROPULSORTHRUSTFACTOR, CCS, TAPERTAIL, &
& TAPERFIN, SWEEPTAIL, SWEEPFIN, SWEEPHALFTAIL, SWEEPHALFFIN, SWEEPTAILMASTER, &
& SWEEPFINMASTER, ASPECTTAIL, ASPECTFIN, SPANTAIL, SPANFIN, SWEEPTAILLE, SWEEPFINLE, TTIP, &
& TC70, TC40, TCTIP, BHALF, BFHALF, BCSHALF, TROOT, TTO, VC
```

```
INTEGER ANUM, TCNUM, N, J, STEP, ELEMENTTC, ELEMENTA, RESULTELEMENT, ARRAYNUM, ISTEP, &
& JSTEP, THRUSTNUM, INT, INTS, X, TOGPROPULSION, PROPULSORNUMWING, CTOG, I, TOGGNACELLE, &
& BWBTOGG, CLATOGG

DOUBLE PRECISION MUCR, TCMIN, TCMAX, TCSTEP, ASTEP, A, TC, MWING, MACWING, &
& RHOT, SIGMAT, RHOC, SIGMAC, RHOR, RHOS, SHEARMOD, MPAY, MOPS, MFUS, &
& MFRES, SWING, SWINGWET, OEW, CDT, CDW, K, CD0TOT, SFCCLIMB, MTOW, &
& MLW, MPP, MZFW, MBASIC, MPRIM, MSEC, MEMP, SFCTO, RANGE, SFCCR, CDTOT, MFUELTOT, MFUELRES, &
& MEQ, THRUSTTO, MTOWSTORE, ERROR, GAMMA, MFUELTO, MLFC, LFCFUS, LFCEMP, LFCWING, MLFCFUS, &
& MLFCEMP, MLFCWING, MLFCTOT, THRUSTCR, V2, TOL, THRUSTTO2, RHOCEIL, RHOCR, ALTCEILING, &
& PRESSURESLS, ALTITUDECRUISE, PRESSURECR, PROPERTIES, ALTITERATION, ALTITUDECRUISEEND, &
& TEMPCR, PROPULSORFUSELAGEDISTANCE, SWINGPROPULSORS, SWINGBLI, PROPULSORWINGLENGTH, &
& CFACTOR, CD0FIN, CD0TAIL, FUELVOLUMETOTAL, FUELVOLUMEOUTER, FUELVOLUMEINNER, &
& FUELAREAOUTER, FUELLENGTHOUTER, FUELAREAINNER, TFUELOUTER, T40, C40, &
& FUELVOLUMEREQ, FUELDENSITY, TCCS, B70, B40, MPPFIXED, Z, CD0WING, CD0FUS, CD0NAC, CDI, &
& TCR, MFUELCR, RANGECR, MFUELL, TTOTAL, OSWALDFACTOR, GROSSFACTOR, THETAAREA, DPFINFRAC



!************************************************************************** ASPECT
RATIO AND THICKNESS/CHORD INPUT ARRAYS

DOUBLE PRECISION,ALLOCATABLE :: ASPECT(:)
DOUBLE PRECISION,ALLOCATABLE :: TCHORD(:)


!**************************************************************************  ---   OPEN
AND READ INPUT FILE ---


OPEN(UNIT=10,FILE='INPUT\INPUT.TXT',STATUS='OLD')

READ (10,*)BWBTOGG
READ (10,*)RANGE
READ (10,*)MCR
READ (10,*)VA

READ (10,*)Z
READ (10,*)Z
READ (10,*)Z
READ (10,*)CL
READ (10,*)CLA

!READ FUSELAGE INPUTS

READ (10,*)PAY
READ (10,*)CABPRESS


READ (10,*)W
READ (10,*)H
READ (10,*)L
READ (10,*)CM
READ (10,*)CO
READ (10,*)C2
READ (10,*)LNOSE
READ (10,*)LTAIL

READ (10,*)ALTITUDECRUISE
READ (10,*)ALTITUDECRUISEEND
READ (10,*)MUCR
READ (10,*)VC



READ (10,*) (ALT(I), I = 1, 12)
READ (10,*) (CAS(I), I = 1, 12)
READ (10,*) (EAS(I), I = 1, 12)
READ (10,*) (TAS(I), I = 1, 12)

READ (10,*) (ALTD(I), I = 1, 11)
READ (10,*) (TASD(I), I = 1, 11)
```

```
READ (10,*)AMIN
READ (10,*)AMAX
READ (10,*)ASTEP


READ (10,*)TCMIN
READ (10,*)TCMAX
READ (10,*)TCSTEP


READ (10,*)TAPER
READ (10,*)BFPERC
READ (10,*)SWEEPMASTER
READ (10,*)STEPERC
READ (10,*)SSLATPERC
READ (10,*)SKRUGPERC

READ (10,*)RHOT
READ (10,*)SIGMAT
READ (10,*)RHOC
READ (10,*)SIGMAC
READ (10,*)RHOR
READ (10,*)RHOS
READ (10,*)NULT
READ (10,*)SHEARMOD
READ (10,*)LETOG
READ (10,*)FF

READ (10,*)TCEMP
READ (10,*)SWEEPTAILMASTER
READ (10,*)SWEEPFINMASTER
READ (10,*)CRTAIL
READ (10,*)CRFIN
READ (10,*)ATAIL
READ (10,*)AFIN
READ (10,*)TAPERTAIL
READ (10,*)TAPERFIN
READ (10,*)CT
READ (10,*)CF
READ (10,*)TCTAIL
READ (10,*)TCFIN

READ (10,*)Z
READ (10,*)Z
READ (10,*)Z
READ (10,*)Z
READ (10,*)Z
READ (10,*)Z
READ (10,*)Z
READ (10,*)Z
READ (10,*)Z
READ (10,*)Z
READ (10,*)Z
READ (10,*)Z
READ (10,*)Z
READ (10,*)Z
READ (10,*)Z
READ (10,*)Z
READ (10,*)Z
READ (10,*)Z
READ (10,*)Z
READ (10,*)Z
READ (10,*)Z
READ (10,*)Z
READ (10,*)Z


READ (10,*)TOGPROPULSION
READ (10,*)PROPULSORNUMWING
READ (10,*)PROPULSORWINGDISTANCE
READ (10,*)PROPULSORWINGLENGTH
READ (10,*)PROPULSORNUMFUSELAGE
```

```
READ (10,*)PROPULSORFUSELAGEDISTANCE
READ (10,*)PROPULSORTHRUSTFACTOR
READ (10,*)PPNUM
READ (10,*)ETAPP
READ (10,*)THETAAREA
READ (10,*)DPFINFRAC

READ (10,*)LNAC
READ (10,*)HNAC
READ (10,*)WNAC
READ (10,*)C3
READ (10,*)MPPFIXED
READ (10,*)THRUSTLOAD

READ (10,*)LAMPERCWING
READ (10,*)LAMPERCFUS
READ (10,*)LAMPERCNAC
READ (10,*)LAMPERCEMP
READ (10,*)LFCFUS
READ (10,*)LFCEMP
READ (10,*)LFCWING
READ (10,*)CDT
READ (10,*)CDW
READ (10,*)TCK

READ (10,*)SFCCLIMB
READ (10,*)SFCTO
READ (10,*)SFCCR
READ (10,*)SFCD

READ (10,*)C4
READ (10,*)DELTASFACT


READ (10,*)SFC
READ (10,*)THRUSTFACTOR
READ (10,*)ALTITERATION

CLOSE(10)

!-------------------------------------------------------------------------------------------------
------------------ INITIAL CALCULATIONS AND VARIABLES -----------------------------


ALTITERATION=ALTITERATION/3.281             !CONVERT TO METRES - SEE PERFORMANCE SUBROUTINE
FOR DEFINITION

DO X=1,12

ALT(X)=ALT(X)/3.281 !CONVERT TO METRES
TAS(X)=TAS(X)*0.5144   !CONVERT TO M/S
EAS(X)=EAS(X)*0.5144
CAS(X)=CAS(X)*0.5144

END DO

!****************************************** -- CLIMB AIR PROPERTIES --

GAMMA=1.4     !GAS CONSTANTS
R=287.05


DO X=1,12


        IF (ALT(X)<11000) THEN

            TEMP(X)=288.15-0.0065*ALT(X)
            PRESSURE(X)=101325*(288.15/TEMP(X))**(-5.25588)

        END IF


        IF (ALT(X)>=11000 .AND. ALT(X)<24994) THEN
```

```
            TEMP(X)=216.65
            PRESSURE(X)=22.63253/EXP(0.000157689*(ALT(X)-10998.1))*1000

        END IF


        IF (ALT(X)>=24994 .AND. ALT(X)<30000) THEN

            TEMP(X)=216.65+0.0029892*(ALT(X)-24994)
            PRESSURE(X)=2.5237*(216.65/TEMP(X))**11.8*1000

        END IF



        RHO(X)=PRESSURE(X)/(R*TEMP(X))

END DO


!********************************************** -- CRUISE AIR PROPERTIES --

ALTITUDECRUISE=ALTITUDECRUISE/3.281    !CONVERSION TO METRES
ALTITUDECRUISEEND=ALTITUDECRUISEEND/3.281



        IF (ALTITUDECRUISE<11000) THEN

            TEMPCR=288.15-0.0065*ALTITUDECRUISE
            PRESSURECR=101325*(288.15/TEMPCR)**(-5.25588)

        END IF

        IF (ALTITUDECRUISE>=11000 .AND. ALTITUDECRUISE<24994) THEN

            TEMPCR=216.65
            PRESSURECR=22.63253/EXP(0.000157689*(ALTITUDECRUISE-10998.1))*1000

        END IF

        IF (ALTITUDECRUISE>=24994 .AND. ALTITUDECRUISE<30000) THEN

            TEMPCR=216.65+0.0029892*(ALTITUDECRUISE-24994)
            PRESSURECR=2.5237*(216.65/TEMPCR)**11.8

        END IF


RHOCR=PRESSURECR/(R*TEMPCR)
PRESSURESLS=101325
!MUCR=1.015D-6*TEMPCR**1.5/(TEMPCR+120)


!************************************


ACR=SQRT(GAMMA*R*TEMPCR)                                          !CRUISE SPEED OF SOUND

VD=ACR*MCR                                                          !DESIGN SPEED

VS=93.86/1.3                                                          !STALL SPEED

RHOSLS=1.2248

!*********************************************************************  FIXED MASSES


MPAY=PAY*95.17                                                       !95KG PAX
```

```
MOPS=PAY*CO                                                              !OPERATIONAL ITEMS
MASS

MFUS=C2*CABPRESS*(9.75+(5.84*W))*(((2*L)/(W+H))-1.5)*((W+H)**2)*CM       !FUSELAGE MASS -
EMPIRICAL 'Howe' METHOD



!------------------------------------------------------------------------------------------ LOOP
SPECIFACTIONS ------------------------------------------------------------------------


ANUM=((AMAX-AMIN)/ASTEP)+1                   !ALLOCATING 'TC' AND 'A' ARRAYS FOR GIVEN RANGE
TCNUM=((TCMAX-TCMIN)/TCSTEP)+1

ALLOCATE(ASPECT(ANUM))
ALLOCATE(TCHORD(TCNUM))



DO ISTEP=1,ANUM                              !FILL INPUT VARIABLE ARRAYS
    ASPECT(ISTEP)=AMIN+ASTEP*(ISTEP-1)
END DO


DO JSTEP=1,TCNUM
    TCHORD(JSTEP)=TCMIN+TCSTEP*(JSTEP-1)
END DO


ARRAYNUM=ANUM*TCNUM                          ! SIZE OF OUTPUT ARRAYS

RESULTELEMENT=0                              !NULL THE RESULT ARRAY NUMBERS



ALLOCATE(ARESULT(ARRAYNUM))                 !ALLOCATE ARRAY SIZE TO EACH OUTPUT ARRAY
ALLOCATE(TCRESULT(ARRAYNUM))
ALLOCATE(SWINGRESULT(ARRAYNUM))
ALLOCATE(LDRESULT(ARRAYNUM))

ALLOCATE(CD0WINGRESULT(ARRAYNUM))
ALLOCATE(CD0FUSRESULT(ARRAYNUM))
ALLOCATE(CD0NACRESULT(ARRAYNUM))
ALLOCATE(CD0TAILRESULT(ARRAYNUM))
ALLOCATE(CD0FINRESULT(ARRAYNUM))

ALLOCATE(CD0TOTRESULT(ARRAYNUM))
ALLOCATE(CDIRESULT(ARRAYNUM))
ALLOCATE(CDTRESULT(ARRAYNUM))
ALLOCATE(CDWRESULT(ARRAYNUM))
ALLOCATE(CDTOTRESULT(ARRAYNUM))

ALLOCATE(MTOWRESULT(ARRAYNUM))
ALLOCATE(OEWRESULT(ARRAYNUM))
ALLOCATE(MLWRESULT(ARRAYNUM))
ALLOCATE(MFUSRESULT(ARRAYNUM))
ALLOCATE(MEMPRESULT(ARRAYNUM))
ALLOCATE(MWINGRESULT(ARRAYNUM))
ALLOCATE(MEQRESULT(ARRAYNUM))
ALLOCATE(MOPSRESULT(ARRAYNUM))
ALLOCATE(MPAYRESULT(ARRAYNUM))
ALLOCATE(MPPRESULT(ARRAYNUM))
ALLOCATE(MFUELTOTRESULT(ARRAYNUM))
ALLOCATE(MFUELRESRESULT(ARRAYNUM))
ALLOCATE(MFUELTORESULT(ARRAYNUM))
ALLOCATE(ALTRESULT(ARRAYNUM))
ALLOCATE(THRUSTCEILINGRESULT(ARRAYNUM))
ALLOCATE(THRUSTCRRESULT(ARRAYNUM))
ALLOCATE(MLFCTOTRESULT(ARRAYNUM))
```

```
ALTMASTER=ALT                        !STORING ORIGINALLY READ ARRAYS
TEMPMASTER=TEMP
RHOMASTER=RHO
PRESSUREMASTER=PRESSURE
TASMASTER=TAS
CASMASTER=CAS

CTOG=0 !STOPS EMMPENAGE VOLUME COEFS. CHANGING REPEATEDLY - SEE 'WING'
TOGGNACELLE=0  !NACCELLE DRAG BLI

!-------------------------------------------------------------------------------------------
-- MAIN LOOP FOR VARYING INPUT VARIABLES ----------------------------------------

DO JSTEP=1,TCNUM                     !MAIN LOOP FOR RANGED VARIABLES

TC=TCHORD(JSTEP)

    DO ISTEP=1,ANUM
    A=ASPECT(ISTEP)

    ALT=ALTMASTER                     !RENEWING ORIGINALLY READ PARAMETERS ('ALT' SUBROUTINE
CAN CHANGE THESE DURING LOOP)
    TEMP=TEMPMASTER
    RHO=RHOMASTER
    PRESSURE=PRESSUREMASTER
    TAS=TASMASTER
    CAS=CASMASTER







     !***********************************           !INITIAL MASSES

    MLW=MFUS+MOPS+(2*MPAY)           !MAX LANDING WEIGHT

    MWING=0
    MTOWSTORE=0
    MPP=0
    MZFW=0
    MFUELTOT=0
    MFUELRES=0              !FUEL RESERVE
    MEQ=0
    MTOW=MLW
    OEW=MFUS+MOPS
    !***********************************


! -------------------------------------------------------------------------------------------
--------- MTOW ITERATION LOOP -----------------------------------------------------



    DO



        CALL WING(MLW, RHOSLS, CLA, VS, SWING, A, TC, TAPER, BFPERC, SWEEPMASTER, SWINGWET,
STEPERC, &
        & SSLATPERC, SKRUGPERC, MTOW, MWING, ETAPP, MPP, PPNUM, MZFW, RHOT, SIGMAT, RHOC,
SIGMAC, &
        & RHOR, NULT, SHEARMOD, RHO(11), MCR, LETOG, RHOS, FF, VD, MBASIC, MPRIM, MSEC, MEMP,
TCEMP, &
        & CRTAIL, CRFIN, ATAIL, AFIN, MACTAIL, MACFIN, CT, CF, L, MACWING, STAIL, &
        & SFIN, SWEEPHALF, TCROOT, SWEEPLE, DELTASFACT, CROOT, CTIP, SPAN, TCS, &
        & SWEEP, TOGPROPULSION, PROPULSORNUMWING, PROPULSORWINGDISTANCE, PROPULSORNUMFUSELAGE,
&
```

```
        & PROPULSORTHRUSTFACTOR, CCS, CTOG, CFACTOR, TAPERTAIL, TAPERFIN, SWEEPTAIL, SWEEPFIN,
&
        & SWEEPHALFTAIL, SWEEPHALFFIN, SWEEPTAILMASTER, SWEEPFINMASTER, ASPECTTAIL, ASPECTFIN,
&
        & SPANTAIL, SPANFIN, SWEEPTAILLE, SWEEPFINLE, FUELVOLUMETOTAL, FUELVOLUMEOUTER,
FUELVOLUMEINNER, &
        & FUELAREAOUTER, FUELLENGTHOUTER, FUELAREAINNER, TFUELOUTER, T40, C40, MFUELTOT,
FUELVOLUMEREQ, &
        & FUELDENSITY, TTIP, TC70, TCCS, TC40, TCTIP, MFUELRES, BHALF, BFHALF, B70, B40,
BCSHALF, &
        & TROOT, VA)



        CALL DRAG(RHOCR, MACWING, VD, MUCR, MCR, LAMPERCWING, TC, SWEEPHALF, TCROOT, SWING, L,
LAMPERCFUS, &
        & H, W, LNOSE, LTAIL, LNAC, LAMPERCNAC, HNAC, WNAC, MACTAIL, MACFIN, LAMPERCEMP,
TCTAIL, &
        & TCFIN, STAIL, SFIN, CL, CDT, CDW, A, K, CD0TOT, CDTOT, PPNUM, LD, SWETFUS, TCK,
SWEEP, TAPER, &
        & PROPULSORFUSELAGEDISTANCE, TOGPROPULSION, CCS, PROPULSORWINGDISTANCE, SWEEPLE,
SWINGPROPULSORS, &
        & SWINGBLI, PROPULSORWINGLENGTH, CROOT, PROPULSORNUMFUSELAGE, SWEEPHALFTAIL,
SWEEPHALFFIN, CD0FIN, &
        & CD0TAIL, PROPULSORTHRUSTFACTOR, TOGGNACELLE, CD0WING, CD0FUS, CD0NAC, CDI,
OSWALDFACTOR, THETAAREA)



         CALL PERFORMANCE(TAS, MACH, EAS, MASS, CLC, CD, DRAGS, THRUST, ROC, CORR, ROCCORR,
ROCMEAN, T, &
         & TCUM, FFLOW, F, FCUM, RANG, RCUM, ALT, TEMP, RHO, RHOSLS, MFUELTO, MTOW, SWING, K,
CD0TOT, &
         & SFCCLIMB, MCR, RANGE, SFCTO, VS, SFCCR, VD, CL, CDTOT, MFUELTOT, MFUELRES, R,
GAMMA, CAS, &

         & TASD, MACHD, CASD, MASSD, CLD, CDD, DRAGSD, THRUSTD, ROCD, CORRD, ROCCORRD,
ROCMEAND, TD, &             !DESCENT VARIABLES
         & TCUMD, FFLOWD, FD, FCUMD, RANGD, RCUMD, ALTD, TEMPD, RHOD, THRUSTTO, SFCD,
THRUSTCR, SFC, &
         & THRUSTFACTOR, RHOCEIL, RHOCR, ALTCEILING, VA, PRESSURESLS, PRESSURE, ALTITERATION,
&
         & ALTITUDECRUISEEND, TEMPCR, PRESSURECR, ALTITUDECRUISE, TTO, TCR, MFUELCR, RANGECR,
MFUELL, TTOTAL, &
         & VC, GROSSFACTOR)



         !********************************************************************** --
POWERPLANT/EQUIPMENT MASS --

         IF (MPPFIXED==0.0) THEN

            MPP=((THRUSTTO*1.325)/(THRUSTLOAD*9.81))*C3   !!!!!!!!!!!!!!!!!  -- *1.325 TO MAKE
UP TO STATIC (TRENT XWB 95K LBF EMPIRICAL CONSTANT)

         ELSE

            MPP=MPPFIXED

         END IF

         MEQ=C4*MTOW

         MLFCFUS=LFCFUS*SWETFUS*LAMPERCFUS/100            !WHOLE WETTED AREA

         MLFCEMP=LFCEMP*(STAIL+SFIN)*LAMPERCEMP/100

         MLFCWING=LFCWING*SWING*LAMPERCWING/100              !UPPER SURFACE (REFERENCE AREA)

         MLFCTOT=MLFCFUS+MLFCEMP+MLFCWING

         !**********************************************************************
```

```
      OEW=MOPS+MFUS+MEMP+MWING+MPP+MEQ+MLFCTOT        !OVERALL MASSES

      MTOW=OEW+MFUELTOT+MFUELRES+MPAY

      MLW=OEW+(2*MPAY)+MFUELRES


      ERROR=((MTOW-MTOWSTORE)**2)**0.5            !CHECK MASS CONVERGENCE

      IF(ERROR<0.01) EXIT


      MTOWSTORE=MTOW                              !RENEW MTOW



  END DO

!*****************************************************************************************
**! -- DIMENSIONS OUTPUT --


  OPEN(UNIT=110,FILE='OUTPUT\DIMENSIONS.TXT',STATUS='UNKNOWN')

     WRITE(110,*)'ROOT CHORD', CROOT
  WRITE(110,*)'ROOT THICKNESS', TROOT
  WRITE(110,*)'ROOT T/C', TCROOT
  WRITE(110,*)
  WRITE(110,*)'CENTRE SECTION CHORD', CCS
  WRITE(110,*)'CENTRE SECTION THICKNESS', TCS
  WRITE(110,*)'CENTRE SECTION T/C', TCCS
  WRITE(110,*)'CENTRE SECTION SPAN', BCSHALF
  WRITE(110,*)
  WRITE(110,*)'KINK CHORD', C40
  WRITE(110,*)'KINK THICKNESS', T40
  WRITE(110,*)'KINK T/C', TC40
  WRITE(110,*)'CENTRE SECTION TO KINK DISTANCE', B40
  WRITE(110,*)
  WRITE(110,*)'70% T/C', TC70
  WRITE(110,*)'70% SPAN', B70
  WRITE(110,*)
  WRITE(110,*)'FUEL TANK LENGTH', BFHALF
  WRITE(110,*)
  WRITE(110,*)'TIP CHORD', CTIP
  WRITE(110,*)'TIP THICKNESS', TTIP
  WRITE(110,*)'TIP T/C', TCTIP
  WRITE(110,*)'TIP SPAN', BHALF
  WRITE(110,*)
  WRITE(110,*)'LEADING-EDGE SWEEP', SWEEPLE
  WRITE(110,*)
  WRITE(110,*)'TAIL ROOT CHORD', CRTAIL
  WRITE(110,*)'TAIL SWEEP LE', SWEEPTAILLE
  WRITE(110,*)'TAIL SPAN', SPANTAIL
  WRITE(110,*)'TAIL TAPER', TAPERTAIL
  WRITE(110,*)
  WRITE(110,*)'FIN ROOT CHORD', CRFIN
  WRITE(110,*)'FIN SWEEP LE', SWEEPFINLE
  WRITE(110,*)'FIN SPAN', SPANFIN
  WRITE(110,*)'FIN TAPER', TAPERFIN



  CLOSE (110)


!*****************************************************************************************
**  -- THRUST FILE OUTPUTS --
```

```
    OPEN(UNIT=20,FILE='OUTPUT\THRUST.TXT',STATUS='UNKNOWN')

    30 FORMAT(150F15.6)

    WRITE(20,*) 'ASPECT RATIO = ', A

    WRITE(20,*) 'T/C = ', TC

    DO THRUSTNUM=1,11

        WRITE(20,*) 'THRUST ', THRUSTNUM, ' = ', THRUST(THRUSTNUM)

        WRITE(20,*) 'ALTITUDE ', THRUSTNUM, ' = ', ALT(THRUSTNUM)

    END DO

    WRITE(20,*) 'THRUST CEILING = ', THRUST(12)

    WRITE(20,*) 'CEILING ALTITUDE = ', ALTCEILING

    WRITE(20,*) 'THRUST CRUISE  = ', THRUSTCR

    WRITE(20,*) 'THRUST TAKEOFF', THRUSTTO

    WRITE(20,*) 'CLIMB TIME =', TCUM(11)

    WRITE(20,*) 'DESCENT TIME =', TCUMD(11)

    WRITE(20,*) 'CRUISE ALTITUDE  = ', ALTITUDECRUISE

    WRITE(20,*) 'EoR THRUST =', THRUSTTO



    CLOSE(20)

    PRINT *, THRUSTTO, ALTITUDECRUISE, CROOT, CCS, SPANFIN, CRFIN, SPANTAIL, CRTAIL, SFIN,
STAIL, SWEEPTAILLE, SWEEPHALFTAIL, &
    & SWEEPTAIL, SWEEPFINLE, SWEEPHALFFIN, SWEEPFIN, TFUELOUTER, TTIP, T40, FUELVOLUMETOTAL,
FUELVOLUMEREQ, MFUELTOT, TCCS, &
    & TC40, TCROOT, TCS, C40, FCUM(11), OSWALDFACTOR



!*****************************************************************************************
****************-- MISSION OUTPUT --  ***************************************



    OPEN(UNIT=130,FILE='OUTPUT\MISSION.TXT',STATUS='UNKNOWN')

    40 FORMAT(A231)
    60 FORMAT(A200)
    50 FORMAT(150F15.1)
    70 FORMAT(A45)
    80 FORMAT(A90)
    90 FORMAT(A20)
    100 FORMAT(A60)
    110 FORMAT(A30)

    SFC=SFC*1000  !BETTER UNITS FOR WRITING TO FILE
    SFCD=SFCD*1000

    WRITE(130,*)
    WRITE(130,*)'*************************!!   TAKEOFF   !!*******************************'
    WRITE(130,*)
    WRITE(130,70) '  Fuel burnt (kg)    Thrust (N)      Time (s)  '
    WRITE(130,50) MFUELTO, THRUSTTO, TTO

    WRITE(130,*)
    WRITE(130,*)
    WRITE(130,*)'*************************!!   CLIMB   !!*******************************'
    WRITE(130,*)
```

```
    WRITE(130,40) '    Altitude (m)      Time (s)    Cum time (s)    Thrust (N)      SFC
(mg/Ns)   Seg fuel (kg)    Cum fuel (kg)   CAS (m/s)     EAS (m/s)      TAS (m/s)  Climb rate
(m/s)  Seg range (m)   Cum range (m)    Lift coef.    Drag coef.'

    DO I=1,11

        WRITE(130,50) ALT(I), T(I), TCUM(I), THRUST(I), SFC(I), F(I), FCUM(I), CAS(I), EAS(I),
TAS(I), ROC(I), RANG(I), RCUM(I), CLC(I), CD(I)

    END DO

    WRITE(130,*)
    WRITE(130,*)
    WRITE(130,*)'*************************!!   CRUISE   !!*****************************'
    WRITE(130,*)
    WRITE(130,80) '    Altitude (m)      Time (s)    Thrust (N)     Fuel (kg)     Range (m)
Lift/Drag'
    WRITE(130,50) ALTITUDECRUISE, TCR, THRUSTCR, MFUELCR, RANGECR, LD

    WRITE(130,*)
    WRITE(130,*)
    WRITE(130,*)'*************************!!   DESCENT   !!*****************************'
    WRITE(130,*)
    WRITE(130,60) '    Altitude (m)     Time (s)    Cum time (s)    Thrust (N)      SFC
(mg/Ns)   Seg fuel (kg)    Cum fuel (kg)   CAS (m/s)  Descent rate (m/s)  Seg range (m)   Cum
range (m)    Lift coef.    Drag coef.'

    DO I=1,11

        WRITE(130,50) ALTD(I), TD(I), TCUMD(I), THRUSTD(I), SFCD, FD(I), FCUMD(I), CASD(I),
ROCCORRD(I), RANGD(I), RCUMD(I), CLD(I), CDD(I)

    END DO

    WRITE(130,*)
    WRITE(130,*)
    WRITE(130,*)'*************************!!   LANDING   !!*****************************'
    WRITE(130,*)
    WRITE(130,110) '  Fuel burnt (kg)  Approach cl'
    WRITE(130,50) MFUELL, CLA

    WRITE(130,*)
    WRITE(130,*)
    WRITE(130,*)'*************************!!   MISSION TOTAL
!!*****************************'
    WRITE(130,*)
    WRITE(130,100) '  Mission fuel (kg)  Reserve fuel (KG)  Mission time (s)'
    WRITE(130,50) MFUELTOT, MFUELRES, TTOTAL

    CLOSE(130)

    SFC=SFC/1000
    SFCD=SFCD/1000


!*********************************************************************************************
-- MAIN OUTPUT --   ***************************************************************



    RESULTELEMENT=RESULTELEMENT+1  ! counts through result array - FOR EVERY DIFFERENT
VARIABLE INPUT (A,TC)


    ARESULT(RESULTELEMENT)=A
    TCRESULT(RESULTELEMENT)=TC
    SWINGRESULT(RESULTELEMENT)=SWING
    LDRESULT(RESULTELEMENT)=LD

    CD0WINGRESULT(RESULTELEMENT)=CD0WING
    CD0FUSRESULT(RESULTELEMENT)=CD0FUS
    CD0NACRESULT(RESULTELEMENT)=CD0NAC
```

```
    CD0TAILRESULT(RESULTELEMENT)=CD0TAIL
    CD0FINRESULT(RESULTELEMENT)=CD0FIN

    CD0TOTRESULT(RESULTELEMENT)=CD0TOT
    CDIRESULT(RESULTELEMENT)=CDI
    CDTRESULT(RESULTELEMENT)=CDT
    CDWRESULT(RESULTELEMENT)=CDW
    CDTOTRESULT(RESULTELEMENT)=CDTOT

    MTOWRESULT(RESULTELEMENT)=MTOW
    OEWRESULT(RESULTELEMENT)=OEW
    MLWRESULT(RESULTELEMENT)=MLW
    MFUSRESULT(RESULTELEMENT)=MFUS
    MEMPRESULT(RESULTELEMENT)=MEMP
    MWINGRESULT(RESULTELEMENT)=MWING
    MEQRESULT(RESULTELEMENT)=MEQ
    MOPSRESULT(RESULTELEMENT)=MOPS
    MPAYRESULT(RESULTELEMENT)=MPAY
    MPPRESULT(RESULTELEMENT)=MPP
    MFUELTOTRESULT(RESULTELEMENT)=MFUELTOT
    MFUELRESRESULT(RESULTELEMENT)=MFUELRES
    MFUELTORESULT(RESULTELEMENT)=MFUELTO
    ALTRESULT(RESULTELEMENT)=ALT(11)
    THRUSTCEILINGRESULT(RESULTELEMENT)=THRUST(11)
    THRUSTCRRESULT(RESULTELEMENT)=THRUSTCR
    MLFCTOTRESULT(RESULTELEMENT)=MLFCTOT




   IF (RESULTELEMENT==ARRAYNUM) EXIT


    END DO

END DO

!-------------------------------------------------------------------------------------------------
OUTPUT FILE ------------------------------------------------------------------

OPEN(UNIT=100,FILE='OUTPUT\OUTPUT.TXT',STATUS='UNKNOWN')

 10 FORMAT(150F15.6)




 WRITE(100,*) 'ASPECT RATIO', ARESULT
 WRITE(100,*) 'THICKNESS/CHORD', TCRESULT
 WRITE(100,*)
 WRITE(100,*) 'WING AREA', SWINGRESULT
 WRITE(100,*) 'LIFT/DRAG', LDRESULT
 WRITE(100,*) 'WAVE DRAG', CDWRESULT
 WRITE(100,*)
 WRITE(100,*) 'WING CD0 ', CD0WINGRESULT
 WRITE(100,*) 'FUSELAGE CD0', CD0FUSRESULT
 WRITE(100,*) 'NACELLE CD0', CD0NACRESULT
 WRITE(100,*) 'TAIL CD0', CD0TAILRESULT
 WRITE(100,*) 'FIN CD0', CD0FINRESULT
 WRITE(100,*) 'TOTAL CD0', CD0TOTRESULT
 WRITE(100,*)
 WRITE(100,*) 'INDUCED DRAG', CDIRESULT
 WRITE(100,*) 'TRIM DRAG', CDTRESULT
 WRITE(100,*) 'WAVE DRAG', CDWRESULT
 WRITE(100,*) 'TOTAL DRAG', CDTOTRESULT
 WRITE(100,*)
 WRITE(100,*) 'MTOW', MTOWRESULT
 WRITE(100,*) 'OEW', OEWRESULT
 WRITE(100,*) 'MLW', MLWRESULT
 WRITE(100,*)
 WRITE(100,*) 'FUSELAGE MASS', MFUSRESULT
 WRITE(100,*) 'WING MASS', MWINGRESULT
```

```
 WRITE(100,*) 'EMPENNAGE MASS', MEMPRESULT
 WRITE(100,*) 'EQUIPMENT MASS', MEQRESULT
 WRITE(100,*) 'OPERATIONAL ITEMS MASS', MOPSRESULT
 WRITE(100,*) 'PAYLOAD MASS', MPAYRESULT
 WRITE(100,*) 'POWERPLANT MASS', MPPRESULT
 WRITE(100,*)
 WRITE(100,*) 'LFC MASS TOTAL', MLFCTOTRESULT
 WRITE(100,*) 'TOTAL MISSION FUEL', MFUELTOTRESULT




CLOSE(100)
!DEALLOCATE




RETURN
END
```

3. ‘BWBMAIN’ subroutine – BWB version of T&W main subroutine

```
    SUBROUTINE BWBMAIN(BWBTOGG)


    IMPLICIT NONE



    !************************************************ CLIMB ARRAYS

    DOUBLE PRECISION,DIMENSION(12)::ALT
    DOUBLE PRECISION, DIMENSION(12)::TEMP
    DOUBLE PRECISION,DIMENSION(12)::RHO
    DOUBLE PRECISION,DIMENSION(12)::TAS
    DOUBLE PRECISION,DIMENSION(12)::EAS

    DOUBLE PRECISION,DIMENSION(12)::ALTMASTER
    DOUBLE PRECISION, DIMENSION(12)::TEMPMASTER
    DOUBLE PRECISION,DIMENSION(12)::RHOMASTER
    DOUBLE PRECISION,DIMENSION(12)::PRESSUREMASTER
    DOUBLE PRECISION,DIMENSION(12)::TASMASTER
    DOUBLE PRECISION,DIMENSION(12)::CASMASTER

    DOUBLE PRECISION,DIMENSION(12)::MACH
    DOUBLE PRECISION,DIMENSION(12)::CAS
    DOUBLE PRECISION,DIMENSION(12)::MASS
    DOUBLE PRECISION,DIMENSION(12)::CLC
    DOUBLE PRECISION,DIMENSION(12)::CD
    DOUBLE PRECISION,DIMENSION(12)::DRAGS
    DOUBLE PRECISION,DIMENSION(12)::THRUST
    DOUBLE PRECISION,DIMENSION(12)::SFC
    DOUBLE PRECISION,DIMENSION(12)::ROC
    DOUBLE PRECISION,DIMENSION(12)::CORR
    DOUBLE PRECISION,DIMENSION(12)::ROCCORR
    DOUBLE PRECISION,DIMENSION(12)::ROCMEAN
    DOUBLE PRECISION,DIMENSION(12)::T
    DOUBLE PRECISION,DIMENSION(12)::TCUM
    DOUBLE PRECISION,DIMENSION(12)::FFLOW
    DOUBLE PRECISION,DIMENSION(12)::F
    DOUBLE PRECISION,DIMENSION(12)::FCUM
    DOUBLE PRECISION,DIMENSION(12)::RANG
    DOUBLE PRECISION,DIMENSION(12)::RCUM

    DOUBLE PRECISION,DIMENSION(12)::THRUSTFACTOR
    DOUBLE PRECISION,DIMENSION(12)::PRESSURE
```

```
!************************************************************** DESCENT ARRAYS

DOUBLE PRECISION,DIMENSION(11)::ALTD
REAL,DIMENSION(11)::TEMPD
DOUBLE PRECISION,DIMENSION(11)::RHOD

DOUBLE PRECISION,DIMENSION(11)::TASD
DOUBLE PRECISION,DIMENSION(11)::MACHD
DOUBLE PRECISION,DIMENSION(11)::CASD
DOUBLE PRECISION,DIMENSION(11)::MASSD
DOUBLE PRECISION,DIMENSION(11)::CLD
DOUBLE PRECISION,DIMENSION(11)::CDD
DOUBLE PRECISION,DIMENSION(11)::DRAGSD
DOUBLE PRECISION,DIMENSION(11)::THRUSTD
DOUBLE PRECISION,DIMENSION(11)::ROCD
DOUBLE PRECISION,DIMENSION(11)::CORRD
DOUBLE PRECISION,DIMENSION(11)::ROCCORRD
DOUBLE PRECISION,DIMENSION(11)::ROCMEAND
DOUBLE PRECISION,DIMENSION(11)::TD
DOUBLE PRECISION,DIMENSION(11)::TCUMD
DOUBLE PRECISION,DIMENSION(11)::FFLOWD
DOUBLE PRECISION,DIMENSION(11)::FD
DOUBLE PRECISION,DIMENSION(11)::FCUMD
DOUBLE PRECISION,DIMENSION(11)::RANGD
DOUBLE PRECISION,DIMENSION(11)::RCUMD

DOUBLE PRECISION,DIMENSION(41)::FUELBURN   !POWERPLANT SENSITIVITY ANALYSIS


!*****************************************************************  -- OUTPUT ARRAYS
--

DOUBLE PRECISION,ALLOCATABLE :: ARESULT(:)
DOUBLE PRECISION,ALLOCATABLE :: TCRESULT(:)
DOUBLE PRECISION,ALLOCATABLE :: SWINGRESULT(:)
DOUBLE PRECISION,ALLOCATABLE :: LDRESULT(:)

DOUBLE PRECISION,ALLOCATABLE :: CD0INNERWINGRESULT(:)
DOUBLE PRECISION,ALLOCATABLE :: CD0OUTERWINGRESULT(:)
DOUBLE PRECISION,ALLOCATABLE :: CD0NACRESULT(:)
DOUBLE PRECISION,ALLOCATABLE :: CD0FINRESULT(:)

DOUBLE PRECISION,ALLOCATABLE :: CD0TOTRESULT(:)
DOUBLE PRECISION,ALLOCATABLE :: CDIRESULT(:)
DOUBLE PRECISION,ALLOCATABLE :: CDTRESULT(:)
DOUBLE PRECISION,ALLOCATABLE :: CDWRESULT(:)
DOUBLE PRECISION,ALLOCATABLE :: CDTOTRESULT(:)

DOUBLE PRECISION,ALLOCATABLE :: MTOWRESULT(:)
DOUBLE PRECISION,ALLOCATABLE :: OEWRESULT(:)
DOUBLE PRECISION,ALLOCATABLE :: MLWRESULT(:)
DOUBLE PRECISION,ALLOCATABLE :: MFUSRESULT(:)
DOUBLE PRECISION,ALLOCATABLE :: MEMPRESULT(:)
DOUBLE PRECISION,ALLOCATABLE :: MWINGRESULT(:)
DOUBLE PRECISION,ALLOCATABLE :: MEQRESULT(:)
DOUBLE PRECISION,ALLOCATABLE :: MOPSRESULT(:)
DOUBLE PRECISION,ALLOCATABLE :: MPAYRESULT(:)
DOUBLE PRECISION,ALLOCATABLE :: MPPRESULT(:)
DOUBLE PRECISION,ALLOCATABLE :: MFUELTOTRESULT(:)
DOUBLE PRECISION,ALLOCATABLE :: MFUELRESRESULT(:)
DOUBLE PRECISION,ALLOCATABLE :: MFUELTORESULT(:)
DOUBLE PRECISION,ALLOCATABLE :: ALTRESULT(:)
DOUBLE PRECISION,ALLOCATABLE :: THRUSTCEILINGRESULT(:)
DOUBLE PRECISION,ALLOCATABLE :: THRUSTCRRESULT(:)
DOUBLE PRECISION,ALLOCATABLE :: MLFCTOTRESULT(:)




REAL MCR, L, CABPRESS, CM, NULT, LAMPERCWING, RHOSLS, &
```

```
& VA, PAY, W, H, CO, C2, AMIN, AMAX, CLA, TAPER, BFPERC, SWEEPMASTER, STEPERC, SSLATPERC,
&
& SKRUGPERC, ETAPP, PPNUM, LETOG, FF, TCEMP, CRTAIL, CRFIN, ATAIL, AFIN, CT, &
& CF, R, ACR, VD, VS, SWEEPHALF, TCROOT, LAMPERCFUS, LNOSE, LTAIL, LNAC, LAMPERCNAC, HNAC,
&
& WNAC, MACTAIL, LAMPERCEMP, TCTAIL, STAIL, SFIN, CL, THRUSTLOAD, &
& C3, SFCD, SWEEPLE, LD, C4, SWETFUS, DELTASFACT, CROOT, CTIP, SPAN, TCS, TCK, &
& SWEEP, PROPULSORWINGDISTANCE, PROPULSORNUMFUSELAGE, PROPULSORTHRUSTFACTOR, CCS,
TAPERTAIL, &
& TAPERFIN, SWEEPTAIL, SWEEPFIN, SWEEPHALFTAIL, SWEEPTAILMASTER, &
& SWEEPFINMASTER, ASPECTTAIL, ASPECTFIN, SPANTAIL, SPANFIN, SWEEPTAILLE, SWEEPFINLE, TTIP,
&
& TC70, TC40, TCTIP, BHALF, BFHALF, BCSHALF, TROOT, RHOBWB, Z, TTO, VC

INTEGER ANUM, TCNUM, N, J, STEP, ELEMENTTC, ELEMENTA, RESULTELEMENT, ARRAYNUM, ISTEP, &
& JSTEP, THRUSTNUM, INT, INTS, X, TOGPROPULSION, PROPULSORNUMWING, CTOG, I, TOGGNACELLE, &
& BWBTOGG, GEARINNERNUM, ANUMINNER, ANUMOUTER, TCNUMINNER, TCNUMOUTER, SRATIONUM,
ISTEPINNER, &
& ISTEPOUTER, JSTEPINNER, JSTEPOUTER, CLATOGG, FUELBURNELEMENT

DOUBLE PRECISION MUCR, TCMIN, TCMAX, TCSTEP, ASTEP, A, TC, MWING, MACWING, &
& RHOT, SIGMAT, RHOC, SIGMAC, RHOR, RHOS, SHEARMOD, MOPS, MFUS, &
& MFRES, SWINGWET, OEW, CDT, CDW, K, CD0TOT, SFCCLIMB, &
& MZFW, MBASIC, MPRIM, MSEC, MEMP, SFCTO, SFCCR, CDTOT, MFUELTOT, MFUELRES, &
& MEQ, THRUSTTO, MTOWSTORE, ERROR, GAMMA, MFUELTO, MLFC, LFCFUS, LFCEMP, LFCWING, MLFCFUS,
&
& MLFCEMP, MLFCWING, MLFCTOT, THRUSTCR, V2, TOL, THRUSTTO2, RHOCEIL, RHOCR, ALTCEILING, &
& PRESSURESLS, ALTITUDECRUISE, PRESSURECR, PROPERTIES, ALTITERATION, ALTITUDECRUISEEND, &
& TEMPCR, PROPULSORFUSELAGEDISTANCE, SWINGPROPULSORS, SWINGBLI, PROPULSORWINGLENGTH, &
& CFACTOR, CD0FIN, CD0TAIL, FUELVOLUMETOTAL, FUELVOLUMEOUTER, FUELVOLUMEINNER, &
& FUELAREAOUTER, FUELLENGTHOUTER, FUELAREAINNER, TFUELOUTER, T40, C40, &
& FUELVOLUMEREQ, FUELDENSITY, TCCS, B70, B40, MPPFIXED, AMININNER, AMAXINNER, ASTEPINNER,
&
& AMINOUTER, AMAXOUTER, ASTEPOUTER, TCMININNER, TCMAXINNER, TCSTEPINNER, TCMINOUTER, &
& TCMAXOUTER, TCSTEPOUTER, SRATIOMIN, SRATIOMAX, SRATIOSTEP, TAPEROUTER, &
& SWEEPLEINNER, SWEEPTEINNER, SWEEPLEOUTER, SWEEPTEOUTER, TCOUTER, TCINNER, &


& SWING, MLW, SINNER, SOUTER, BINNER, AINNER, BINNERHALF, &
!VARIABLES FROM BWB SUBROUTINE
& BOUTER, AOUTER, BOUTERHALF, B, QOUTER, QINNER, E, ABAR, FABAR, BRATIO, SOUTERCORR,
DELTAFIN, &
& MASSFIN, ROUTER, RANGE, MTOW, MASSOUTERCOVERS, SWEEPQUARTEROUTER, SWEEPHALFOUTER, &
& FBAR, CKOUTER, TCKOUTER, MASSOUTERRIBS, TKOUTER, DELTALE, DELTATE, DELTASPOILER,
DELTACARBON, &
& DELTAPP, DELTAGEAR, MASSOUTERSEC, MASSOUTERTOTAL, TCRATIO, TCKINNER, TCRINNER, &
& RINNER, MFIN, MPAY, CRINNER, CKINNER, MPP, RRATIO, MASSINNERCOVERS, SWEEPQUARTERINNER, &
& SWEEPHALFINNER, MASSINNERRIBS, TRINNER, TAPERINNER, MASSINNERSEC, MASSINNERTOTAL,
NOSEDIAMETER, FTBAR, &
& MASSNOSESHELL, SNOSECELL, MASSNOSELE, SNOSELE, MASSNOSEGEARATTACH, SNOSESCREEN,
MASSNOSEFLOOR, &
& SNOSEFLOOR, MASSNOSEMISC, MASSNOSETOTAL, RIBSPACING, CABINVOLUMESUM, CABINVOLUME,
MASSCABINMEMBRANE, HBAR, &
& MASSCABINBULK, MASSNOSESCREEN, SCABINBULK, MASSCABINFLOOR, SCABINFLOOR, MASSCABINTOTAL,
MASSWINDOW, &
& SWINDOW, MASSAPERTURE, SAPERTURE, MASSRAMPDOOR, SRAMPDOOR, RAMPWIDTH, MASSSECTOTAL,
MASSFUSELAGE, &
& MASSAIRFRAME, SRATIO, MACWINGINNER, MACWINGOUTER, TCFIN, SWEEPHALFFIN, MACFIN, &


& XOUTERWING, SKOUTER, S1, S2, &                !VARIABLES FROM STABILITY SUBROUTINE
& BFUELOUTER, XFUELOUTER, XINNERCOVER, XINNERSPAR, &
& CABINLENGTH, NOSELENGTH, XINNERWING, XPAY, XNACELLE, ZNACELLE, XNOSE, XMASSSUM, &
& XCG, INNERMOMENT, INNERLIFTSLOPE, OUTERMOMENT, OUTERLIFTSLOPE, INNERLIFT, OUTERLIFT, &
& XACQUARTER, XAC, STATICMARGINMTOW, STATICMARGINMLW, TTOUTER, CTOUTER, &

& CD0INNERWING, CD0OUTERWING, CDI, CD0NAC, CFUELTIP, FUELLENGTHINNER, CFUELROOT,
TRFUELINNER, TFUELINNER, &
& TKINNER, SWEEPLEFIN, TCR, MFUELCR, RANGECR, MFUELL, TTOTAL, OSWALDFACTOR, SGROSS,
GROSSFACTOR, CEILINGTHRUSTREQ, &
& THETAAREA, DPFINFRAC, DELTAPLANT, PLANFORMAREAFACTOR
```

```
!******************************************************************************** ASPECT
RATIO AND THICKNESS/CHORD INPUT ARRAYS

DOUBLE PRECISION,ALLOCATABLE :: ASPECTINNER(:)  !BWB ARRAYS
DOUBLE PRECISION,ALLOCATABLE :: ASPECTOUTER(:)
DOUBLE PRECISION,ALLOCATABLE :: TCHORDINNER(:)
DOUBLE PRECISION,ALLOCATABLE :: TCHORDOUTER(:)
DOUBLE PRECISION,ALLOCATABLE :: AREARATIO(:)


!********************************************************************************  ---
OPEN AND READ INPUT FILE ---


OPEN(UNIT=10,FILE='INPUT\INPUT.TXT',STATUS='OLD')

READ (10,*)Z
READ (10,*)RANGE
READ (10,*)MCR
READ (10,*)VA
READ (10,*)CL
READ (10,*)CLATOGG
READ (10,*)CLA
READ (10,*)Z
READ (10,*)Z
READ (10,*)PLANFORMAREAFACTOR
!READ FUSELAGE INPUTS

READ (10,*)PAY
READ (10,*)CABPRESS
READ (10,*)W
READ (10,*)H
READ (10,*)L
READ (10,*)CM
READ (10,*)CO
READ (10,*)C2
READ (10,*)LNOSE
READ (10,*)LTAIL

READ (10,*)ALTITUDECRUISE
READ (10,*)ALTITUDECRUISEEND
READ (10,*)MUCR
READ (10,*)VC



READ (10,*) (ALT(I), I = 1, 12)
READ (10,*) (CAS(I), I = 1, 12)
READ (10,*) (EAS(I), I = 1, 12)
READ (10,*) (TAS(I), I = 1, 12)

READ (10,*) (ALTD(I), I = 1, 11)
READ (10,*) (TASD(I), I = 1, 11)



!*****************************************--T&W INPUTS--
**************************************************

READ (10,*)AMIN
READ (10,*)AMAX
READ (10,*)ASTEP

READ (10,*)TCMIN
READ (10,*)TCMAX
READ (10,*)TCSTEP

READ (10,*)TAPER
READ (10,*)BFPERC
READ (10,*)SWEEPMASTER
READ (10,*)STEPERC
READ (10,*)SSLATPERC
READ (10,*)SKRUGPERC
```

```
READ (10,*)RHOT
READ (10,*)SIGMAT
READ (10,*)RHOC
READ (10,*)SIGMAC
READ (10,*)RHOR
READ (10,*)RHOS
READ (10,*)NULT
READ (10,*)SHEARMOD
READ (10,*)LETOG
READ (10,*)FF

READ (10,*)TCEMP
READ (10,*)SWEEPTAILMASTER
READ (10,*)SWEEPFINMASTER
READ (10,*)CRTAIL
READ (10,*)CRFIN
READ (10,*)ATAIL
READ (10,*)AFIN
READ (10,*)TAPERTAIL
READ (10,*)TAPERFIN
READ (10,*)CT
READ (10,*)CF
READ (10,*)TCTAIL
READ (10,*)TCFIN

!*****************************************--BWB INPUTS--
**************************************************
READ (10,*)AMININNER
READ (10,*)AMAXINNER
READ (10,*)ASTEPINNER

READ (10,*)AMINOUTER
READ (10,*)AMAXOUTER
READ (10,*)ASTEPOUTER

READ (10,*)TCMININNER
READ (10,*)TCMAXINNER
READ (10,*)TCSTEPINNER

READ (10,*)TCMINOUTER
READ (10,*)TCMAXOUTER
READ (10,*)TCSTEPOUTER

READ (10,*)SRATIOMIN
READ (10,*)SRATIOMAX
READ (10,*)SRATIOSTEP


READ (10,*)TAPERINNER
READ (10,*)TAPEROUTER
READ (10,*)SWEEPLEINNER
READ (10,*)SWEEPTEINNER
READ (10,*)SWEEPLEOUTER
READ (10,*)SWEEPTEOUTER
READ (10,*)RHOBWB
READ (10,*)GEARINNERNUM
READ (10,*)NOSEDIAMETER

!*********************************************************************************************
**********************

READ (10,*)TOGPROPULSION
READ (10,*)PROPULSORNUMWING
READ (10,*)PROPULSORWINGDISTANCE
READ (10,*)PROPULSORWINGLENGTH
READ (10,*)PROPULSORNUMFUSELAGE
READ (10,*)PROPULSORFUSELAGEDISTANCE
READ (10,*)PROPULSORTHRUSTFACTOR
READ (10,*)PPNUM
READ (10,*)ETAPP
READ (10,*)THETAAREA
READ (10,*)DPFINFRAC

READ (10,*)LNAC
```

```
READ (10,*)HNAC
READ (10,*)WNAC
READ (10,*)C3
READ (10,*)MPPFIXED
READ (10,*)THRUSTLOAD

READ (10,*)LAMPERCWING
READ (10,*)LAMPERCFUS
READ (10,*)LAMPERCNAC
READ (10,*)LAMPERCEMP
READ (10,*)LFCFUS
READ (10,*)LFCEMP
READ (10,*)LFCWING
READ (10,*)CDT
READ (10,*)CDW
READ (10,*)TCK

READ (10,*)SFCCLIMB
READ (10,*)SFCTO
READ (10,*)SFCCR
READ (10,*)SFCD

READ (10,*)C4
READ (10,*)DELTASFACT


READ (10,*)SFC
READ (10,*)THRUSTFACTOR
READ (10,*)ALTITERATION

CLOSE(10)

!-------------------------------------------------------------------------------------------
---------------------- INITIAL CALCULATIONS AND VARIABLES -----------------------------


ALTITERATION=ALTITERATION/3.281         !CONVERT TO METRES - SEE PERFORMANCE SUBROUTINE
FOR DEFINITION

DO X=1,12

    ALT(X)=ALT(X)/3.281                 !CONVERT TO METRES
    TAS(X)=TAS(X)*0.5144                !CONVERT TO M/S
    EAS(X)=EAS(X)*0.5144
    CAS(X)=CAS(X)*0.5144

END DO

SWEEPLEOUTER=SWEEPLEOUTER*3.14159/180   !CONVERT TO RADIANS
SWEEPTEOUTER=SWEEPTEOUTER*3.14159/180
SWEEPLEINNER=SWEEPLEINNER*3.14159/180
SWEEPTEINNER=SWEEPTEINNER*3.14159/180

!****************************************** -- CLIMB AIR PROPERTIES --

GAMMA=1.4     !GAS CONSTANTS
R=287.05


DO X=1,12


        IF (ALT(X)<11000) THEN

            TEMP(X)=288.15-0.0065*ALT(X)
            PRESSURE(X)=101325*(288.15/TEMP(X))**(-5.25588)

        END IF


        IF (ALT(X)>=11000 .AND. ALT(X)<24994) THEN

            TEMP(X)=216.65
            PRESSURE(X)=22.63253/EXP(0.000157689*(ALT(X)-10998.1))*1000
```

```
        END IF


        IF (ALT(X)>=24994 .AND. ALT(X)<30000) THEN

            TEMP(X)=216.65+0.0029892*(ALT(X)-24994)
            PRESSURE(X)=2.5237*(216.65/TEMP(X))**11.8*1000

        END IF



        RHO(X)=PRESSURE(X)/(R*TEMP(X))

END DO


!********************************************** -- CRUISE AIR PROPERTIES --

ALTITUDECRUISE=ALTITUDECRUISE/3.281    !CONVERSION TO METRES
ALTITUDECRUISEEND=ALTITUDECRUISEEND/3.281



        IF (ALTITUDECRUISE<11000) THEN

            TEMPCR=288.15-0.0065*ALTITUDECRUISE
            PRESSURECR=101325*(288.15/TEMPCR)**(-5.25588)

        END IF

        IF (ALTITUDECRUISE>=11000 .AND. ALTITUDECRUISE<24994) THEN

            TEMPCR=216.65
            PRESSURECR=22.63253/EXP(0.000157689*(ALTITUDECRUISE-10998.1))*1000

        END IF

        IF (ALTITUDECRUISE>=24994 .AND. ALTITUDECRUISE<30000) THEN

            TEMPCR=216.65+0.0029892*(ALTITUDECRUISE-24994)
            PRESSURECR=2.5237*(216.65/TEMPCR)**11.8

        END IF


RHOCR=PRESSURECR/(R*TEMPCR)

PRESSURESLS=101325

!MUCR=1.015D-6*TEMPCR**1.5/(TEMPCR+120)


!*************************************


ACR=SQRT(GAMMA*R*TEMPCR)                                          !CRUISE SPEED OF
SOUND

VD=ACR*MCR                                                          !DESIGN SPEED

VS=93.86/1.3                                                           !STALL SPEED

RHOSLS=1.2248


!************************************************ FIXED MASSES


MPAY=PAY*95.17                                                       !95KG PAX
```

```
MOPS=PAY*CO                                                              !OPERATIONAL ITEMS
MASS


!------------------------------------------------------------------------------------ BWB
LOOP SPECIFICATIONS ------------------------------------------------------------------------
--------

ANUMINNER=((AMAXINNER-AMININNER)/ASTEPINNER)+1                  !ALLOCATING 'TC' AND 'A'
ARRAYS FOR GIVEN RANGE

ANUMOUTER=((AMAXOUTER-AMINOUTER)/ASTEPOUTER)+1

TCNUMINNER=((TCMAXINNER-TCMININNER)/TCSTEPINNER)+1

TCNUMOUTER=((TCMAXOUTER-TCMINOUTER)/TCSTEPOUTER)+1

SRATIONUM=((SRATIOMAX-SRATIOMIN)/SRATIOSTEP)+1


ALLOCATE(ASPECTINNER(ANUMINNER))

ALLOCATE(ASPECTOUTER(ANUMOUTER))

ALLOCATE(TCHORDINNER(TCNUMINNER))

ALLOCATE(TCHORDOUTER(TCNUMOUTER))

ALLOCATE(AREARATIO(SRATIONUM))


DO ISTEPINNER=1,ANUMINNER                              !FILL INPUT VARIABLE ARRAYS
    ASPECTINNER(ISTEPINNER)=AMININNER+ASTEPINNER*(ISTEPINNER-1)
END DO

DO ISTEPOUTER=1,ANUMOUTER                              !FILL INPUT VARIABLE ARRAYS
    ASPECTOUTER(ISTEPOUTER)=AMINOUTER+ASTEPOUTER*(ISTEPOUTER-1)
END DO


DO JSTEPINNER=1,TCNUMINNER
    TCHORDINNER(JSTEPINNER)=TCMININNER+TCSTEPINNER*(JSTEPINNER-1)
END DO

DO JSTEPOUTER=1,TCNUMOUTER
    TCHORDOUTER(JSTEPOUTER)=TCMINOUTER+TCSTEPOUTER*(JSTEPOUTER-1)
END DO

DO SRATIOSTEP=1,SRATIONUM
    AREARATIO(SRATIOSTEP)=SRATIOMIN+SRATIOMAX*(SRATIOSTEP-1)
END DO


ARRAYNUM=ANUMINNER*ANUMOUTER*TCNUMINNER*TCNUMOUTER*SRATIONUM                    ! SIZE
OF OUTPUT ARRAYS



!------------------------------------------------------------------------------------------
------------------------------------------------------------------------------------------
---------
RESULTELEMENT=0                            !NULL THE RESULT ARRAY NUMBERS



ALLOCATE(ARESULT(ARRAYNUM))               !ALLOCATE ARRAY SIZE TO EACH OUTPUT ARRAY
ALLOCATE(TCRESULT(ARRAYNUM))
ALLOCATE(SWINGRESULT(ARRAYNUM))
ALLOCATE(LDRESULT(ARRAYNUM))

ALLOCATE(CD0INNERWINGRESULT(ARRAYNUM))
```

```
ALLOCATE(CD0OUTERWINGRESULT(ARRAYNUM))
ALLOCATE(CD0NACRESULT(ARRAYNUM))
ALLOCATE(CD0FINRESULT(ARRAYNUM))

ALLOCATE(CD0TOTRESULT(ARRAYNUM))
ALLOCATE(CDIRESULT(ARRAYNUM))
ALLOCATE(CDTRESULT(ARRAYNUM))
ALLOCATE(CDWRESULT(ARRAYNUM))
ALLOCATE(CDTOTRESULT(ARRAYNUM))

ALLOCATE(MTOWRESULT(ARRAYNUM))
ALLOCATE(OEWRESULT(ARRAYNUM))
ALLOCATE(MLWRESULT(ARRAYNUM))
ALLOCATE(MFUSRESULT(ARRAYNUM))
ALLOCATE(MEMPRESULT(ARRAYNUM))
ALLOCATE(MWINGRESULT(ARRAYNUM))
ALLOCATE(MEQRESULT(ARRAYNUM))
ALLOCATE(MOPSRESULT(ARRAYNUM))
ALLOCATE(MPAYRESULT(ARRAYNUM))
ALLOCATE(MPPRESULT(ARRAYNUM))
ALLOCATE(MFUELTOTRESULT(ARRAYNUM))
ALLOCATE(MFUELRESRESULT(ARRAYNUM))
ALLOCATE(MFUELTORESULT(ARRAYNUM))
ALLOCATE(ALTRESULT(ARRAYNUM))
ALLOCATE(THRUSTCEILINGRESULT(ARRAYNUM))
ALLOCATE(THRUSTCRRESULT(ARRAYNUM))
ALLOCATE(MLFCTOTRESULT(ARRAYNUM))



ALTMASTER=ALT                        !STORING ORIGINALLY READ ARRAYS
TEMPMASTER=TEMP
RHOMASTER=RHO
PRESSUREMASTER=PRESSURE
TASMASTER=TAS
CASMASTER=CAS

CTOG=0         !STOPS EMMPENAGE VOLUME COEFS. CHANGING REPEATEDLY - SEE 'WING'
TOGGNACELLE=0  !NACCELLE DRAG BLI

!-------------------------------------------------------------------------------------------
------ MAIN LOOP FOR VARYING INPUT VARIABLES ----------------------------------------

DO SRATIOSTEP=1,SRATIONUM

SRATIO=AREARATIO(SRATIOSTEP)

        DO JSTEPOUTER=1,TCNUMOUTER                    !MAIN LOOP FOR RANGED VARIABLES

        TCOUTER=TCHORDOUTER(JSTEPOUTER)

            DO JSTEPINNER=1,TCNUMINNER                    !MAIN LOOP FOR RANGED VARIABLES

            TCINNER=TCHORDINNER(JSTEPINNER)

                DO ISTEPOUTER=1,ANUMOUTER

                AOUTER=ASPECTOUTER(ISTEPOUTER)

                    DO ISTEPINNER=1,ANUMINNER

                    AINNER=ASPECTINNER(ISTEPINNER)
```

```
    ALT=ALTMASTER                    !RENEWING ORIGINALLY READ PARAMETERS ('ALT'
SUBROUTINE CAN CHANGE THESE DURING LOOP)
    TEMP=TEMPMASTER
    RHO=RHOMASTER
    PRESSURE=PRESSUREMASTER
    TAS=TASMASTER
    CAS=CASMASTER



     !*************************************************   --INITIAL MASSES--
    MFUS=0.0
    MLW=MFUS+MOPS+(2*MPAY)           !MAX LANDING WEIGHT

    MWING=0.0001
    MTOWSTORE=0.0001
    MPP=MPPFIXED
    MZFW=0.0001
    MFUELTOT=0.0001
    MFUELRES=0.0001                       !FUEL RESERVE
    MEQ=0.0001
    MTOW=MLW
    OEW=MFUS+MOPS
    !*************************************************

    !***** POWERPLANT SENSITIVITY ANALYSIS******!

    FUELBURNELEMENT=0

   ! DO MPP=10000,30000,500


    FUELBURNELEMENT=FUELBURNELEMENT+1
! ------------------------------------------------------------------------------------
-------------  MTOW ITERATION LOOP ------------------------------------------------



    DO



        CALL BWB(MWING, SRATIO, TCOUTER, TCINNER, AOUTER, AINNER, MLW, RHOSLS, CLA, VS,
VD, MTOW, &
        & PPNUM, RANGE, NULT, TAPERINNER, TAPEROUTER, SWEEPLEINNER, SWEEPTEINNER,
SWEEPLEOUTER, SWEEPTEOUTER, &
        & RHOBWB, GEARINNERNUM, NOSEDIAMETER, CABPRESS, SWING, MACFIN, TCFIN, SFIN,
SWEEPHALFINNER, &
        & SWEEPHALFOUTER, CKINNER, CRINNER, SWEEPHALFFIN, MACWINGINNER, MACWINGOUTER,
SINNER, SOUTER, BINNER, BOUTER, &
        & SWEEPQUARTERINNER, SWEEPQUARTEROUTER, TTOUTER, CTOUTER, CKOUTER, TKOUTER,
NOSELENGTH, CABINLENGTH, BINNERHALF, &
        & BOUTERHALF, MASSINNERTOTAL, MASSOUTERTOTAL, MASSCABINTOTAL, MASSNOSETOTAL, PAY,
TCKOUTER, TCKINNER, &
        & FUELDENSITY, FUELVOLUMEREQ, MFUELTOT, MFUELRES, FUELLENGTHOUTER, CFUELTIP,
TFUELOUTER, FUELAREAOUTER, &
        & FUELVOLUMEOUTER, FUELLENGTHINNER, CFUELROOT, TRFUELINNER, TFUELINNER,
FUELAREAINNER, FUELVOLUMEINNER, &
        & FUELVOLUMETOTAL, VA, B, TKINNER, SWEEPLEFIN, TRINNER, TCRINNER, CL, CLATOGG,
MPP, MPAY, SGROSS, TOGPROPULSION, ETAPP, &
        & PROPULSORTHRUSTFACTOR, PROPULSORNUMWING, PROPULSORWINGDISTANCE, DPFINFRAC,
DELTAPLANT, PLANFORMAREAFACTOR)


       ! IF (SOUTER<=200) GROSSFACTOR=0.822   !FACTOR FOR GROSS WING AREA  (CL INPUT
ACCOUNTS FOR THIS). ALSO FOR CONVERGENCE IS LEFT UNTIL OUTER WING INCREASES
       ! IF (SOUTER>200) GROSSFACTOR=0.822

        CALL DRAGBWB(RHOCR, MACWINGINNER, VD, MUCR, MCR, LAMPERCWING, TCINNER, &
        & SWING, L, LAMPERCFUS, H, W, LNOSE, LTAIL, LNAC, LAMPERCNAC, HNAC, WNAC, TCOUTER,
&
```

```
        & MACTAIL, MACFIN, LAMPERCEMP, TCTAIL, TCFIN, STAIL, SFIN, CL, CDT,
SWEEPHALFINNER, &
        & CDW, A, K, CD0TOT, CDTOT, PPNUM, LD, SWETFUS, TCK, SWEEP, TAPERINNER,
SWEEPHALFOUTER, &
        & PROPULSORFUSELAGEDISTANCE, TOGPROPULSION, CKINNER, PROPULSORWINGDISTANCE, &
        & SWINGPROPULSORS, SWINGBLI, PROPULSORWINGLENGTH, CRINNER, PROPULSORNUMFUSELAGE, &
        & SWEEPHALFTAIL, SWEEPHALFFIN, CD0FIN, CD0TAIL, PROPULSORTHRUSTFACTOR,
TOGGNACELLE, &
        & SWEEPLEINNER, SWEEPLEOUTER, MACWINGOUTER, SINNER, SOUTER, BINNER, BOUTER,
AINNER, &
        & SWEEPQUARTERINNER, AOUTER, TAPEROUTER, TCKOUTER, SWEEPQUARTEROUTER, TCKINNER,
CD0INNERWING, &
        & CD0OUTERWING, CDI, CD0NAC, BOUTERHALF, SWEEPTEINNER, OSWALDFACTOR, GROSSFACTOR,
SGROSS, THETAAREA)



       ! SWING=SWING*GROSSFACTOR

        CALL PERFORMANCE(TAS, MACH, EAS, MASS, CLC, CD, DRAGS, THRUST, ROC, CORR, ROCCORR,
ROCMEAN, T, &
        & TCUM, FFLOW, F, FCUM, RANG, RCUM, ALT, TEMP, RHO, RHOSLS, MFUELTO, MTOW, SGROSS,
K, CD0TOT, &
        & SFCCLIMB, MCR, RANGE, SFCTO, VS, SFCCR, VD, CL, CDTOT, MFUELTOT, MFUELRES, R,
GAMMA, CAS, &

        & TASD, MACHD, CASD, MASSD, CLD, CDD, DRAGSD, THRUSTD, ROCD, CORRD, ROCCORRD,
ROCMEAND, TD, &            !DESCENT VARIABLES
        & TCUMD, FFLOWD, FD, FCUMD, RANGD, RCUMD, ALTD, TEMPD, RHOD, THRUSTTO, SFCD,
THRUSTCR, SFC, &
        & THRUSTFACTOR, RHOCEIL, RHOCR, ALTCEILING, VA, PRESSURESLS, PRESSURE,
ALTITERATION, &
        & ALTITUDECRUISEEND, TEMPCR, PRESSURECR, ALTITUDECRUISE, TTO, TCR, MFUELCR,
RANGECR, MFUELL, &
        & TTOTAL, VC, GROSSFACTOR)



        CALL STABILITY(XOUTERWING, BINNERHALF, SWEEPLEINNER, BOUTER, SWEEPLEOUTER,
SKOUTER, SWEEPTEOUTER, S1, S2, &
        & TKOUTER, TTOUTER, CTOUTER, BFUELOUTER, XFUELOUTER, XINNERCOVER, CRINNER,
SWEEPTEINNER, XINNERSPAR, &
        & CABINLENGTH, NOSELENGTH, XINNERWING, XPAY, XNACELLE, LNAC, ZNACELLE, HNAC,
XNOSE, XMASSSUM, &
        & MASSOUTERTOTAL, CKOUTER, MFUELTOT, MFUELRES, MASSCABINTOTAL, MASSINNERTOTAL,
MPAY, MPP, &
        & MASSNOSETOTAL, XCG, INNERMOMENT, INNERLIFTSLOPE, OUTERMOMENT, OUTERLIFTSLOPE,
INNERLIFT, OUTERLIFT, &
        & XACQUARTER, XAC, STATICMARGINMTOW, STATICMARGINMLW, SWEEPQUARTERINNER,
SWEEPQUARTEROUTER, BINNER, BOUTERHALF, &
        & THRUSTCR, MEQ, MOPS, MLFC, MASSSECTOTAL)



         !********************************************************************** --
POWERPLANT/EQUIPMENT MASS --

         IF (MPPFIXED==0.0)  MPP=((THRUSTTO*1.325)/(THRUSTLOAD*9.81))*C3
!!!!!!!!!!!!!!!!!  -- *1.325 TO MAKE UP TO STATIC (TRENT XWB 95K LBF EMPIRICAL CONSTANT)


         MEQ=C4*MTOW

       !  MLFCFUS=LFCFUS*SWETFUS*LAMPERCFUS/100            !WHOLE WETTED AREA

         MLFCEMP=LFCEMP*(STAIL+SFIN)*LAMPERCEMP/100

         MLFCWING=LFCWING*SOUTER*LAMPERCWING/100              !UPPER SURFACE (REFERENCE
AREA)

         MLFCTOT=MLFCEMP+MLFCWING

         !**********************************************************************
```

```
        OEW=MOPS+MFUS+MEMP+MWING+MPP+MEQ+MLFCTOT        !OVERALL MASSES

        MTOW=OEW+MFUELTOT+MFUELRES+MPAY

        MLW=OEW+(2*MPAY)+MFUELRES



        ERROR=((MTOW-MTOWSTORE)**2)**0.5            !CHECK MASS CONVERGENCE

        IF(ERROR<0.1) EXIT



        MTOWSTORE=MTOW                              !RENEW MTOW

       ALT=ALTMASTER                     !RENEWING ORIGINALLY READ PARAMETERS ('ALT'
SUBROUTINE CAN CHANGE THESE DURING LOOP)
       TEMP=TEMPMASTER
       RHO=RHOMASTER
       PRESSURE=PRESSUREMASTER
       TAS=TASMASTER
       CAS=CASMASTER



    END DO

    FUELBURN(FUELBURNELEMENT)=MFUELTOT

   ! END DO ! POWERPLANT SENSITIVITY ANALYSIS

    OPEN(UNIT=140,FILE='OUTPUT\BWBFUELBURN.TXT',STATUS='UNKNOWN')

    140 FORMAT(1F6.0)

    WRITE(140,140)FUELBURN

    CLOSE(140)

!*******************************************************************************
******  !! DIMENSIONS OUTPUT !! ************************************************************



    OPEN(UNIT=110,FILE='OUTPUT\DIMENSIONS.TXT',STATUS='UNKNOWN')


    WRITE(110,*)'OUTER WING AREA          ', SOUTER
    WRITE(110,*)'INNER WING AREA          ', SINNER
    WRITE(110,*)
    WRITE(110,*)'INNER ROOT CHORD         ', CRINNER
    WRITE(110,*)'INNER ROOT THICKNESS     ', TRINNER
    WRITE(110,*)'INNER ROOT T/C           ', TCRINNER
    WRITE(110,*)
    WRITE(110,*)'INNER KINK CHORD         ', CKINNER
    WRITE(110,*)'INNER KINK THICKNESS     ', TKINNER
    WRITE(110,*)'INNER KINK T/C           ', TCKINNER
    WRITE(110,*)'INNER KINK HALF SPAN     ', BINNERHALF
    WRITE(110,*)
    WRITE(110,*)'OUTER KINK CHORD         ', CKOUTER
    WRITE(110,*)'OUTER KINK THICKNESS     ', TKOUTER
    WRITE(110,*)'OUTER KINK STRUCTURAL T/C', TCKOUTER
    WRITE(110,*)'OUTER KINK AERO T/C      ', TCKINNER
    WRITE(110,*)
    WRITE(110,*)'OUTER TIP CHORD          ', CTOUTER
    WRITE(110,*)'OUTER TIP THICKNESS      ', TTOUTER
    WRITE(110,*)'OUTER TIP T/C            ', TCOUTER
```

```
    WRITE(110,*)'AIRCRAFT SPAN           ', B
    WRITE(110,*)
    WRITE(110,*)'INNER LEADING-EDGE SWEEP ', SWEEPLEINNER
    WRITE(110,*)'INNER TRAILING-EDGE SWEEP', SWEEPTEINNER
    WRITE(110,*)'OUTER LEADING-EDGE SWEEP ', SWEEPLEOUTER
    WRITE(110,*)'OUTER TRAILING-EDGE SWEEP', SWEEPTEOUTER
    WRITE(110,*)
    WRITE(110,*)'FIN ROOT CHORD          ', CTOUTER
    WRITE(110,*)'FIN SWEEP LE            ', SWEEPLEFIN
    WRITE(110,*)'FIN TAPER               ', TAPERFIN
    WRITE(110,*)'FIN AREA  PER FIN       ', SFIN



    CLOSE (110)


!*********************************************************************************
******  -- THRUST FILE OUTPUTS --   ************************************************


    OPEN(UNIT=20,FILE='OUTPUT\THRUST.TXT',STATUS='UNKNOWN')

    30 FORMAT(150F15.6)

    WRITE(20,*) 'OUTER ASPECT RATIO = ', AOUTER

    WRITE(20,*) ' OUTER T/C = ', TCOUTER

    DO THRUSTNUM=1,11

        WRITE(20,*) 'THRUST ', THRUSTNUM, ' = ', THRUST(THRUSTNUM)

        WRITE(20,*) 'ALTITUDE ', THRUSTNUM, ' = ', ALT(THRUSTNUM)

    END DO

    WRITE(20,*) 'THRUST CEILING = ', THRUST(12)

    WRITE(20,*) 'CEILING ALTITUDE = ', ALTCEILING

    WRITE(20,*) 'THRUST CRUISE  = ', THRUSTCR

    WRITE(20,*) 'THRUST TAKEOFF', THRUSTTO

    WRITE(20,*) 'CLIMB TIME =', TCUM(11)

    WRITE(20,*) 'DESCENT TIME =', TCUMD(11)

    WRITE(20,*) 'START CRUISE ALTITUDE  = ', ALT(11)

    WRITE(20,*) 'CRUISE ALTITUDE  = ', ALTITUDECRUISE

    WRITE(20,*) 'END CRUISE ALTITUDE  = ', ALTD(1)

    WRITE(20,*) 'EoR THRUST =', THRUSTTO



    CLOSE(20)

    PRINT *, THRUSTTO, ALTITUDECRUISE, STATICMARGINMTOW, STATICMARGINMLW, MWING,
cd0innerWING, CD0OUTERWING, CDI, &

    & CD0NAC, CD0FIN, FUELVOLUMETOTAL, FUELVOLUMEREQ, CRINNER, BINNERHALF, MACWINGINNER,
OSWALDFACTOR, deltaplant



!*********************************************************************************
********************-- MISSION OUTPUT --  ***************************************
```

```
    OPEN(UNIT=130,FILE='OUTPUT\MISSION.TXT',STATUS='UNKNOWN')

    40 FORMAT(A231)
    60 FORMAT(A200)
    50 FORMAT(150F15.1)
    55 FORMAT(150F15.2)
    70 FORMAT(A45)
    80 FORMAT(A90)
    90 FORMAT(A20)
    100 FORMAT(A60)
    110 FORMAT(A30)


    SFC=SFC*1000  !BETTER UNITS FOR WRITING TO FILE
    SFCD=SFCD*1000

    WRITE(130,*)
    WRITE(130,*)'*************************!!   TAKEOFF   !!*******************************'
    WRITE(130,*)
    WRITE(130,70) '  Fuel burnt (kg)     Thrust (N)      Time (s)  '
    WRITE(130,50) MFUELTO, THRUSTTO, TTO

    WRITE(130,*)
    WRITE(130,*)
    WRITE(130,*)'*************************!!   CLIMB   !!*******************************'
    WRITE(130,*)
    WRITE(130,40) '    Altitude (m)     Time (s)    Cum time (s)    Thrust (N)      SFC
(mg/Ns)   Seg fuel (kg)    Cum fuel (kg)   CAS (m/s)     EAS (m/s)      TAS (m/s)  Climb
rate (m/s)  Seg range (m)   Cum range (m)    Lift coef.    Drag coef.'

    DO I=1,11

        WRITE(130,50) ALT(I), T(I), TCUM(I), THRUST(I), SFC(I), F(I), FCUM(I), CAS(I),
EAS(I), TAS(I), ROCCORR(I), RANG(I), RCUM(I), CLC(I), CD(I)

    END DO

    WRITE(130,*)
    WRITE(130,*)
    WRITE(130,*)'*************************!!   CRUISE   !!*******************************'
    WRITE(130,*)
    WRITE(130,80) '    Altitude (m)      Time (s)    Thrust (N)     Fuel (kg)     Range
(m)      Lift/Drag'
    WRITE(130,50) ALTITUDECRUISE, TCR, THRUSTCR, MFUELCR, RANGECR, LD

    WRITE(130,*)
    WRITE(130,*)
    WRITE(130,*)'*************************!!   DESCENT   !!*******************************'
    WRITE(130,*)
    WRITE(130,60) '    Altitude (m)     Time (s)    Cum time (s)    Thrust (N)      SFC
(mg/Ns)   Seg fuel (kg)    Cum fuel (kg)   CAS (m/s)   Descent rate (m/s)  Seg range (m)
Cum range (m)    Lift coef.    Drag coef.'

    DO I=1,11

        WRITE(130,50) ALTD(I), TD(I), TCUMD(I), THRUSTD(I), SFCD, FD(I), FCUMD(I),
CASD(I), ROCCORRD(I), RANGD(I), RCUMD(I), CLD(I), CDD(I)

    END DO

    WRITE(130,*)
    WRITE(130,*)
    WRITE(130,*)'*************************!!   APPROACH
!!*******************************'
    WRITE(130,*)
    WRITE(130,110) '  Fuel burnt (kg)  Approach cl'
    WRITE(130,55) MFUELL, CLA

    WRITE(130,*)
    WRITE(130,*)
```

```
    WRITE(130,*)'************************!!   MISSION TOTAL
!!*****************************'
    WRITE(130,*)
    WRITE(130,100) '  Mission fuel (kg)  Reserve fuel (KG)  Mission time (s)'
    WRITE(130,50) MFUELTOT, MFUELRES, TTOTAL

    CLOSE(130)

    SFC=SFC/1000
    SFCD=SFCD/1000


!*******************************************************************************************
**** -- MAIN OUTPUT --
*****************************************************************




    RESULTELEMENT=RESULTELEMENT+1  ! counts through result array - FOR EVERY DIFFERENT
VARIABLE INPUT (A,TC)


    ARESULT(RESULTELEMENT)=AOUTER
    TCRESULT(RESULTELEMENT)=TCOUTER
    SWINGRESULT(RESULTELEMENT)=SWING
    LDRESULT(RESULTELEMENT)=LD

    CD0INNERWINGRESULT(RESULTELEMENT)=CD0INNERWING
    CD0OUTERWINGRESULT(RESULTELEMENT)=CD0OUTERWING
    CD0NACRESULT(RESULTELEMENT)=CD0NAC
    CD0FINRESULT(RESULTELEMENT)=CD0FIN

    CD0TOTRESULT(RESULTELEMENT)=CD0TOT
    CDIRESULT(RESULTELEMENT)=CDI
    CDTRESULT(RESULTELEMENT)=CDT
    CDWRESULT(RESULTELEMENT)=CDW
    CDTOTRESULT(RESULTELEMENT)=CDTOT

    MTOWRESULT(RESULTELEMENT)=MTOW
    OEWRESULT(RESULTELEMENT)=OEW
    MLWRESULT(RESULTELEMENT)=MLW
    MFUSRESULT(RESULTELEMENT)=MFUS
    MEMPRESULT(RESULTELEMENT)=MEMP
    MWINGRESULT(RESULTELEMENT)=MWING
    MEQRESULT(RESULTELEMENT)=MEQ
    MOPSRESULT(RESULTELEMENT)=MOPS
    MPAYRESULT(RESULTELEMENT)=MPAY
    MPPRESULT(RESULTELEMENT)=MPP
    MFUELTOTRESULT(RESULTELEMENT)=MFUELTOT
    MFUELRESRESULT(RESULTELEMENT)=MFUELRES
    MFUELTORESULT(RESULTELEMENT)=MFUELTO
    ALTRESULT(RESULTELEMENT)=ALT(11)
    THRUSTCEILINGRESULT(RESULTELEMENT)=THRUST(11)
    THRUSTCRRESULT(RESULTELEMENT)=THRUSTCR
    MLFCTOTRESULT(RESULTELEMENT)=MLFCTOT




   IF (RESULTELEMENT==ARRAYNUM) EXIT

               END DO

           END DO

        END DO

    END DO

END DO
```

```
!-------------------------------------------------------------------------------------------
---- OUTPUT FILE ------------------------------------------------------------------

OPEN(UNIT=100,FILE='OUTPUT\OUTPUT.TXT',STATUS='UNKNOWN')

 10 FORMAT(150F15.6)




 WRITE(100,*) 'OUTER ASPECT RATIO', ARESULT
 WRITE(100,*) 'OUTER THICKNESS/CHORD', TCRESULT
 WRITE(100,*)
 WRITE(100,*) 'WING AREA', SWINGRESULT
 WRITE(100,*) 'LIFT/DRAG', LDRESULT
 WRITE(100,*)
 WRITE(100,*) 'INNER WING CD0 ', CD0INNERWINGRESULT
 WRITE(100,*) 'OUTER WING CD0', CD0OUTERWINGRESULT
 WRITE(100,*) 'NACELLE CD0', CD0NACRESULT
 WRITE(100,*) 'FIN CD0', CD0FINRESULT
 WRITE(100,*) 'TOTAL CD0', CD0TOTRESULT
 WRITE(100,*)
 WRITE(100,*) 'INDUCED DRAG', CDIRESULT
 WRITE(100,*) 'TRIM DRAG', CDTRESULT
 WRITE(100,*) 'WAVE DRAG', CDWRESULT
 WRITE(100,*) 'TOTAL DRAG', CDTOTRESULT
 WRITE(100,*)
 WRITE(100,*) 'MTOW', MTOWRESULT
 WRITE(100,*) 'OEW', OEWRESULT
 WRITE(100,*) 'MLW', MLWRESULT
 WRITE(100,*)
 WRITE(100,*) 'FUSELAGE MASS', MFUSRESULT
 WRITE(100,*) 'WING MASS', MWINGRESULT
 WRITE(100,*) 'EMPENNAGE MASS', MEMPRESULT
 WRITE(100,*) 'EQUIPMENT MASS', MEQRESULT
 WRITE(100,*) 'OPERATIONAL ITEMS MASS', MOPSRESULT
 WRITE(100,*) 'PAYLOAD MASS', MPAYRESULT
 WRITE(100,*) 'POWERPLANT MASS', MPPRESULT
 WRITE(100,*)
 WRITE(100,*) 'LFC MASS TOTAL', MLFCTOTRESULT
 WRITE(100,*) 'TOTAL MISSION FUEL', MFUELTOTRESULT




CLOSE(100)
!DEALLOCATE

CALL TMATCH(THRUSTCR)



!************************************** -- 3000NM MISSION --
****************************************

!MTOWSTORE=0.001

!SFCCR=0.013343

!SFC(11)=0.013909

!DO                 !ITERATE FUEL REDUCTION ONLY- SAME AIRCRAFT DESIGN

!RANGE=5557500   !(m)(3000NM MISSION)

        !CALL PERFORMANCE(TAS, MACH, EAS, MASS, CLC, CD, DRAGS, THRUST, ROC, CORR,
ROCCORR, ROCMEAN, T, &
       ! & TCUM, FFLOW, F, FCUM, RANG, RCUM, ALT, TEMP, RHO, RHOSLS, MFUELTO, MTOW,
SGROSS, K, CD0TOT, &
       ! & SFCCLIMB, MCR, RANGE, SFCTO, VS, SFCCR, VD, CL, CDTOT, MFUELTOT, MFUELRES, R,
GAMMA, CAS, &
```

```
       ! & TASD, MACHD, CASD, MASSD, CLD, CDD, DRAGSD, THRUSTD, ROCD, CORRD, ROCCORRD,
ROCMEAND, TD, &            !DESCENT VARIABLES
       ! & TCUMD, FFLOWD, FD, FCUMD, RANGD, RCUMD, ALTD, TEMPD, RHOD, THRUSTTO, SFCD,
THRUSTCR, SFC, &
       ! & THRUSTFACTOR, RHOCEIL, RHOCR, ALTCEILING, VA, PRESSURESLS, PRESSURE,
ALTITERATION, &
       ! & ALTITUDECRUISEEND, TEMPCR, PRESSURECR, ALTITUDECRUISE, TTO, TCR, MFUELCR,
RANGECR, MFUELL, &
       ! & TTOTAL, VC, GROSSFACTOR)



!OEW=MOPS+MFUS+MEMP+MWING+MPP+MEQ+MLFCTOT        !OVERALL MASSES -

!MTOW=OEW+MFUELTOT+MFUELRES+MPAY

!MLW=OEW+(2*MPAY)+MFUELRES



!ERROR=ABS(MTOWSTORE-MTOW)

!IF (ERROR<=0.001) EXIT

!MTOWSTORE=MTOW



!END DO

!CEILINGTHRUSTREQ=THRUST(12)


!PRINT *, MFUELTOT, ALTITUDECRUISE, THRUSTCR, ALTCEILING, CEILINGTHRUSTREQ, THRUSTTO

!*************************************************************************************
***************



RETURN
END
```

4. ‘Wing’ subroutine – Wing structural mass calculations

```
SUBROUTINE WING(MLW, RHOSLS, CLA, VS, SWING, A, TC, TAPER, BFPERC, SWEEPMASTER, &
& SWINGWET, STEPERC, SSLATPERC, SKRUGPERC, MTOW, MWING, ETAPP, MPP, &
& PPNUM, MZFW, RHOT, SIGMAT, RHOC, SIGMAC, RHOR, NULT, SHEARMOD, RHOCR, &
& MCR, LETOG, RHOS, FF, VD, MBASIC, MPRIM, MSEC, MEMP, TCEMP, &
& CRTAIL, CRFIN, ATAIL, AFIN, MACTAIL, MACFIN, CT, CF, L, MACWING, &
& STAIL, SFIN, SWEEPHALF, TCROOT, SWEEPLE, DELTASFACT, &
& CROOT, CTIP, SPAN, TCS, SWEEP, TOGPROPULSION, PROPULSORNUMWING, PROPULSORWINGDISTANCE, &
& PROPULSORNUMFUSELAGE, PROPULSORTHRUSTFACTOR, CCS, CTOG, CFACTOR, TAPERTAIL, TAPERFIN, &
& SWEEPTAIL, SWEEPFIN, SWEEPHALFTAIL, SWEEPHALFFIN, SWEEPTAILMASTER, SWEEPFINMASTER, &
& ASPECTTAIL, ASPECTFIN, SPANTAIL, SPANFIN, SWEEPTAILLE, SWEEPFINLE, FUELVOLUMETOTAL, &
& FUELVOLUMEOUTER, FUELVOLUMEINNER, FUELAREAOUTER, FUELLENGTHOUTER, FUELAREAINNER, &
& TFUELOUTER, T40, C40, MFUELTOT, FUELVOLUMEREQ, FUELDENSITY, TTIP, TC70, TCCS, TC40, &
& TCTIP, MFUELRES, BHALF, BFHALF, B70, B40, BCSHALF, TROOT, VA)
IMPLICIT NONE
REAL NULT, MCR, L, LETOG, CLA, VS, TCTIP, TCROOT, BHALF, BCSHALF, CROOT, &
& TAPER, CTIP, TTIP, TROOT, TC70, BFHALF, BFPERC, RHOSLS, &
& SWEEPLE, SWEEPMASTER, SWEEP, SWEEPHALF, STE, STEPERC, SSLAT, SSLATPERC, SKRUG,
SKRUGPERC, &
& BSHALF, ETAPP, PPNUM, TAPERF, VD, FF, CRTAIL, CRFIN, IARM, CT, CF, TCEMP, &
& ATAIL, AFIN, MACTAIL, MACFIN, STAIL, SFIN, TC40, CCS, TCS, &
& DELTASFACT, SPAN, PROPULSORWINGDISTANCE, PROPULSORNUMFUSELAGE, &
```

```
& PROPULSORTHRUSTFACTOR, CFSTORE, CTSTORE, TAPERTAIL, TAPERFIN, SWEEPTAIL, SWEEPFIN, &
& SWEEPHALFTAIL, SWEEPHALFFIN, SWEEPTAILMASTER, SWEEPFINMASTER, ASPECTTAIL, ASPECTFIN, &
& SPANTAIL, SPANFIN, SWEEPTAILLE, SWEEPFINLE, VA

INTEGER TOGPROPULSION, PROPULSORELEMENT, PROPULSORNUMWING, CTOG

DOUBLE PRECISION KR, A, TC, MWING, MACWING, SWING, SWINGWET, &
& RHOT, SIGMAT, RHOC, SIGMAC, SHEARMOD, RHOS, RHOR, RC, ETACP, DELTAW, &
& DELTAPP, DELTAF, R, SIGMAMEAN, SIGMATOR, ETAT, WBASIC, DELTAS, DELTAA, DELTAPA, &
& DELTAST, WPRIM, WLE, WTE, WSLAT, WKRUGER, WAI, WSPLD, WTSUPP, WASUPP, WSEC, RHOCR, &
& MTOW, MLW, MPP, MZFW, MBASIC, MPRIM, MSEC, MEMP, AL, WT, PROPULSORMASS, DELTAPROPULSOR,
&
& ETAPROPULSOR, ST, CFACTOR, FUELVOLUMETOTAL, FUELVOLUMEOUTER, FUELVOLUMEINNER,
FUELAREAOUTER, &
& FUELLENGTHOUTER, FUELAREAINNER, TFUELOUTER, T40, C40, MFUELTOT, FUELVOLUMEREQ,
FUELDENSITY, &
& B40, B70, TCCS, MFUELRES

SWING=(2*MLW*9.81)/(RHOSLS*CLA*(VA**2))  ! WING AREA

!TCTIP=0.7652*TC
!TCROOT=1.1652*TC

TCTIP=0.74*TC
TCROOT=1.17*TC

!*****************************************     - INITIAL CALCS -

BHALF=SQRT(A*SWING)/2

SPAN=BHALF*2

BCSHALF=BHALF*0.1

BFHALF=(BHALF-BCSHALF)*BFPERC



SWEEP=SWEEPMASTER    !CONVERTS BACK TO DEGS - RESET

SWEEP=SWEEP*(3.14159/180) !converts to radians

SWEEPLE=(SWEEP+((1-TAPER)/(A*(1+TAPER))))!*(3.14159/180)

SWEEPHALF=(SWEEP-((1-TAPER)/(A*(1+TAPER))))!*(3.14159/180)


SWINGWET=SWING*(1.977+(0.52*TC))

STE=(STEPERC/100)*SWINGWET

SSLAT=(SSLATPERC/100)*SWINGWET

SKRUG=(SKRUGPERC/100)*SWING



BSHALF=BHALF/COS(SWEEPHALF)

CROOT=(SWING)/((1+TAPER)*BHALF)*1.3      !ROOT CHORD DIMENSION - for straight-taper wing
(no sweep) - INCLUDES FACTOR FOR KINK & sweep

CTIP=CROOT*TAPER

MACWING=(0.66667)*CROOT*(1+TAPER+TAPER**2)/(1+TAPER)

TTIP=CTIP*TCTIP

TROOT=CROOT*TCROOT

CCS=CROOT-BCSHALF*TAN(SWEEPLE)
```

```
B40=(BHALF-BCSHALF)*0.25

C40=CCS-(B40*TAN(SWEEPLE))    !0.25 MEASURED FRACTION TO KINK FROM CENTRE SECTION

TC40=TCTIP*0.99

T40=TC40*C40

B70=0.7*BHALF

TC70=(B70-B40)*(TCTIP-TC40)/(BHALF-B40)+TC40   !INTERPOLATES BETWEEN TC40 AND TCTIP

TCCS=(BCSHALF)*(TC40-TCROOT)/(B40)+TCROOT   !INTERPOLATES BETWEEN TC40 AND TCROOT

TCS=TCCS*CCS

!TCS=(TCROOT+((BCSHALF/BHALF)*(TCTIP-TCROOT)))*CCS*0.8

!************************************************************  !WING GEOMETRY



!*****************************************          - BASIC WEIGHT & RELIEF FACTORS -


RC=((BHALF-BCSHALF)/TCS)*((0.66667)+(0.33333)*(TCROOT/TC40))

ETACP=(2/(3*3.14159))+((1+(2*TAPER))/(6*(1+TAPER)))


IF (MTOW/=MLW) THEN

DELTAW=-0.8*MWING/MTOW

!*************************************   !CHECKS FOR DISTRIBUTED PROPULSION CASE

RELIEF: SELECT CASE(TOGPROPULSION)

CASE(1)

DELTAPP=-1.5*((ETAPP**2/ETACP)*((MPP/PPNUM)/(MTOW/2)))

CASE(2)

DELTAPP=-1.5*((ETAPP**2/ETACP)*((MPP*(1-PROPULSORTHRUSTFACTOR)/PPNUM)/(MTOW/2)))
!PROPULSORTHRUSTFACTOR REDUCES WEIGHT DUE TO LESS THRUST REQUIRED

PROPULSORMASS=MPP*PROPULSORTHRUSTFACTOR/((PROPULSORNUMWING*2)+PROPULSORNUMFUSELAGE)

DO PROPULSORELEMENT=1,PROPULSORNUMWING  !CALCULATES PROPULSOR DISTANCE RATIO 'ETAPP' FOR
HALF WING

ETAPROPULSOR=(BCSHALF+(PROPULSORWINGDISTANCE/PROPULSORNUMWING*PROPULSORELEMENT))/BHALF

DELTAPROPULSOR=-1.5*((ETAPROPULSOR**2/ETACP)*(PROPULSORMASS/(MTOW/2)))

DELTAPP=DELTAPP+DELTAPROPULSOR  !ADDS PROPULSORS TO THE MAIN ENGINE RELIEF CONTRIBUTION


END DO


END SELECT RELIEF

!*************************************

TAPERF=TAPER*1.1
```

```
DELTAF=((-1*(1+(3*TAPERF)))/4)*(BFHALF/(BHALF-BCSHALF))**2*(1-(MZFW/MTOW))

R=1+DELTAW+DELTAPP+DELTAF

ELSE

R=1

END IF

SIGMAMEAN=0.5*(((RHOT*9.81)/SIGMAT)+((RHOC*9.81)/(0.8*SIGMAC)))

SIGMATOR=1.2*2

ETAT=0.8  !ASSUMED VALUE

KR=0.0005 !ASSUMED VALUE

WBASIC=(0.3333*SIGMAMEAN*R*NULT*(MTOW*9.81)*BSHALF*2*ETACP* &
& (((1.08*RC)/ETAT)+(1.5*SIGMATOR)))+(KR*RHOR*9.81*SWING* &
& (1+((TROOT+TTIP)/2)))



!************************         NON OPTIMUM ADDED WEIGHTS - PRIMARY WEIGHT


DELTAS=RHOR*9.81*SWING*(1+(2*TC))*0.001*DELTASFACT      !SHEET TAPER CORRECTION
(DELTASFACT IS A FACTOR FOR MODERN AIRCRAFT WEIGHT REDUCTION)

DELTAA=(0.001*(9.81*MTOW))+(0.002*(9.81*(MLW)))   !FUSELAGE AND UNDERCARRIAGE ATTACHMENTS


ATTACHMENTS: SELECT CASE(TOGPROPULSION)

CASE(1)

DELTAPA=0.025*(1+(0.2*PPNUM))*(MPP*9.81)           !EXTRA RIB WEIGHT FOR ATTACHMENTS

CASE(2)

DELTAPA=0.025*(1+(0.2*PPNUM))*(MPP*9.81)


END SELECT ATTACHMENTS

DELTAST=0.05*((9.81*RHOT)/SHEARMOD)*(0.5*RHOCR*VD**2)*(BHALF*2*COS(SWEEPLE))**3 &
& *(1-SIN(SWEEPHALF))/(TC70**2*(1-(MCR*COS(SWEEPHALF)**2))**0.5)

WPRIM=WBASIC+DELTAS+DELTAA+DELTAPA+DELTAST



!************************         SECONDARY WEIGHTS


WLE=0.18*SWINGWET*LETOG*(1+SQRT((MTOW*9.81)/10**6))*(1.33333)*(0.0008*9.81*RHOS) ! LEADING
EDGE SUPPORT


CONTROLSURFACES: SELECT CASE(TOGPROPULSION)

CASE(1)

ST=0.16*SWING

CASE(2)

STE=STE-(STE/3)*PROPULSORWINGDISTANCE/B40 !  /3 FOR 3RD INNER FLAPS AND 0.25* FOR QUARTER
KINK TO SPAN RATIO
```

```
ST=0.16*SWING                                !INITIAL ST BEFORE DISTRIBUTED ENGINE AREA
REDUCTION

ST=ST-(ST/3)*PROPULSORWINGDISTANCE/B40 !  /3 FOR 3RD INNER FLAPS AND 0.25* FOR QUARTER
KINK TO SPAN RATIO


END SELECT CONTROLSURFACES


WTE=STE*((1+(1.6*SQRT((MTOW*9.81)/10**6)))*(0.000857*9.81*RHOS)+FF) !TRAILING EDGE SUPPORT
MASS

WT=(9.81*0.00364*2.9*RHOR)*ST*(1+SQRT((9.81*MTOW)/10**6))  !TRAILING EDGE DEVICES MASS

WSLAT=1.7*0.0016*9.81*RHOS*(1+(0.7*SQRT((MTOW*9.81)/10**6)))*SSLAT !LEADING EDGE SLATS

WKRUGER=0.02*(RHOR/10)*SWING  !LEADING EDGE KRUGER FLAPS

WAI=0.04*SWING*(1+(0.5*((9.81*MTOW)/10**6)**0.25))*(9.81*RHOR*0.00455)   !AILERONS

WSPLD=15*SWING

WTSUPP=0.05*WT

WASUPP=0.2*WAI


WSEC=WLE+WTE+WSLAT+WKRUGER+WT+WAI+WSPLD+WTSUPP+WASUPP


!**************************      TOTAL WING MASS

MWING=(WPRIM+WSEC)/9.81


!************************     WING DIMENSIONS


FUELLENGTHOUTER=((BHALF-BCSHALF)*BFPERC-B40)

TFUELOUTER=FUELLENGTHOUTER/((0.75*(BHALF-BCSHALF))/(TTIP-T40))+T40

FUELLENGTHOUTER=FUELLENGTHOUTER/COS(SWEEPLE)


!************************     FUEL VOLUME CHECK


FUELDENSITY=817.15  !KEROSENE

FUELVOLUMEREQ=(MFUELTOT+MFUELRES)/FUELDENSITY


FUELAREAINNER=(C40*B40+(CCS-C40)*B40/2)   !FOR HALF WING

FUELVOLUMEINNER=FUELAREAINNER*(T40+TCS)/2

FUELAREAOUTER=CTIP*FUELLENGTHOUTER+(C40-CTIP)*FUELLENGTHOUTER/2

FUELVOLUMEOUTER=FUELAREAOUTER*(T40+TFUELOUTER)/2

FUELVOLUMETOTAL=(FUELVOLUMEOUTER+FUELVOLUMEINNER)*2*(100-STEPERC-SSLATPERC-
SKRUGPERC)/100*0.8   !*0.8 FOR T/C VARIATION ALLOWANCE


!*******************************************************************************
EMPENNAGE GEOMETRY (FOR DRAG CALCULATIONS)
```

```
IARM=0.6*L     !MOMENT ARM

IF (CTOG==0) THEN !STOPS CHANGING CT/CF

VOLUME: SELECT CASE(TOGPROPULSION)  !VOLUME COEFFICIENT REDUCTION ACCOUNTING FOR ENGINE
LOCATION SPREAD (EMPENNAGE MOMENT REQ.)

CASE(1)

CFACTOR=1

CASE(2)

CTOG=CTOG+1    !STOPS EMMPENAGE VOLUME COEFS. CHANGING REPEATEDLY


CFSTORE=PROPULSORTHRUSTFACTOR*(CF*0.975)+(1-PROPULSORTHRUSTFACTOR)*CF !0.975 REPRESENTS
50% PROPULSORS PRODUCING 95% CF  (50% PRODUCING 100%CF); TOTAL 97.5% OVERALL

CTSTORE=PROPULSORTHRUSTFACTOR*(CT*0.95)+(1-PROPULSORTHRUSTFACTOR)*CT  ! 0.95=5% FROM CT
FOR UPPER ENGINE MOUNTS AND *FACTOR FOR JUST THOSE ENGINES

CFACTOR=(CFSTORE+CTSTORE)/(CF+CT)  !CREATE STORES TO COMPARE AGAINST ORIGINAL; GIVES
FACTOR FOR MEMP

CF=CFSTORE  !COPY COEFFICIENTS FROM STORE TO ACTUAL CT/CF

CT=CTSTORE



END SELECT VOLUME

ELSE
END IF

STAIL=CT*MACWING*SWING/IARM

SFIN=CF*BHALF*SWING/IARM*2

!-----  SPAN EQUATIONS ASSUME EMPENNAGE ROOT CHORD AND TIP CHORD ALIGN VERTICALLY TO GIVE
TWO TRIANGLES -----


SPANTAIL=SQRT(STAIL*ATAIL)/2 !HALF SPAN OF TAIL

SPANFIN=SQRT(SFIN*AFIN)


CRTAIL=(STAIL/2)*2/(SPANTAIL*(TAPERTAIL+1))

CRFIN=SFIN*2/(SPANFIN*(TAPERFIN+1))


MACTAIL=0.66667*CRTAIL*(1+TAPERTAIL+(TAPERTAIL**2))/(1+TAPERTAIL)

MACFIN=0.66667*CRFIN*(1+TAPERFIN+(TAPERFIN**2))/(1+TAPERFIN)



SWEEPTAILLE=ATAN(CRTAIL/SPANTAIL)

SWEEPFINLE=ATAN(CRFIN/SPANFIN)


 SWEEPTAIL=SWEEPTAILLE-((1-TAPERTAIL)/(ATAIL*(1+TAPERTAIL)))

 SWEEPFIN=SWEEPFINLE-((1-TAPERFIN)/(AFIN*(1+TAPERFIN)))


 SWEEPHALFTAIL=SWEEPTAIL-((1-TAPERTAIL)/(ATAIL*(1+TAPERTAIL)))

 SWEEPHALFFIN=SWEEPFIN-((1-TAPERFIN)/(AFIN*(1+TAPERFIN)))
```

```
!**************************      EMPENNAGE MASS

MEMP=(MWING/7.96)*CFACTOR    ! /7.96 IS AN empirical proportion. CF


RETURN
END
```

5. ‘BWB’ subroutine – BWB structural mass calculations

```
!ST=TRAILING EDGE FLAP AREA


SUBROUTINE WING(MLW, RHOSLS, CLA, VS, SWING, A, TC, TAPER, BFPERC, SWEEPMASTER, &
& SWINGWET, STEPERC, SSLATPERC, SKRUGPERC, MTOW, MWING, ETAPP, MPP, &
& PPNUM, MZFW, RHOT, SIGMAT, RHOC, SIGMAC, RHOR, NULT, SHEARMOD, RHOCR, &
& MCR, LETOG, RHOS, FF, VD, MBASIC, MPRIM, MSEC, MEMP, TCEMP, &
& CRTAIL, CRFIN, ATAIL, AFIN, MACTAIL, MACFIN, CT, CF, L, MACWING, &
& STAIL, SFIN, SWEEPHALF, TCROOT, SWEEPLE, DELTASFACT, &
& CROOT, CTIP, SPAN, TCS, SWEEP, TOGPROPULSION, PROPULSORNUMWING, PROPULSORWINGDISTANCE, &
& PROPULSORNUMFUSELAGE, PROPULSORTHRUSTFACTOR, CCS, CTOG, CFACTOR, TAPERTAIL, TAPERFIN, &
& SWEEPTAIL, SWEEPFIN, SWEEPHALFTAIL, SWEEPHALFFIN, SWEEPTAILMASTER, SWEEPFINMASTER, &
& ASPECTTAIL, ASPECTFIN, SPANTAIL, SPANFIN, SWEEPTAILLE, SWEEPFINLE, FUELVOLUMETOTAL, &
& FUELVOLUMEOUTER, FUELVOLUMEINNER, FUELAREAOUTER, FUELLENGTHOUTER, FUELAREAINNER, &
& TFUELOUTER, T40, C40, MFUELTOT, FUELVOLUMEREQ, FUELDENSITY, TTIP, TC70, TCCS, TC40, &
& TCTIP, MFUELRES, BHALF, BFHALF, B70, B40, BCSHALF, TROOT, VA)

IMPLICIT NONE



REAL NULT, MCR, L, LETOG, CLA, VS, TCTIP, TCROOT, BHALF, BCSHALF, CROOT, &
& TAPER, CTIP, TTIP, TROOT, TC70, BFHALF, BFPERC, RHOSLS, &
& SWEEPLE, SWEEPMASTER, SWEEP, SWEEPHALF, STE, STEPERC, SSLAT, SSLATPERC, SKRUG,
SKRUGPERC, &
& BSHALF, ETAPP, PPNUM, TAPERF, VD, FF, CRTAIL, CRFIN, IARM, CT, CF, TCEMP, &
& ATAIL, AFIN, MACTAIL, MACFIN, STAIL, SFIN, TC40, CCS, TCS, &
& DELTASFACT, SPAN, PROPULSORWINGDISTANCE, PROPULSORNUMFUSELAGE, &
& PROPULSORTHRUSTFACTOR, CFSTORE, CTSTORE, TAPERTAIL, TAPERFIN, SWEEPTAIL, SWEEPFIN, &
& SWEEPHALFTAIL, SWEEPHALFFIN, SWEEPTAILMASTER, SWEEPFINMASTER, ASPECTTAIL, ASPECTFIN, &
& SPANTAIL, SPANFIN, SWEEPTAILLE, SWEEPFINLE, VA

INTEGER TOGPROPULSION, PROPULSORELEMENT, PROPULSORNUMWING, CTOG

DOUBLE PRECISION KR, A, TC, MWING, MACWING, SWING, SWINGWET, &
& RHOT, SIGMAT, RHOC, SIGMAC, SHEARMOD, RHOS, RHOR, RC, ETACP, DELTAW, &
& DELTAPP, DELTAF, R, SIGMAMEAN, SIGMATOR, ETAT, WBASIC, DELTAS, DELTAA, DELTAPA, &
& DELTAST, WPRIM, WLE, WTE, WSLAT, WKRUGER, WAI, WSPLD, WTSUPP, WASUPP, WSEC, RHOCR, &
& MTOW, MLW, MPP, MZFW, MBASIC, MPRIM, MSEC, MEMP, AL, WT, PROPULSORMASS, DELTAPROPULSOR,
&
& ETAPROPULSOR, ST, CFACTOR, FUELVOLUMETOTAL, FUELVOLUMEOUTER, FUELVOLUMEINNER,
FUELAREAOUTER, &
& FUELLENGTHOUTER, FUELAREAINNER, TFUELOUTER, T40, C40, MFUELTOT, FUELVOLUMEREQ,
FUELDENSITY, &
& B40, B70, TCCS, MFUELRES



SWING=(2*MLW*9.81)/(RHOSLS*CLA*(VA**2))  ! WING AREA

!TCTIP=0.7652*TC
!TCROOT=1.1652*TC

TCTIP=0.74*TC
TCROOT=1.17*TC
```

```
!*****************************************     - INITIAL CALCS -

BHALF=SQRT(A*SWING)/2

SPAN=BHALF*2

BCSHALF=BHALF*0.1

BFHALF=(BHALF-BCSHALF)*BFPERC



SWEEP=SWEEPMASTER    !CONVERTS BACK TO DEGS - RESET

SWEEP=SWEEP*(3.14159/180) !converts to radians

SWEEPLE=(SWEEP+((1-TAPER)/(A*(1+TAPER))))!*(3.14159/180)

SWEEPHALF=(SWEEP-((1-TAPER)/(A*(1+TAPER))))!*(3.14159/180)

SWINGWET=SWING*(1.977+(0.52*TC))

STE=(STEPERC/100)*SWINGWET

SSLAT=(SSLATPERC/100)*SWINGWET

SKRUG=(SKRUGPERC/100)*SWING


BSHALF=BHALF/COS(SWEEPHALF)

CROOT=(SWING)/((1+TAPER)*BHALF)*1.3      !ROOT CHORD DIMENSION - for straight-taper wing
(no sweep) - INCLUDES FACTOR FOR KINK & sweep

CTIP=CROOT*TAPER

MACWING=(0.66667)*CROOT*(1+TAPER+TAPER**2)/(1+TAPER)

TTIP=CTIP*TCTIP

TROOT=CROOT*TCROOT

CCS=CROOT-BCSHALF*TAN(SWEEPLE)

B40=(BHALF-BCSHALF)*0.25

C40=CCS-(B40*TAN(SWEEPLE))    !0.25 MEASURED FRACTION TO KINK FROM CENTRE SECTION

TC40=TCTIP*0.99

T40=TC40*C40

B70=0.7*BHALF

TC70=(B70-B40)*(TCTIP-TC40)/(BHALF-B40)+TC40   !INTERPOLATES BETWEEN TC40 AND TCTIP

TCCS=(BCSHALF)*(TC40-TCROOT)/(B40)+TCROOT   !INTERPOLATES BETWEEN TC40 AND TCROOT

TCS=TCCS*CCS

!TCS=(TCROOT+((BCSHALF/BHALF)*(TCTIP-TCROOT)))*CCS*0.8

!*********************************************************  !WING GEOMETRY
```

```
!*****************************************          - BASIC WEIGHT & RELIEF FACTORS -


RC=((BHALF-BCSHALF)/TCS)*((0.66667)+(0.33333)*(TCROOT/TC40))

ETACP=(2/(3*3.14159))+((1+(2*TAPER))/(6*(1+TAPER)))


IF (MTOW/=MLW) THEN

    DELTAW=-0.8*MWING/MTOW

    !*************************************   !CHECKS FOR DISTRIBUTED PROPULSION CASE

    RELIEF: SELECT CASE(TOGPROPULSION)

        CASE(1)

            DELTAPP=-1.5*((ETAPP**2/ETACP)*((MPP/PPNUM)/(MTOW/2)))

        CASE(2)

            DELTAPP=-1.5*((ETAPP**2/ETACP)*((MPP*(1-
PROPULSORTHRUSTFACTOR)/PPNUM)/(MTOW/2))) !PROPULSORTHRUSTFACTOR REDUCES WEIGHT DUE TO LESS
THRUST REQUIRED


PROPULSORMASS=MPP*PROPULSORTHRUSTFACTOR/((PROPULSORNUMWING*2)+PROPULSORNUMFUSELAGE)

            DO PROPULSORELEMENT=1,PROPULSORNUMWING  !CALCULATES PROPULSOR DISTANCE RATIO
'ETAPP' FOR HALF WING


ETAPROPULSOR=(BCSHALF+(PROPULSORWINGDISTANCE/PROPULSORNUMWING*PROPULSORELEMENT))/BHALF

                DELTAPROPULSOR=-1.5*((ETAPROPULSOR**2/ETACP)*(PROPULSORMASS/(MTOW/2)))

                DELTAPP=DELTAPP+DELTAPROPULSOR  !ADDS PROPULSORS TO THE MAIN ENGINE RELIEF
CONTRIBUTION


            END DO


    END SELECT RELIEF

    !*************************************

    TAPERF=TAPER*1.1

    DELTAF=((-1*(1+(3*TAPERF)))/4)*(BFHALF/(BHALF-BCSHALF))**2*(1-(MZFW/MTOW))

    R=1+DELTAW+DELTAPP+DELTAF

ELSE

    R=1

END IF

SIGMAMEAN=0.5*(((RHOT*9.81)/SIGMAT)+((RHOC*9.81)/(0.8*SIGMAC)))

SIGMATOR=1.2*2

ETAT=0.8  !ASSUMED VALUE

KR=0.0005 !ASSUMED VALUE

WBASIC=(0.3333*SIGMAMEAN*R*NULT*(MTOW*9.81)*BSHALF*2*ETACP* &
& (((1.08*RC)/ETAT)+(1.5*SIGMATOR)))+(KR*RHOR*9.81*SWING* &
```

```
& (1+((TROOT+TTIP)/2)))



!************************         NON OPTIMUM ADDED WEIGHTS - PRIMARY WEIGHT


DELTAS=RHOR*9.81*SWING*(1+(2*TC))*0.001*DELTASFACT      !SHEET TAPER CORRECTION
(DELTASFACT IS A FACTOR FOR MODERN AIRCRAFT WEIGHT REDUCTION)

DELTAA=(0.001*(9.81*MTOW))+(0.002*(9.81*(MLW)))   !FUSELAGE AND UNDERCARRIAGE ATTACHMENTS


ATTACHMENTS: SELECT CASE(TOGPROPULSION)

    CASE(1)

        DELTAPA=0.025*(1+(0.2*PPNUM))*(MPP*9.81)           !EXTRA RIB WEIGHT FOR
ATTACHMENTS

    CASE(2)

        DELTAPA=0.025*(1+(0.2*PPNUM))*(MPP*9.81)


END SELECT ATTACHMENTS

DELTAST=0.05*((9.81*RHOT)/SHEARMOD)*(0.5*RHOCR*VD**2)*(BHALF*2*COS(SWEEPLE))**3 &
& *(1-SIN(SWEEPHALF))/(TC70**2*(1-(MCR*COS(SWEEPHALF)**2))**0.5)

WPRIM=WBASIC+DELTAS+DELTAA+DELTAPA+DELTAST



!************************         SECONDARY WEIGHTS


WLE=0.18*SWINGWET*LETOG*(1+SQRT((MTOW*9.81)/10**6))*(1.33333)*(0.0008*9.81*RHOS) ! LEADING
EDGE SUPPORT


CONTROLSURFACES: SELECT CASE(TOGPROPULSION)

    CASE(1)

        ST=0.16*SWING

    CASE(2)

        STE=STE-(STE/3)*PROPULSORWINGDISTANCE/B40 !  /3 FOR 3RD INNER FLAPS AND 0.25* FOR
QUARTER KINK TO SPAN RATIO

        ST=0.16*SWING                              !INITIAL ST BEFORE DISTRIBUTED ENGINE
AREA REDUCTION

        ST=ST-(ST/3)*PROPULSORWINGDISTANCE/B40 !  /3 FOR 3RD INNER FLAPS AND 0.25* FOR
QUARTER KINK TO SPAN RATIO


END SELECT CONTROLSURFACES



WTE=STE*((1+(1.6*SQRT((MTOW*9.81)/10**6)))*(0.000857*9.81*RHOS)+FF) !TRAILING EDGE SUPPORT
MASS

WT=(9.81*0.00364*2.9*RHOR)*ST*(1+SQRT((9.81*MTOW)/10**6))  !TRAILING EDGE DEVICES MASS

WSLAT=1.7*0.0016*9.81*RHOS*(1+(0.7*SQRT((MTOW*9.81)/10**6)))*SSLAT !LEADING EDGE SLATS

WKRUGER=0.02*(RHOR/10)*SWING  !LEADING EDGE KRUGER FLAPS

WAI=0.04*SWING*(1+(0.5*((9.81*MTOW)/10**6)**0.25))*(9.81*RHOR*0.00455)   !AILERONS
```

```
WSPLD=15*SWING

WTSUPP=0.05*WT

WASUPP=0.2*WAI

WSEC=WLE+WTE+WSLAT+WKRUGER+WT+WAI+WSPLD+WTSUPP+WASUPP

!*************************      TOTAL WING MASS

MWING=(WPRIM+WSEC)/9.81

!************************     WING DIMENSIONS


FUELLENGTHOUTER=((BHALF-BCSHALF)*BFPERC-B40)

TFUELOUTER=FUELLENGTHOUTER/((0.75*(BHALF-BCSHALF))/(TTIP-T40))+T40

FUELLENGTHOUTER=FUELLENGTHOUTER/COS(SWEEPLE)


!************************     FUEL VOLUME CHECK

FUELDENSITY=817.15  !KEROSENE

FUELVOLUMEREQ=(MFUELTOT+MFUELRES)/FUELDENSITY

FUELAREAINNER=(C40*B40+(CCS-C40)*B40/2)   !FOR HALF WING

FUELVOLUMEINNER=FUELAREAINNER*(T40+TCS)/2

FUELAREAOUTER=CTIP*FUELLENGTHOUTER+(C40-CTIP)*FUELLENGTHOUTER/2

FUELVOLUMEOUTER=FUELAREAOUTER*(T40+TFUELOUTER)/2

FUELVOLUMETOTAL=(FUELVOLUMEOUTER+FUELVOLUMEINNER)*2*(100-STEPERC-SSLATPERC-
SKRUGPERC)/100*0.8   !*0.8 FOR T/C VARIATION ALLOWANCE

!*****************************************************************************
EMPENNAGE GEOMETRY (FOR DRAG CALCULATIONS)



IARM=0.6*L     !MOMENT ARM

IF (CTOG==0) THEN !STOPS CHANGING CT/CF

     VOLUME: SELECT CASE(TOGPROPULSION)  !VOLUME COEFFICIENT REDUCTION ACCOUNTING FOR
ENGINE LOCATION SPREAD (EMPENNAGE MOMENT REQ.)

        CASE(1)

            CFACTOR=1

        CASE(2)

            CTOG=CTOG+1    !STOPS EMMPENAGE VOLUME COEFS. CHANGING REPEATEDLY


            CFSTORE=PROPULSORTHRUSTFACTOR*(CF*0.975)+(1-PROPULSORTHRUSTFACTOR)*CF !0.975
REPRESENTS 50% PROPULSORS PRODUCING 95% CF  (50% PRODUCING 100%CF); TOTAL 97.5% OVERALL
```

```
            CTSTORE=PROPULSORTHRUSTFACTOR*(CT*0.95)+(1-PROPULSORTHRUSTFACTOR)*CT  !
0.95=5% FROM CT FOR UPPER ENGINE MOUNTS AND *FACTOR FOR JUST THOSE ENGINES

            CFACTOR=(CFSTORE+CTSTORE)/(CF+CT)  !CREATE STORES TO COMPARE AGAINST ORIGINAL;
GIVES FACTOR FOR MEMP

            CF=CFSTORE  !COPY COEFFICIENTS FROM STORE TO ACTUAL CT/CF

            CT=CTSTORE


    END SELECT VOLUME

ELSE
END IF

STAIL=CT*MACWING*SWING/IARM

SFIN=CF*BHALF*SWING/IARM*2

!-----  SPAN EQUATIONS ASSUME EMPENNAGE ROOT CHORD AND TIP CHORD ALIGN VERTICALLY TO GIVE
TWO TRIANGLES -----


SPANTAIL=SQRT(STAIL*ATAIL)/2 !HALF SPAN OF TAIL

SPANFIN=SQRT(SFIN*AFIN)


CRTAIL=(STAIL/2)*2/(SPANTAIL*(TAPERTAIL+1))

CRFIN=SFIN*2/(SPANFIN*(TAPERFIN+1))


MACTAIL=0.66667*CRTAIL*(1+TAPERTAIL+(TAPERTAIL**2))/(1+TAPERTAIL)

MACFIN=0.66667*CRFIN*(1+TAPERFIN+(TAPERFIN**2))/(1+TAPERFIN)



SWEEPTAILLE=ATAN(CRTAIL/SPANTAIL)

SWEEPFINLE=ATAN(CRFIN/SPANFIN)


SWEEPTAIL=SWEEPTAILLE-((1-TAPERTAIL)/(ATAIL*(1+TAPERTAIL)))

SWEEPFIN=SWEEPFINLE-((1-TAPERFIN)/(AFIN*(1+TAPERFIN)))


SWEEPHALFTAIL=SWEEPTAIL-((1-TAPERTAIL)/(ATAIL*(1+TAPERTAIL)))

SWEEPHALFFIN=SWEEPFIN-((1-TAPERFIN)/(AFIN*(1+TAPERFIN)))



!**************************      EMPENNAGE MASS


MEMP=(MWING/7.96)*CFACTOR    ! /7.96 IS AN empirical proportion. CF


RETURN
END
```

6. ‘Drag’ subroutine – T&W drag calculations

```
SUBROUTINE DRAG(RHOCR, MACWING, VD, MUCR, MCR, LAMPERCWING, TC, SWEEPHALF, TCROOT, &
& SWING, L, LAMPERCFUS, H, W, LNOSE, LTAIL, LNAC, LAMPERCNAC, HNAC, WNAC, &
& MACTAIL, MACFIN, LAMPERCEMP, TCTAIL, TCFIN, STAIL, SFIN, CL, CDT, &
& CDW, A, K, CD0TOT, CDTOT, PPNUM, LD, SWETFUS, TCK, SWEEP, TAPER, &
& PROPULSORFUSELAGEDISTANCE, TOGPROPULSION, CCS, PROPULSORWINGDISTANCE, SWEEPLE, &
& SWINGPROPULSORS, SWINGBLI, PROPULSORWINGLENGTH, CROOT, PROPULSORNUMFUSELAGE, &
& SWEEPHALFTAIL, SWEEPHALFFIN, CD0FIN, CD0TAIL, PROPULSORTHRUSTFACTOR, TOGGNACELLE, &
& CD0WING, CD0FUS, CD0NAC, CDI, OSWALDFACTOR, THETAAREA)

IMPLICIT NONE

DOUBLE PRECISION MACWING, MUCR, TC, RE, SWING, CFTURB, CFLAM, CFMEAN, FSTAR, &
& FORMFAC, SWET, CD0WING, R, CD0FUS, RHOCR, CD0NAC, CD0TAIL, CD0FIN, CD0WINGIMP, &
& CD0FUSEMPIMP, CD0NACIMP, CD0WINDIMP, CD0IMP, CD0TOT, CDT, CDW, AEFF, A, OSWALDFACTOR, &
& K, CDI, CDTOT, SSWPA, MDES, RSWPA, SWPA, RTP, ERRORMDES, DELTA, ERRORSTORE, &
& PROPULSORFUSELAGEDISTANCE, SWINGPROPULSORS, SWINGBLI, PROPULSORWINGLENGTH, &
& SFUSELAGEBLI, THETAAREA

REAL MCR, LAMPERCWING, LAMPERCFUS, H, W, L, Q, LNOSE, LTAIL, VD, SWEEPHALF, &
& TCROOT, DEFF, LNAC, LAMPERCNAC, HNAC, WNAC, MACTAIL, MACFIN, &
& LAMPERCEMP, TCTAIL, TCFIN, STAIL, SFIN, CL, PPNUM, LD, SWETFUS, TCK, SWEEP, &
& CL2D, RTPC, MDESSTORE, TAPER, CCS, PROPULSORWINGDISTANCE, SWEEPLE, CROOT, &
& PROPULSORNUMFUSELAGE, SWEEPHALFTAIL, SWEEPHALFFIN, PROPULSORTHRUSTFACTOR


INTEGER IMDES, TOGPROPULSION, TOGGNACELLE



!*******************************************************************************************
************     -- WING DRAG CALCULATIONS --

RE=(RHOCR*MACWING*VD/MUCR)                                        !REYNOLDS NUMBER AT MEAN
CHORD

CFTURB=0.455/(((LOG10(RE))**2.58)*(1+(0.144*MCR**2))**0.65)   !FRICTION COEFFICIENT-
TURBULENT

CFLAM=1.328/(RE**0.5)                                          !FRICTION COEFFICIENT-LAMINA

CFMEAN=((LAMPERCWING/100)*CFLAM)+((1-(LAMPERCWING/100))*CFTURB)      !MEAN FRICTION
COEFFICIENT

FSTAR=1+(3.3*TC)-(0.008*(TC**2))+(27*(TC**3))  !FORM FACTOR COEFFICIENT

FORMFAC=((FSTAR-1)*COS(SWEEPHALF)**2)+1   !FORM FACTOR

Q=1                                        !INTERFERENCE FACTOR

SWET=(1.977+(0.52*TC))*SWING        !WETTED SURFACE AREA

CD0WING=CFMEAN*FORMFAC*Q*SWET/(SWING)      !ZERO LIFT DRAG COEFFICIENT


WINGBLI: SELECT CASE (TOGPROPULSION)   !DISTRIBUTED PROPULSION TOGGLE

    CASE(1)  !LEFT BLANK FOR NORMAL CONDITIONS (NO BLI)


    CASE(2)

       ! SWINGBLI=(CCS*PROPULSORWINGDISTANCE)-
(PROPULSORWINGDISTANCE*PROPULSORWINGDISTANCE*TAN(SWEEPLE)/2)

       ! SWINGPROPULSORS=PROPULSORWINGDISTANCE*PROPULSORWINGLENGTH

       ! SWET=SWET-(2*SWINGBLI)+(SWINGPROPULSORS*2)        !- BLI AREA SUBTRACTED AND
PROPULSOR BOX ADDED - *2 FOR BOTH SIDES
```

```
END SELECT WINGBLI


!*******************************************************************************************
***********     -- FUESLAGE DRAG CALCULATIONS --


RE=(RHOCR*L*VD/MUCR)                                        !REYNOLDS NUMBER AT MEAN CHORD

CFTURB=0.455/(((LOG10(RE))**2.58)*(1+(0.144*MCR**2))**0.65)   !FRICTION COEFFICIENT-
TURBULENT

CFLAM=1.328/(RE**0.5)                                         !FRICTION COEFFICIENT-LAMINA

CFMEAN=((LAMPERCFUS/100)*CFLAM)+((1-(LAMPERCFUS/100))*CFTURB)      !MEAN FRICTION
COEFFICIENT

R=(H-W)/(H+W)     !DEFF COEFFICIENT

DEFF=((W/2)+(H/2))*((64-R**4)/(64-(19*R**2)))    !EFFECTIVE DIAMTER OF FUSELAGE

FORMFAC=1+(2.2/(L/((4/3.142)*((3.142*DEFF**2)/4))**0.5)**1.5)-(0.9/(L/((4/3.142) &
& *((3.142*DEFF**2)/4))**0.5))**3   !FORM FACTOR

Q=1                                       !INTERFERENCE FACTOR

SWETFUS=(3.142*DEFF*(L-LNOSE-LTAIL))+(0.75*3.142*DEFF*(LNOSE+LTAIL))        !WETTED
SURFACE AREA

CD0FUS=CFMEAN*FORMFAC*Q*SWETFUS/SWING      !ZERO LIFT DRAG COEFFICIENT

FUSELAGEBLI: SELECT CASE (TOGPROPULSION)

    CASE(1)

    CASE(2)

      !  SFUSELAGEBLI=PROPULSORFUSELAGEDISTANCE*(L-LTAIL-LNOSE-PROPULSORWINGLENGTH)+ &
!CALCULATES AREA PROPULSORS COVER
      !  & 0.75*PROPULSORFUSELAGEDISTANCE*LNOSE

      !  SWETFUS=SWETFUS-SFUSELAGEBLI           !WETTED SURFACE AREA MINUS BLI AREA


END SELECT FUSELAGEBLI



!*******************************************************************************************
***********        -- NACELLES DRAG --

IF (TOGGNACELLE==0) THEN

    TOGGNACELLE=TOGGNACELLE+1

    NACELLEBLI: SELECT CASE (TOGPROPULSION)

            CASE(1)

        CASE(2)

                LNAC=LNAC*(1-PROPULSORTHRUSTFACTOR)
            HNAC=HNAC*(1-PROPULSORTHRUSTFACTOR)
           WNAC=WNAC*(1-PROPULSORTHRUSTFACTOR)

    END SELECT NACELLEBLI

END IF

RE=(RHOCR*LNAC*VD/MUCR)                                     !REYNOLDS NUMBER AT MEAN CHORD
```

```
CFTURB=0.455/(((LOG10(RE))**2.58)*(1+(0.144*MCR**2))**0.65)   !FRICTION COEFFICIENT-
TURBULENT

CFLAM=1.328/(RE**0.5)                                        !FRICTION COEFFICIENT-LAMINA

CFMEAN=((LAMPERCNAC/100)*CFLAM)+((1-(LAMPERCNAC/100))*CFTURB)      !MEAN FRICTION
COEFFICIENT

R=(HNAC-WNAC)/(HNAC+WNAC)     !DEFF COEFFICIENT

DEFF=((WNAC/2)+(WNAC/2))*((64-R**4)/(64-(19*R**2)))    !EFFECTIVE DIAMTER OF FUSELAGE

FORMFAC=1.25   !FORM FACTOR

Q=1.0                                  !INTERFERENCE FACTOR


SWET=(3.14159*DEFF*LNAC)                   !WETTED SURFACE AREA

CD0NAC=(CFMEAN*FORMFAC*Q*SWET/SWING)*PPNUM      !ZERO LIFT DRAG COEFFICIENT


!*****************************************************************************************
************       -- TAIL DRAG --


RE=(RHOCR*MACTAIL*VD/MUCR)                                    !REYNOLDS NUMBER AT MEAN
CHORD

CFTURB=0.455/(((LOG10(RE))**2.58)*(1+(0.144*MCR**2))**0.65)   !FRICTION COEFFICIENT-
TURBULENT

CFLAM=1.328/(RE**0.5)                                        !FRICTION COEFFICIENT-LAMINA

CFMEAN=((LAMPERCEMP/100)*CFLAM)+((1-(LAMPERCEMP/100))*CFTURB)      !MEAN FRICTION
COEFFICIENT

FSTAR=1+(3.52*TCTAIL) !FORMFACTOR COEFFICIENT

FORMFAC=((FSTAR-1)*COS(SWEEPHALFTAIL)**2)+1   !FORM FACTOR

Q=1.                                  !INTERFERENCE FACTOR

SWET=STAIL*(1.977+(0.52*TCTAIL))               !WETTED SURFACE AREA

CD0TAIL=CFMEAN*FORMFAC*Q*SWET/SWING      !ZERO LIFT DRAG COEFFICIENT


!*****************************************************************************************
************       -- FIN DRAG --


RE=(RHOCR*MACFIN*VD/MUCR)                                     !REYNOLDS NUMBER AT MEAN CHORD

CFTURB=0.455/(((LOG10(RE))**2.58)*(1+(0.144*MCR**2))**0.65)   !FRICTION COEFFICIENT-
TURBULENT

CFLAM=1.328/(RE**0.5)                                        !FRICTION COEFFICIENT-LAMINA

CFMEAN=((LAMPERCEMP/100)*CFLAM)+((1-(LAMPERCEMP/100))*CFTURB)      !MEAN FRICTION
COEFFICIENT

FSTAR=1+(3.52*TCFIN) !FORMFACTOR COEFFICIENT

FORMFAC=((FSTAR-1)*COS(SWEEPHALFFIN)**2)+1   !FORM FACTOR

Q=1.                                  !INTERFERENCE FACTOR

SWET=SFIN*(1.977+(0.52*TCFIN))               !WETTED SURFACE AREA
```

```
CD0FIN=CFMEAN*FORMFAC*Q*SWET/SWING      !ZERO LIFT DRAG COEFFICIENT

!*****************************************************************************************
************     -- IMPERFECTIONS DRAG COEFF --

CD0WINGIMP=0.06*CD0WING                                    !WING
CD0FUSEMPIMP=0.07*CD0FUS                                   !FUSELAGE/EMPENNAGE
CD0NACIMP=0.15*CD0NAC                                      !NACELLE INSTALLATION
CD0WINDIMP=0.02*CD0FUS                                     !WINDSHIELD

!CD0IMP=CD0WINGIMP+CD0FUSEMPIMP+CD0NACIMP+CD0WINDIMP        !IMPERFECTIONS TOTAL

CD0TOT=(CD0WING+CD0FUS+CD0NAC+CD0TAIL+CD0FIN) !*1.3  !TOTAL - 3% TOTAL PROFILE DRAG FOR
SYSTEMS


AEFF=A*1.2

OSWALDFACTOR=(1.78*(1-(0.045*A**0.68))-0.64)**1.2    !OSWALD SPANWISE EFFICIENCY FACTOR
WITH 1.1 FACTOR FOR SWEEP

K=1/(AEFF*OSWALDFACTOR*3.142)                   !INDUCED DRAG FACTOR

CDI=K*CL**2                         !INDUCED DRAG COEFFICIENT


!*****************************************************************  -- WAVE DRAG --


!SWPA=(ATAN(TAN(SWEEP)-((1/A)*(1-TAPER)/(1+TAPER)*((1.6*RTP)-0.28)))) --UNUSED--
CL2D=CL/(0.9*COS(SWEEP))
RTPC=0.52
MDESSTORE=MCR
ERRORSTORE=0

DO IMDES=1,10001

    !RTP=0.5015

    SSWPA=1.6*RTPC*(1-TAPER)/(MDESSTORE**2*A*(1-TAPER))

    RSWPA=TAN(SWEEP)-(1-TAPER)/(1+TAPER)*(1.32+(1.6*RTPC))/A

    SWPA=ACOS(SQRT(((1-(2*RSWPA*SSWPA)+(1-
(4*SSWPA*(RSWPA+SSWPA)))**0.5))/(2*(1+RSWPA**2))))

    RTP=1+(RTPC*(1-(1/(MDESSTORE*COS(SWPA))**2)))

    MDES=TCK*(((2.78+(2.03*RTP)+((12.68+(3.87*RTP))*TC/COS(SWPA))))-
(CL2D/CL)*CL/(COS(SWPA))**2) &

    & /(((2.65+(2.25*RTP))+(27.8*TC/COS(SWPA)))*COS(SWPA))

    ERRORMDES=((MDESSTORE-MDES)**2)**0.5

    IF (ERRORMDES<0.00001) EXIT

    IF ((ERRORSTORE<=ERRORMDES) .AND. (IMDES>1)) THEN

        PRINT *, 'WAVE DRAG ERROR INCREASING'
        PAUSE

        STOP

    END IF

    IF (IMDES==1000) THEN
        PRINT *, 'WAVE DRAG NON-CONVERGENCE'
        PAUSE
        STOP
    END IF

    MDESSTORE=MDES
```

```
        ERRORSTORE=ERRORMDES

    END DO

    DELTA=0.03+MCR-MDES

    CDW=0.007*DELTA+(155*DELTA**4.5)




    !*********************************************************************


    CDTOT=CD0TOT+CDI+CDT+CDW           !TOTAL DRAG COEFFICIENT

    LD=CL/CDTOT


    RETURN
    END
```

7. ‘DragBWB’ subroutine – BWB drag calculations

```
SUBROUTINE DRAGBWB(RHOCR, MACWINGINNER, VD, MUCR, MCR, LAMPERCWING, TCINNER, &
& SWING, L, LAMPERCFUS, H, W, LNOSE, LTAIL, LNAC, LAMPERCNAC, HNAC, WNAC, TCOUTER, &
& MACTAIL, MACFIN, LAMPERCEMP, TCTAIL, TCFIN, STAIL, SFIN, CL, CDT, SWEEPHALFINNER, &
& CDW, A, K, CD0TOT, CDTOT, PPNUM, LD, SWETFUS, TCK, SWEEP, TAPERINNER, SWEEPHALFOUTER, &
& PROPULSORFUSELAGEDISTANCE, TOGPROPULSION, CKINNER, PROPULSORWINGDISTANCE, &
& SWINGPROPULSORS, SWINGBLI, PROPULSORWINGLENGTH, CRINNER, PROPULSORNUMFUSELAGE, &
& SWEEPHALFTAIL, SWEEPHALFFIN, CD0FIN, CD0TAIL, PROPULSORTHRUSTFACTOR, TOGGNACELLE, &
& SWEEPLEINNER, SWEEPLEOUTER, MACWINGOUTER, SINNER, SOUTER, BINNER, BOUTER, AINNER, &
& SWEEPQUARTERINNER, AOUTER, TAPEROUTER, TCKOUTER, SWEEPQUARTEROUTER, TCKINNER, CD0INNERWING,
&
& CD0OUTERWING, CDI, CD0NAC, BOUTERHALF, SWEEPTEINNER, OSWALDFACTOR, GROSSFACTOR, SGROSS,
THETAAREA)

IMPLICIT NONE

DOUBLE PRECISION MACWING, MUCR, TCINNER, RE, SWING, CFTURB, CFLAM, CFMEAN, FSTAR, &
& FORMFAC, SWET, CD0WING, R, CD0FUS, RHOCR, CD0NAC, CD0TAIL, CD0FIN, CD0WINGIMP, &
& CD0FUSEMPIMP, CD0NACIMP, CD0WINDIMP, CD0IMP, CD0TOT, CDT, CDW, AEFF, A, OSWALDFACTOR, &
& K, CDI, CDTOT, SSWPA, MDES, RSWPA, SWPA, RTP, ERRORMDES, DELTA, ERRORSTORE, &
& PROPULSORFUSELAGEDISTANCE, SWINGPROPULSORS, SWINGBLI, PROPULSORWINGLENGTH, &
& SFUSELAGEBLI, MACWINGINNER, SWEEPHALFINNER, SINNER, CD0INNERWING, MACWINGOUTER, &
& TCOUTER, SWEEPHALFOUTER, SOUTER, CD0OUTERWING, BINNER, BOUTER, TC, TAPERINNER, &
& CKINNER, SWEEPLEINNER, SWEEPLEOUTER, CTOUTER, TAPERFIN, TCFIN, SWEEPHALFFIN, &
& CRINNER, MACFIN, AINNER, SWEEPQUARTERINNER, AOUTER, TAPEROUTER, TCKOUTER, &
& SWEEPQUARTEROUTER, TCKINNER, BOUTERHALF, SWEEPTEINNER, GROSSFACTOR, SGROSS, THETAAREA

REAL MCR, LAMPERCWING, LAMPERCFUS, H, W, L, Q, LNOSE, LTAIL, VD, SWEEPHALF, &
& DEFF, LNAC, LAMPERCNAC, HNAC, WNAC, MACTAIL, &
& LAMPERCEMP, TCTAIL, STAIL, SFIN, CL, PPNUM, LD, SWETFUS, TCK, SWEEP, &
& CL2D, RTPC, MDESSTORE, TAPER, CCS, PROPULSORWINGDISTANCE, SWEEPLE, CROOT, &
& PROPULSORNUMFUSELAGE, SWEEPHALFTAIL, PROPULSORTHRUSTFACTOR


INTEGER IMDES, TOGPROPULSION, TOGGNACELLE



!*********************************************************************************************
********     -- INNER WING DRAG CALCULATIONS --
```

```
RE=(RHOCR*MACWINGINNER*VD/MUCR)                                    !REYNOLDS NUMBER AT MEAN
CHORD

!re=96961474

CFTURB=0.455/(((LOG10(RE))**2.58)*(1+(0.144*MCR**2))**0.65)   !FRICTION COEFFICIENT-TURBULENT

CFLAM=1.328/(RE**0.5)                                          !FRICTION COEFFICIENT-LAMINA

CFMEAN=((LAMPERCWING/100)*CFLAM)+((1-(LAMPERCWING/100))*CFTURB)      !MEAN FRICTION
COEFFICIENT

FSTAR=1+(3.3*TCINNER)-(0.008*(TCINNER**2))+(27*(TCINNER**3))  !FORM FACTOR COEFFICIENT

FORMFAC=((FSTAR-1)*COS(SWEEPHALFINNER)**2)+1   !FORM FACTOR

Q=1                                      !INTERFERENCE FACTOR

SWET=(1.97+(0.52*TCINNER))*SINNER       !WETTED SURFACE AREA - 1.970 from  1.977 for tip area
removal

CD0INNERWING=CFMEAN*FORMFAC*Q*SWET/(SGROSS)      !ZERO LIFT DRAG COEFFICIENT


WINGBLI: SELECT CASE (TOGPROPULSION)   !DISTRIBUTED PROPULSION TOGGLE


CASE(1)  !LEFT BLANK FOR NORMAL CONDITIONS (NO BLI)




CASE(2)

       ! SWINGBLI=(CRINNER*PROPULSORWINGDISTANCE)-
PROPULSORWINGDISTANCE*PROPULSORWINGDISTANCE*(TAN(SWEEPLEINNER)+TAN(SWEEPTEINNER))/2

       ! SWINGPROPULSORS=PROPULSORWINGDISTANCE*PROPULSORWINGLENGTH

       ! SWET=SWET-(SWINGBLI-SWINGPROPULSORS)*2        !- BLI AREA SUBTRACTED AND PROPULSOR
BOX ADDED - *2 FOR BOTH SIDES

        ! CD0INNERWING=CD0INNERWING-(THETAAREA/(0.5*SGROSS))   !bwb DP BLI area given from
Rolls royce-SRC


END SELECT WINGBLI



!*****************************************************************************************
********     -- OUTER WING DRAG CALCULATIONS --


RE=(RHOCR*MACWINGOUTER*VD/MUCR)                                    !REYNOLDS NUMBER AT MEAN
CHORD

CFTURB=0.455/(((LOG10(RE))**2.58)*(1+(0.144*MCR**2))**0.65)   !FRICTION COEFFICIENT-TURBULENT

CFLAM=1.328/(RE**0.5)                                          !FRICTION COEFFICIENT-LAMINA

CFMEAN=((LAMPERCWING/100)*CFLAM)+((1-(LAMPERCWING/100))*CFTURB)      !MEAN FRICTION
COEFFICIENT

FSTAR=1+(3.3*TCOUTER)-(0.008*(TCOUTER**2))+(27*(TCOUTER**3))  !FORM FACTOR COEFFICIENT

FORMFAC=((FSTAR-1)*COS(SWEEPHALFOUTER)**2)+1   !FORM FACTOR

Q=1                                      !INTERFERENCE FACTOR

SWET=(1.977+(0.52*TCOUTER))*SOUTER        !WETTED SURFACE AREA
```

```
CD0OUTERWING=CFMEAN*FORMFAC*Q*SWET/(SGROSS)      !ZERO LIFT DRAG COEFFICIENT


!*****************************************************************************************
*******        -- NACELLES DRAG --

IF (TOGGNACELLE==0) THEN

        TOGGNACELLE=TOGGNACELLE+1

        NACELLEBLI: SELECT CASE (TOGPROPULSION)

         CASE(1)

             CASE(2)

                        !LNAC=LNAC*(1-PROPULSORTHRUSTFACTOR)
           ! HNAC=HNAC*(1-PROPULSORTHRUSTFACTOR)
                !WNAC=WNAC*(1-PROPULSORTHRUSTFACTOR)

        END SELECT NACELLEBLI

END IF

RE=(RHOCR*LNAC*VD/MUCR)                                    !REYNOLDS NUMBER AT MEAN CHORD

CFTURB=0.455/(((LOG10(RE))**2.58)*(1+(0.144*MCR**2))**0.65)   !FRICTION COEFFICIENT-TURBULENT

CFLAM=1.328/(RE**0.5)                                      !FRICTION COEFFICIENT-LAMINA

CFMEAN=((LAMPERCNAC/100)*CFLAM)+((1-(LAMPERCNAC/100))*CFTURB)      !MEAN FRICTION COEFFICIENT

R=(HNAC-WNAC)/(HNAC+WNAC)     !DEFF COEFFICIENT

DEFF=((WNAC/2)+(WNAC/2))*((64-R**4)/(64-(19*R**2)))    !EFFECTIVE DIAMTER OF FUSELAGE

FORMFAC=1.25   !FORM FACTOR

Q=1.0                                  !INTERFERENCE FACTOR

SWET=(3.14159*DEFF*LNAC)                 !WETTED SURFACE AREA

CD0NAC=(CFMEAN*FORMFAC*Q*SWET/(SGROSS))*PPNUM      !ZERO LIFT DRAG COEFFICIENT



!*****************************************************************************************
********       -- FIN DRAG --


RE=(RHOCR*MACFIN*VD/MUCR)                                   !REYNOLDS NUMBER AT MEAN CHORD

CFTURB=0.455/(((LOG10(RE))**2.58)*(1+(0.144*MCR**2))**0.65)   !FRICTION COEFFICIENT-TURBULENT

CFLAM=1.328/(RE**0.5)                                      !FRICTION COEFFICIENT-LAMINA

CFMEAN=((LAMPERCEMP/100)*CFLAM)+((1-(LAMPERCEMP/100))*CFTURB)      !MEAN FRICTION COEFFICIENT

FSTAR=1+(3.52*TCFIN) !FORMFACTOR COEFFICIENT

FORMFAC=((FSTAR-1)*COS(SWEEPHALFFIN)**2)+1   !FORM FACTOR

Q=1.                                  !INTERFERENCE FACTOR

SWET=SFIN*(1.977+(0.52*TCFIN))               !WETTED SURFACE AREA

CD0FIN=CFMEAN*FORMFAC*Q*SWET/(SGROSS)      !ZERO LIFT DRAG COEFFICIENT

!*****************************************************************************************
********     -- INDUCED DRAG COEFF --
```

```
CD0TOT=(CD0OUTERWING+CD0INNERWING+CD0NAC+CD0FIN) !*1.3  !TOTAL - 3% TOTAL PROFILE DRAG FOR
SYSTEMS


A=(BOUTER+BINNER)**2/SWING


AEFF=A*1.2

OSWALDFACTOR=(1.78*(1-(0.045*A**0.68))-0.64)**1.2    !OSWALD SPANWISE EFFICIENCY FACTOR WITH
1.1 FACTOR FOR SWEEP

K=1/(AEFF*OSWALDFACTOR*3.142)                    !INDUCED DRAG FACTOR

CDI=K*(CL-0.054)**2                          !INDUCED DRAG COEFFICIENT


!*****************************************************************  -- WAVE DRAG --


!SWPA=(ATAN(TAN(SWEEP)-((1/A)*(1-TAPER)/(1+TAPER)*((1.6*RTP)-0.28)))) --UNUSED--


IF (AOUTER<3) AOUTER=3

IF (SOUTER<100) THEN

    CL2D=CL

ELSE

    CL2D=CL/(0.9*COS(SWEEPQUARTEROUTER))

END IF

RTPC=0.52

MDESSTORE=MCR

ERRORSTORE=0


DO IMDES=1,10001

    !RTP=0.5015

    SSWPA=1.6*RTPC*(1-TAPEROUTER)/(MDESSTORE**2*AOUTER*(1-TAPEROUTER))

    RSWPA=TAN(SWEEPQUARTEROUTER)-(1-TAPEROUTER)/(1+TAPEROUTER)*(1.32+1.6*RTPC)/AOUTER

    SWPA=ACOS(SQRT((1-2*RSWPA*SSWPA+SQRT(1-4*SSWPA*(RSWPA+SSWPA)))/(2*(1+RSWPA**2))))

    RTP=1+RTPC*(1-1/(MDESSTORE*COS(SWPA))**2)

    MDES=TCK*(((2.78+(2.03*RTP)+((12.68+(3.87*RTP))*TCKINNER/COS(SWPA))))-
(CL2D/CL)*CL/(COS(SWPA))**2) &

    & /(((2.65+(2.25*RTP))+(27.8*TCKINNER/COS(SWPA)))*COS(SWPA))

    ERRORMDES=((MDESSTORE-MDES)**2)**0.5


    IF (ERRORMDES<0.00001) EXIT

    IF ((ERRORSTORE<=ERRORMDES) .AND. (IMDES>100)) THEN

       PRINT *, 'WAVE DRAG ERROR INCREASING'
      PAUSE
```

```
        STOP

    END IF

    IF (IMDES==1000) THEN

        PRINT *, 'WAVE DRAG NON-CONVERGENCE'

        PAUSE
        STOP

    END IF

    MDESSTORE=MDES

    ERRORSTORE=ERRORMDES

END DO

DELTA=0.03+MCR-MDES

IF (DELTA<0) DELTA=0

CDW=0.007*DELTA+(155*DELTA**4.5)


!*********************************************************************


CDTOT=CD0TOT+CDI+CDT+CDW           !TOTAL DRAG COEFFICIENT

LD=CL/CDTOT


RETURN
END
```

8. ‘Performance’ subroutine – performance calculations for mission for both aircraft types

```
SUBROUTINE PERFORMANCE(TAS, MACH, EAS, MASS, CLC, CD, DRAGS, THRUST, ROC, CORR, ROCCORR,
ROCMEAN, T, &
& TCUM, FFLOW, F, FCUM, RANG, RCUM, ALT, TEMP, RHO, RHOSLS, MFUELTO, MTOW, SWING, K, CD0TOT, &
& SFCCLIMB, MCR, RANGE, SFCTO, VS, SFCCR, VD, CL, CDTOT, MFUELTOT, MFUELRES, R, GAMMA, CAS, &

& TASD, MACHD, CASD, MASSD, CLD, CDD, DRAGSD, THRUSTD, ROD, CORRD, RODCORR, RODMEAN, TD, &
!DESCENT VARIABLES
& TCUMD, FFLOWD, FD, FCUMD, RANGD, RCUMD, ALTD, TEMPD, RHOD, THRUSTTO, SFCD, THRUSTCR, SFC, &
& THRUSTFACTOR, RHOCEIL, RHOCR, ALTCEILING, VA, PRESSURESLS, PRESSURE, ALTITERATION, &
& ALTITUDECRUISEEND, TEMPCR, PRESSURECR, ALTITUDECRUISE, TTO, TCR, MFUELCR, RANGECR, MFUELL,
TTOTAL, &
& VC, GROSSFACTOR)

IMPLICIT NONE

REAL MCR, TOL, V2, VS, CLT, TTO, LL, VD, CL, RHOSLS, VC, SFCD, TEMP1, TEMP2, &
& R, VA
INTEGER X, Y, W, TOG, CHECK, COUNT
DOUBLE PRECISION MFUELTO, MTOW, SWING, K, CD0TOT, SFCCLIMB, MFUEL, ERROR, ERRORFAC, THRUSTTO,
&
& SFCTO, MTOWCR1, RANGECR, RANGE, SFCCR, CDTOT, MTOWCR2, RCUMSTORE, MFUELCR, TCR, MFUELL,
MFUELTOT, &
& MFUELRES, THRUSTSTORE, D, KTO, ERRORTHRUST, THRUSTBIG, ALT1, ALT2, DENS1, DENS2, &
& GAMMA, ALTCEILING, THRUSTCR, RHOCEIL, RHOCR, DELTAPRESSURE, PRESSURESLS, ERRORTAS, TASSTORE,
V, &
& MACHCLIMB, XFACTOR, EASSTORE, ALTITERATION, TEMPITERATION, RHOITERATION, PRESSUREITERATION,
&
& TEMPCR, PRESSURECR, ALTITUDECRUISE, ALTITUDECRUISEEND, TTOTAL, ERRORTHRUST2, SGROSS,
GROSSFACTOR
```

```
!************************************************ CLIMB ARRAYS

DOUBLE PRECISION,DIMENSION(12)::TAS
DOUBLE PRECISION,DIMENSION(12)::CAS
DOUBLE PRECISION,DIMENSION(12)::MACH
DOUBLE PRECISION,DIMENSION(12)::EAS
DOUBLE PRECISION,DIMENSION(12)::MASS
DOUBLE PRECISION,DIMENSION(12)::CLC
DOUBLE PRECISION,DIMENSION(12)::CD
DOUBLE PRECISION,DIMENSION(12)::DRAGS
DOUBLE PRECISION,DIMENSION(12)::THRUST
DOUBLE PRECISION,DIMENSION(12)::SFC
DOUBLE PRECISION,DIMENSION(12)::ROC
DOUBLE PRECISION,DIMENSION(12)::CORR
DOUBLE PRECISION,DIMENSION(12)::ROCCORR
DOUBLE PRECISION,DIMENSION(12)::ROCMEAN
DOUBLE PRECISION,DIMENSION(12)::T
DOUBLE PRECISION,DIMENSION(12)::TCUM
DOUBLE PRECISION,DIMENSION(12)::FFLOW
DOUBLE PRECISION,DIMENSION(12)::F
DOUBLE PRECISION,DIMENSION(12)::FCUM
DOUBLE PRECISION,DIMENSION(12)::RANG
DOUBLE PRECISION,DIMENSION(12)::RCUM
DOUBLE PRECISION,DIMENSION(12)::ALT
DOUBLE PRECISION,DIMENSION(12)::TEMP
DOUBLE PRECISION,DIMENSION(12)::RHO

DOUBLE PRECISION,DIMENSION(12)::THRUSTFACTOR
DOUBLE PRECISION,DIMENSION(12)::PRESSURE


!********************************************** DESCENT ARRAYS

DOUBLE PRECISION,DIMENSION(11)::ALTD
REAL,DIMENSION(11)::TEMPD
DOUBLE PRECISION,DIMENSION(11)::RHOD

DOUBLE PRECISION,DIMENSION(11)::TASD
DOUBLE PRECISION,DIMENSION(11)::MACHD
DOUBLE PRECISION,DIMENSION(11)::CASD
DOUBLE PRECISION,DIMENSION(11)::MASSD
DOUBLE PRECISION,DIMENSION(11)::CLD
DOUBLE PRECISION,DIMENSION(11)::CDD
DOUBLE PRECISION,DIMENSION(11)::DRAGSD
DOUBLE PRECISION,DIMENSION(11)::THRUSTD
DOUBLE PRECISION,DIMENSION(11)::ROD
DOUBLE PRECISION,DIMENSION(11)::CORRD
DOUBLE PRECISION,DIMENSION(11)::RODCORR
DOUBLE PRECISION,DIMENSION(11)::RODMEAN
DOUBLE PRECISION,DIMENSION(11)::TD
DOUBLE PRECISION,DIMENSION(11)::TCUMD
DOUBLE PRECISION,DIMENSION(11)::FFLOWD
DOUBLE PRECISION,DIMENSION(11)::FD
DOUBLE PRECISION,DIMENSION(11)::FCUMD
DOUBLE PRECISION,DIMENSION(11)::RANGD
DOUBLE PRECISION,DIMENSION(11)::RCUMD


!----------------VARIABLES---------------

!RHOITERATION, TEMPITER... == INPUT ALTITUDE FOR CEILING IN PREVIOUS ITERATION FROM ROLLS-
ROYCE VALUES


!-----------------------------------------


CHECK=0
COUNT=0

!*****************************************************************   --- TAKEOFF ---
```

```
TOL=3048    !RUNWAY LENGTH - 10500FT MINUS 500FT FOR CONTINGENCY

V2=VS*1.114  !ORIGINALLY VA*1.2 , ALTHOUGH R.WILSON ADVISED AN INCREASE IN VA FROM 67.0 TO
93.86 I.E. VS=140KTS

THRUSTTO=(V2**2*MTOW/(2*TOL))*2    !TAKEOFF THRUST AT END OF RUNWAY, MACH 0.25 - (*2 FOR TWO
ENGINE EQUIVALENT (NORMALLY ONE ENGINE INOPERATIVE)

TTO=120                            !2 MINS TAKEOFF THRUST

MFUELTO=SFCTO*(THRUSTTO/1000)*TTO



!*********************************************************************   --- CLIMB ---

!DO X=1,8                                    !FILL TAS ARRAY


        !DELTAPRESSURE=PRESSURE(X)/PRESSURESLS

        !CAS=EAS(X)*0.5144     !CAS ARRAY (NAMED EAS) CONVERTED TO M/S

    !DO   !ITERATION TO GET TASSTORE=TAS(X) FOR MACH NO.

   ! MACHCLIMB=(TASSTORE/SQRT(GAMMA*R*TEMP(X)))  !MACH NO. AT ALTITUDE

    !XFACTOR=(((0.2*MACHCLIMB**2+1)**3.5-1)*DELTAPRESSURE+1)**(0.4/1.4)-1

    !CAS=SQRT(5*1.4*287.05307*288.15)*SQRT(XFACTOR)


        !EASSTORE=CAS/(1+(0.125*(CAS/SQRT(GAMMA*R*TEMP(X)))**2*(1-DELTAPRESSURE))+ &
        !& (0.0046875*(1-
(10*DELTAPRESSURE)+(9*DELTAPRESSURE**2))*(CAS/SQRT(GAMMA*R*TEMP(X)))**4))   !CONVERT CAS TO
EAS - CALIBRATAED AIRSPEED USED BEFORE CONSTANT MACH NO. CLIMB FROM V4.2

        !TAS(X)=EASSTORE*SQRT(RHOSLS/RHO(X)) !CONVERT EAS TO TAS

    !TAS(X)=CAS*0.5144           !CONVERTING TO M/S

   ! ERRORTAS=((TASSTORE-TAS(X))**2)**0.5

    !IF (ERRORTAS<0.1) EXIT

    !TASSTORE=TAS(X)

!END DO



MASS(1)=MTOW-MFUELTO                    ! SET INITIAL VALUES FOR INPUTS
TCUM(1)=0
FCUM(1)=0
RCUM(1)=0
MFUEL=0
ERROR=0
X=1
Y=2
TOG=1                                   !TOGGLE


!************************************************************ -- CEILING AIR PROPERTIES FROM
THRUST FACTOR INPUT - required for RHOITERATION --

CALL PROPERTIES(RHOITERATION, TEMPITERATION, PRESSUREITERATION, ALTITERATION,R)


RHO(12)=RHOITERATION !INITIAL VALUE FOR INITAL THRUST


!************************************************************
```

```
IF (MFUELCR<1) MFUELCR=10000

!*****************************************************   -- INITIAL THRUST AT MASS(1)--
CALL ALTITUD(ALT, MCR, MASS(1), CL, SWING, RHO, TAS, X, ALT1, ALT2, DENS1, DENS2, TEMP, R,
GAMMA, &
& ALTITUDECRUISEEND, RHOCR, TEMPCR, PRESSURECR, ALTITUDECRUISE, MFUELCR, ALTD, VD, SGROSS,
GROSSFACTOR)

D=CDTOT*SWING*0.5*RHOCR*TAS(11)**2                  !INITAL DRAG AND THRUST CALCULATION AT
CEILING



THRUST(12)=(((VC/TAS(11))*MASS(1))*9.81)+D

!*****************************************************



DO !*************** -- THRUST REQUIREMENT LOOP--


    DO !******************** -- MASS ITERATION LOOP --



        CLC(X)=(MASS(X)*9.81)/(SWING*0.5*RHO(X)*TAS(X)**2)

        CD(X)=CD0TOT+(K*CLC(X)**2)



        DRAGS(X)=0.5*RHO(X)*(TAS(X)**2)*SWING*CD(X)



        !******************************************************* ITERATES CEILING THRUST



         !THRUSTBIG=THRUSTSTORE+(ALT(11)*0.003281*0.05*THRUSTSTORE)     **CHANGE THRUSTSTORE
TO THRUST(12)***          !THRUST BIG IS SLS VALUE HIGHER THAN THRUSTTO TO CONVERGE

         !THRUSTBIG=THRUSTTO

         !THRUST(X)=THRUSTBIG-((THRUSTBIG-THRUSTSTORE)/ALT(11))*ALT(X)            !THRUST FOR
SET CEILING (I.E. THRUST STORE)



         THRUST(X)=THRUSTFACTOR(X)*THRUST(12)*RHOITERATION/RHO(12)                       !
THRUST CALIBRATED WITH TOC


        !*******************************************************  RATE OF CLIMB CALC;
DIFFERENT FOR ACCELERATION AT CONST. ALT AND CEILING



        ROC(X)=((THRUST(X)-DRAGS(X))/(MASS(X)*9.81))*TAS(X)

        IF (X==3 .OR. X==9 .OR. X==11) THEN

            CORR(X)=(TAS(X)/9.81)*((TAS(X)-TAS(W))/(ALT(X)-ALT(W)))+1

        ELSE

            CORR(X)=(TAS(X)/9.81)*((TAS(Y)-TAS(X))/(ALT(Y)-ALT(X)))+1

        END IF
```

```
        ROCCORR(X)=ROC(X)/CORR(X)

        !*************************************************************************  !
PREVIOUS FUEL AND ERROR BETWEEN NEW AND OLD FUEL

        IF (X>1) THEN

        ROCMEAN(W)=(ROCCORR(W)+ROCCORR(X))/2

            IF (X==4) THEN                                              !CONSTANT ALT
ACCELERATION EQUATION AT 4


                T(W)=(CAS(X)-CAS(W))/((((THRUST(X)+THRUST(W))/2)-
((DRAGS(X)+DRAGS(W))/2))/((MASS(X)+MASS(W))/2))

            ELSE

                T(W)=(ALT(X)-ALT(W))/ROCMEAN(W)

            ENDIF


            TCUM(X)=TCUM(W)+T(W)

            FFLOW(W)=SFC(W)*(THRUST(X)+THRUST(W))/(2*10**3)

            F(W)=T(W)*FFLOW(W)

            ERROR=F(W)-MFUEL



        ELSE                                                            ! FIRST ALTITUDE REQUIRES
SECOND ALTITUDE DATA -  LOOP

            X=X+1
            W=X-1
            Y=X+1

            GOTO 50

        ENDIF

        !*************************************************************************


        ERRORFAC=(ERROR**2)**(0.5)              ! MODULUS OF ERROR

        IF (ERRORFAC<0.01) THEN                 ! ERROR SIZE CHECK, SMALL PROCEED

            CHECK=0             !RESET CHECK


        !*************************************************************************


            FCUM(X)=F(W)+FCUM(W)                !CUMULATIVE VALUES

            RANG(X)=CAS(W)*T(W)

            RCUM(X)=RANG(X)+RCUM(W)

            X=X+1                               ! NEXT ARRAY ELEMENT VALUES
            W=X-1
            Y=X+1

            IF (X<12) THEN                      !CHECK FOR END OF ARRAY

            MASS(X)=MASS(W)
            CYCLE

            ELSE
```

```
            EXIT  !LEAVE CLIMB CALCS

            END IF

                                ! REITERATE IF ERROR IS LARGE
        ENDIF

        !*********************************************************************

        CHECK=CHECK+1
        IF (CHECK>1000) THEN

        !ALT(X)=ALT(W)+1
        PRINT *, 'ALTITUDE TOO HIGH FOR CONVERGENCE (SMALL ASPECT RATIO OR HIGH T/C), CHANGE
FROM ALTITUDE ', ALT(W)
        PAUSE
        STOP
        END IF


        !*********************************************************************


        50 CONTINUE

        MFUEL=MFUEL+ERROR  ! FUEL MASS GUESS

        MASS(X)=MASS(W)-MFUEL    ! NEXT TOTAL MASS

        !**************


    END DO




!*************************************************************************************************
************************************************************
    !!!!!!!!!!!!!! CHECK NEW OPTIMUM ALTITUDE FOR NEW THRUST WITH LOWER MASS (BURNED FUEL)



    CALL ALTITUD(ALT, MCR, MTOW, CL, SWING, RHO, TAS, W, ALT1, ALT2, DENS1, DENS2, TEMP, R,
GAMMA, &
    & ALTITUDECRUISEEND, RHOCR, TEMPCR, PRESSURECR, ALTITUDECRUISE, MFUELCR, ALTD, VD, SGROSS,
GROSSFACTOR)   !FIND ALT(11)


    !*****************************************CEILING ALTITUDE FOR THRUST, CL=CLIMB


    MASS(12)=MASS(11)-(MTOW*0.00167)*0      !MINUS PERCENTAGE OF MTOW TO SIMULATE FUEL BURN
FROM 11 TO 12(*0 TO CANCEL - CLIMB altitude TIME HIGH)

    ALTCEILING=ALT(11)+(3000/3.281)    !  +3000ft for ceiling climb

    !********

    CALL PROPERTIES(RHO(12), TEMP(12), PRESSURE(12), ALTCEILING, R)

    !********

    TAS(12)=MCR*SQRT(GAMMA*R*TEMP(12))

    CLC(12)=(MASS(12)*9.81)/(SWING*0.5*RHO(12)*TAS(12)**2)

    CD(12)=CD0TOT+(K*CLC(12)**2)

    DRAGS(12)=SWING*CD(12)*0.5*RHO(12)*TAS(12)**2
```

```
    THRUSTSTORE=((VC/TAS(12))*9.81*MASS(12))+DRAGS(12)



    ERRORTHRUST2=ERRORTHRUST

    ERRORTHRUST=((THRUST(12)-THRUSTSTORE)**2)**0.5                                  !ERROR BETWEEN
NEW/OLD THRUST


    IF (ERRORTHRUST2<ERRORTHRUST .AND. COUNT>=1) EXIT

    COUNT=COUNT+1
    check=0

        IF (ERRORTHRUST>0.01) THEN

            THRUST(12)=THRUSTSTORE

            X=1                                     !RESETS INTEGERS
            Y=2


            IF (COUNT>1000) THEN

                PRINT *, 'WARNING: THRUST LOWER THAN DRAG, "ERROR THRUST CYCLIC" ERROR;
DECREASE CLA?'
                COUNT=0
                check=0
                EXIT

            END IF

            CYCLE

        ELSE

            COUNT=0
            check=0
            EXIT


        END IF

ENDDO




!*************************************************************************************************
--- CRUISE AND DESCENT/LANDING PHASES ---
*************************************************

THRUSTCR=CDTOT*SWING*0.5*RHOCR*VD**2                                  ! CRUISE THRUST

MTOWCR1=MTOW-MFUELTO-FCUM(11)

RCUMD(11)=0                                                            !INITIAL DESCENT
RANGE VALUE
RCUMSTORE=0                                                            !INITIAL RANGE
STORE (OLD) VALUE


!*****************
LL=TOL                                                                !LANDING LENGTH
MFUELL=0.5*MFUELTO                                                     !LANDING FUEL
!*****************


DO                                                                        ! LOOP FOR
CRUISE RANGE CORRECTION WITH DESCENT RANGE ACCOUNTED FOR
```

```
    RANGECR=RANGE-RCUM(11)-RCUMD(11)-TOL-LL                                    !CRUISE
RANGE EQUATION

    MFUELCR=(MTOWCR1)*(1-(1/EXP(((RANGECR/1000)*SFCCR*9.81)/(VD*(CL/CDTOT)))))     !CRUISE
FUEL USED
    MTOWCR2=MTOWCR1-MFUELCR                                                    !END OF
CRUISE WEIGHT


    TCR=RANGECR/1000/(VD*LOG(MTOWCR1/MTOWCR2))                                 !CRUISE
TIME




    !******* -- DESCENT CALL AND ITERATION OF CRUISE RANGE

    CALL DESCENT(TASD, MACHD, CASD, MASSD, CLD, CDD, DRAGSD, THRUSTD, &            !DESCENT
VARIABLES
    & ROD, CORRD, RODCORR, RODMEAN, TD, TCUMD, FFLOWD, FD, FCUMD, RANGD, &
    & RCUMD, ALTD, TEMPD, RHOD, RHOSLS, MTOW, SWING, K, CD0TOT, SFCCLIMB, &
    & MCR, MTOWCR2, SFCD, R)

    ERROR=RCUMD(11)-RCUMSTORE                                                  !ERROR
BETWEEN NEW AND OLD DESCENT RANGE
    RCUMSTORE=RCUMD(11)                                                        !NEWLY
ASSIGNED RANGE OF DESCENT TO INPUT INTO CRUISE EQU. VIA STORE VARIABLE

    IF (ERROR<0.01) EXIT


END DO


MFUELTOT=MFUELTO+FCUM(11)+MFUELCR+FCUMD(11)+MFUELL

MFUELRES=MFUELTOT/11

TTOTAL=TCR+TCUM(11)+TCUMD(11)+240  !240=4MINS FOR LANDING/T/O              !TOTAL TIME



RETURN

END
```

9. ‘Altitud’ subroutine – altitude calculations

```
!ALTMARGIN: ENSURES PREVIOUS SEGMENT ALTITUDE IS NOT MARGINALLY DIFFERENT

SUBROUTINE ALTITUD (ALT, MCR, MASSSTORE, CL, SWING, RHO, TAS, X, ALT1, ALT2, DENS1, DENS2,
TEMP, &
& R, GAMMA, ALTITUDECRUISEEND, RHOCR, TEMPCR, PRESSURECR, ALTITUDECRUISE, MFUELCR, ALTD, VD,
SGROSS, GROSSFACTOR)

IMPLICIT NONE

REAL COUNT, TEMP1, TEMP2, CL, MCR, R, VD

INTEGER Z, W, V, X, CHECK

DOUBLE PRECISION ALTGUESS, ALT1, ALT2, DENS1, DENS2, VEL1, VEL2, SWING, ERRORALT, EMOD,
MASSSTORE, &
& ALTMARGIN, PRESSURE1, PRESSURE2, GAMMA, RHOCR, TEMPCR, PRESSURECR, ALTITUDECRUISE,
ALTITUDECRUISEEND, &
& RHOEND, MFUELCR, TASEND, SGROSS, GROSSFACTOR

DOUBLEPRECISION, DIMENSION(12)::MASS
DOUBLEPRECISION, DIMENSION(12)::ALT
DOUBLEPRECISION, DIMENSION(12)::TAS
```

```
DOUBLEPRECISION, DIMENSION(12)::RHO
DOUBLEPRECISION, DIMENSION(12)::PRESSURE
DOUBLEPRECISION, DIMENSION(12)::TEMP
DOUBLEPRECISION, DIMENSION(11)::ALTD

REAL, DIMENSION(100)::E
DOUBLEPRECISION, DIMENSION(100)::ALTITUDE



CHECK=0
ALTITUDE(1)=10000
ALTITUDE(2)=20000
E=0
!SWING=GROSSFACTOR*SWING

 !*********************************************   MAX CRUISE ALTITUDE AT CL=CLEAN; START
OF CRUISE ALTITUDE      ************************************************

DO  Z=1,100
    W=Z-1
    V=W-1



    IF (Z>2) ALTITUDE(Z)=ALTITUDE(W)-(E(W)/((E(V)-E(W))/(ALTITUDE(V)-ALTITUDE(W))))    !NEWTON
RAPHSON METHOD FOR ITERATIVE SEQUENCE




    IF (ALTITUDE(Z)<11000) THEN

        TEMP1=288.15-0.0065*ALTITUDE(Z)
        PRESSURE1=101325*(288.15/TEMP1)**(-5.25588)

    END IF

    IF (ALTITUDE(Z)>=11000 .AND. ALTITUDE(Z)<24994) THEN

         TEMP1=216.65
        PRESSURE1=22.63253/EXP(0.000157689*(ALTITUDE(Z)-10998.1))*1000

    END IF

    IF (ALTITUDE(Z)>=24994 .AND. ALTITUDE(Z)<30000) THEN

        11 CONTINUE

        TEMP1=216.65+0.0029892*(ALTITUDE(Z)-24994)
        PRESSURE1=2.5237*(216.65/TEMP1)**11.8*1000

    END IF


    RHO(11)=PRESSURE1/(R*TEMP1)



    TAS(11)=SQRT(MASSSTORE*9.81/(CL*SWING*0.5*RHO(11)))    !---- MAIN EQUATION FOR ALTITUDE
CONVERGENCE -----!

    TEMP2=(TAS(11)/MCR)**2/(GAMMA*R)



    IF (ALTITUDE(Z)<11000) ALT(11)=(288.15-TEMP2)/0.0065


    IF (ALTITUDE(Z)>=11000 .AND. ALTITUDE(Z)<24994) THEN

        PRESSURE2=RHO(11)*(R*TEMP2)/1000 !IN KPA
```

```
        ALT(11)=LOG(22.63253/PRESSURE2)/0.000157689+10998.1

    END IF


    IF (ALTITUDE(Z)>=24994 .AND. ALTITUDE(Z)<30000) ALT(11)=(TEMP2-216.65)/0.0029892+24994



    E(Z)=ALTITUDE(Z)-ALT(11)

    EMOD=((ALTITUDE(Z)-ALT(11))**2)**0.5


    IF (EMOD<0.01) THEN

        EXIT

    ELSE

        CHECK=CHECK+1
                                                                        !CHECK COUNTER FOR
ITERATION NUMBER
        IF (CHECK>100) THEN

            PRINT *, 'OPTIMUM ALTITUDE NON CONVERGENCE ERROR'
!NOTIFIES FOR NON CONVERGENCE
            STOP

        END IF

    END IF



END DO









!*****************************************************************   END OF CRUISE ALTITUDE
************************************************************

CHECK=0
ALTITUDE(1)=10000
ALTITUDE(2)=20000
E=0


DO  Z=1,100
    W=Z-1
    V=W-1



    IF (Z>2) ALTITUDE(Z)=ALTITUDE(W)-(E(W)/((E(V)-E(W))/(ALTITUDE(V)-ALTITUDE(W))))     !NEWTON
RAPHSON METHOD FOR ITERATIVE SEQUENCE



    IF (ALTITUDE(Z)<11000) THEN

        TEMP1=288.15-0.0065*ALTITUDE(Z)
        PRESSURE1=101325*(288.15/TEMP1)**(-5.25588)
```

```
    END IF

    IF (ALTITUDE(Z)>=11000) THEN

         TEMP1=216.65
        PRESSURE1=22.63253/EXP(0.000157689*(ALTITUDE(Z)-10998.1))*1000

    END IF

   ! IF (ALTITUDE(Z)>=24994 .AND. ALTITUDE(Z)<30000) THEN

    !    TEMP1=216.65+0.0029892*(ALTITUDE(Z)-24994)
   !     PRESSURE1=2.5237*(216.65/TEMP1)**11.8*1000

  !  END IF



    RHOEND=PRESSURE1/(R*TEMP1)




    TASEND=SQRT((MASSSTORE-MFUELCR)*9.81/(CL*SWING*0.5*RHOEND))    !---- MAIN EQUATION FOR
ALTITUDE CONVERGENCE -----!

    TEMP2=(TASEND/MCR)**2/(GAMMA*R)




    IF (ALTITUDE(Z)<11000) ALTD(1)=(288.15-TEMP2)/0.0065


    IF (ALTITUDE(Z)>=11000) THEN

    PRESSURE2=RHOEND*(R*TEMP2)/1000 !IN KPA
    ALTD(1)=LOG(22.63253/PRESSURE2)/0.000157689+10998.1

    END IF

   ! IF (ALTITUDE(Z)>=24994 .AND. ALTITUDE(Z)<30000) ALTD(1)=(TEMP2-216.65)/0.0029892+24994




    E(Z)=ALTITUDE(Z)-ALTD(1)
    EMOD=((ALTITUDE(Z)-ALTD(1))**2)**0.5


    IF (EMOD<0.01) THEN

        EXIT

    ELSE

        CHECK=CHECK+1
                                                                    !CHECK COUNTER FOR
ITERATION NUMBER
        IF (CHECK>100) THEN

            PRINT *, 'OPTIMUM ALTITUDE NON CONVERGENCE ERROR'
!NOTIFIES FOR NON CONVERGENCE
            STOP

        END IF

    END IF



END DO
```

```
!*********************************************************  CHANGES CRUISE ALTITUDE

ALTITUDECRUISE=(0.375)*(ALTD(1)-ALT(11))+ALT(11)  !0.375 (3/8) IS EMPIRICAL RATIO (FROM A350)-
3000FT ABOVE START CRUISE AND 8000FT FROM END CRUISE

!ALTITUDECRUISE=ALT(11)

CALL PROPERTIES(RHOCR, TEMPCR, PRESSURECR, ALTITUDECRUISE,R)

VD=MCR*SQRT(GAMMA*R*TEMPCR)

!*************************************************************CHANGE ALTITUDES BELOW ALT(11) IF
THEY ARE HIGHER THAN ALT(11); ALSO REQUIRED TEMP, RHO CALCS AND TAS INTERPOLATION

IF (ALT(11)<=ALT(10) .AND. ALT(11)>ALT(9)) THEN


    ALT(10)=((ALT(11)-ALT(9))/2)+ALT(9)




            IF (ALT(10)<11000) THEN

                TEMP(10)=288.15-0.0065*ALT(10)
                PRESSURE(10)=101325*(288.15/TEMP(10))**(-5.25588)

            END IF

            IF (ALT(10)>=11000 .AND. ALT(10)<24994) THEN

               TEMP(10)=216.65
               PRESSURE(10)=22.63253/EXP(0.000157689*(ALT(10)-10998.1))*1000

            END IF

            IF (ALT(10)>=24994 .AND. ALT(10)<30000) THEN

                TEMP(10)=216.65+0.0029892*(ALT(10)-24994)
                PRESSURE(10)=2.5237*(216.65/TEMP(10))**11.8*1000

            END IF


    RHO(10)=PRESSURE(10)/(R*TEMP(10))

    TAS(10)=(ALT(10)-ALT(9))*(TAS(11)-TAS(9))/(ALT(11)-ALT(9))+TAS(9)

    PRINT *, 'ALT(10) REPLACED'
    PAUSE

!************************************************************************


ELSE IF (ALT(11)<=ALT(9) .AND. ALT(11)>ALT(8))  THEN


    ALT(9)=((ALT(11)-ALT(8))/3)+ALT(8)




            IF (ALT(9)<11000) THEN

                TEMP(9)=288.15-0.0065*ALT(9)
                PRESSURE(9)=101325*(288.15/TEMP(9))**(-5.25588)

            END IF

            IF (ALT(9)>=11000 .AND. ALT(9)<24994) THEN

                TEMP(10)=216.65
```

```
            PRESSURE(10)=22.63253/EXP((0.000157689*ALT(9)-10998.1))*1000

        END IF

        IF (ALT(9)>=24994 .AND. ALT(9)<30000) THEN

        TEMP(9)=216.65+0.0029892*(ALT(9)-24994)
        PRESSURE(9)=2.5237*(216.65/TEMP(9))**11.8*1000

        END IF


    RHO(9)=PRESSURE(9)/(R*TEMP(9))

    TAS(9)=(ALT(9)-ALT(8))*(TAS(11)-TAS(8))/(ALT(11)-ALT(8))+TAS(8)


    !*****


    ALT(10)=ALT(11)-((ALT(11)-ALT(8))/3)


        IF (ALT(10)<11000) THEN

            TEMP(10)=288.15-0.0065*ALT(10)
            PRESSURE(10)=101325*(288.15/TEMP(10))**(-5.25588)

        END IF

        IF (ALT(10)>=11000 .AND. ALT(10)<24994) THEN

            TEMP(10)=216.65
            PRESSURE(10)=22.63253/EXP(0.000157689*(ALT(10)-10998.1))*1000

        END IF

        IF (ALT(10)>=24994 .AND. ALT(10)<30000) THEN

            TEMP(10)=216.65+0.0029892*(ALT(10)-24994)
            PRESSURE(10)=2.5237*(216.65/TEMP(10))**11.8*1000

        END IF


    RHO(10)=PRESSURE(10)/(R*TEMP(10))

    TAS(10)=(ALT(10)-ALT(8))*(TAS(11)-TAS(8))/(ALT(11)-ALT(8))+TAS(8)


    PRINT *, 'ALT(10,9) REPLACED'
    PAUSE



!*************************************************************************   --- ASSUMES
ALTITUDE(8) < 11000 METRES ---


ELSE IF (ALT(11)<=ALT(8) .AND. ALT(11)>ALT(7))  THEN


    ALT(8)=((ALT(11)-ALT(7))/4)+ALT(7)

    TEMP(8)=288.15-0.0065*ALT(8)

    PRESSURE(8)=101325*(288.15/TEMP(8))**(-5.25588)

    RHO(8)=PRESSURE(8)/(R*TEMP(8))

    TAS(8)=(ALT(8)-ALT(7))*(TAS(11)-TAS(7))/(ALT(11)-ALT(7))+TAS(7)
```

```
!******

    ALT(9)=((ALT(11)-ALT(7))/2)+ALT(7)

    TEMP(9)=288.15-0.0065*ALT(9)

    PRESSURE(9)=101325*(288.15/TEMP(9))**(-5.25588)

    RHO(9)=PRESSURE(9)/(R*TEMP(9))

    TAS(9)=(ALT(9)-ALT(7))*(TAS(11)-TAS(7))/(ALT(11)-ALT(7))+TAS(7)

 !*****

    ALT(10)=((ALT(11)-ALT(7))*(3/4))+ALT(7)

    TEMP(10)=288.15-0.0065*ALT(10)

    PRESSURE(10)=101325*(288.15/TEMP(10))**(-5.25588)

    RHO(10)=PRESSURE(10)/(R*TEMP(10))

    TAS(10)=(ALT(10)-ALT(7))*(TAS(11)-TAS(7))/(ALT(11)-ALT(7))+TAS(7)


    PRINT *, 'ALT(10,9,8) REPLACED'
    PAUSE

    ELSE IF (ALT(11)<=ALT(7)) THEN

    PRINT *, 'ALTITUDE NUMBER 7 HIGHER THAN CEILING'
    PAUSE
    STOP

END IF

!*********************************************************************************


  !SWING=SWING/GROSSFACTOR



RETURN
END
```

10. ‘Properties’ subroutine – Air properties at altitude calculations

```
   SUBROUTINE PROPERTIES(RHO, TEMP, PRESSURE, ALT, R)

   DOUBLE PRECISION RHO, TEMP, PRESSURE, ALT

   REAL R


           IF (ALT<11000) THEN

               TEMP=288.15-0.0065*ALT
               PRESSURE=101325*(288.15/TEMP)**(-5.25588)

           END IF
```

```
        IF (ALT>=11000 .AND. ALT<24994) THEN

           TEMP=216.65
           PRESSURE=22.63253/EXP(0.000157689*(ALT-10998.1))*1000

        END IF

        IF (ALT>=24994 .AND. ALT<30000) THEN

            TEMP=216.65+0.0029892*(ALT-24994)
            PRESSURE=2.5237*(216.65/TEMP)**11.8*1000

        END IF


RHO=PRESSURE/(R*TEMP)


RETURN

END-
```

11. ‘Descent’ subroutine – descent performance calculations

```
SUBROUTINE DESCENT(TAS, MACH, CAS, MASS, CLC, CD, DRAGS, THRUST, &
& ROD, CORR, RODCORR, RODMEAN, T, TCUM, FFLOW, F, FCUM, RANG, &
& RCUM, ALT, TEMP, RHO, RHOSLS, MTOW, SWING, K, CD0TOT, SFCCLIMB, &
& MCR, MTOWCR2, SFCD, R)


IMPLICIT NONE

REAL MCR, RHOSLS, SFCD, R
INTEGER X, Y, W, INTS
DOUBLE PRECISION MTOF, MFUEL, ERROR, ERRORFAC, MTOWCR2, MTOW, SWING, K, &
& CD0TOT, SFCCLIMB, PRESSURRE

DOUBLE PRECISION,DIMENSION(11)::TAS  !SUBROUTINE ARRAYS PASS THROUGH INTO PERFORMANCE
SUBROUTINE WITH 'D' SUFFIX TO DISTINGUISH FROM CLIMB
DOUBLE PRECISION,DIMENSION(11)::CAS
DOUBLE PRECISION,DIMENSION(11)::MACH
DOUBLE PRECISION,DIMENSION(11)::EAS
DOUBLE PRECISION,DIMENSION(11)::MASS
DOUBLE PRECISION,DIMENSION(11)::CLC
DOUBLE PRECISION,DIMENSION(11)::CD
DOUBLE PRECISION,DIMENSION(11)::DRAGS
DOUBLE PRECISION,DIMENSION(11)::THRUST
DOUBLE PRECISION,DIMENSION(11)::ROD
DOUBLE PRECISION,DIMENSION(11)::CORR
DOUBLE PRECISION,DIMENSION(11)::RODCORR
DOUBLE PRECISION,DIMENSION(11)::RODMEAN
DOUBLE PRECISION,DIMENSION(11)::T
DOUBLE PRECISION,DIMENSION(11)::TCUM
DOUBLE PRECISION,DIMENSION(11)::FFLOW
DOUBLE PRECISION,DIMENSION(11)::F
DOUBLE PRECISION,DIMENSION(11)::FCUM
DOUBLE PRECISION,DIMENSION(11)::RANG
DOUBLE PRECISION,DIMENSION(11)::RCUM
DOUBLE PRECISION,DIMENSION(11)::ALT
REAL,DIMENSION(11)::TEMP
DOUBLE PRECISION,DIMENSION(11)::RHO
DOUBLE PRECISION,DIMENSION(11)::PRESSURE


!********************************************** AIR PROPERTIES

 DO X=1,11

            IF (ALT(X)<11000) THEN

                TEMP(X)=288.15-0.0065*ALT(X)
                PRESSURE(X)=101325*(288.15/TEMP(X))**(-5.25588)
```

```
            END IF

            IF (ALT(X)>=11000 .AND. ALT(X)<24994) THEN

                TEMP(X)=216.65
                PRESSURE(X)=22.63253/EXP(0.000157689*(ALT(X)-10998.1))*1000

            END IF

            IF (ALT(X)>=24994 .AND. ALT(X)<30000) THEN

                TEMP(X)=216.65+0.0029892*(ALT(X)-24994)
                PRESSURE(X)=2.5237*(216.65/TEMP(X))**11.8*1000

            END IF


    RHO(X)=PRESSURE(X)/(R*TEMP(X))

END DO



!*********************************************************************   --- DESCENT ---

DO X=1,11
CAS(X)=TAS(X)/SQRT(RHOSLS/RHO(X))
END DO



MASS(1)=MTOWCR2
TCUM(1)=0
FCUM(1)=0
RCUM(1)=0
X=1
Y=2


30 CONTINUE

MFUEL=0
ERROR=0



DO



!*********   GET RODCORR WITH GUESSED/NEW MASS

CLC(X)=(MASS(X)*9.81)/(SWING*0.5*RHO(X)*TAS(X)**2)

CD(X)=CD0TOT+(K*CLC(X)**2)

DRAGS(X)=0.5*RHO(X)*(TAS(X)**2)*SWING*CD(X)

THRUST(X)=10000

ROD(X)=((DRAGS(X)-THRUST(X))/(MASS(X)*9.81))*TAS(X)

    IF (X==11) THEN

        CORR(X)=(TAS(X)/9.81)*((TAS(X)-TAS(W))/(ALT(X)-ALT(W)))+1

    ELSE

        CORR(X)=(TAS(X)/9.81)*((TAS(Y)-TAS(X))/(ALT(Y)-ALT(X)))+1

    END IF

RODCORR(X)=ROD(X)/CORR(X)
```

```
!**************

IF (X>1) THEN                                ! PREVIOUS FUEL AND ERROR



RODMEAN(W)=(RODCORR(W)+RODCORR(X))/2

T(W)=(ALT(W)-ALT(X))/RODMEAN(W)



TCUM(X)=TCUM(W)+T(W)
FFLOW(W)=SFCD*((THRUST(X)+THRUST(W))/2)/10**3

F(W)=T(W)*FFLOW(W)

ERROR=F(W)-MFUEL



ELSE     ! FIRST ALTITUDE REQUIRES SECOND ALTITUDE DATA -  LOOP

    X=X+1
    W=X-1
    Y=X+1

    GOTO 50

ENDIF

!***************

ERRORFAC=(ERROR**2)**(0.5)
IF (ERRORFAC<0.01) THEN                ! ERROR SIZE CHECK

    FCUM(X)=F(W)+FCUM(W)
    RANG(X)=CAS(W)*T(W)
    RCUM(X)=RANG(X)+RCUM(W)


    X=X+1                         ! NEXT ALTITUDE FOR SMALL ERROR
    W=X-1
    Y=X+1
    IF (X<12) THEN

    MASS(X)=MASS(W)
    GOTO 30

    ELSE
    GOTO 200

    END IF

                          ! REITERATE IF ERROR IS LARGE
ENDIF


!*************


50 CONTINUE

MFUEL=MFUEL+ERROR  ! FUEL MASS GUESS

MASS(X)=MASS(W)-MFUEL    ! NEXT TOTAL MASS

!**************


END DO
```

```
200 CONTINUE


RETURN

END
```

12. ‘Stability’ subroutine – Aircraft static Stability calculations

```
SUBROUTINE STABILITY(XOUTERWING, BINNERHALF, SWEEPLEINNER, BOUTER, SWEEPLEOUTER, SKOUTER,
SWEEPTEOUTER, S1, S2, &
    & TKOUTER, TTOUTER, CTOUTER, BFUELOUTER, XFUELOUTER, XINNERCOVER, CRINNER,
SWEEPTEINNER, XINNERSPAR, &
    & CABINLENGTH, NOSELENGTH, XINNERWING, XPAY, XNACELLE, LNAC, ZNACELLE, HNAC, XNOSE,
XMASSSUM, &
    & MASSOUTERTOTAL, CKOUTER, MFUELTOT, MFUELRES, MASSCABINTOTAL, MASSINNERTOTAL, MPAY,
MPP, &
    & MASSNOSETOTAL, XCG, INNERMOMENT, INNERLIFTSLOPE, OUTERMOMENT, OUTERLIFTSLOPE,
INNERLIFT, OUTERLIFT, &
    & XACQUARTER, XAC, STATICMARGINMTOW, STATICMARGINMLW, SWEEPQUARTERINNER,
SWEEPQUARTEROUTER, BINNER, &
    & BOUTERHALF, THRUSTCR, MEQ, MOPS, MLFC, MASSSECTOTAL)

IMPLICIT NONE

REAL LNAC, HNAC

DOUBLE PRECISION XOUTERWING, BINNERHALF, SWEEPLEINNER, BOUTER, SWEEPLEOUTER, SKOUTER,
SWEEPTEOUTER, S1, S2, &
    & TKOUTER, TTOUTER, CTOUTER, BFUELOUTER, XFUELOUTER, XINNERCOVER, CRINNER,
SWEEPTEINNER, XINNERSPAR, &
    & CABINLENGTH, NOSELENGTH, XINNERWING, XPAY, XNACELLE, ZNACELLE, XNOSE, XMASSSUM, &
    & MASSOUTERTOTAL, CKOUTER, MFUELTOT, MFUELRES, MASSCABINTOTAL, MASSINNERTOTAL, MPAY,
MPP, &
    & MASSNOSETOTAL, XCG, INNERMOMENT, INNERLIFTSLOPE, OUTERMOMENT, OUTERLIFTSLOPE,
INNERLIFT, OUTERLIFT, &
    & XACQUARTER, XAC, STATICMARGINMTOW, SWEEPQUARTERINNER, SWEEPQUARTEROUTER, BINNER,
BOUTERHALF, XCGMLW, &
    & STATICMARGINMLW, THRUSTCR, XLFC, XSEC, XEQOPS, MEQ, MOPS, MLFC, MASSSECTOTAL


!*********----------------------------  CENTRE OF GRAVITY (C.G)  ----------------------
*******

!C.G MOMENTS TAKEN ABOUT NOSE TIP

!X-AXIS LIES ON CENTRE LINE, Z-AXIS PARALLEL TO WING THICKNESS


XOUTERWING=BINNERHALF*TAN(SWEEPLEINNER)+0.35*BOUTER*TAN(SWEEPLEOUTER)+0.6*(CKOUTER+0.35*BO
UTER*(TAN(SWEEPTEOUTER)- &

& TAN(SWEEPLEOUTER)))  !60% C.G FROM LE, 35% SPAN FROM OUTER ROOT (KINK)

S1=TKOUTER*CKOUTER

S2=TTOUTER*CTOUTER

BFUELOUTER=0.85*BOUTERHALF/4*(S1+3*S2+2*SQRT(S1*S1))/(S1+S2+SQRT(S1*S2))  !STRUCTURAL SPAN
FROM KINK TO FUEL C.G - 85% length

XFUELOUTER=BINNERHALF*TAN(SWEEPLEINNER)+BFUELOUTER*TAN(SWEEPLEOUTER)+0.40*(CKOUTER+BFUELOU
TER*(TAN(SWEEPTEOUTER)- &

& TAN(SWEEPLEOUTER)))  ! 40% FROM LE (15+25)%, FUEL TANK C.G POINT


!ASSUMPTION THAT COVER MASS = SPAR MASS
```

```
XINNERCOVER=0.35*BINNERHALF*TAN(SWEEPLEINNER)+0.6*(CRINNER+0.35*BINNERHALF*(TAN(SWEEPTEINN
ER)-TAN(SWEEPLEINNER))) ! 60% FROM L.E. BECAUSE SPAR=40%, BOTH =50%

XINNERSPAR=0.35*BINNERHALF*TAN(SWEEPLEINNER)+0.08*(CRINNER+0.35*BINNERHALF*(TAN(SWEEPTEINN
ER)-TAN(SWEEPLEINNER)))+ &  !8% GAP FROM FRONT SPAR TO L.E.

& 0.5*(CABINLENGTH-0.35*BINNERHALF*TAN(SWEEPQUARTERINNER)) ! 50%  spar box c.g.

XLFC=NOSELENGTH+0.35*BINNERHALF*TAN(SWEEPQUARTERINNER)

XSEC=XINNERSPAR

XEQOPS=XINNERSPAR

XINNERWING=(XINNERSPAR+XINNERCOVER)/2  !spar mass = cover mass

XPAY=XINNERSPAR !0.35*BINNERHALF*TAN(SWEEPLEINNER)+0.8*((CABINLENGTH+NOSELENGTH)-
0.35*BINNERHALF*TAN(SWEEPLEINNER))

!XFUELINNER=

XNACELLE=BINNERHALF*TAN(SWEEPLEINNER)-0.5*LNAC

ZNACELLE=0.5*HNAC  !ONLY FOR A.C CALCS

XNOSE=0.667*NOSELENGTH

XMASSSUM=XOUTERWING*MASSOUTERTOTAL+XFUELOUTER*(MFUELTOT+MFUELRES)+XINNERWING*(MASSCABINTOT
AL+MASSINNERTOTAL)+ &   !SUM OF X AND MASS PRODUCTS

&
XPAY*MPAY+XNACELLE*MPP+XNOSE*MASSNOSETOTAL+THRUSTCR/9.81*ZNACELLE+XEQOPS*(MEQ+MOPS)+XLFC*M
LFC+XSEC*MASSSECTOTAL

XCG=XMASSSUM/(MASSOUTERTOTAL+MFUELTOT+MFUELRES+MASSCABINTOTAL+MASSINNERTOTAL+MPAY+MPP+MASS
NOSETOTAL+THRUSTCR/9.81+ &
& MEQ+MOPS+MLFC+MASSSECTOTAL)   !X FROM NOSE ON CENTRE LINE



!*********----------------------------  AERODYNAMIC CENTRE (A.C)  -----------------------
*******

INNERLIFTSLOPE=0.1193

OUTERLIFTSLOPE=0.1141


INNERMOMENT=INNERLIFTSLOPE*TAN(SWEEPQUARTERINNER)*(BINNERHALF**2/2*CRINNER-
BINNERHALF**3/3*(TAN(SWEEPLEINNER)+TAN(SWEEPTEINNER)))                                  !
INTEGRAL OF LOCAL MOMENT FORCES

!OUTERMOMENT=OUTERLIFTSLOPE*(BINNERHALF*TAN(SWEEPQUARTERINNER)+TAN(SWEEPQUARTEROUTER))*(BO
UTERHALF**2/2*CKOUTER-BOUTERHALF**3/3*(TAN(SWEEPLEOUTER)-TAN(SWEEPTEOUTER)))


!OUTERMOMENT=OUTERLIFTSLOPE*(BINNERHALF*TAN(SWEEPQUARTEROUTER)*CKOUTER+BOUTERHALF**2/2*(CK
OUTER*TAN(SWEEPQUARTERINNER)-BINNERHALF* &

!& TAN(SWEEPQUARTEROUTER)*(TAN(SWEEPLEOUTER)-TAN(SWEEPTEOUTER)))-
BOUTERHALF**3/3*TAN(SWEEPQUARTERINNER)*(TAN(SWEEPLEOUTER)-TAN(SWEEPTEOUTER)))

OUTERMOMENT=OUTERLIFTSLOPE*(BINNERHALF*BOUTERHALF*TAN(SWEEPQUARTERINNER)*CKOUTER+BOUTERHAL
F**2/2*(CKOUTER*TAN(SWEEPQUARTEROUTER)-BINNERHALF* &

& TAN(SWEEPQUARTERINNER)*(TAN(SWEEPLEOUTER)-TAN(SWEEPTEOUTER)))-
BOUTERHALF**3/3*TAN(SWEEPQUARTEROUTER)*(TAN(SWEEPLEOUTER)-TAN(SWEEPTEOUTER)))
```

```
INNERLIFT=INNERLIFTSLOPE*(BINNERHALF*CRINNER-
BINNERHALF**2/2*(TAN(SWEEPLEINNER)+TAN(SWEEPTEINNER)))
! INTEGRAL OF LOCAL LIFT FORCES

OUTERLIFT=OUTERLIFTSLOPE*(BOUTERHALF*CKOUTER-BOUTERHALF**2/2*(TAN(SWEEPLEOUTER)-
TAN(SWEEPTEOUTER)))


XACQUARTER=(INNERMOMENT+OUTERMOMENT)/(INNERLIFT+OUTERLIFT)  ! A.C DISTANCE FROM QUATER
CHORD POINT ON CENTRE LINE

XAC=XACQUARTER+0.276*CRINNER  ! A.C DISTANCE FROM NOSE POINT ON CENTRE LINE



!********---------------------------------  STATIC MARGIN ----------------------------------
*******


STATICMARGINMTOW=(XAC-XCG)/CRINNER*100  ! NOTE: THIS IS READ MANUALLY FROM OUTPUT - SHOULD
BE BELOW 5%



XCGMLW=(XOUTERWING*MASSOUTERTOTAL+XINNERWING*(MASSCABINTOTAL+MASSINNERTOTAL)+MFUELRES*XFUE
LOUTER+ &   !SUM OF X AND MASS PRODUCTS

&
XPAY*2*MPAY+XNACELLE*MPP+XNOSE*MASSNOSETOTAL+ZNACELLE*THRUSTCR/9.81+XEQOPS*(MEQ+MOPS)+XLFC
*MLFC+XSEC*MASSSECTOTAL)/ &

&
(MASSOUTERTOTAL+MASSCABINTOTAL+MASSINNERTOTAL+MFUELRES+2*MPAY+MPP+MASSNOSETOTAL+THRUSTCR/9
.81+MEQ+MOPS+MLFC+MASSSECTOTAL)


STATICMARGINMLW=(XAC-XCGMLW)/CRINNER*100



RETURN
END
```